In Vivo Confocal Microscopy of The Abnormal Cornea:

A Clinical and Clinico-Pathological Correlation

Thaer Saad Alomar

M.B.Ch.B, DO, FRCSEd

School of Clinical Sciences

Thesis submitted to the University of Nottingham

for the degree of Doctor in Medicine (Ophthalmology)

July 2012

“In the name of Allah, the most gracious and the most merciful.”

Abstract

In vivo confocal microscopy (IVCM) offers a unique real time non-invasive imaging method to explore live tissues at cellular and subcellular levels of histological detail with magnifications very much comparable to conventional 'ex vivo' light microscopy. Therefore it has been widely used over the past two decades to investigate the ocular surface and cornea in health, disease and following surgical procedures. One of the main challenges in understanding IVCM is to get a proper interpretation of the images that present various figures and patterns of tissue structures all in black and white with variable degree of reflectivity, being whiter (or brighter) when they are more (or hyper) reflective. The lack of good correlation between IVCM and corresponding light microscopy for the same tissue samples has lead to speculative interpretations of IVCM images in the literature.

In this work we tried to fill that gap through performing IVCM to patients with various corneal and ocular surface disorders just few days prior to obtaining the tissue samples (corneal graft, excisional biopsy or alcohol delamination) for histopathological examination to make sure that IVCM images were truly representative to the tissue details that might change if more time was left to elapse between IVCM and tissue sampling.

In ocular surface disease group (chapter three) we contrasted IVCM criteria in conjunctival epithelial overgrowth onto the cornea in limbal stem cell deficiency and Pterygium-like disorders with those seen in Corneal/Conjunctival Intraepithelial neoplasia (CIN) to confirm reliable diagnostic criteria of CIN with IVCM.

In corneal oedema (chapter four) IVCM viewing of (histologically confirmed) subepithelial fibroblasts without clinically visible corneal scarring has been reported for the first time in IVCM literature particularly in Fuchs endothelial dystrophy. Sub-basal corneal nerve reduction as well as stromal keratocytes and endothelial changes were clearly illustrated with IVCM.

In keratoconus cases (chapter five) morphological epithelial changes related to regenerative atypia have been studied for the first time and compared to those seen in CIN through light microscopy and IVCM in addition to other epithelial changes associated with keratoconus. Novel IVCM criteria for Bowman's zone breaks have been described and compared carefully with histological sections.

In corneal dystrophies (chapter six) IVCM criteria in Thiel-Behnke's corneal dystrophy (CDBII) as well as in macular, granular and lattice dystrophy correlated well with light microscopic findings with a novel IVCM pattern in one Macular dystrophy case.

In Acanthamoeba keratitis (chapter seven) a new form of Acanthamoeba cysts has been described for the first time through IVCM.

Moreover this study presented for the first time IVCM diagnostic criteria in corneal intraepithelial neoplasia, keratoconus, Acanthamoeba keratitis and some corneal dystrophies. A comprehensive IVCM illustration of various types and stages of corneal fibrosis has been achieved as well.

Dedication

I hereby dedicate my fruitful work to my lord “Allah” the most gracious, for his overwhelming care and provision with health, wealth and strength until the whole work was done. Secondly I dedicate my achievement to my beloved wife ‘Sura’ for her endless support and patience throughout my life; and to my loving parents for their continuous supplication to finish the work, And finally to my lovely daughters Omama, Danea and Ranea.

Acknowledgements

I would like to forward my sincere thanks and appreciation to Professor Harminder S Dua for his kind supervision all the way through. For me he is a role model in implementing ethical and moral values at the highest standards with which he treats his patients, researchers and colleagues. At the same level of appreciation I deeply acknowledge the efforts of Professor James Lowe in the analysis of the histopathological material of my project. I used to tell my colleagues how much I enjoyed the time spent with him in studying the cases backed by his vast knowledge from which I took an invaluable part in the field of ocular pathology. I never forget in particular those moments when comparable things were seen in light and confocal microscopy to add new fruits to my work.

"Knowledgeable without arrogance" that is how I simply describe my two special supervisors.

I also forward my sincere gratitude to Trevor Gray, Linda Dewdney, Anne Kane and Clair Boag in the Department of Histopathology for their help & provision of laboratory materials.

Finally I do acknowledge all the emotional & scientific back up from my special colleagues, Mouhamed Al-Aqaba, Ammar Miri, Usama Faris and Muneer Otri who let me live a friendly atmosphere during the years of stressful work.

Contents

List of figures

List of tables

Chapter One

1 Introduction

A Confocal Microscope (CM) is a diffraction - limited scanning spot microscope in which both the light source and the detector take the form of micrometer-scale pinholes (Dabbs and Glass, 1992).

CM is an innovative development of the conventional light microscopy. Despite being described first by Marvin Minsky in 1955 (Minsky, 1988), it was not before the late 1980s that advanced technology yielded powerful clinically useful confocal microscopes to explore the living tissues of the human eye at literally cellular level, hence the term "In vivo confocal microscopy" (IVCM) (Cavanagh et al., 1990). Since then an increasing number of articles have been published on the clinical applications and features of in vivo confocal microscopy (IVCM) of the human cornea indicating the rising popularity and importance of this unique imaging paradigm for clinical and pathological evaluation in ophthalmology (Dhaliwal et al., 2007).

1.1 BASICS OF CONFOCAL OPTICS:

In conventional light microscopy for a thick specimen illumination light involves layers out of the focal plane of the microscope objective,

thus the backscattered light coming from these layers would degrade the resolution quality of images of the area at the focal plane.

In Confocal Optics (Figure 1-1) the problem is eliminated through the following steps:

1. Point light source is focused onto a small volume within the specimen, i.e. diffraction limited illumination.
2. Point detection, through a pinhole, of reflected light rays for inspection by observer's eye or camera.
3. The pinhole is conjugate to the focal point of the lens, hence the name ''Confocal'' pinhole or microscope (Mathers et al., 1995).

This results in a reduction of the amount of out-of-focus signal from above and below the focal plane that contributes to the detected image and produces a marked increase in both transverse (x,y) and axial (z) resolution as well as the contrast of image details (Mathers et al., 1995).

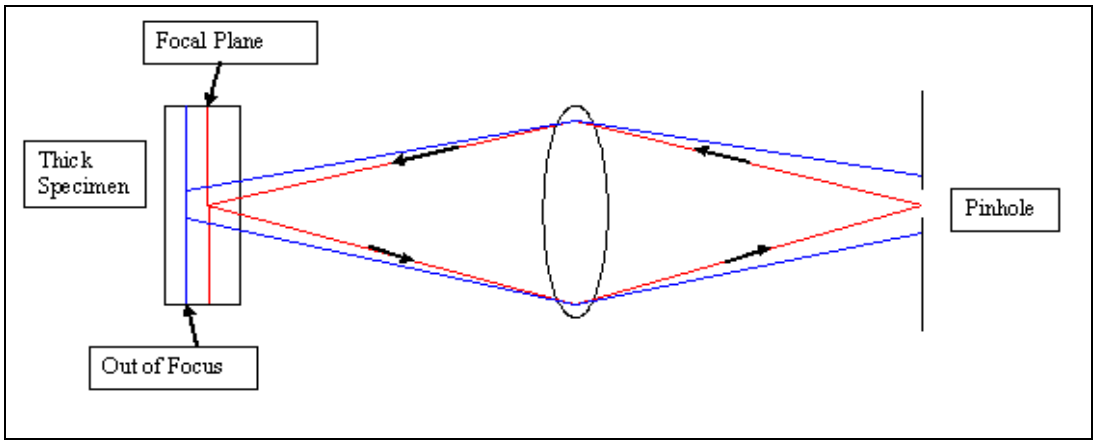

Figure 1-1 Basic confocal optics.

The sophisticated built-up of CM can be simplified in the following diagram:

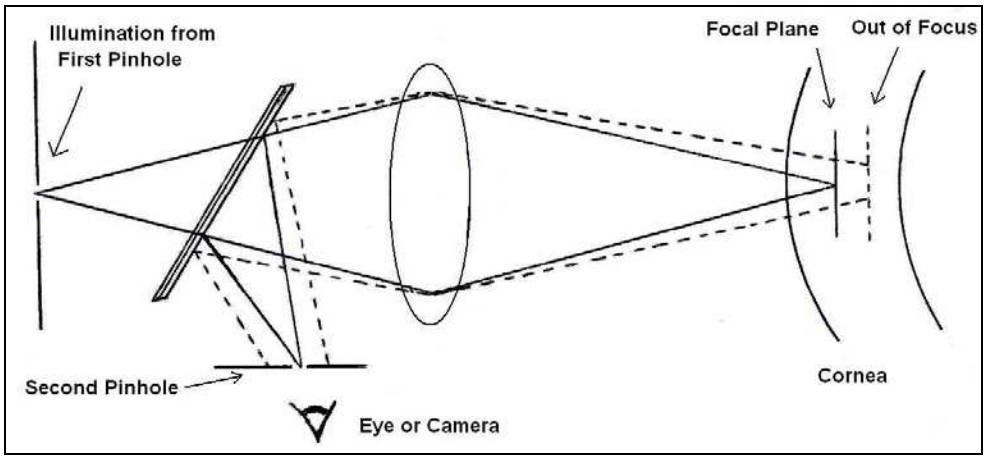

Figure 1-2: A diagram illustrating the basic optical principles of in vivo confocal microscopy of human cornea. Illumination from the first pinhole is focused by the objective lens at the desired section within the cornea (focal plane). Out- of- Focus sections are more or less illuminated. Backscattered light passes through the microscope objective to be focused for inspection at the Second Pinhole which cuts away Out-of-Focus light. The first and Second Pinholes as well as the Focal Plane of the objective are Conjugate points .(reproduced from Jalbert et al. 2003).

4. Because only one tiny volume element of the specimen is illuminated by each point source the detected field of view would be very tiny as well i.e. trading field of view for enhanced resolution, therefore a useful full-field view of the specimen as a whole must be regained by mechanically scanning the specimen (Cavanagh et al., 1990), a function that can be performed in two ways:

   a. Lateral scanning in x and y axes through which the full image is constructed. The speed of this scanning would determine the temporal resolution (t) of the microscope (Mathers et al., 1995).

   b. Axial scanning in z axis by varying the focal plane at different depths through the whole thickness of the cornea thus

producing optical sectioning and 3 dimensional viewing of the examined tissues. In fact this non-invasive sectioning is one of the powerful features of confocal microscopy which allows clinicians to observe truly in situ live histological and pathological details at literally cellular and subcellular levels.

1.2 SCANNING METHODS AND IMAGE ACQUISITION:

As images in confocal microscopy are built up through continuous scanning, the scanning speed is the time required to create one image thus different microscopes have different scanning speeds (Bohnke and Masters, 1999). Rapid scanning in x-y axes produces multiple sequential images that are going to be collected by the detector (a charged couple device or CCD) attached to a computer, which builds up the image one pixel at a time. Thus rapid scanning that yields images at 30 frames / sec or faster is called real – time scanning. In fact this helps the clinician to observe CM images as a video display on the PC monitor and chose the best frames required (Bohnke and Masters, 1999).

The most common scanning methods are the following:

1. Spinning Nipkow Disc system: Nipkow disc contains thousands of pinholes 20 – 80μm size each, arranged in Archimedean spirals (Figure

1-3). The illuminating and reflected beams pass through these pinholes. On spinning the disc many points in x and y planes will be scanned rapidly to yield video rate image display. Because the illumination and detection of light through conjugate pinholes occurs in tandem, this microscope was named the tandem scanning confocal microscope (Mathers et al., 1995, Parmar et al., 2006).

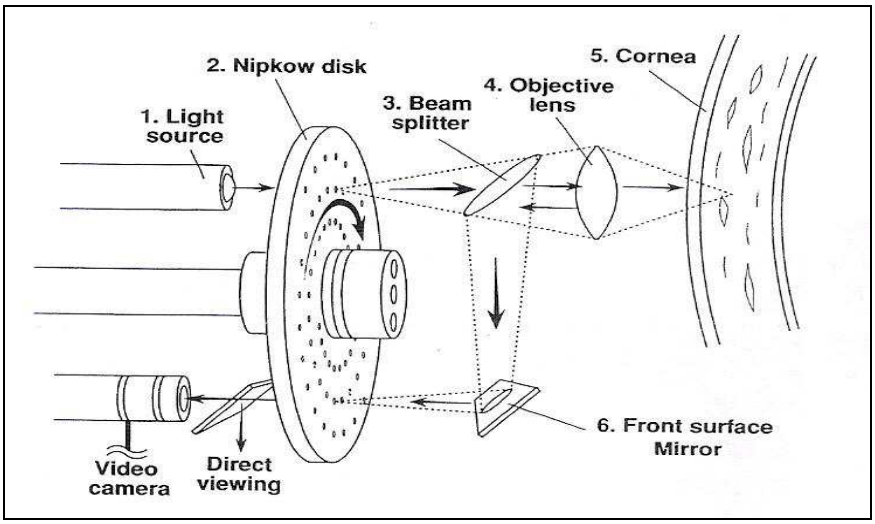

Figure 1-3: Nipkow disc scanning system (reproduced from Cavanagh et al. 2000)

The holes in the disk are arranged so that a large number of beams uniformly scan the image field as the disk rotates, completely covering the specimen at a high rate which allows real-time focusing and imaging of dynamic processes. In the setup by Xiao, Corle, and Kino it was possible to generate 700 frames per second on rotating the disc at 2500 rpm (Cavanagh et al., 1990). Because disk-scanning microscopes form a real image, a CCD camera may be located directly in the image plane. Several shortcomings have

limited the practical utility of disk-scanning confocal systems. One of the most serious ones is the typical reliance on conventional broad-spectrum light sources, and the extreme light loss that occurs at the disk as it transmits only 1% of the incident illumination (Mathers et al., 1995).

2. Oscillating mirrors: Two high-speed oscillating mirrors, driven by galvanometric motors, pivot on perpendicular axes, one scanning along the x axis and the other on the y-axis. This system is used in scanning slit confocal microscopes (SSCM) and laser scanning microscope (LSCM) (Bohnke and Masters, 1999).
3. Axial scanning at z axis is another feature of CM that is achieved by advancing the focal plane of the objective through the thick specimen (Cornea) thus obtaining section images at certain depths. A modification of z scanning, called Confocal Microscopy Through Focusing (CMTF) is achieved by optically advancing a thin (9µm) focal plane at a constant speed through the cornea while recording video images, thus enables the clinicians to measure corneal thickness (Pachymetry) as well as determining corneal sub-layer or lesion depth (Mohay et al., 1997, Patel et al., 2001). Changing or advancing the focal plane can be done manually or through the use of a microstepper motor to drive the fine-focus control of the microscope (Bohnke and Masters, 1999).

1.3 TYPES OF CONFOCAL MICROSCOPE

1. Tandem scanning confocal microscope (TSCM): using spinning Nipkow disc system. Ideally this is the best tool to perform z-scanning and measure corneal thickness (pachymetry).
2. Slit scanning confocal microscope (SSCM): Apart from using the oscillating mirrors for scanning, this design uses two slits, one for the illuminating beam and the other for backscattered light. This system has that advantage that many points are scanned in parallel, markedly decreasing the scanning time. Another important advantage is the superior light throughput compared with that in the point-scanning Nipkow disk systems. The disadvantage is that the microscope is truly confocal only in the axis perpendicular to the slit height (Masters and Bohnke, 2001a).
3. Laser scanning confocal microscope (LSCM): Laser illumination can result in marked increase in amount of reflected / backscattered light from the specimen thus yielding sharp images with more details. Laser sources are currently used with either of scanning systems i.e. rotating disc and oscillating mirrors. This the type of the machine used in this study.

1.4 CHARACTERISTIC FEATURES OF IVCM IMAGES:

The abbreviation (IVCM) is going to be used in the rest of the text to stand for "in vivo confocal microscopy". The images obtained by IVCM are en-face i.e. parallel to the surface of the cornea with a lateral resolution of 1 – 2μm and axial resolution of 5 – 10μm (Jalbert et al., 2003). Consequently they have a restricted field of view which is 400 X 400μm for 300x magnification in HRT II Rostock Cornea Module, the machine used in this study. The objective lens used in corneal confocal microscopy is of water immersion type with magnification power rage of 25x – 100x, Numerical Aperture of 0.6 – 1.0 and working distance of 0 – 2mm (Bohnke and Masters, 1999, Mathers et al., 1995, Jalbert et al., 2003). A 40x lens can be used to give a general overview of the cornea while a 63x lens would help observe the details in a smaller region of interest (Masters and Bohnke, 2001b). Oblique views comparable to cross-sectional light micrographs could be obtained in this study as well to provide further evaluation of relative depth and location of various tissue elements.

1.5 UNIQUE ADVANTAGES OF IVCM IN OPHTHALMOLOGY:

1. It represents the only non-invasive in vivo imaging method to visualize cellular and sub-cellular corneal details
2. It offers the feature of optical sectioning in z axis with ability to sub-layer depth measurement & pachymetry.
3. Enhanced image contrast & resolution axially and laterally compared to. conventional microscopy
4. Ability to see through moderately opaque tissues (corneal oedema & scarring).
5. Adaptable to real time observation of dynamic processes in the living eye e.g. wound healing in refractive surgery and therapeutic response in microbial keratitis (Cavanagh et al., 1993).

1.6 LIMITATIONS OF IVCM:

1. Involuntary movements due to pulse, respiration, and ocular microsaccades frequently result in significant blurring of the images, a problem that could be minimized by the use of rapid image capture systems (video and/or digital) (Jalbert et al., 2003).
2. It requires a good level of patient's compliance to efficiently perform the examination due to the short working distance of the

confocal microscope with the need to apply a coupling gel between the eye and the surface of microscope objective. Moreover to sustain good opening of lid aperture during the test makes sensitive patients or those with sore eye poor candidates for IVCM.

3. No dye or enhancement material can be used in IVCM to specifically identify tissue or cellular components as in histopathological processing. Hence all IVCM images come in black and white presenting the histological and pathological tissue changes in patterns and shapes at various degrees of reflectivity i.e. hyper-reflectivity presents bright or white areas in contrast with hypo-reflective darker areas.

Proper interpretation of the details seen on confocal images is a real challenge to the clinicians in terms of diagnosis. Unless well correlated with cytological and histopathological work up IVCM imagery interpretation would remain hypothetical (Masters and Bohnke, 2001b). That is why the vast majority of published literature so far has been descriptive rather than quantitative in nature as more investigators are trying to put proper interpretations of IVCM images taken for a wide variety of corneal conditions (Kaufman et al., 2004).

1.7 ACHIEVEMENTS OF IN VIVO CONFOCAL MICROSCOPY:

1.7.1 IVCM of Normal Cornea

1.7.1.1 Epithelium

The superficial cell layer is difficult to image with the confocal microscope and is only occasionally seen in some subjects (Nathan Efron et al., 2001). The cells are 40 – 50μm in diameter with hyper-reflective cytoplasmic along and bright nuclei of 10μm size (Masters and Thaer, 1994, Nathan Efron et al., 2001, Guthoff et al., 2006, Mastropasqua and Nubile, 2002) (Figure 1-4). The smaller middle (wing) cells are 20 – 30μm in diameter presenting more homogenous pattern with very thin bright borders and invisible nuclei (Nathan Efron et al., 2001, Masters and Thaer, 1994, Popper et al., 2004, Guthoff et al., 2006, Mastropasqua and Nubile, 2002). The average middle cell density is around 5000cell/mm² (Guthoff et al., 2006, Eckard et al., 2006). The basal cell layer has tightly packed cells of 20μm height and 10μm diameter each with dark cytoplasm, bright borders, and invisible nucleus (Nathan Efron et al., 2001, Masters and Thaer, 1994, Popper et al., 2004). This layer shows a honeycomb pattern of cell arrangement on enface images sometimes with sub-basal nerves being visible as well (Figure 1-4) (Mastropasqua and Nubile, 2002). The average basal epithelial cell density varies among

different studies between 3601 and 8996cells/ mm² (Vanathi M et al., 2003, Eckard et al., 2006).

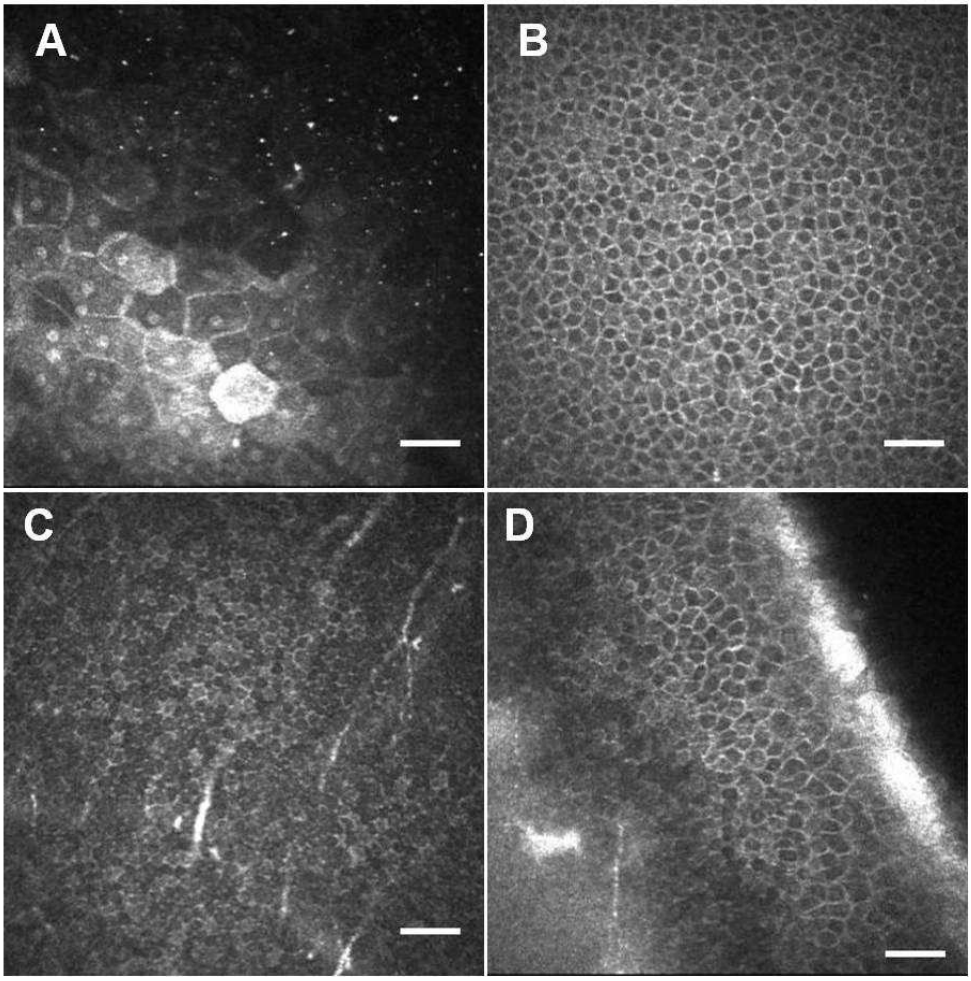

Figure 1-4: IVCM images of normal corneal epithelium. A, superficial desquamating cells with well demarcated borders as well as hyper-reflective nuclei and cytoplasm. B, middle (wing) cell layer presents with regular pattern, dark cytoplasm and invisible nuclei. C, the basal cell layer includes smaller cells in close association to the sub-basal corneal nerves. D, oblique view showing all corneal epithelial layers in relation to sub-basal nerves and Bowman zone. Scale bar 50µm.

1.7.1.2 Bowman's Layer

This layer is identified on ivcm by its reflectivity which starts at the level of sub-basal nerves down to the level of the first visible anterior keratocytes. With white light TSCM Bowman zone showed amorphous reflectivity without any specific features (Bohnke and Masters, 1999, Nathan Efron et al., 2001, Mustonen et al., 1998b, Mastropasqua and Nubile, 2002). However with HRTII RCM machine this layer shows moderately hyper-reflective linear structures 5-15µm wide running within darker areas (Figure 1-5A). In a recent study these structures were named as (K-structures) and considered as a feature of Bowman zone on IVCM in normal cornea (Kobayashi et al., 2006). They are not clearly identified in oblique views (Figure 1-5B).

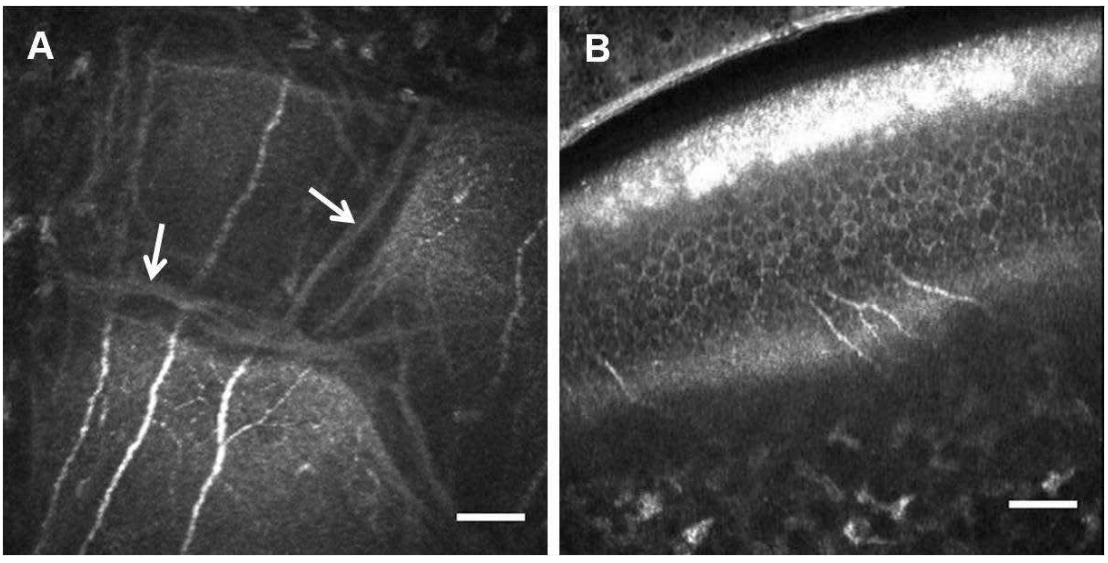

Figure 1-5: IVCM images in normal cornea at the level of Bowman zone. A, shows linear K-structures (arrows). They are less bright than the sub-basal nerves and unidentifiable on oblique view (B). Scale bar 50µm.

1.7.1.3 Stroma

This layer comprises 90% of the corneal thickness and the most noticeable component on confocal microscopy is the keratocyte nuclei which appear as hyper-reflective oval to kidney-shaped figures within a darker background representing the extra cellular matrix. The cell bodies, cytoplasmic processes as well as the stromal collagen fibrils are not visible on confocal microscopy of the normal cornea (Nathan Efron et al., 2001, Erie, 2003, Popper et al., 2004, Mastropasqua and Nubile, 2002). The apparent diameter of the nuclei ranges from 5 – 30µm, a variation that is explained by the variable 3 dimensional orientations of keratocytes within the stroma (Nathan Efron et al., 2001). (Figure 1-6).

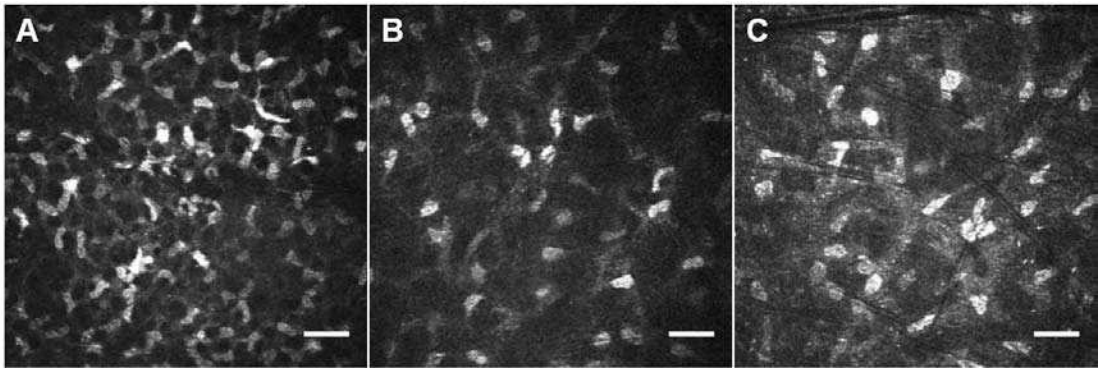

Figure 1-6: IVCM enface images of normal cornea showing keratocyte nuclei in anterior (A), middle (B) and posterior (C) stromal layers. Note the highest density seen in (A) compared to the lowest seen in (B). Focal plane depth is 53µm, 226µm and 426µm in A, B and C respectively. Scale bar 50 µm.

Keratocyte nuclei density has been calculated with IVCM in cell/mm^2 as shown in table 1 (Mustonen et al., 1998b, Hollingsworth et al., 2001, Vanathi M et al., 2003, Niederer et al., 2007b) as well as in cell/mm^3 as

shown in table 2 (Patel et al., 2001, Berlau et al., 2002, Popper et al., 2004). Keratocyte density is greatest in the anterior stroma 50 to 100µm immediately posterior to Bowman's zone where cell density is greatest in the most anterior countable confocal image (Bohnke and Masters, 1999, Patel et al., 2001). The posterior stroma showed the second highest density while the least density value was found in the middle layers (Mustonen et al., 1998b, Hollingsworth et al., 2001, Berlau et al., 2002, Vanathi M et al., 2003). The variable values reported in the literature may be explained by variation in axial resolution and contrast of different confocal microscopes used in various studies (Niederer and McGhee, 2010).

Table 1-1: Keratocyte cell density in cell/mm² measured through IVCM. (reproduced from (Niederer and McGhee, 2010)

Study	Number of eyes	Anterior stroma (cell/mm²)	Posterior stroma (cell/mm²)
Mustonen et al., 1998b*	58	1058	771
Hollingsworth et al., 2001*	120	1037	571
Vanathi et al., 2003*	100	1005	654
Niederer et al., 2007a**	85	765	315

* Slit scanning confocal microscopy (SSCM), **Laser scanning confocal microscopy (LSCM)

Table 1-2: Keratocyte density in cell/mm³ measured through IVCM. (reproduced from (Niederer and McGhee, 2010)

Study	Number of eyes	Anterior stroma (Cell/mm³)	Posterior stroma (Cell/mm³)
Patel et al., 2001*	70	33050	19947
Berlau et al., 2002**	49	24320	18850
Popper et al., 2004**	20	28616	26073

* Tandem scanning confocal microscope (TSCM), ** SSCM

Moreover confocal microscopy in vivo has been used to determine corneal keratocyte density in normal corneas (Berlau et al., 2002, Patel et al., 2001, Popper et al., 2004), in contact lens wearers (Patel et al., 2002), in keratoconus (Erie et al., 2002a), in Fuchs' Endothelial dystrophy (Mustonen et al., 1998a), after penetrating keratoplasty (Bourne, 2001), after myopic LASIK (Pisella et al., 2001, Bragheeth, 2004) and after myopic PRK (Erie et al., 2003).

1.7.1.4 Endothelium:

In confocal microscopy, the endothelium is clearly visible in normal corneas when the focusing in the z axis is performed properly (Bohnke and Masters, 1999). The regular honeycomb pattern of endothelial cells is well visualised in IVCM where the cell borders appear darker than the cell bodies with no identifiable nuclei (Nathan Efron et al., 2001, Bohnke and

Masters, 1999, Patel et al., 2006a, Popper et al., 2004, Vanathi M et al., 2003, Mastropasqua and Nubile, 2002) (Figure 1-7).

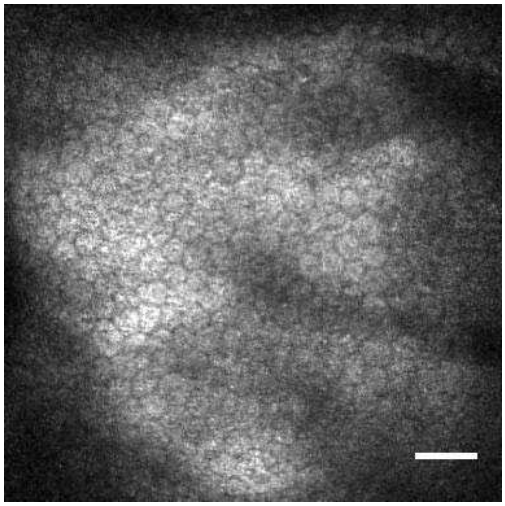

Figure 1-7: IVCM enface image of normal corneal endothelium. Note the hyper-reflective cytoplasm with the dark cell borders in a regular honeycomb pattern. Scale bar 50µm.

The Average endothelial cell density ranged between 2743 and 3061 cell/mm² through SSCM (Popper et al., 2004, Vanathi M et al., 2003, Mustonen et al., 1998b, Hollingsworth et al., 2001) while in studies using HRTII RCM the average density value ranged between 2553 and 2720 cell/mm² (Niederer et al., 2008, Niederer et al., 2007b).

1.7.1.5 Corneal thickness:

IVCM has shown poor agreement in corneal thickness measurements when it was compared with ultrasound pachymetry. With IVCM central corneal thickness was to be less than the ultrasound-measured value by 25 – 39µm even with the use of special devices to

stabilise the eye (McLaren et al., 2004, Ivarsen et al., 2002, Brugin et al., 2007, McLaren et al., 2007). The investigators admitted that the length of time taken to get full corneal thickness measurement would be associated with more involuntary eye movements that collectively degraded the precision and accuracy of pachymetry results during IVCM. In HRTII RCM machine used in our study it takes 4 seconds to complete volumetric (axial) scanning for just 60µm of corneal thickness and 10 seconds for manual sequence scanning through the full corneal thickness. This is too long a time compared to the time needed by ultrasound pachymetry.

1.7.1.6 Corneal Nerves:

Nerve bundles enter the peripheral mid-stroma in a radial pattern (Al-Aqaba et al., 2010). These nerves lose their peri-neurium and myelin sheath within 1mm of the limbus, preserving the corneal transparency, and are subsequently surrounded by only Schwann cell sheaths (Muller et al., 2003, Oliveira-Soto L and N., 2001). The nerves course anteriorly, giving rise to multiple branches innervating the anterior and mid-stroma (Masters and Thaer, 1994, Patel and McGhee, 2005, Oliveira-Soto L and N., 2001). Nerve bundles within the anterior stroma penetrate through Bowman's zone at approximately 400 points located in the mid-peripheral cornea to form the sub-basal nerve plexus that runs parallel to the corneal surface (Masters and Thaer, 1994, Muller et al., 1997, Patel and McGhee, 2005, Al-Aqaba et al., 2010). These sub-basal nerves consist of

straight and beaded fibres where the beads have been identified to consist of accumulations of mitochondria and glycogen particles (Muller et al., 1997). Only the beaded fibres subsequently form branches that enter the corneal epithelium where they terminate (Guthoff et al., 2005, Muller et al., 1997). Corneal nerves are easily identified by confocal microscopy. The sub-basal epithelial nerves are seen as hyper-reflective linear structures with beaded appearance running in straight and curved courses with numerous interconnecting and branching points in (H) and (Y) patterns (Oliveira-Soto and Efron, 2001, Bragheeth and Dua, 2005, Erie et al., 2005, Patel and McGhee, 2005). In IVCM studies the superior contrast and resolution of images produced by HRTII RCM (which is an LSCM) resulted in more detailed visibility of sub-basal nerves in comparison with the images of white light confocal microscopes i.e. TSCM and SSCM (Figure 1-8).

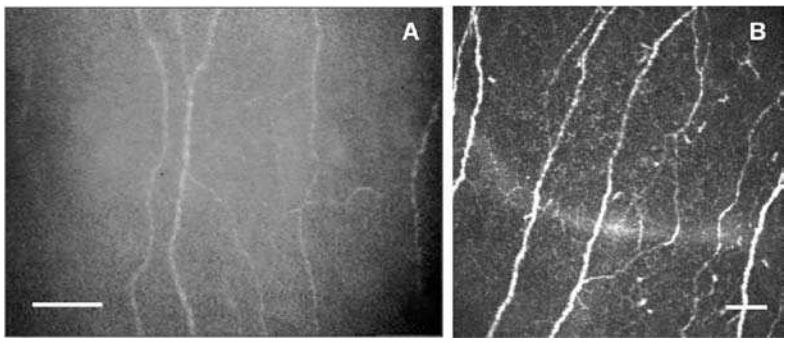

Figure 1-8: IVCM images of sub-basal corneal nerves obtained with SSCM (A) and LSCM (B). High resolution and better contrast permits the visibility of fine branches in B not well visualised in A. With clearer demarcation in B assessment of nerve width can be more accurate. Scale bar 50µm. (A is reproduced from Oliveira-Soto and Efron, 2001).

The sub-basal nerve diameter can range from 0.52µm (Grupcheva et al., 2002) to 4.68 um (Hosal et al., 2005). Sub-basal nerve density varied among different studies basically due to different types of confocal microscopes in addition to different methods in measuring and counting the nerves per frame among various investigators. The density values reported in studies using laser scanning confocal microscope (HRTII RCM) ranged between 21.6mm/mm² (Niederer et al., 2007a) and 25.96mm/mm² (Patel and McGhee, 2008) that are higher than values reported with slit scanning confocal microscopes i.e. 11.10 mm/mm² (Oliveira-Soto and Efron, 2001) and 15.18mm/mm² (Zhang et al., 2005). Recently the work of Patel & McGhee has achieved for the first time a map representing the pattern of distribution of the sub-basal corneal nerve fibres within the central 5 – 6mm area of normal cornea (Patel and McGhee, 2005). Apart from the complex series of anastomoses, nerve fibre bundles were arranged in a radiating pattern, converging toward an area approximately 1 – 2mm inferior to the central cornea to form a clockwise whorl or vortex pattern (Figure 1-9).

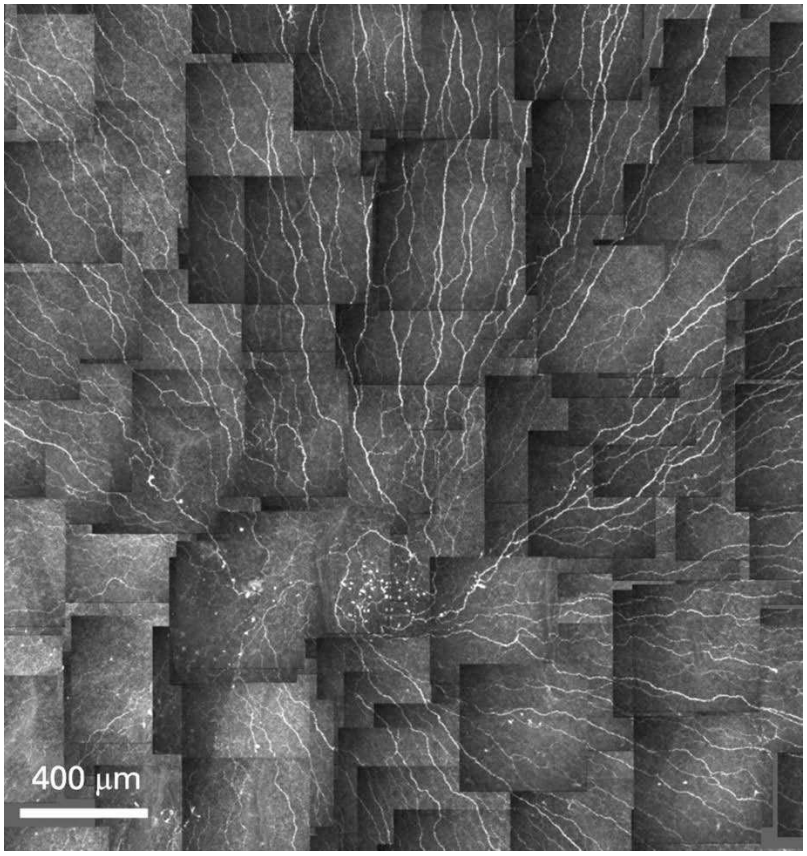

Figure 1-9: Montage of IVCM en face images showing sub-basal nerves distribution in normal human cornea with the whorl-like pattern located infero-centrally. (reproduced from Patel and McGhee 2009).

On the other hand stromal nerves can be divided into 2 main groups: the sub-Bowman's and mid-stromal nerves. The sub-Bowman's (alternatively called sub-epithelial) nerves are visible on IVCM in the first frames after Bowman zone (i.e. when the focal plane is advanced towards the stroma). They appear as hyper-reflective linear and curvilinear 1 – 5μm thick structures (Figure 1-10 A) apparently limited to the mid-peripheral cornea (Stachs et al., 2007, Patel et al., 2007). The thicker mid-stromal nerves run straight courses in various directions showing clear points of dichotomous bifurcation (Figure 1-10B). Their width on IVCM has been

reported to range between 5.5µm (Simo Mannion et al., 2005) to 11.6µm (Benitez del Castillo et al., 2004), a variation that could be explained by the obliquity of these nerves relative to en face view in IVCM that makes the nerve appear thinner (Patel and McGhee, 2009).

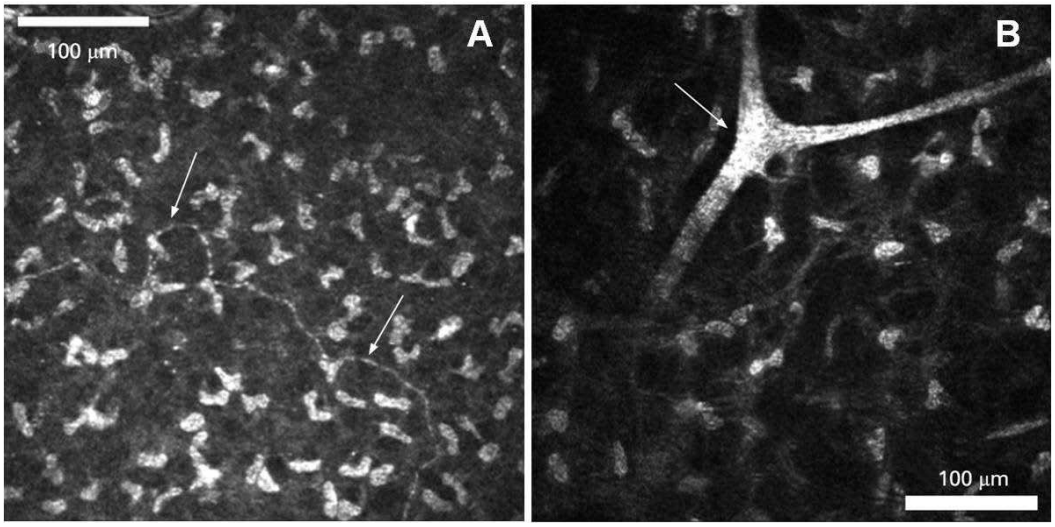

Figure 1-10: IVCM images of stromal nerves in normal cornea showing the sub-epithelial (sub-Bowman's) nerves (A) in anterior stroma and thicker mid-stromal nerves (B) with dichotomous branching pattern. (reproduced from Patel and McGhee 2009).

In addition to these straight nerves another population of mid-stromal nerves has been described recently as tortuous beaded nerves that are thought to represent a functionally different nerves (Visser et al., 2009).

Due to these powerful features in visualising and detecting the corneal nerves at various levels IVCM has been used to explore corneal innervation following keratoplasty (Patel et al., 2007) and refractive surgeries like Photorefractive Keratectomy (PRK) and laser in situ keratomileusis (LASIK) as well as in non surgical conditions like dry eyes, contact lens wear and in diabetic neuropathy.

1.7.2 IVCM of Ocular surface

Apart from corneal epithelium IVCM has been applied to identify the reflectivity features of the epithelium in the corneal limbus and bulbar conjunctiva. This is a relatively new field of application that started since the introduction of HRT II RCM thanks to its superior features of contrast and resolution compared to TSCM generation of confocal microscopes.

At the limbus the 'conjunctival' epithelial cells overlying the palisades of Vogts were brighter on IVCM compared to the hypo-reflective 'corneal' cells on the inter-palisade rete pegs (Guthoff et al., 2006, Messmer et al., 2006b, Patel et al., 2006b). The demarcation between the 2 epithelial phenotypes was clear on IVCM (Figure 1-11).

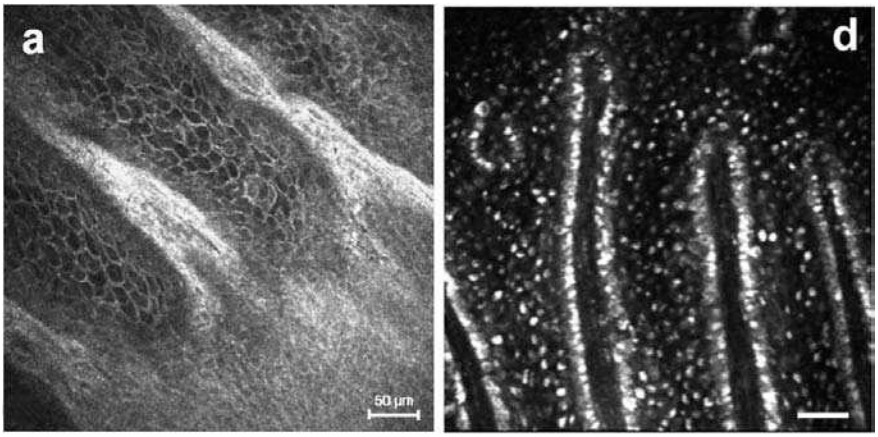

Figure 1-11: IVCM images of the limbal epithelium in normal cornea showing hyper-reflective cells on the palisades (a) alternating with darker corneal epithelium of the rete pegs. In pigmented subjects hyper-reflective dots were seen in the palisade basal cells in addition to those in the rete pegs. (a reproduced from Messmer et al 2006, b reproduced from Patel et al 2006).

Within the bulbar conjunctiva the superficial cells were hyper-reflective with bright nuclei while the middle and basal cells were smaller and

darker with well-demarcated borders and hardly visible nuclei compared to superficial cells (Messmer et al., 2006b, Efron et al., 2009) (Figure 1-12).

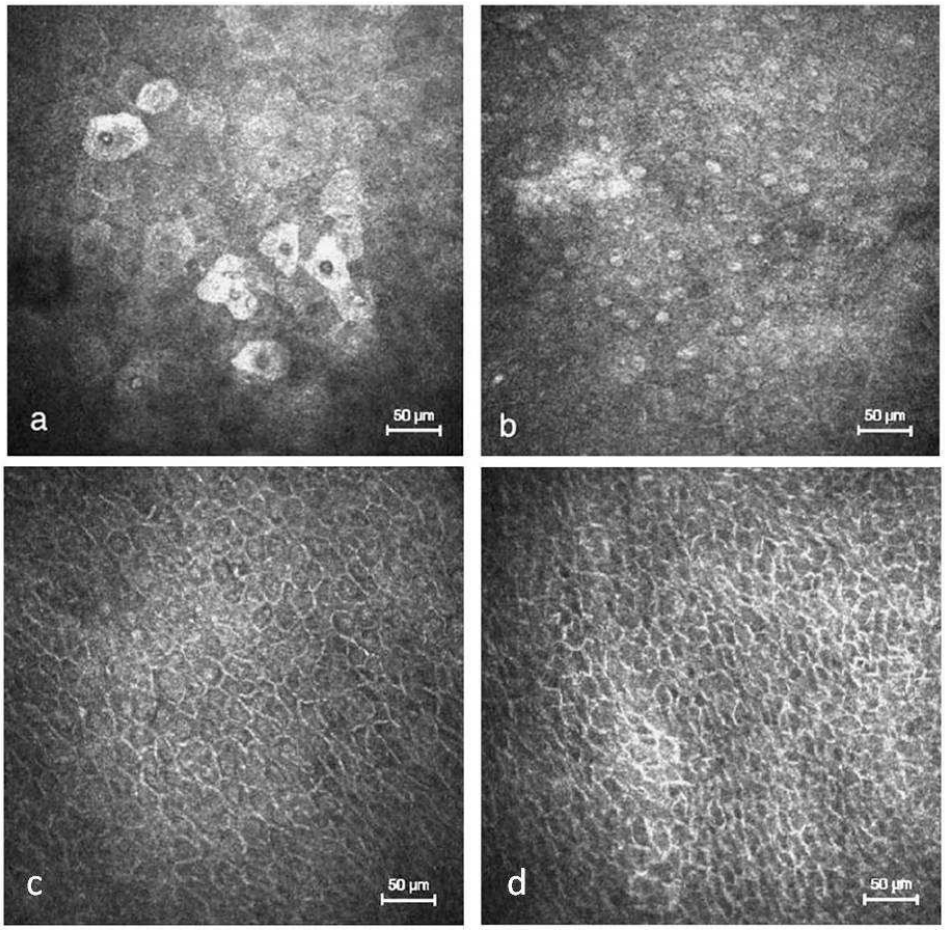

Figure 1-12: IVCM images of the epithelium in normal bulbar conjunctiva showing desquamating superficial cells (a), superficial cells with bright nuclei and ill-defined borders(b), middle layer cells (c), and basal cells (d). (reproduced from Messmer et al 2006).

Goblet cells were visible as roundish figures of moderate hyper-reflectivity compared to the nuclei (De Nicola et al., 2005, Messmer et al., 2006b, Kobayashi et al., 2005) (Figure 1-13A). Cystic changes within the

bulbar conjunctival epithelium as well as Langerhans cell were visible on IVCM (Mastropasqua et al., 2006, Efron et al., 2009) (Figure 1-13 B & C).

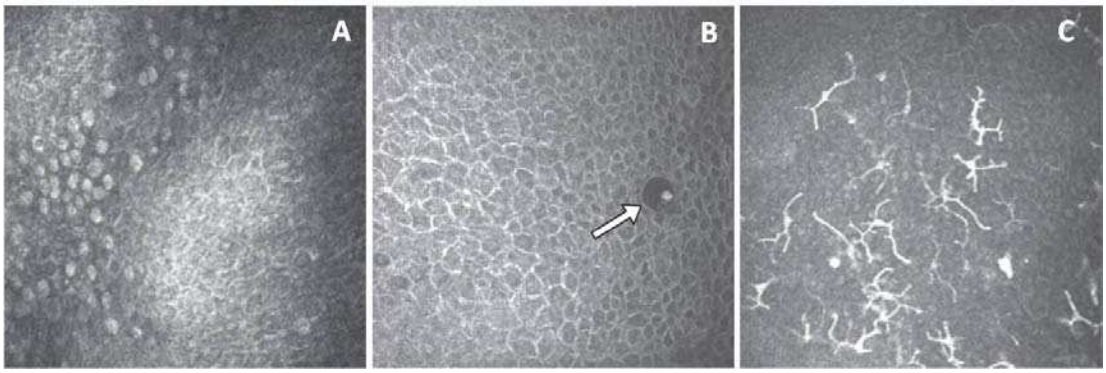

Figure 1-13: IVCM images of normal bulbar conjunctiva showing goblet cells (A), cystic changes (B) and Langerhan cells (C). (reproduced from Efron et al., 2009).

1.7.3 IVCM in Refractive surgery

CM has been used to investigate corneas pre and post LASIK, PRK and Keratoplasty as regard to corneal re-innervation, keratocyte density, postoperative haze as well as postoperative changes in various corneal layers (Buhren et al., 2001, Bragheeth and Dua, 2005, Calvillo et al., 2004, Dawson et al., 2005, Erie et al., 2005, Erie et al., 2003, Erie et al., 2002b, Grupcheva et al., 2001c, Hollingsworth et al., 2006, Kaufman et al., 2004, Lee et al., 2002, Linna et al., 2000, Moilanen et al., 2003, Moller-Pedersen et al., 2000, Moller-Pedersen et al., 1998, Pisella et al., 2001, Timo Tervo and Moilanen, 2003, Vesaluoma et al., 2000, Bragheeth, 2004, Mitooka et al., 2002, Buhren and Kohnen, 2003). Some of these findings can be summarised as follows:

1. Sub- basal Nerve plexus density was found to recover to near normal preoperative values in 2years and 5years following PRK and LASIK respectively (Erie et al., 2005). However this morphologic recovery of sub-basal nerves appeared to be slower than the recovery of corneal sensation even after long term evaluation suggesting a degree of redundancy in the existing nerves (Bragheeth and Dua, 2005, Calvillo et al., 2004, Erie et al., 2005, Erie, 2003).
2. Keratocyte density remained below preoperative values within the anterior 10% of stroma even 3 years following PRK and LASIK (Erie, 2003, Bragheeth, 2004, Erie et al., 2003, Mitooka et al., 2002). IVCM was able to visualise activated keratocytes with hyper-reflective cell processes within the anterior stroma (Figure 1-14) in the first postoperative month (Bragheeth, 2004, Erie, 2003, Erie et al., 2003, Buhren and Kohnen, 2003, Sonigo et al., 2006).
3. Flap Interface: Interspersed high and low reflective particles were noticed nearly in all cases of LASIK, not seen preoperatively (Bragheeth, 2004), similar to those found in contact lens wearers (Masters and Bohnke, 2001b). Low reflective particles decreased over time while highly reflective particles remained constant (Perez-Gomez and Efron, 2003, Bragheeth, 2004).

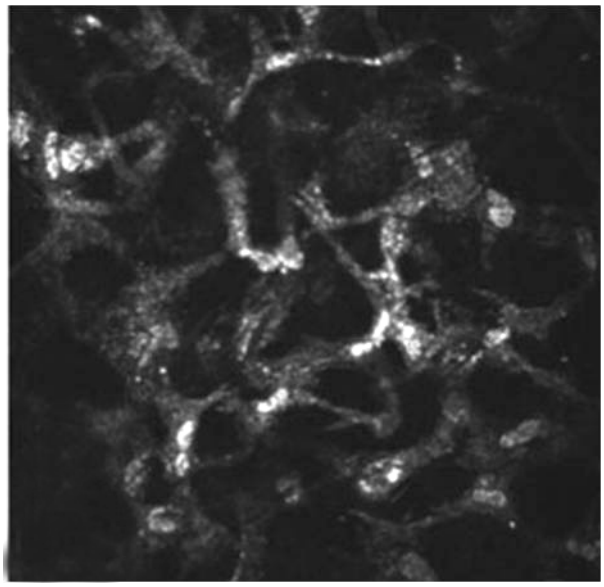

Figure 1-14: IVCM en face image showing activated keratocytes with increased reflectivity and visible cytoplasmic processes following LASIK. (reproduced from Sonigo et al., 2006)

1.7.4 IVCM of corneal nerves in diabetic patients:

Rosenberg et al found significantly reduced sub-basal nerve density in all patients with diabetic neuropathy compared to normal controls (Rosenberg et al., 2000a). However corneal sensation was only reduced in severe neuropathy. They concluded that IVCM appeared to detect the beginning neuropathy earlier than measuring corneal mechanical sensitivity. Similar results were published by Malik et al 3 years later with a general conclusion that IVCM would offer a rapid, non-invasive and reiterative imaging technique to quantify corneal nerve changes as well as assessing the response to certain topically applied therapies deemed to be beneficial for somatic human diabetic neuropathy (Malik et al., 2003). Kallinikos et al stressed that corneal nerve tortuosity as observed by

IVCM was significantly more severe in patients with severe diabetic neuropathy compared to those with mild to moderate neuropathy, a feature that may reflect an alteration in the degree of nerve degeneration and regeneration in diabetes mellitus (Kallinikos et al., 2004).

1.7.5 IVCM in Microbial Keratitis

1.7.5.1 Acanthamoeba Keratitis

IVCM offers a rapid and accurate non-invasive clinical method for diagnosing Acanthamoeba keratitis as well as assessing the efficacy of topical applications used for its treatment (Cavanagh et al., 2000, Mathers et al., 1996, Parmar et al., 2006).

The cystic forms appear as round double- walled hyper-reflective objects about 10 – 25µm in diameter (figure15) seen at the level of epithelium and anterior stroma (Kaufman et al., 2004, Mathers et al., 1996, Parmar et al., 2006, Winchester et al., 1995). The tophozoites show more elongated less bright figures (Cavanagh et al., 2000).

Mathers et al identified 43 patients who had keratitis and positive epithelial biopsy for Acanthamoeba with acridine orange staining. Thirty-six (84%) of these patients showed highly refractile ovoid bodies typical of Acanthamoeba cysts by tandem scanning confocal microscopy (TSCM) (Mathers et al., 1996). More recently Parmer et al performed IVCM in 63 cases of suspected AK. In 54 cases (85.7%) cysts were detected and all

of them showed a favourable response to treatment (Parmar et al., 2006). However, the yield of positive cultures in their study was relatively low (9/29 [31%]), whereas the yield of positive corneal biopsy was only 50% (2/4). The rapidity of diagnosis with the relative ease of use and non-invasive nature of in vivo confocal microscopy are clearly advantageous features when compared with traditional laboratory techniques which all rely on blind invasive sampling of the cornea and are associated with a subsequent delay in the culture result (Parmar et al., 2006, Mathers et al., 1996, Kaufman et al., 2004).

It's worth mentioning the superior quality of IVCM images taken by HRT II RCM compared to TSCM as regard to detailed features of Acanthamoeba cysts (Figure 1-9).

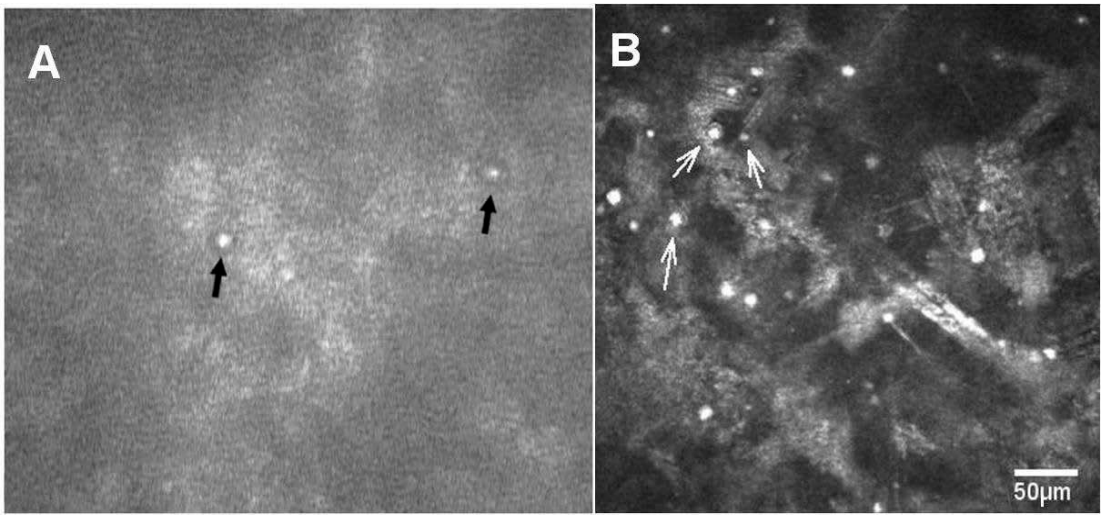

Figure 1-15: Acanthamoeba cysts in IVCM images taken with TSCM in A (black arrows) and with HRT II RCM in B (white arrows). (A reproduced from Parmar et al 2006, image width = 400µm).

1.7.5.2 Fungal Keratitis

This is a serious potentially blinding condition that can be induced by corneal infection with filamentous fungal species like *Aspergillus fumigatus* and *Fusarium solani* or spor forming *Candida albicans*. IVCM has been successfully used to identify the hyphae in fungal keratitis.

Winchester et al used TSCM to image the corneas in two culture-proven cases of *A fumigatus* keratitis (Winchester et al., 1997). Fungal hyphae were imaged as bright interlocking lines around 6µm wide and 200 to 400 µm long. More recently Brasnu et al published similar results in 4 corneas infected with *F solani* that correlated well with culture and smear staining of corneal scrapings (Figure 1-16) (Brasnu et al., 2007). The investigators concluded that IVCM can be applied to establish early diagnosis even before culture results that are associated with low positive yield and long delay.

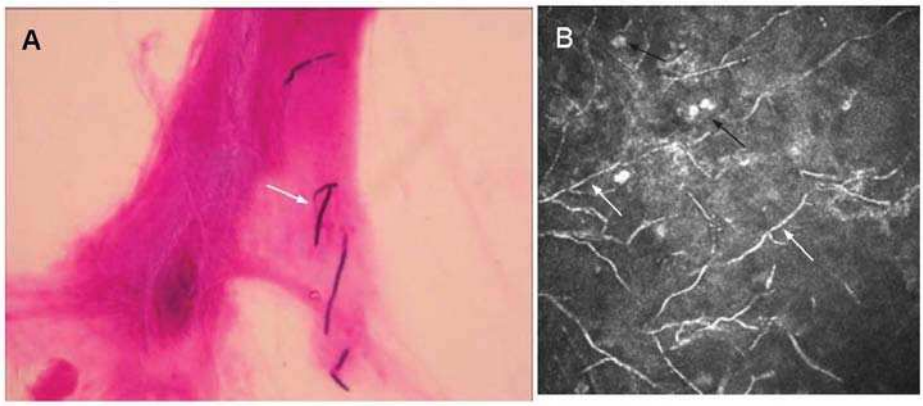

Figure 1-16: Microscopic findings in F solani – infected cornea. A, light micrograph of corneal smear showing hyphae (arrow) (Gram stain; 400x magnification). B, IVCM 400x400µm image of F solani – infected cornea showing high-contrast bright linear structures resembling the fungal hyphae (white arrows) with inflammatory cells (black arrows). (reproduced from Brasnu et al 2007).

1.7.6 IVCM in Corneal Dystrophies

Corneal dystrophies are genetically inherited disorders affecting various corneal layers resulting in progressive loss of corneal clarity in the majority of cases. Over the last two decades, an exponential increase in the field of molecular genetics has allowed elucidation of many chromosomal defects linked to such corneal disorders (Vincent et al., 2005). This is particularly important as inherited corneal diseases typically affect those of working age for whom the support and rehabilitation contributes to a significant social and economic cost (Vincent et al., 2005). Over the past decade many investigators were interested in describing the IVCM features of different types of these dystrophies with the possibility of correlating these findings with histological sections obtained following keratoplasty. The following conditions have been well investigated with IVCM:

1.7.6.1 Epithelial Basement Membrane Dystrophy (EBMD) (Cogan's Dystrophy, Map – Dot – Fingerprint):

This dominantly inherited corneal dystrophy is characterized histologically by an anomalous basement membrane within the epithelial layers associated with intraepithelial microcysts as well as abnormalities of epithelial cell morphology (Laibson, 1976, Labbé et al., 2006).

IVCM features in EBMD have been described in previous studies as ridges, curved linear structures and cyst-like formations all within epithelial layers (Bohnke and Masters, 1999, Hernandez-Quintela et al., 1998, Rosenberg et al., 2000b). Recently Labbe et al published the changes seen in EBMD nicely visualised with HRT II RCM (Labbé et al., 2006) . Folds of thickened epithelial basement membrane were illustrated as bright lines (Figure 1-17a) running through epithelial layers in oblique views (Figure 1-17 b & c) as well as ring-like structures at the basal epithelium (Figure 1-17d). Microcysts were visualised as bright round figures ranging in size from 400µm down to the size of a single cell (Figure 1-17e). Epithelial cells with irregular borders in association with basement membrane abnormalities were reported as well (Figure 1-17f).

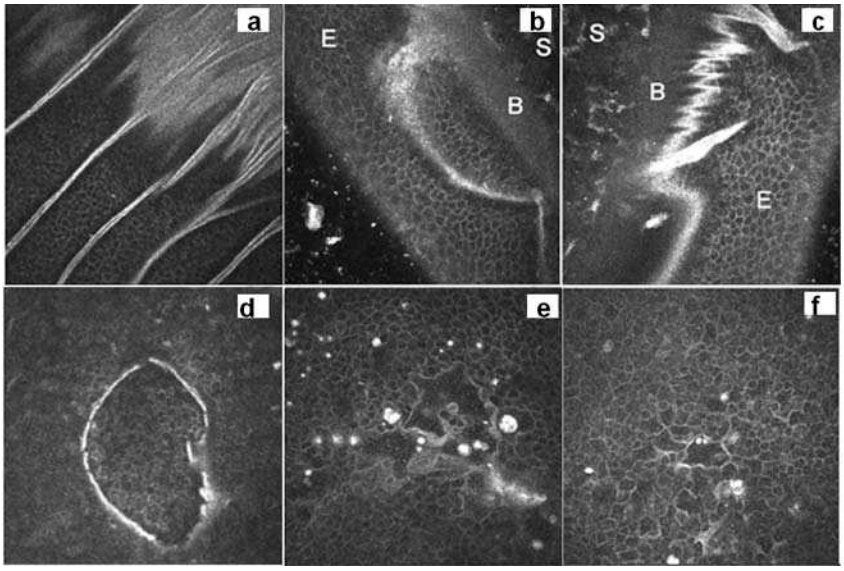

Figure 1-17: IVCM images in epithelial basement membrane dystrophy (EBMD) showing thickened basement membrane folds seen as bright lines on en face view (a), sharp insinuations within epithelial layers in oblique view (b & c) or ring-like structures at the level of basal epithelium (d). Microcysts appear as bright round structures of variable sizes (e) associated with cells of irregular borders. (images are 400x400µm, reproduced from Bransu et al 2007).

1.7.6.2 Meesmann's Dystrophy (MCD):

This corneal dystrophy is inherited as an autosomal dominant trait with incomplete penetrance that manifests in the first decade of life with multiple bilateral corneal intraepithelial cystic lesions. The condition is usually asymptomatic until recurrent corneal erosions develop from ruptured cysts. On IVCM these microcystic lesions were identified by some investigators as round or oval hyporeflective areas within the basal epithelium ranging between 5 – 145µm in diameter with occasional bright material seen within these lesions (Figure 1-18) (Patel et al., 2005a). The surrounding epithelium as well as the rest of corneal layers showed normal patterns on IVCM.

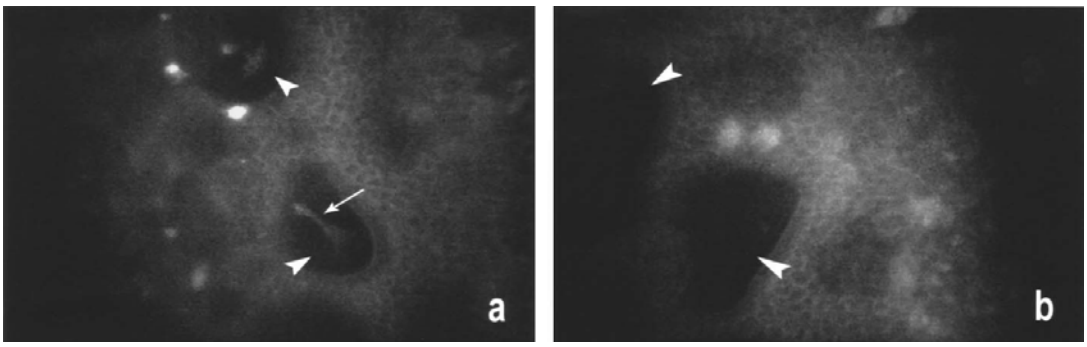

Figure 1-18: IVCM in Meesmann's corneal dystrophy. Multiple dark round and oval areas are seen at the level of middle and basal epithelium (arrowheads) measuring 67x106µm in (a) and 87x145µm in (b). Hyper-reflective material can be seen in some lesions (arrow). Frame size 340x255µm. (reproduced from Patel et al., 2005a).

.

1.7.6.3 Corneal Dystrophy of Bowman's Zone (CDB):

In corneal dystrophy of Bowman's zone (CDB) 2 types have been identified histologically: Reis-Bucklers' (CDBI) and Thiel-Behnke's (CDBII)

dystrophy (Kuchle et al., 1995, Ridgway et al., 2000). The first type is associated with earlier onset of visual impairment, usually in the second decade of life, along with epithelial irregularity and geographical opacities / deposits at the level of Bowman's zone seen on slitlamp examination. The second type presents with later onset of visual impairment with a honeycomb-shaped opacities at the level of Bowmans zone (Kuchle et al., 1995, Ridgway et al., 2000).

These opacities are confined to the central and mid-peripheral cornea whereas the extreme periphery almost always remains transparent. They gradually increase to become more diffuse and uniform in appearance, with corneal epithelial erosions commencing at an early age (Vincent et al., 2005). Histology shows a dystrophic Bowman's layer with the accumulation of granular deposits in (CDBI) and fibrocellular material in (CDBII), that may extend into the anterior stroma (Kuchle et al., 1995, Ridgway et al., 2000).

Kobayashi & Sugiyama (2007) published quality IVCM images of corneas with Reis-Bucklers' (CDBI) and Thiel-Behnke's (CDBII) dystrophy (Kobayashi and Sugiyama, 2007). Highly reflective granular deposits in CDBI (Figure 1-19A) and homogenous moderately reflective material in CDBII (Figure 1-19B) were seen at the level of Bowman's zone using HRTII-RCM confocal microscope.

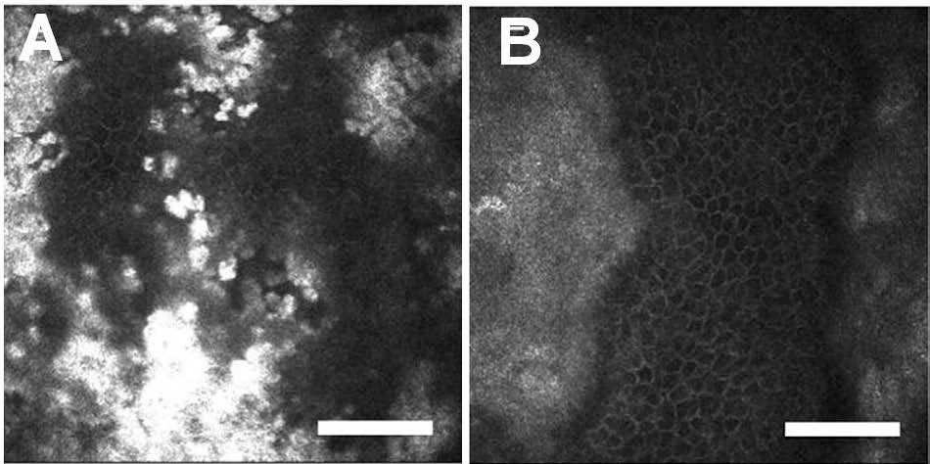

Figure 1-19: IVCM en face images of corneas with Bowman's zone dystrophy. (A) shows hyper-reflective granular deposits in Reis-Bucklers' dystrophy (CDBI) while (B) presents homogenous reflective material in Thiel-Behnke's (CDBII) dystrophy all seen at the level of Bowman's zone. Scale bar 100µm. (reproduced from Kobayashi & Sugiyama 2007).

1.7.6.4 Lattice Dystrophy type I:

In lattice dystrophy deposits of amyloid material are localised within subepithelial and stromal layers presenting clinically as filamentous branching opacities (Rodrigues and Krachmer, 1988).

This dystrophy manifests in the first or second decade of life with the appearance of double contour linear refractile branching deposits within the anterior stroma, usually confined to the central cornea, leaving a clear periphery (Vincent et al., 2005). IVCM images showed hyper-reflective linear branching deposits at subepithelial level (Figure 1-20A) as well as anterior and mid stromal layers (Figure 1-20B) , 50 – 100µm wide, representing the lattice lines visible on slit lamp biomicroscopy (Chiou et al., 1999a, Rosenberg et al., 2001, Kobayashi et al., 2007) .

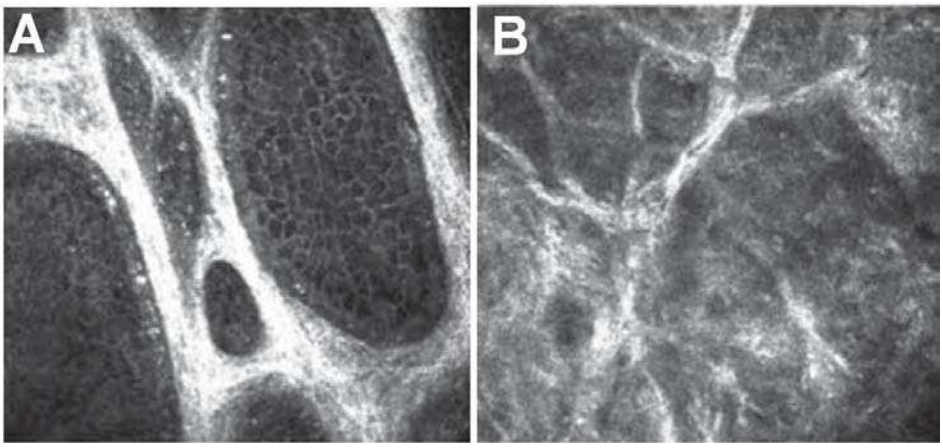

Figure 1-20: IVCM en face images in Lattice corneal dystrophy. Hyper-reflective linear branching deposits are visualised at subepithelial level in (A) and within anterior stroma in (B). Images are 400x400µm. (reproduced from Kobayashi et al 2007).

1.7.6.5 Granular Dystrophy type 1:

Granular corneal dystrophy is an autosomal dominant disorder characterised by the accumulation of circumscribed discrete breadcrumb like opacities within the central corneal anterior stroma sparing the periphery (Rodrigues and Krachmer, 1988) (Figure 1-21A). These corneal changes manifest within the first decade of life without visual symptoms. The intervening stroma remains clear but later in life accumulates the granular deposits. Superficial stromal deposits result in epithelial irregularity with painful episodes of recurrent corneal erosion (Rodrigues and Krachmer, 1988). Histologically the dystrophic “hyaline” material is eosinophilic on light microscopy and electron-dens on electron microscopy (Rodrigues and Krachmer, 1988). IVCM images show intensely hyper-reflective areas in mid-epithelial layers, Bowman’s zone, anterior and mid- stroma (Werner et al., 1999a, Vincent et al., 2005) (Figure 1-21B).

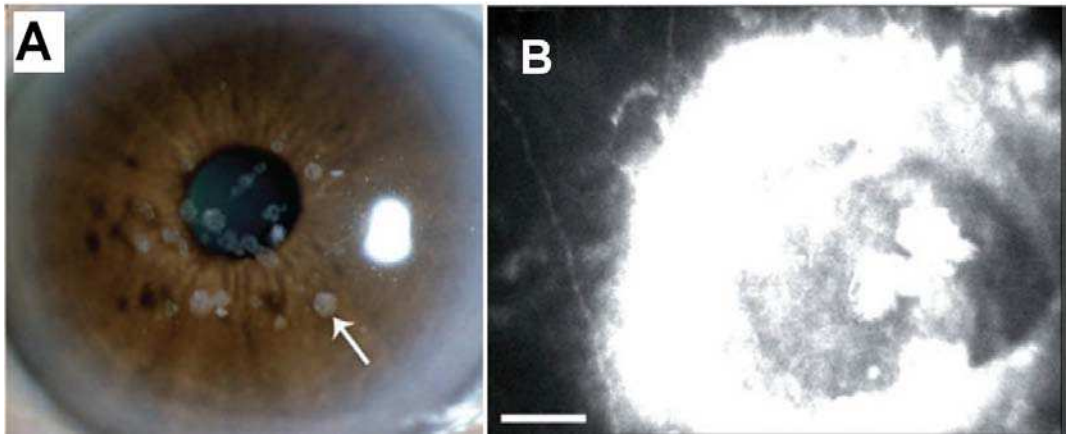

Figure 1-21: Granular corneal dystrophy. A, diffuse slitlamp photograph of showing central breadcrumb like deposits. B, IVCM image shows hyper-reflective deposits within anterior stroma. Scale bar 50µm. (reproduced from Vincent et al., 2005).

1.7.6.6 Central Crystalline Dystrophy of Schnyder:

This autosomal dominant corneal dystrophy involves deposition of cholesterol or lipid material in the central and peripheral stroma (Vesaluoma et al., 1999, Ciancaglini et al., 2001a). It primarily presents with a central discoid opacity just posterior to Bowman's zone in the anterior stroma. The opacity consists of small, needle-shaped refractile crystals that are either white or polychromatic and have the appearance of 'glass wool' (Figure 1-22 A). These deposits may extend irregularly into deeper layers, but the epithelium and corneal sensitivity are normal (Vincent et al., 2005). IVCM illustrates the presence of highly reflective needle-like deposits in the subepithelial and anterior stromal layers (Figure 1-22 B), as well as absence of subepithelial nerve plexus especially in adult patients (Vesaluoma et al., 1999). The extracellular matrix showed increased reflectivity that was enough to impair good

visualisation of deeper stromal keratocytes and endothelium (Vesaluoma et al., 1999, Ciancaglini et al., 2001a).

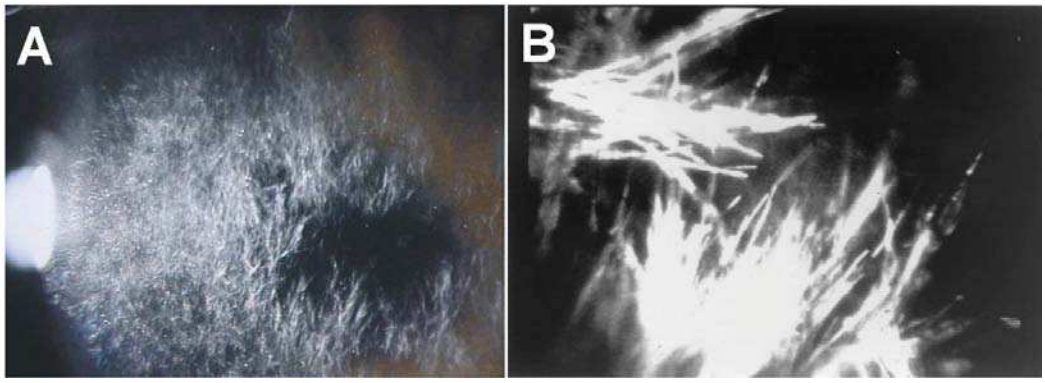

Figure 1-22: Central Crystalline dystrophy of Schnyder. A, slitlamp photograph of corneal deposits. B, IVCM shows highly refractile needle like crystals in the anterior stroma. (IVCM objective 40x. A & B reproduced from Ciancaglini et al., 2001)

1.7.6.7 Fuchs Endothelial Dystrophy (FED):

FED is the most common primary disorder of the corneal endothelium inherited as an autosomal dominant and sporadic disorder. Clinical onset usually occurs over the age of 40, with wart-like excrescences (or guttae) of Descemet's membrane visible in the central cornea. The endothelial cells show polymegathism (reduced numbers with irregular shapes) associated with abnormal thickening of Descemet's membrane due to deposition of excessive collagen , which gives a beaten metal appearance on slit-lamp examination (Bergmanson et al., 1999). The gradual compromise in function can lead to corneal oedema which may present as bullous keratopathy with resultant painful vision loss.

Mustonen et al published a detailed description of IVCM features in FED cases (Mustonen et al., 1998a). Intra-epithelial bullae 5 – 50 µm in diameter were seen as well as anterior stromal lacunae , 7 – 70 µm in diameter observed immediately below Bowman's zone (Figure 1-23 A). The corneal guttae appear as multiple round hypo-reflective areas, 20 – 40 µm in diameter, with bright 5 – 10 µm centres scattered at the level of endothelium described as Strawberry-like changes (Vincent et al., 2005, Mustonen et al., 1998a) (Figure 1-23 B). When they were visible on IVCM the endothelial cells showed polymorphism and polymegathism (Chiou et al., 1999b, Vincent et al., 2005).

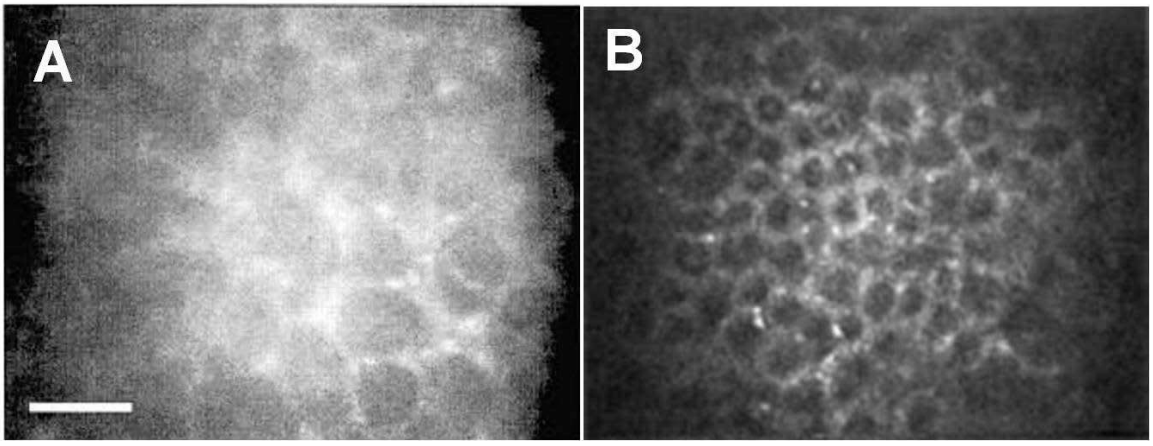

Figure 1-23: Fuch's Endothelial corneal dystrophy on IVCM. A, anterior stromal lacunae (scale bar 50µm). B, IVCM at the level of endothelium shows dark round figures with bright centres representing the guttae of Descemets membrane (magnification 210x). (A reproduced from Mustonen et al., 1998a. B reproduced from Chiou et al., 1999b)

1.7.6.8 Posterior Polymorphous Endothelial Dystrophy (PPD):

Clinically, PPD is characterized by the presence of endothelial lesions, which have been classified into three main forms: vesicular, band and diffuse. Vesicles appear as endothelial blisters or blebs on slit-lamp examination and these may be isolated or form clusters of curvilinear patterns often associated with corneal oedema (Vincent et al., 2005, Grupcheva et al., 2001a). IVCM in PPD was best described by Patel et al (2005) where dark round and oval areas were seen at the level of endothelium with occasional clusters of dark and bright bodies (Figure 1-24) (Patel et al., 2005b)

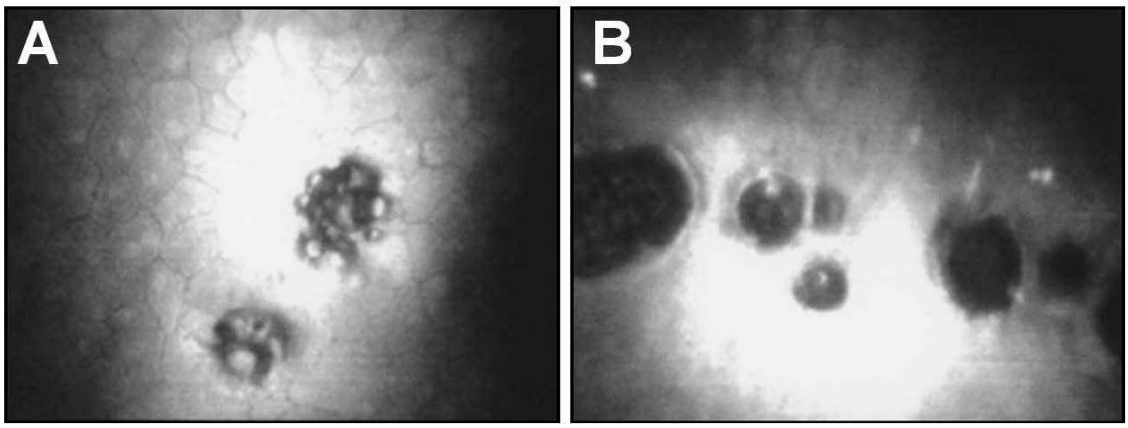

Figure 1-24: IVCM in Posterior Polymorphous Dystrophy (PPD). A, cluster of dark and bright bodies at the level of endothelium. B, dark round and oval areas at the level of endothelium. (frames 340x 255µm. Reproduced from Patel et al., 2005).

1.7.7 Iridocorneal Endothelial Syndrome:

Iridocorneal endothelial syndrome (ICE) involves a spectrum of disorders that includes Cogan–Reese syndrome, Chandler's syndrome and essential iris atrophy that do not always present with clear clinical features. ICE is most commonly unilateral and progressive with no identifiable pattern of inheritance but exhibiting a female predominance. The main clinical features of the syndrome are varying degrees of corneal endothelial abnormality, iris atrophy and secondary glaucoma (Grupcheva et al., 2004). Progressive corneal oedema usually results in significant drop of vision. IVCM revealed epithelial-like changes of endothelial cells, namely bright prominent nuclei with irregular ill-defined cell borders (Figure 1-25 A&B) (Grupcheva et al., 2004, Chiou et al., 1999c).

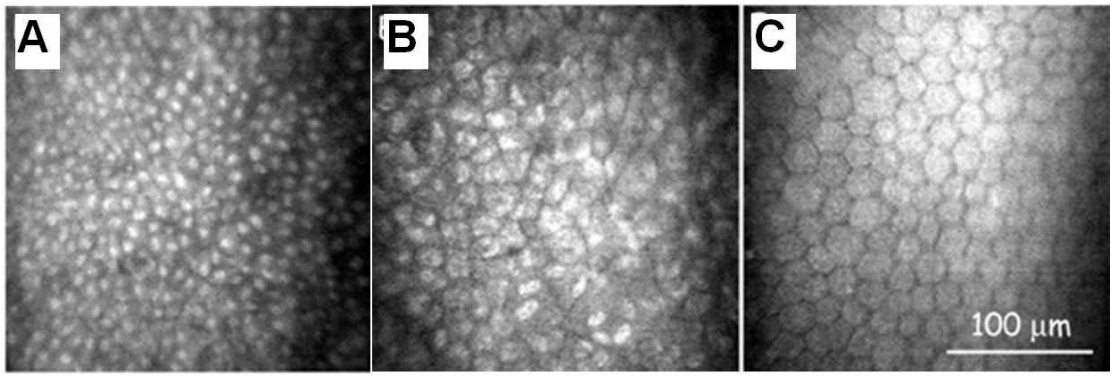

Figure 1-25: IVCM in Iridocorneal Endothelial syndrome. Bright nuclei are seen within ill-defined endothelial cells in (A) and within irregular endothelial cells in (B). Normal endothelial pattern is represented in (C). (reproduced from Grupcheva et al., 2004)

1.7.8 IVCM in Keratoconus:

Keratoconus is a progressive, asymmetric, non-inflammatory corneal deformity characterized by an axial corneal ectasia, leading to irregular astigmatism and myopia. IVCM has been use to investigate microstructural changes including keratocyte and corneal nerve densities in keratoconic corneas (Erie et al., 2002a, Hollingsworth et al., 2005b, Weed et al., 2006). Changes in the epithelium included larger cell size in all three layers with reduction in basal cell density (Hollingsworth et al., 2005b). Hollingsworth et al reported a reduced density of anterior and posterior keratocytes (Hollingsworth et al., 2005b) that was recently found to be increased in the work of Weed et al (Weed et al., 2006), a deference that was explained by the latter group to be due to the area scanned by IVCM [central cornea (Hollingsworth et al., 2005b) vs corneal apex (Weed et al., 2006)]. Corneal sub-basal nerve plexus was recently investigated by Patel and McGhee (Patel and McGhee, 2006) who reported significantly lower nerve density in keratoconic (10,478 +/- 2,188um/mm^2) compared to normal corneas (21,668 +/- 1,411um/mm^2). Stromal folds have been illustrated with IVCM as alternate dark and bright bands throughout stromal layers (Ucakhan et al., 2006, Efron and Hollingsworth, 2008).

1.8 IMPORTANCE OF THIS STUDY

In the majority of IVCM literature there has been limited consideration to correlate histopathological with confocal microscopic details for the same tissue samples. In fact the number of published articles illustrating correlative light and in vivo confocal microscopic findings is limited to 4 (Hollingsworth et al., 2005a, Brasnu et al., 2007, Kobayashi and Sugiyama, 2007, Messmer et al., 2006a). The lack of this kind of research work has lead to speculative interpretation of IVCM patterns and details in a significant number of publications in a way that lead to poor enthusiasm among the majority of eye clinicians to rely on this imaging modality in clinical practice. Based on this fact we believe that our study to establish reasonable correlation between IVCM and histopathology will achieve the following:

1. Appropriate and scientific interpretation of IVCM features in various corneal disorders that helps clinicians towards better understanding of IVCM illustrations.
2. Reliable diagnostic criteria with IVCM that supports other investigative facilities to establish proper diagnosis as well as quantitative evaluation of different corneal and ocular surface disorders.

Chapter Two

2 Materials and Methods

2.1 RECRUITMENT & INCLUSION CRITERIA:

Patients who routinely attend the cornea clinic at Nottingham University Hospitals, Queens Medical centre, Nottingham, UK, have been selected according to the nature of their corneal and ocular surface pathology. Those who were deemed appropriate for undergoing corneal transplantation for the treatment of their condition or undergoing corneal or conjunctival biopsy for diagnostic purposes were recruited in the study as well as those who were managed conservatively.

This project was approved by the local ethics research committee (reference number 06/Q2403/46) and the Research and Development department of Nottingham University Hospitals NHS Trust (reference number 07/H0403/140). Informed, written consent was obtained from all patients.

2.2 ANTERIOR SEGMENT PHOTOGRAPHY:

Diffuse slitlamp photographs were taken to illustrate the majority of corneal and ocular surface disorders included in this study. Anterior

segment camera from Topcon has been used to obtain corneal photos with and without fluorescein staining.

2.3 IN VIVO CONFOCAL MICROSCOPY (IVCM)

2.3.1 Technical Features of Rostock Cornea Module (RCM):

Each patient was examined with HRTII-Rostock Cornea Module (HRTII-RCM) (Heidelberg engineering GmbH, Heidelberg, Germany). Rostock Cornea Module (RCM) is the true confocal microscope that is designed to work in conjunction with Heidelberg Retina Tomogram II (HRTII). We refer to the combination by the abbreviation (HRTII-RCM) (Figure 2-1).

Figure 2-1: HRT II and RCM set up for in vivo confocal microscopy

A small light weight charge-coupled device camera mounted on a side arm furnishes a lateral view of the eye and the objective lens to help

adjusting the position of the eye with the objective lens and the illuminating laser beam (figure 23). It produces 640 x 480pixels colour images at a rate of 15 frames per second.

Figure 2-2: HRTII-RCM with side-mounted digital camera. A, overall view. B, display view on the screen shows alignment of the cornea with the objective and illuminating beam.

Other technical specifications include:

1. Light source: Class I Diod laser 670nm wavelength
2. Objective Lens: 63X water immersion, Numerical Aperture 0.95.
3. Magnification on screen: 300X
4. Image size: 384 x 384pixels equivalent to 400 X 400 um
5. Optical resolution: Lateral 2um, depth 4um.
6. Digital Transverse resolution: approximately 1um/pixel
7. Image Acquisition time 24msec.

2.3.2 Steps of IVCM scanning

In vivo confocal microscopy was carried out as an outpatient procedure under topical anaesthesia with Minims Oxybuprocaine Hydrochloride 0.4% (Chauvin Pharmaceuticals Ltd, UK). The microscope objective is covered with a sterile PMMA cap (tomocap) the surface of which comes in gentle touch with the patient's corneal surface. A drop of thick viscous 0.2% polyacrylic gel (Viscotears Liquid gel, Novartis pharmaceuticals UK Ltd) serves as coupling medium between the contact cap and objective of the LSCM.

The patient sits at the equipment with the chin on a rest and the forehead pressed against a band. The IVCM scanning is started at the central 3-4mm of the cornea then moved across to the superior, inferior, temporal and nasal quadrants. This dynamic scanning is guided by a side mounted digital camera attached to HRTII-RCM the view of which is displayed next to IVCM view on the screen to help ascertain the location of the cornea being scanned (Figure 2-3). Images were captured at each point through the thickness of the cornea, giving a total number of 300-500 frames per cornea. For qualitative analysis of pathological findings 6-10 images for each layer were analysed to avoid inclusion of artefacts or chance findings. When corneal grafting was done, the tissue was marked for the 12 O'clock position so that histological examination could be carried out specifically in the quadrant of interest. Each examination may take 5 to 15 minutes depending on patient's cooperation, however intervening

periods of rest may be needed should the patient feel any discomfort. A repeat examination was undertaken in certain cases to evaluate the tissue changes in response to topical treatment or surgical procedures.

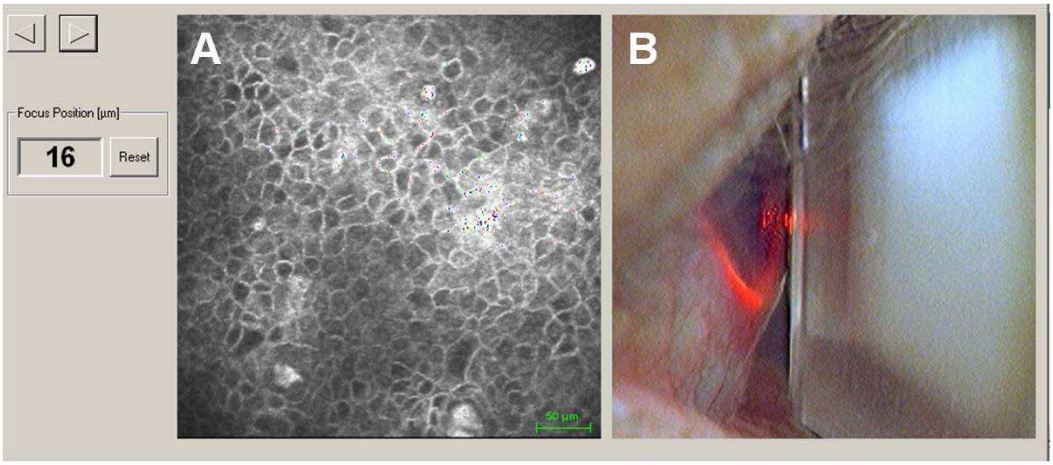

Figure 2-3: On-screen display of IVCM image (A) and view of the side mounted digital camera (B) in HRTII-RCM confocal microscope. The left-side figure indicates the focal plane depth in micrometers.

2.4 HISTOPATHOLOGY

2.4.1 Procedures for tissue sampling:

All excised tissue samples/buttons were routinely subjected to histological examination. Tissue samples were obtained though one of the following procedures:

1. Exicisional or diagnostic biopsy in ocular surface lesions.
2. Penetrating keratoplasty (PK) for full thickness corneal buttons or Deep Anterior Lamellar Keratoplasty (DALK) for partial thickness corneal samples.

3. Alcohol delamination: in this method 20% ethanol was applied to the central 6mm of the dysplastic corneal epithelium for 40 seconds using an optical zone marker (Bausch & Lomb, Kingston-upon-Thames, Surrey, UK). The alcohol was then drained from the well with a surgical sponge (K-Sponge-Katena Products, Denville, New Jersey, USA) and the surface washed with saline solution before peeling off the loosened epithelium. Biopsy specimens were floated on a few drops of saline placed on non absorbent paper and unfolded with fine forceps by gentle stroking. The saline was absorbed with a K-sponge such that the epithelial sheet lay flat on the paper. The sheet was then covered with a few drops of 10% formalin and kept covered for 15 - 20 minutes before transferring to a formalin pot for transfer to the laboratory.

2.4.2 Light Microscopy:

Tissue samples were fixed with 10% formalin then embedded in resin or wax blocks to obtain cross-sections of 5µm for Heamatoxylin & Eosin (H&E) and 1µm for toluidine blue staining for light microscopic examination. Alcian blue stain was used in full thickness corneal samples from 2 cases clinically diagnosed with macular corneal dystrophy. Slides were viewed with the Nanozoomer Digital Pathology System (NDP C9600 series, Hamamatsu Photoincs K.K. Hamamatsu city, Japan). This scanning machine delivers automated high throughput scanning with excellent

image quality through virtual microscopy to yield high resolution whole-slide images. These images are then viewed in digital format at various magnifications on a computer or over a network. Hamamatsu NDP viewer (Hamamatsu Photonics, Hamamatsu City, Japan) is the principal software program provided by the manufacturer of the NanoZoomer digital pathology microscope to serve slide viewing at various magnifications, provision of images for the region of interest with scale bars as well as performing reliable cell morphometry measurements.

2.4.3 Electron microscopy

Tissue samples were prepared for transmission electron microscopy (TEM) following standard procedures. Briefly, samples were fixed in 2.5% glutaraldehyde (in 0.1 mol/l cacodylate buffer, pH 7.4) for 16 to 24 hours. Each sample was then cut into 1-mm–wide slices and washed in cacodylate buffer, followed by secondary fixation in 1% osmium tetroxide for 1 hour. The tissue samples were then processed by dehydration in ascending concentrations of ethanol followed by acetone before infiltration and embedding in TER resin (TAAB Laboratories, London, UK). The orientated embedded blocks were polymerized at 60℃ for 16 hours before cutting 0.5µm sections using an ultramicrotome (Leica Microsystems Ltd, Milton Keynes, UK). Suitable areas for TEM were then selected from 0.5-µm toluidine blue-stained sections. After trimming, 80-nm sections were cut and mounted on copper grids before double staining

with uranyl acetate and lead citrate. A JEOL transmission electron microscope (JEOL 1010, Welwyn Garden City, UK) was used to examine the prepared sections.

2.5 IMAGE ANALYSIS & PROCESSING:

2.5.1 Heidelberg Eye Explorer

Heidelberg eye explorer (version 1.5.10.0; Heidelberg Engineering, Heidelberg, Germany) is the driver software of HRT-II-RCM confocal microscope. Through this program the images are directly digitized and stored into PC hard drive. It serves the following functions:

1. Section scan which enables single image capture in one focal plane
2. Volume scan: This mode functions through an automated scan over 60µm of corneal thickness in 4seconds. A total of 30 images are captured in 4seconds, one every 2microns.
3. Sequence Scan: This function captures 100 frames in 10 seconds each time. The focal plane in this mode can be advanced manually from the epithelium to the endothelium to enable whole corneal thickness scan in one go.
4. Cell density count (cell/mm^2): This is a semi-automated function that could be done on the screen (Figure 2-4).

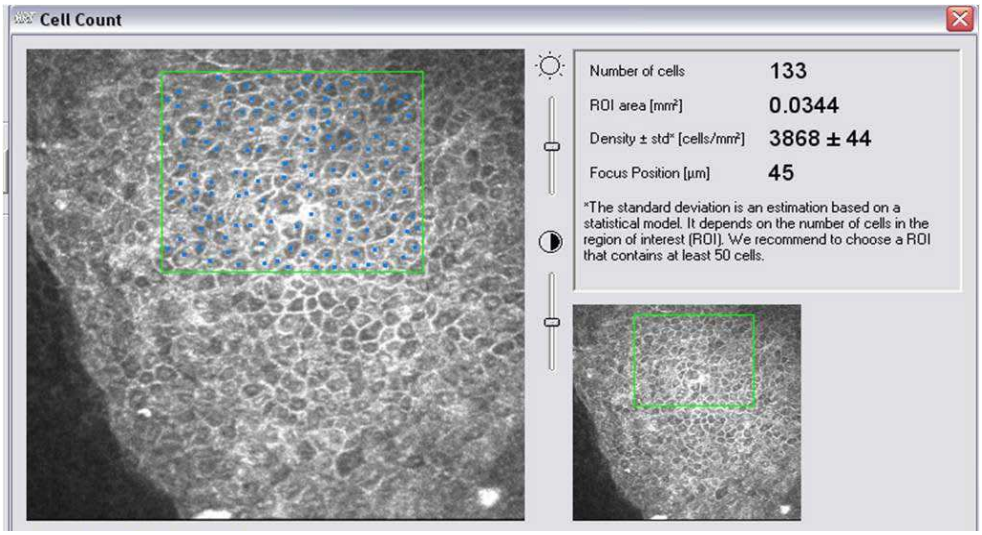

Figure 2-4: Display of cell density count in HRTII-RCM confocal microscope.

For qualitative analysis of pathological findings 6-10 images for each layer were analysed to avoid inclusion of artefacts or chance findings. For quantitative analysis of cell density an average of 3 images for each cornea, excluding duplicates, was analysed through the built-in feature of Heidelberg eye explorer (version 1.5.10.0).

2.5.2 ImageJ:

ImageJ (Version 1.31, Wayne Rasband, Research Services Branch, National Institute of Mental Health, Bethesda, Maryland, USA), is an open-source image processing program that was used in the analysis of IVCM images with provision of reference scale bars. For sub-basal nerve density "NeuronJ" plug-in, developed by Meijering et al, was used with ImageJ to facilitate the tracing and length measurement of sub-basal

corneal nerves in IVCM images semi-manually (Figure 2-5) (Meijering et al., 2004). An average of 3-5 images was chosen in each case.

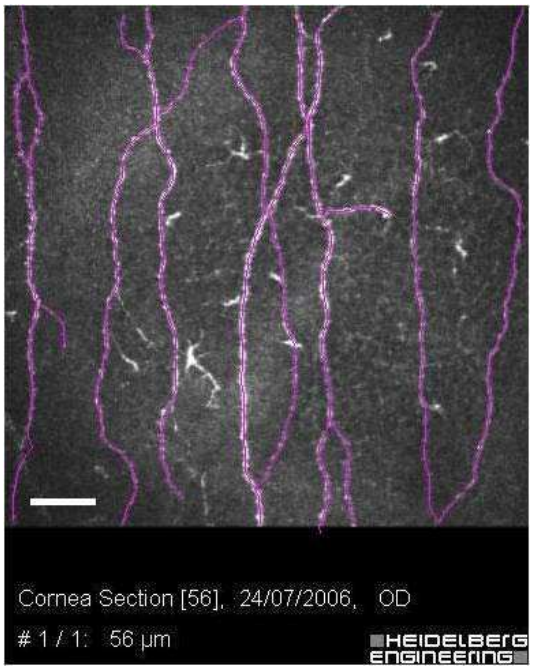

Figure 2-5: An IVCM image shows nerve tracing in NeuronJ to facilitate reliable sub-basal corneal nerve length measurements. ImageJ is used to provide a scale bar of 50µm in each image.

2.5.3 NDP viewer

Hamamatsu NDP viewer (Hamamatsu Photonics, Hamamatsu City, Japan) is the principal software program provided by the manufacturer of the NanoZoomer digital pathology microscope. Main features are mentioned above.

2.6 DATA ANALYSIS

2.6.1 Microsoft excel

Microsoft Excel 2007 (Microsoft Corp., Redmond, WA, USA) was used to compile all the data and to generate descriptive figures.

2.6.2 Statistical Package for Social Sciences (SPSS)

SPSS 16.0 (SPSS, Chicago, IL) was used to perform the statistical analysis. A p value of < 0.05 was taken as the threshold of statistical significance. The Student‟s t-test for independent samples was used to test the difference between two groups of normally distributed data. One way ANOVA with Post Hoc test was used to detect the difference among three or more groups of normally distributed data.

2.7 VALIDATION STRATEGY OF IVCM CORRELATION WITH LIGHT MICROSCOPY:

IVCM provides en face images of cells compared to cross sectional images of tissue histology. The comparison therefore is not like-for-like but as IVCM imaging will always remain predominantly en face and histology will be cross sectional, the comparison is important. It is only by such comparison that some validity can be ascribed to cell morphology revealed on IVCM images. In order to validate the outcomes of correlative

analysis of IVCM and light microscopy (LM) in this study the following principles were carefully considered:

1. **The plane** of the microstructural detail should be the same in both IVCM and LM sections. In IVCM a focal depth indicator in micrometers is shown on each en face image created by HRTII-RCM machine used in this study as well as the characteristic patterns of reflectivity for each corneal layer well known and reported in the literature (see chapter one). Oblique IVCM views, which are partly comparable to LM cross sections, as well as volumetric scanning in (z) axis were also used to determine the exact level of certain tissue details within corneal layers e.g. subepithelial fibroblasts (chapter four) and Bowman's zone breaks (chapter five).
2. The close similarity between various figures seen in IVCM and LM in terms of **shape and size**. In LM the powerful features of the driver software of the Nanozoomer (NDP) were used to perform accurate morphometric measurements in basal nuclei and nucleoli in corneal intraepithelial neoplasia (CIN) and regenerative atypia (chapter three & five), subepithelial fibroblasts in Fuchs endothelial dystrophy (FED) (chapter four) and some Bowman's zone breaks in keratoconus (chapter five). In IVCM each en face frame measures 384x384 pixel corresponding to 400x400µm of transverse resolution based on manufacturer's specifications for HRTII-RCM machine. This pixel/micron ratio was used to create the reference scale bar in each

IVCM image (50µm=48pixel). Since formalin fixation causes negligible shrinkage of tissue, a size comparison, taken in this study can still be appropriate.

3. **Accuracy of location** of pathological changes. The side-mounted digital camera attached to HRTII-RCM machine monitors the exact position of contact of the microscope objective lens with the cornea. By continuously moving the IVCM objective lens over the corneal / ocular surface various areas would be dynamically scanned guided by previous slitlamp features. Lesion borders in cases of corneal intraepithelial neoplasia (CIN) and limbal stem cell deficiency (LSCD) were detected and viewed with the help of dynamic IVCM scanning.
4. **Intracellular changes** detected in LM sections should correlate with similar changes in corresponding IVCM frames. Such changes were carefully studied and correlated in both microscopic modalities in cases of LSCD with Dyskeratosis as well as CIN-related changes in middle and basal epithelium (chapter three).

These principles were applied to IVCM and LM section analysis and clearly illustrated throughout different study groups.

Chapter Three

3 In Vivo Confocal Microscopic Features in Ocular Surface Diseases:

This study included a group of conditions where the primary pathological lesion involved an overgrowth of conjunctival tissue onto the corneal surface with or without limited degree of subepithelial changes like scarring.

The total number of cases included in this study was 13 divided into 2 main groups:

1. Non-neoplastic Conjunctivalisation of corneal surface in the following conditions:
    a. Corneal fibrovascular lesion: 3 cases
    b. Diffuse Keratoconjunctival Proliferation (DKP): 1 case
    c. Limbal stem cell deficiency (LSCD): 7 cases
2. Corneal Intraepithelial Neoplasia (CIN): 4 cases

CIN patients were considered separately in order to compare their IVCM findings with those seen in cases of corneal conjunctivalisation. The final outcome was to establish 2 sets of IVCM criteria that could help differentiate CIN from conjunctivalisation disorders on clinical basis before -or even without- the need for histopathological sampling. The rationale for this work comes from the fact that CIN is commonly

misdiagnosed as one of the benign ocular surface disorders long before accurate diagnosis is established through histological examination of proper tissue samples that are recommended to be prepared as unfolded epithelial sheets (Waring et al., 1984).

3.1 IVCM IN NON–NEOPLASTIC CORNEAL CONJUNCTIVALISATION:

3.1.1 Background:

A healthy epithelium of the corneal limbus represents the natural anatomical border between the conjunctival and corneal epithelia acting as a barrier against conjunctival epithelial overgrowth onto the cornea (Dua et al., 1994). This area is well known to be populated with corneal epithelial stem cells residing in niches termed as Limbal Epithelial Crypts that are distributed around the limbal circumference (Dua et al., 2005). These stem cells are responsible for replacing any loss in the corneal epithelium caused by chemical, physical, infectious or autoimmune insult provided sufficient circumference of healthy limbus is preserved. However when the limbus, with its stem cell reservoir, is damaged partially or totally the conjunctival epithelium takes the role of healing the surface defect and invades the corneal surface partially or totally. Therefore conjunctivalisation of the cornea is the hallmark of limbal stem cell deficiency. In vivo confocal

microscopy (IVCM) has been used to explore the reflectivity patterns of conjunctival epithelium in normal eyes (Kobayashi et al., 2005, Messmer et al., 2006b, Efron et al., 2009) as well as in cases with pterygium (Gheck et al., 2007) but without any histological correlation.

In this study we used IVCM to examine the corneal surface in a group of patients affected by conjunctival overgrowth onto the corneal surface of various clinical manifestations and aetiological backgrounds in order to find out differential IVCM features of conjunctival epithelium in pathological location. When histological samples were available through surgical treatment or diagnostic procedures we correlated light microscopic findings with IVCM images to confirm accurate interpretation of the latter. IVCM criteria of conjunctival epithelium in such pathological conditions was then contrasted with those seen in CIN to differentiate between the 2 conditions on the basis of IVCM reflectivity patterns.

3.1.2 Objective:

To establish differential IVCM criteria of conjunctival epithelium overgrowth of various aetiological backgrounds supported with histopathological correlation in order to discriminate corneal from conjunctival epithelium on the basis of IVCM reflectivity patterns.

3.1.3 Patients and methods:

11 patients were included in the study (8males and 3females aged 18-71) all seen in the eye clinic of Queen's Medical Centre, Nottingham, UK and presented with the following ocular surface problems:

1. Recurrent fibrovascular growth (n=1) extending from 3 to 5 o'clock position of the right limbus to involve central corneal zone with subsequent visual impairment. Similar lesion was removed 2years before. The lesion was removed via excisional biopsy.
2. Suspicious asymptomatic limbal lesion at 8 o'clock position of right limbus encroaching the corneal surface (n=1). Surgical treatment through excisional biopsy was done.
3. Bilateral superficial corneal neovascularisation involving the whole limbal circumference with longer loops from the nasal side associated with subepithelial scarring (n=1). The right eye showed more extensive and central involvement with tiny multiple telangiectatic spots on temporal limbus. The patient had history of chronic blepharitis with bilateral ocular irritation and visual impairment for 8years. Diagnostic biopsy was taken from the right temporal limbus.
4. Diffuse kerato-conjunctival proliferation (DKP) (n=1) in the left eye involving limbal circumference between 3 and 9 o'clock positions sparing 6 o'clock and central areas. The diagnosis was based on clinical features and the patient had a history of chronic blepharitis

with moderate but stable visual impairment and hence was treated conservatively.

5. Limbal stem cell deficiency (LSCD) diagnosed clinically in 7 cases among which 2 had partial unilateral LSCD with clear central corneas and good vision, 4 cases had bilateral total LSCD with central corneal involvement and poor vision and 1 case with bilateral total LSCD with clear central island of corneal epithelium albeit poor vision due to history of multiple operations for retinal detachment and cataract in both eyes. Aetiological backgrounds for LSCD cases included chronic blepharitis with recurrent trichiasis (n=1), chemical burn (n=2), Aniridia with Glaucoma (n=2) and multiple ocular surgeries (n=2). 4 of total LSCD cases had their central corneal conjunctivalisation treated by alcohol delamination (n=1) and surgical lamellar excision as part of allolimbal stem cell transplantation (n=3). The rest of LSCD patients were stable and treated conservatively with lubricants.

Table 3-1 shows the demographic and clinical features of the cases included in the study. Figure 3-1 illustrates slitlamp photographs of 9 eyes of the group at time of presentation.

In total 7 tissue samples were sent in 10% formaldehyde to the histopathology department where 5µm thin sections were stained with Heamatoxylin & Eosin then examined under light microscopy with NanoZoomer NDP machine. All eyes were examined with in vivo confocal microscopy (IVCM) as detailed in chapter two prior to any

surgical intervention. Finally IVCM and light microscopic (LM) sections were analysed for appropriate correlation.

Table 3-1: Summary of demographics, clinical features and management of 11 patients with ocular surface disorders included in the study.

No	age /sex /eye	Presenting features	BCVA	Background	Management
1	44 / M / R	Recurrent fibrovascular corneal lesion	6\18	Removal of fibrovascular lesion	Excision
2	60 / M / R	Fleshy limbal lesion with corneal encroachment	6\6	not significant	Excision
3	51 / M / BE	Diffuse limbal corneal neovascularisation with faint scarring + telangiectatic spots on right temporal limbus	R 6\12 L 6\9	Chronic Blepharitis	Right temporal limbal biopsy
4	76 / M / L	Diffuse keratoconjunctival proliferation 3-9o'clock sparing 6o'clock and corneal centre	6\9	Chronic Blepharitis	Conservative
5	71 / M / BE	Total LSCD with central corneal involvement. Left cornea had translucent avascular central surface.	L 6\36 R 6\60	Recurrent Trichiasis with repeated electrolysis	Alcohol delamination of left central corneal epithelium
6	64 / F / L	Total LSCD with central corneal involvement	6\60	Aniridia + Glaucoma	Allolimbal SCT
7	64 / M / L	Total LSCD with central corneal involvement	6\60	Aniridia, Glaucoma, PK	Allolimbal SCT
8	70 / F / L	Total LSCD with central corneal involvement	6\24	Bilateral PK + pseudophakia	Allolimbal SCT
9	43 / M / BE	Total LSCD with clear central island of corneal epithelium	R 6\36 L 6\60	Bilateral RD & cataract operations	Conservative
10	18 / M / R	Partial LSCD with superior and inferior pannus	6\6	Alkali burn 20months ago	Conservative
11	36 / F / R	Partial LSCD with superior conjunctivalisation	6\9	Alkali burn 6months ago	Conservative

BE= both eyes. LSCD= limbal stem cell deficiency. PK= penetrating keratoplasty. RD= retinal detachment. SCT= stem cell transplant.

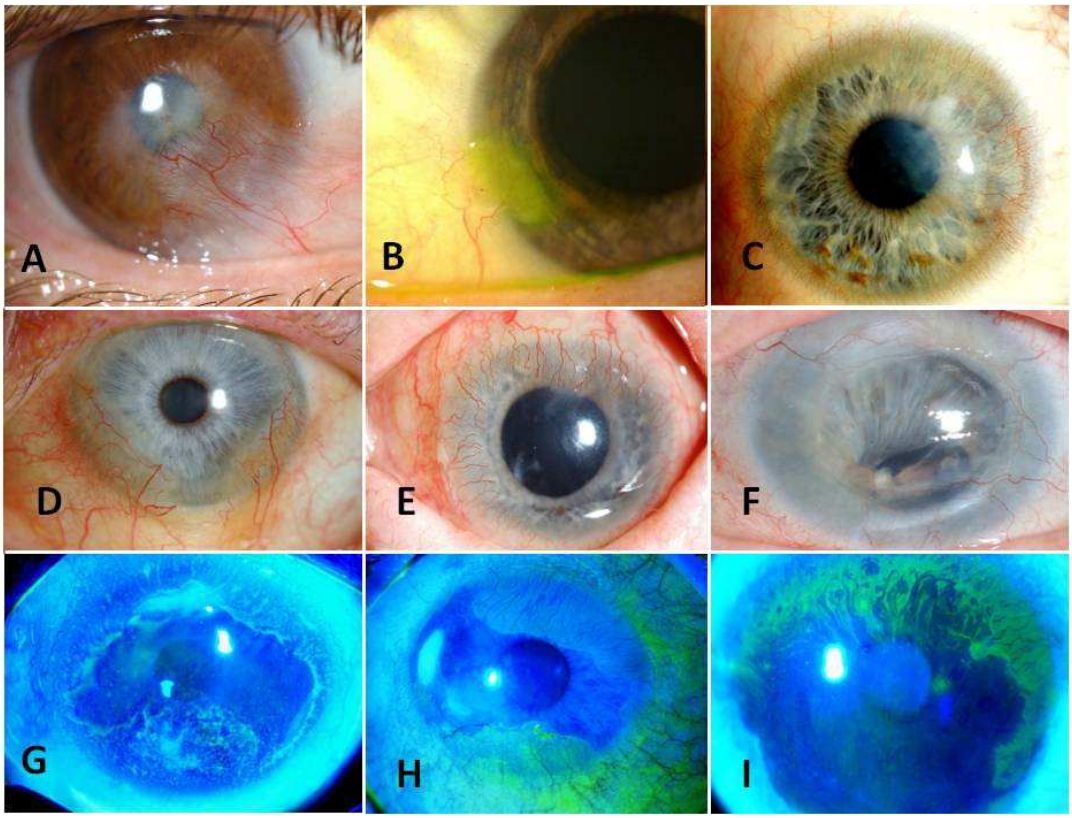

Figure 3-1: Diffuse slitlamp photos of 9 corneas with ocular surface disease. A (case1 right eye), recurrent fibrovascular growth with central corneal involvement. B (case2 right eye), suspicious temporal limbal fleshy lesion with corneal encroachment. C (case3 right eye), 360º limbal superficial neovascularisation with central scarring. D (case4 left eye), Diffuse keratoconjunctival proliferation (DKP). E (case5 left eye), total LSCD with translucent avascular central corneal surface. F (case8 left eye), total LSCD with central corneal involvement. G (case9 left eye), total LSCD with clear central island of corneal epithelium. H (case10 right eye), partial LSCD with superior and inferior pannus. I (case11 right eye), partial LSCD with superior conjunctivalisation. (G, H and I with fluorescein stain).

3.1.4 Results

3.1.4.1 Elastotic degeneration of subepithelial collagen:

Histological examination of samples taken from the first three cases with fibrovascular lesions (Table 3-1) revealed elastotic degeneration of subepithelial stromal collagen fibres consistent with the diagnosis of

Pterygium (Figure 3-2) along with unremarkable overlying stratified squamous surface epithelium.

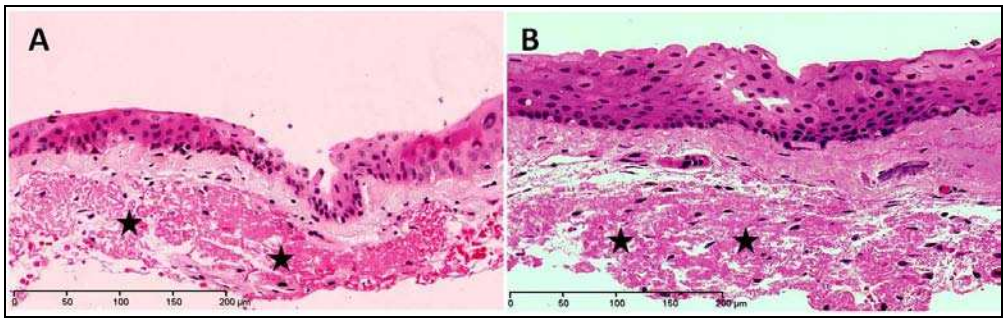

Figure 3-2: Light micrographs showing elastotic degeneration of stromal collagen (stars) in fibrovascular tissue samples taken from a fleshy limbal lesion in csae2 (A) and diffuse corneo-limbal neovascularisation in case3 (B). (H&E stain)

3.1.4.2 Goblet cells

On histological sections goblet cells were seen distributed singly and in rosette-like aggregates (Figure 3-3A) while on IVCM images of corresponding lesions they presented as moderately hyper-reflective round to oval figures randomly distributed in a similar fashion to that seen on light microscopy (Figure 3-3B). The average size of goblet cells calculated in three samples was 15.8 ± 2µm (mean ± SD) (Figure 3-3 C & D) while on IVCM images their size ranged between 15 – 20µm.

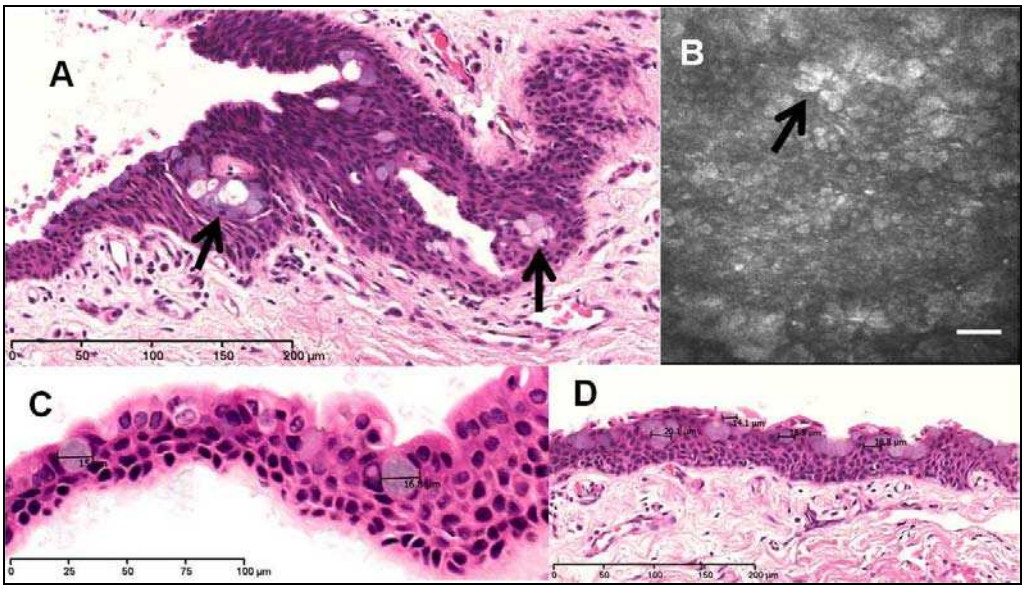

Figure 3-3: Microscopic views of goblet cells. Rosette aggregates of goblet cells (arrows) within epithelial layers are seen in light micrograph (A) and IVCM image (B) of the recurrent fibrovascular growth in case1. Cell morphometry revealed an average size of 15.8 ± 2µm (mean ± SD) on histological sections (C & D). IVCM scale bar 50 µm. H&E stain in A, C & D.

These cells were noticed on histological samples and IVCM in 4 cases (case1 & 2 with fibrovascular growth, case 6 & 8 with total LSCD involving central cornea in Table 3-1). Four more cases (case 1 with DKP and 3 with LSCD sparing the central cornea) showed these cells on IVCM alone as tissue samples were not available. Goblet cells were missing in 3cases (number 3, 5 and 7 Table 3-1).

3.1.4.3 Cystic changes

Cystic changes within the epithelial layers were seen on IVCM in 9cases (number 1, 2, 4 and 6-11 Table 3-1) among which 3cases (1, 6 and 8) showed similar histological evidence, 2 cases (2 and 7) had no cysts on histology samples while the remaining 4 cases had no

samples. Cystic changes were missing in 2 cases histologically and on IVCM (case 3 and 5). Figure 3-4 illustrates these epithelial cysts on light microscopy (Figure 3-4A) as well as IVCM en face (Figure 3-4B) and oblique (Figure 3-4C) views in association with goblet cells.

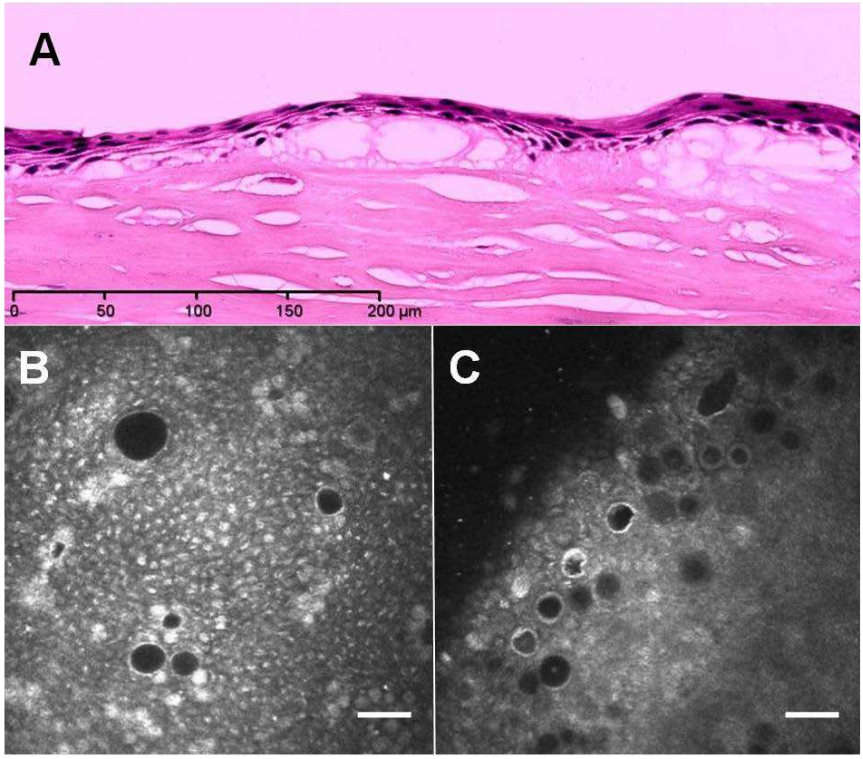

Figure 3-4: Cystic changes adjacent to conjunctival epithelium are seen in light micrograph of cross section in tissue sample from case 6(A) as well as corneal IVCM en face image in case 9 (B) and oblique view in case 8 (C). Scale bar 50µm.H&E stain in (A).

3.1.4.4 Epithelial Reflectivity & pattern of distribution:

On IVCM the conjunctival epithelium appeared as hyper-reflective sheets with ill-defined nuclei and cell borders at all levels (Figure 3-5A). It was clearly demarcated from the adjacent corneal epithelium which assumed a darker honeycomb pattern with invisible nuclei at middle and basal layers. When alternate sheets of conjunctival and

corneal epithelia existed in the same area on IVCM the sub-basal corneal nerves were seen only on the corneal side (Figure 3-5B).

Isolated islands of hyper-reflective epithelium were noticed within the clear corneal epithelium on IVCM (Figure 3-5 C&D). They were located more centrally in cases of LSCD (number 9,10 and 11 Table 3-1) who showed clear central corneal surfaces on slitlamp examination (Figure 3-1 G – I). This conjunctival epithelial demarcation on IVCM was clearly seen in all cases except 2 (number 5 and 6 Table 3-1).

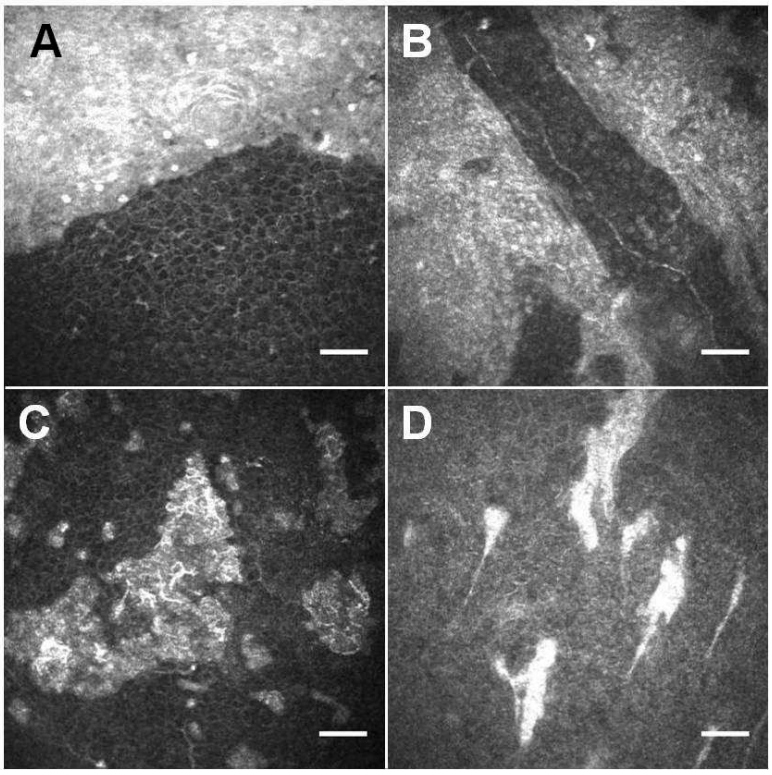

Figure 3-5: IVCM corneal en face images in ocular surface disease. A, (case2) shows sharp demarcation of hyper-reflective conjunctival epithelium from the corneal epithelium. B, (case11) sub-basal corneal nerves are seen in the corneal epithelial side in-between sheets of conjunctival epithelium. C & D (case 9 & 11 respectively)show isolated conjunctival epithelial islands within the corneal epithelium. Scale bar 50µm.

Another form of conjunctival epithelial distribution was noticed in case 3 where the slitlamp examination of the right eye showed tiny multiple telangiectatic spots among the temporal limbal vascular loops (Figure 3-6A). On IVCM of the corresponding area bright epithelial cells were found to surround circular figures containing bright spots consistent with end-on views of capillary blood vessels all seen within the middle epithelial layers (Figure 3-6B). The en face images taken at successive depth of focal plane revealed the vascular nature of the structures (Figure 3-6 C-D).

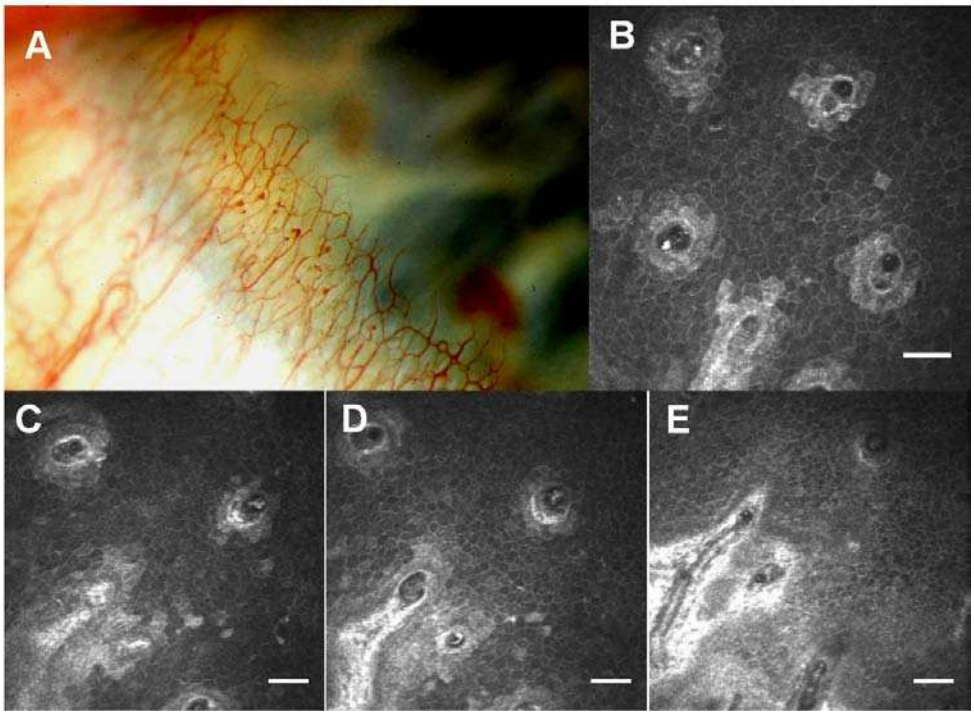

Figure 3-6: Tiny superficial telangiectatic spots close to temporal limbus in case 3 are shown on slitlamp photograph (A). Corresponding IVCM image (B) shows dark circles representing end-on views of these dilated capillary blood vessels surrounded by bright conjunctival epithelial cells all within clear corneal epithelium. IVCM images C – E were taken at successive depths of 37, 43 and 60µm respectively to confirm the vascular nature of these circular patterns. Scale bar 50 µm.

3.1.4.5 Other less frequent pathological findings:

1. Regenerative atypia: In 3 samples histological examination revealed ill-defined epithelial cells with intracytoplasmic vacuoles and enlarged vesicular nuclei with prominent nucleoli (Figure 3-7A-C). However no features of dysplasia i.e. loss of polarity and mitotic figures were seen. These changes were consistent with regenerative atypia and could be seen extensively in tissue samples from case 5, 6 and 7 in table1 who had LSCD with central corneal involvement. Corresponding IVCM images showed hyper-reflective prominent nuclei within ill-defined epithelial cells at the superficial, middle and basal layers consistent with metaplasia (Figure 3-7 D-F).

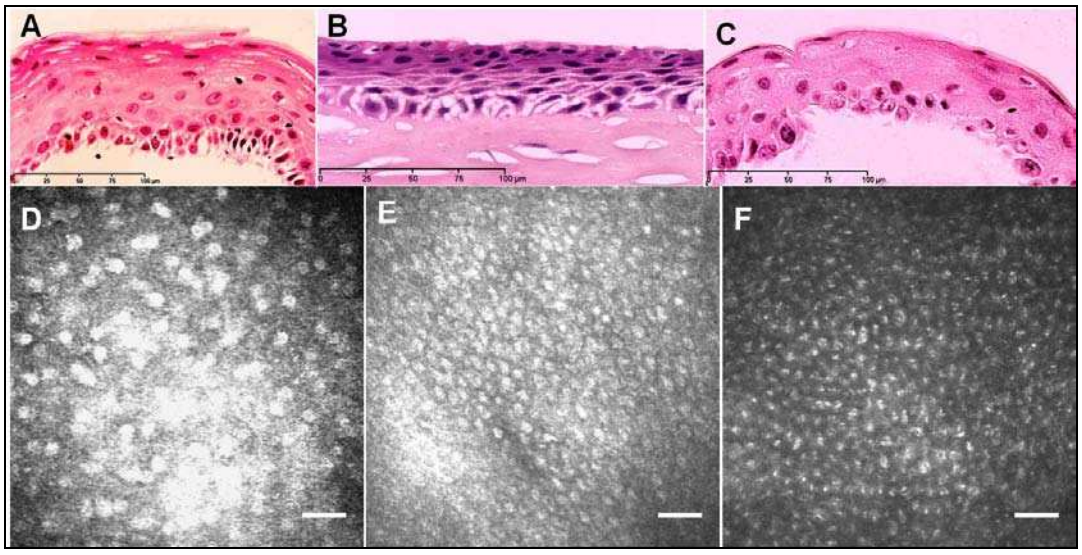

Figure 3-7: Cellular morphological changes in regenerative atypia of corneal epithelium. A – C, light micrographs of epithelial sections in samples taken from cornea in case 7, 6 and 5 respectively showing vacuolation with enlarged vesicular nuclei and prominent nuclei without mitotic figures or disrupted polarity. Corresponding IVCM images show prominent hyper-reflective nuclei within ill-defined cells at superficial (D), middle (E) and basal (F) epithelial layers in case 7, 6 and 5 respectively. IVCM focal depth is 6, 10 and 46µm respectively with scale bar 50µm. H&E stain in A-C.

2. Dyskeratosis of epithelial cells was noticed in the histological sample of case 8 (Table 3-1) as round individual cells having their cytoplasm filled with eosinophilic keratin with a central pyknotic nucleus (Figure 3-8A). The size of these figures ranged between 11.6 – 20.7µm with an average of 17.2 +/- 3.1µm (mean +/- SD). The corresponding IVCM images showed multiple hyper-reflective round to oval structures 10 – 20µm in diameter with occasional double-wall appearance similar to Acanthamoeba cysts (Figure 3-8B&C).

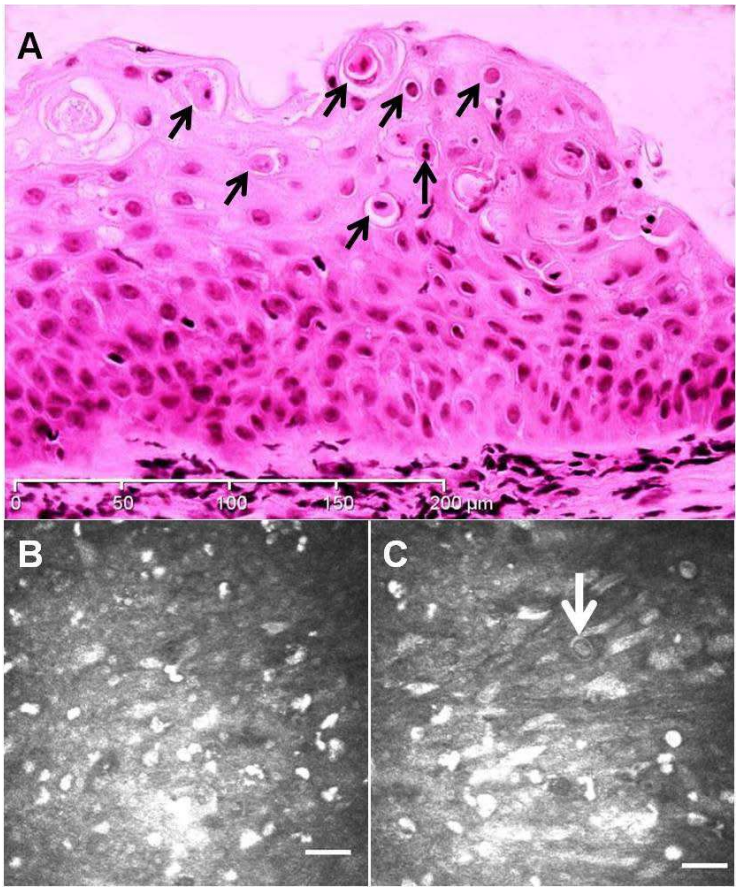

Figure 3-8: Dyskeratosis in limbal stem cell deficiency. A, light micrograph of epithelial section in anterior lamellar corneal sample from case 8 shows multiple dyskeratotic cells (black arrows) expressing eosinophilic keratin-filled cytoplasm with pyknotic nuclei. Corresponding IVCM images show multiple bright round to oval figures within mid-epithelial layers (B) with occasional double- wall shapes (white arrow in C). Scale bar 50µm. H&E stain in A.

3.1.5 Discussion

IVCM has been applied in previous studies to identify the reflectivity features of the epithelium in the corneal limbus and bulbar conjunctiva (Kobayashi et al., 2005, Messmer et al., 2006b, Patel et al., 2006b) (see IVCM of the ocular surface in chapter one). In these studies the demarcation between the 2 epithelial phenotypes was clear on IVCM (see IVCM of the ocular surface in chapter one).

In this study all conditions of pathological conjunctival overgrowth shared the feature of increased hyper-reflectivity resulting in a clear contrast between corneal and conjunctival epithelia similar to the features reported in previous studies of the IVCM of limbal region (Kobayashi et al., 2005, Patel et al., 2006b). These findings are in keeping with the conjunctival nature of the ocular surface pathologies included in our study. The details of cell borders and nuclei were frequently overshadowed on IVCM in these pathological conditions; however prominent nuclei were noticed in association with regenerative atypia seen on histological sections under light microscopy. Despite the apparent diversity of the conditions included in this study all cases shared the common feature of having conjunctival overgrowth past the limbus onto the corneal surface bringing the conjunctival and corneal epithelia next to each other without being separated by a limbal barrier. This disruption of normal anatomical distribution was helpful to contrast the reflectivity criteria of different epithelial phenotypes against each other through IVCM en

face views in a non-invasive method compared to other histological manoeuvres. Some of these disorders like LSCD and DKP were diagnosed clinically while three cases who presented with fibrovascular corneal overgrowth of undetermined appearance were confirmed histologically to bear stromal changes consistent with those of Pterygium overlaid by stratified squamous epithelium of conjunctival phenotype.

Goblet cells on IVCM appeared moderately hyper-reflective round to oval figures that were paler and larger when viewed within bright epithelial nuclei. These cells were comparable in size, shape and pattern of distribution on IVCM and light microscopy. Cystic changes were possibly formed by accumulation of mucin secretion from goblet cells. They were seen more frequently on IVCM compared to histological sections possibly due to dehydrating steps taken during sample preparation for light microscopy.

Dyskeratosis represents premature single cell keratinisation usually termed (corps ronds) (or round bodies) characterised by eosinophilic kertin-filled cytoplasm with pycnotic nucleus (Tripathi and Garner, 1972). Dyskeratotic cells were noticed in one case with total LSCD involving the central corneal surface. The excessive keratin filling these dying cells in a roundish collection could explain their hyper-reflectivity on IVCM. Some of these figures assumed double-wall shapes on IVCM simulating Acanthamoeba cysts. Dyskeratosis could be the early stage towards full keratinization of ocular surface occasionally seen in LSCD.

Regenerative atypia involves certain cellular and nuclear morphological changes seen in response to rapid cell turnover provoked by traumatic or inflammatory causes (Genta and Rugge, 2006). In three cases with total LSCD involving central corneal surface these changes, as seen histologically, could explain the intensely bright nuclei at superficial, middle and basal epithelium seen on IVCM with ill defined cell borders. Possible causes include recurrent trichiasis in case 5 and long-term exposure to topical anti-glaucoma treatment in case 6 & 7.

On IVCM the following patterns of epithelial distribution on the corneal surface were noticed:

1. Continuous straight or undulating borders between conjunctival and corneal epithelia.
2. Alternate finger-like sheets of conjunctival and corneal epithelium with visible sub-basal nerves on the corneal side.
3. Isolated islands of conjunctival epithelium that were more centrally located in cases of LSCD with clear central cornea and absence of inflammatory features subjectively and objectively.

The first 2 patterns are easily identified on slitlamp especially with the use of topical fluorescein dye wherein the conjunctival epithelium takes late staining (Dua et al., 1994). However the isolated epithelial islands on central corneal epithelium were only seen on IVCM even when fluorescein staining was unremarkable. This finding gives another clue to the nature of conjunctival epithelial response in LSCD and needs

further investigation to evaluate the corneal situation in long term follow up of such cases.

3.1.6 Conclusion

IVCM is an effective non-invasive imaging tool to establish specific criteria for qualitative evaluation of conjunctival epithelium overgrowth onto the corneal surface induced by various aetiological factors. It provides more elaborate features of corneal surface in resolved LSCD that could not be detected with slitlamp examination alone.

3.2 IN VIVO CONFOCAL MICROSCOPY OF CORNEAL INTRA-EPITHELIAL NEOPLASIA WITH HISTOPATHOLOGICAL CORRELATION.

3.2.1 Introduction:

The term CIN is widely accepted in the literature to indicate Conjunctival and/or Corneal Intraepithelial Neoplasia which includes dysplasia and Carcinoma in Situ (Erie et al., 1986, Lee and Hirst, 1995). It is a relatively rare condition that more often affects elderly males (Erie et al., 1986, Roberson, 1984). A predominantly corneal type of CIN without conjunctival lesions has been well described and frequently considered as a separate entity by some authors (Waring et al., 1984, Erie et al., 1986, Horatanaruang et al., 2005, Roberson, 1984, Hanssens M et al., 1993, Geggel et al., 1985, Brown HH et al., 1989). This however, almost always occurs in association with corresponding limbal lesions (Hanssens M et al., 1993, Waring et al., 1984). The term “Ocular Surface Squamous Neoplasia (OSSN)” is now used to describe the spectrum of lesions but excludes papillomas, melanomas, and lymphomas (Lee and Hirst, 1995).

The clinical symptoms are generally non specific with chronic ocular irritation, redness and varying degrees of visual involvement determined by the extent of encroachment of the lesion on the visual axis (Waring et al., 1984, Lee and Hirst, 1995, Roberson, 1984,

Hanssens M et al., 1993, Geggel et al., 1985, Cruess et al., 1981). The signs too can vary from a distinct limbal lesion to a gray avascular semi-transparent thickened sheet of epithelium with a lustreless surface (Waring et al., 1984, Lee and Hirst, 1995). For this reason and because of the non-invasive nature of the condition, the diagnosis is often missed or delayed and patients treated for chronic conjunctivitis. Other conditions for which CIN is commonly mistaken include pterygium, corneal pannus, viral keratitis, corneal dystrophy and fatty degeneration (Lee and Hirst, 1995, Erie et al., 1986).

Histological examination of a tissue sample, preferably taken from the limbus, reveals the correct diagnosis (Lee and Hirst, 1995, Erie et al., 1986, Roberson, 1984). In recent years IVCM has proved useful as a non-invasive technique to investigate various ocular surface conditions including CIN (Guthof et al., 2006, Messmer, 2008). However, the diagnostic features of CIN by IVCM are not yet fully established in the published literature (Gentile et al., 2009, Messmer, 2008, Guthof et al., 2006). Single case reports were recently published describing confocal microscopic features of CIN including irregular hyper-reflective cells with bright nuclei (Malandrini et al., 2008, Wakuta et al., 2008). Malendrini et al (2008) mentioned these features in the superficial layers only, whereas Wakuta et al (2008) described similar changes in all epithelial layers. In thischapter we present novel IVCM findings in CIN with emphasis on their diagnostic potential, showing the basal layer heavily populated by dysplastic cells supported by

reliable histopathological correlation. IVCM description of sub-basal corneal nerves in CIN was not mentioned in earlier studies. We also present IVCM changes in patients after treatment with topical chemotherapeutic agents.

3.2.2 Patients and methods.

The study was an observational consecutive case series. The research adhered to the tenets of the Declaration of Helsinki. Informed, written consent was obtained from all patients. We examined 4 eyes of four patients (three men and one woman, (age range 57 to 73) affected by CIN, referred either to the Queens Medical Centre of Nottingham University Hospitals, Nottingham, UK or to the ophthalmology Clinic, University "G d'Annunzio" of Chieti-Pescara, Italy. In addition control eyes of four male patients, two with limbal stem cell deficiency (LSCD), one with a suspicious limbal lesion and one with diffuse keratoconjunctival proliferation (DKP) (Said et al., 2008) were also studied.

3.2.2.1 Patients with corneal/conjunctival intraepithelial neoplasia:

All patients with CIN had superficial corneal opacification confined to the epithelium. Adjacent conjunctival involvement was also observed in all patients. Slit-lamp examination revealed a continuous non-

vascularised semitransparent relatively thick sheet of abnormal epithelium growing over the corneal surface. This abnormal layer showed a rough lustreless surface with superficial punctate staining with fluorescein and Lissamine green. Patient demographics and clinical findings are given in Table 3-2. Representative biomicroscopic findings of the patients at presentation are illustrated in Figure 3-9.

Table 3-2: Demographics and clinical features of patients with CIN and Controls

Patient	Sex	Age	Symptoms	Slit-lamp findings	Diagnostic and Therapeutic intervention	Outcome
CIN						
1	M	69	Ocular irritation, visual impairment	Abnormal corneal epithelium	Alcohol delamination + MMC 0.04%	Complete healing
2	M	57	Ocular irritation, visual impairment	Abnormal corneal and conjunctival epithelium	Alcohol delamination + MMC 0.04%	Partial healing/ recurrence/ complete healing
3	F	70	Photophobia, foreign body sensation	Abnormal corneal and conjunctival epithelium	Excisional biopsy + MMC 0.04%	Complete healing/ recurrence
4	M	73	Ocular irritation, visual impairment	Abnormal corneal epithelium	MMC 0.04%	Complete healing
CONTROLS						
5	M	22	Right alkali burn. Intermittent ocular irritation. Clinical diagnosis: LSCD	Superior and inferior fibrovascular pannus on cornea. Clear visual axis. Temporal corneal scar.	Topical steroids and lubricants. No surgical intervention.	Gradually progressing.
6	M	74	Ocular discomfort and visual impairment. Clinical diagnosis: LSCD	Peripheral superficial vascularization and abnormal corneal epithelium	Alcohol delamination	Clearing of visual axis with improvement in vision
7	M	63	Asymptomatic	Localised fleshy limbal lesion 4x2 mm	Surgical excision	Settled with no recurrence
8	M	66	Ocular discomfort, dry eyes. Clinical diagnosis: DKP	Circumferential encroachment of fibrovascular tissue (conjunctiva like) on cornea. Visual axis clear	Topical lubricants	Stable, no signs of progression

MMC = Mitomycin C

LSCD = Limbal stem cell deficiency. DKP = Diffuse keratoconjunctival proliferation

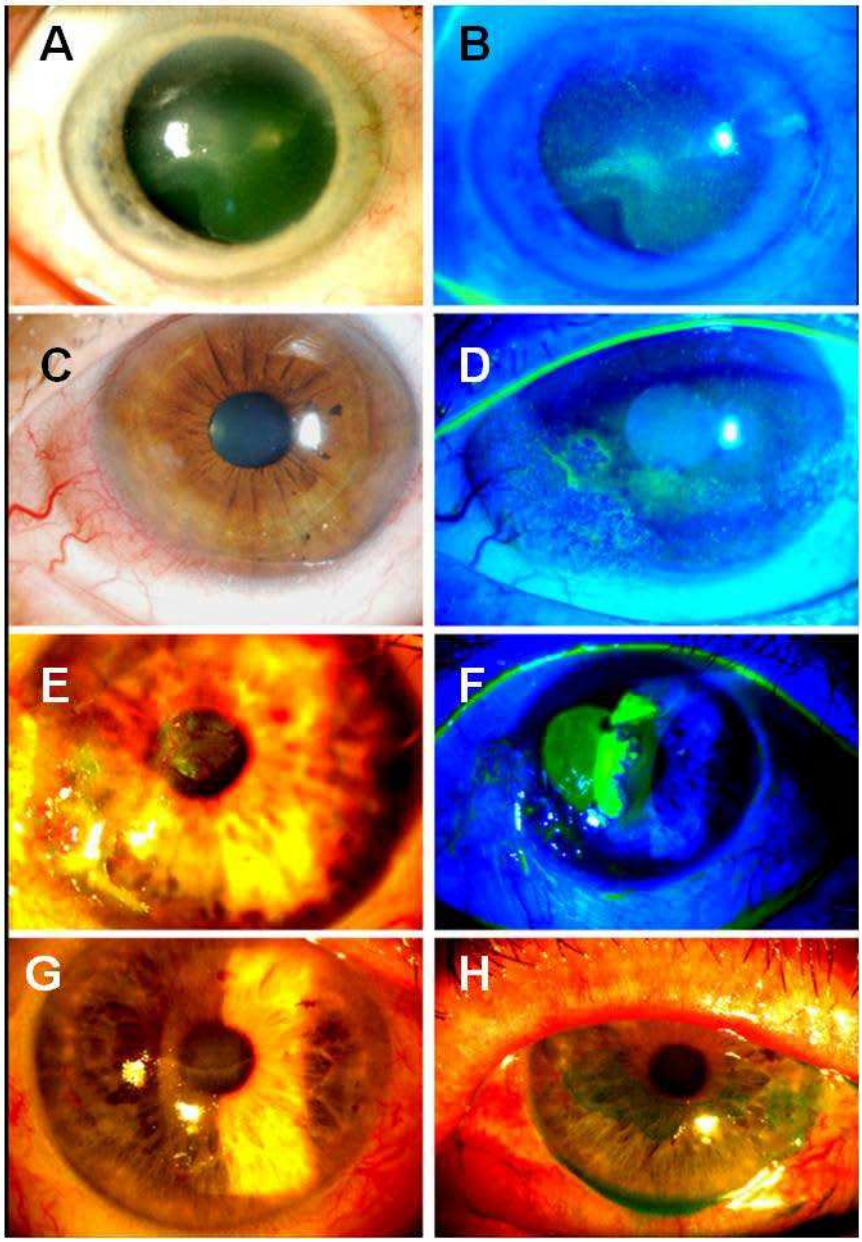

Figure 3-9: Diffuse slit lamp photographs of eyes of the 4 patients with CIN. A: a greyish flat sheet of cells is seen covering approximately 80% of the corneal surface of patient 1. The sheet shows coarse punctuate staining with fluorescein dye (B). C: illustrates patient 2 with a prominent limbal lesion and a flatter extension onto the lower cornea. Here too the abnormal epithelium shows a similar staining pattern with fluorescein dye (D). E: The above pattern was repeated in patient 3. The central patch of abnormal epithelium stained strongly with fluorescein (F). G: Patient 4, the central limit of the inferior CIN lesion is seen as a scalloped line across the pupil. H: Same eye 7 days after topical MMC treatment. Partial regression is seen by Lissamine green stain.

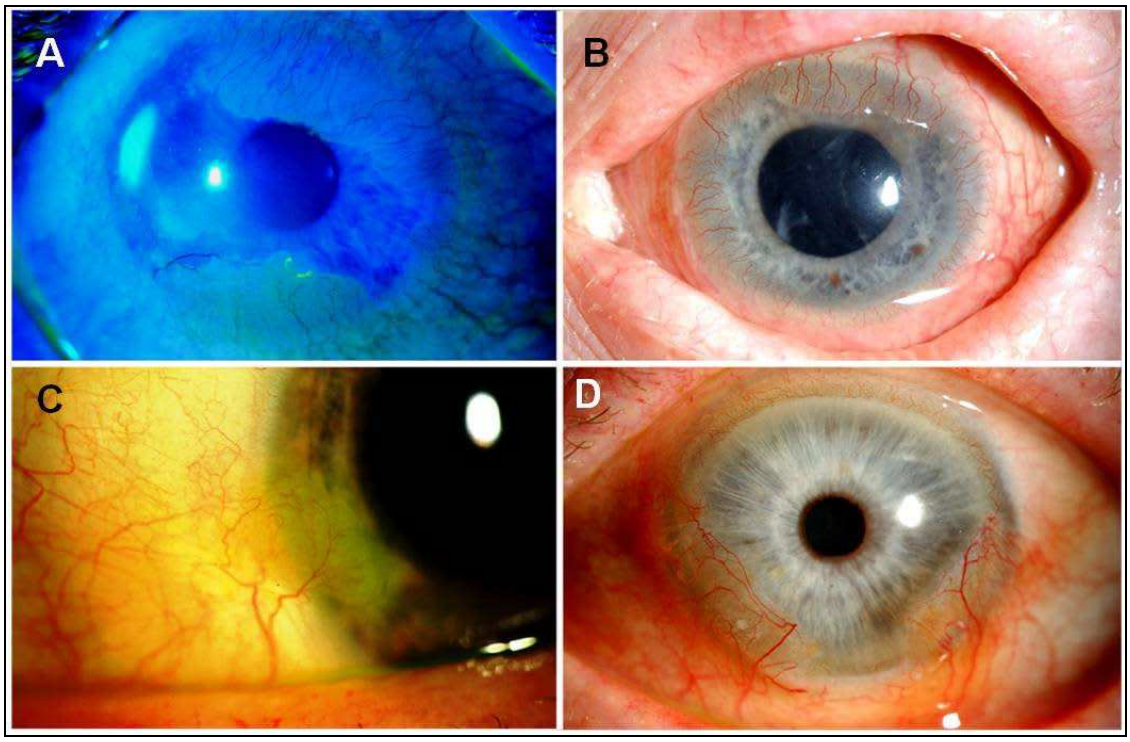

Figure 3-10: Diffuse slitlamp photographs of control eyes. A: Wide sheets of fibrovascular pannus covered with conjunctival epithelium, highlighted with fluorescein, are seen over the superior & inferior parts of cornea in patient 5 with limbal stem cell deficiency following alkali burn. B: A 360^{o} circumferential fibrovascular pannus is seen encroaching on to the cornea in a patient with chronic inflammation. There is associated central corneal haze and scarring (patient 6). C: A fleshy, vascularised slowly progressive limbal lesion with corneal involvement in patient 7 is illustrated. D: Diffuse keratoconjunctival proliferation in patient 8 affecting approximately 6 clock hours.

Previous treatment received included scraping of abnormal epithelium (1 case) topical steroids and lubricants (2 cases). Corneal epithelial samples were taken through impression cytology and biopsy using alcohol delamination (Dua et al., 2006) from each case for histopathology. After histological diagnosis of CIN patients were treated with topical Mitomycin C (MMC) 0.04% four times a day for a week followed by one week off. The number of such cycles required for complete resolution was 2 to 9. One case required additional application of 0.04% MMC soaked sponges

for five minutes, one application per week for a total of 5 applications to achieve complete response.

For histology via alcohol delamination see chapter two. Specimens were paraffin embedded and 5-7µm sections were stained with haematoxylin and eosin (H&E). Slides were reviewed with the help of the Nanozoomer Digital Pathology scanner (NDP C9600 series, Hamamatsu Photoincs K.K. Hamamatsu city, Japan), using the software for high magnification views and cell morphometry. For impression cytology, under topical anaesthesia a cellulose acetate filter paper disc (Millipore. 0.45µm) (Millipore Corp., Bedford, MA, USA), marked for orientation, was applied to the surface of the dysplastic epithelium and firm pressure applied to the paper with a Goldman tonometer headpiece. The paper was allowed to remain in contact with the eye for approximately 5–10 seconds, then peeled off with a forceps and placed in fixative solution before transfer to the laboratory. Cells were stained with haematoxylin and eosin.

IVCM was performed to all patients as described in chapter two. The corneal surface was evaluated in all patients with emphasis on visualizing epithelial cell morphology at the site of CIN and its borders. IVCM examinations were performed in the active stage, after treatment and in the event of recurrence for all cases. Epithelial cell density (cells/mm^2) was calculated, using the analysis software of the instrument.

3.2.2.2 Controls:

Patient demographics and clinical findings are given in Table 3-2 and Figure 3-10. One patient had LSCD secondary to unilateral alkali burn. Abnormal conjunctivalised epithelium covering a fibrovascular pannus had encroached on the cornea superiorly and inferiorly. Another patient with LSCD had central corneal involvement with a thin opaque layer of 'conjunctivalised' epithelium. This was removed by alcohol delamination. One male patient had a suspicious fleshy lesion at the limbus encroaching on the cornea. An excisional biopsy was performed. One male patient had diffuse keratoconjunctival proliferation, affecting the peripheral cornea from 3 o'clock to 10 o'clock with a small relatively unaffected area of 1clock hour at 6 o'clock position. The visual axis was clear. He was managed conservatively.

3.2.3 Results:

3.2.3.1 Corneal /conjunctival intraepithelial neoplasia:

In histology a multilayered epithelium with cellular and nuclear pleomorphism in the basal layer and reversal of the nuclear cytoplasm ratio were observed. Some cells had multiple nuclei and most of the basal cells had prominent nucleoli (Figure 3-11). Such dysplastic cells were also noted in the suprabasal layers in some sections. Representative images

from two patients are given in Figure 3-11A & B. The nucleoli of the basal cells measured from 2.60 to 3.98µm (mean= 2.84 ± SD of 0.60) (Figure 3-12 A & B). [Basal nuclear size in non–metaplastic corneal epithelial cells measured with the nanozoomer is 7.84µm ± 0.40 (Mean ± SD) personal observation]. The basal cell nuclei ranged between 8.2 – 16.6µm (mean 11.9 ± 3.765 SD) while the middle layer nuclei were 6.61 – 11.1µm (mean 8.98 ± 1.52 SD) (Figure 3-12 C).

In impression cytology the dysplastic cells were characterized by enlarged, irregular and hyperchromatic nuclei. Cell groupings with loss of cellular borders and irregularly arranged enlarged nuclei were observed in some areas. The sheets of dysplastic cells also showed large nucleoli (Figure 3-11 C).

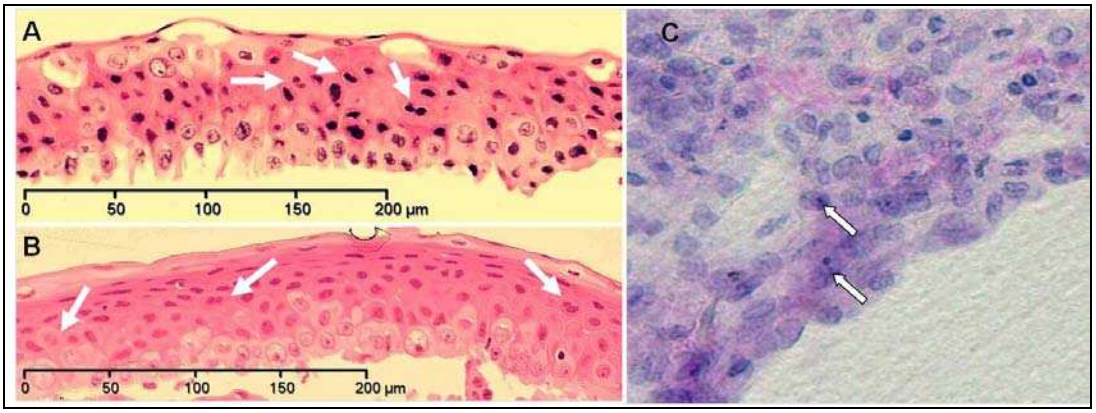

Figure 3-11: Light photomicrographs of CIN of different patients (H & E stained). A & B: histological sections in two patients show mitotic figures (arrows) as well as enlarged nucleoli in basal dysplastic cells. C: impression cytology of another patient with CIN where prominent nucleoli are also visible (arrows).

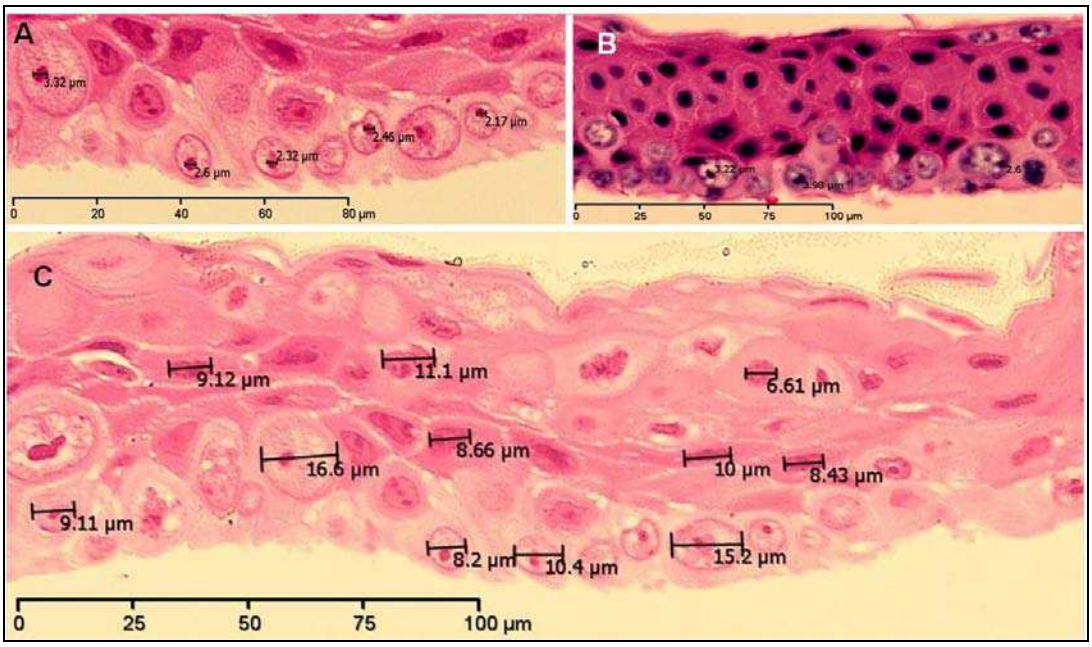

Figure 3-12. Nuclear and nucleolar morphometry in two patients with CIN. A & B: Basal layer nucleoli range from 2.60 - 3.98µm (mean=2.84 ± SD of 0.60). C, basal layer nuclei range from 8.2 – 16.6µm (mean =11.9 ± SD 3.765) while middle layer nuclei range from 6.61 – 11.1µm (mean 8.98 ± SD 1.52). (H & E stained micrographs).

IVCM images of CIN at presentation showed the following:

1. In middle epithelial layers the cells were hyper-reflective and pleomorphic with variation in size and shape but largely maintaining a polygonal morphology. The cell borders were reasonably well defined. Nuclei were prominent and hyper-reflective. Some cells showed mitotic activity (double nuclei) (Figure 3-13 left column).
2. In basal layers the cells showed characteristic bright dots, 2 – 4µm in size located within dark round spaces giving the appearance of a starry sky in a dark night. The cell borders were ill-defined. At places, areas of normal basal cells without the bright dots and with defined borders

were seen amongst the abnormal basal epithelium (Figure 3-13 middle column).

3. At the advancing edge the CIN lesion was well demarcated on confocal images. The distinction between normal and abnormal epithelium was clear with the former being darker with well defined cell borders and the latter appearing as a hyper-reflective sheet with abnormal cell morphology as described above (Figure 3-13 right column). Cell density was remarkably reduced in CIN areas (3162 ± 47 cell/mm²) compared to normal epithelial regions (6301 ± 60 cell/mm²).
4. In the sub-basal layer the sub-basal corneal nerves were not seen in areas of CIN examined by in vivo confocal microscopy. However, where projections of normal epithelium were visible in between CIN epithelium, the sub-basal nerves could be distinctly seen (Figure 3-13 H). No cell invasion in Bowman's zone or anterior stroma was observed in the areas examined.

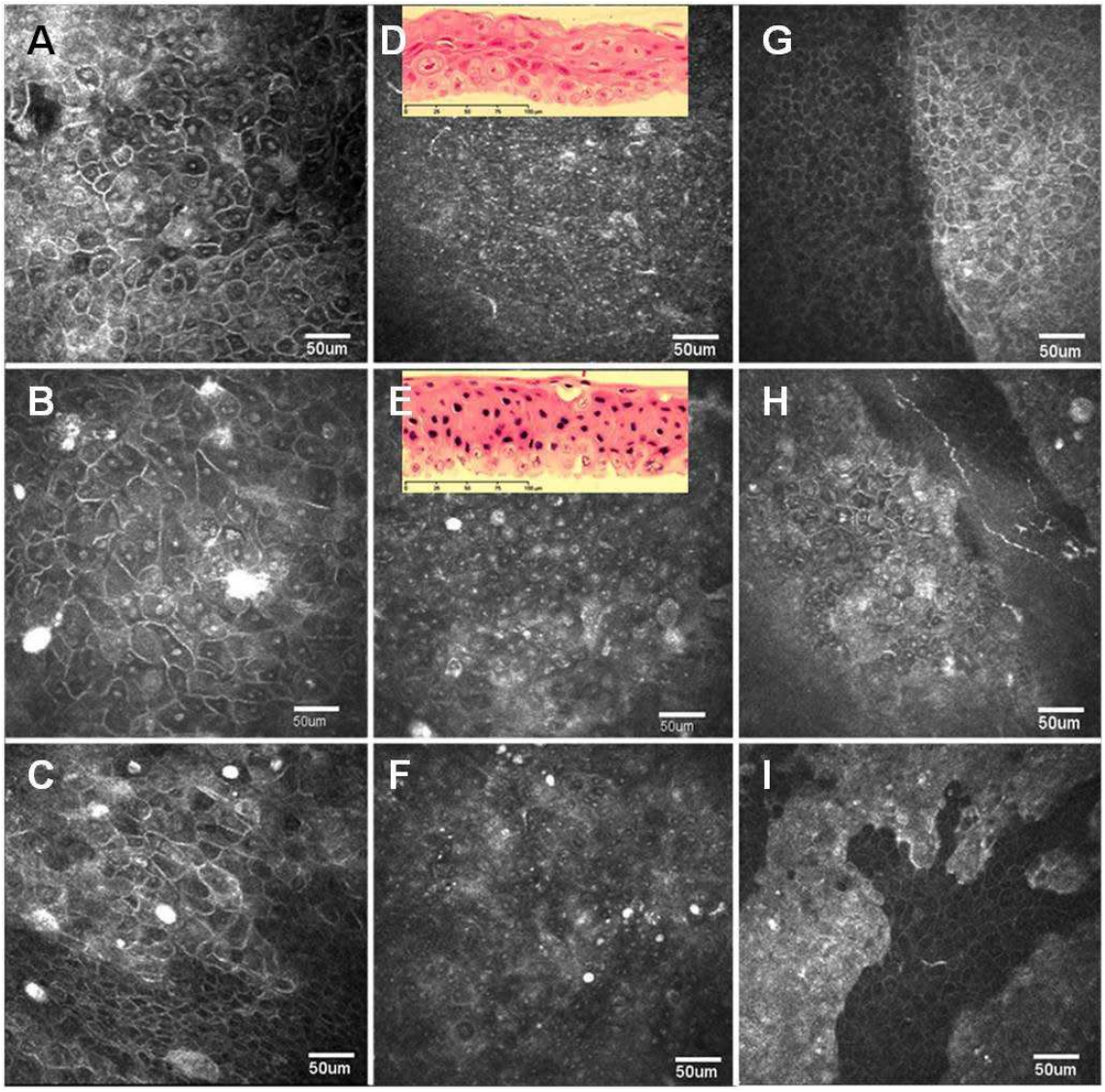

Figure 3-13: IVCM features of patients 1, 2 and 3 with CIN. Each row corresponds to one patient.

Left column: Mid- epithelial layer shows multinucleated bizarre-shaped cells.

Middle column: Basal cells show ill-defined borders with tiny bright spots 2 – 4 µm in size within dark spaces giving a 'starry – sky' pattern. These dots are comparable to prominent nucleoli of enlarged basal nuclei seen in corresponding photomicrograph insets (D & E).

Right column: Images of advancing border of CIN at mid-epithelial layer show higher reflectivity and cell density and pleomorphism in CIN compared to adjacent normal epithelium. H: sub-basal corneal nerves are exclusively seen within normal epithelium between CIN areas. I: fimbriated extensions of CIN are illustrated inter-digitating with normal corneal epithelium.

In response to treatment clinical regression of the lesions was corresponded with reduced reflectivity of the epithelium of the CIN, ill-defined demarcation of the CIN and normal epithelial junction and loss of pleomorphism. The middle layer cells appeared more regular in size (Figure 3-14 A) though at certain areas the nuclei were still prominent and hyper-reflective (Figure 3-14 B). Some mitotic figures were visible. The basal cell borders became distinctly visible and approached normality. The bright dots were no longer visible in these basal cells. The sub-basal nerves were apparent in places where they were previously not seen (Figure 3-14 C & D). When clinical resolution of the lesion occurred, complete normality of all layers was restored on IVCM examination.

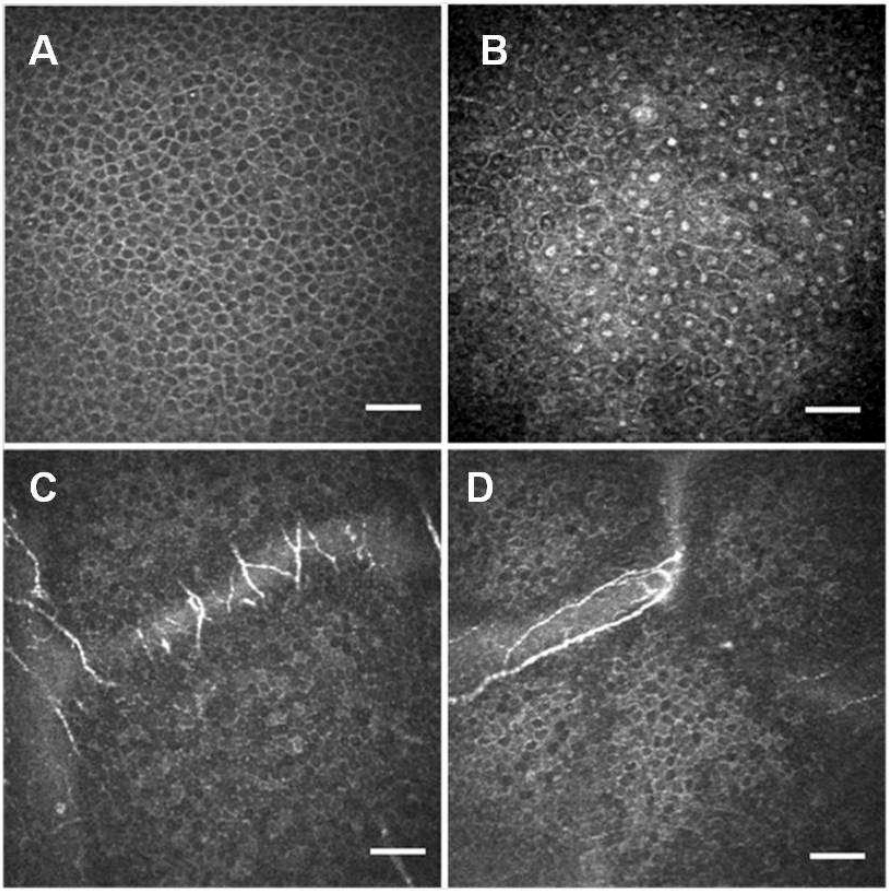

Figure 3-14: IVCM after clinical resolution of CIN. A: normal pattern of mid-epithelial layers. B: occasional areas of prominent nuclei. C & D: normal basal epithelium with visible sub-basal nerves. Scale bar 50µm.

3.2.3.2 Controls:

Tissue samples from two control patients (number 6 and 7,Table 3-2) were available for histology (Figure 3-15). Patient 6, with LSCD secondary to chronic inflammation and recurrent trichiasis, showed regenerative atypia characterised by uniformly enlarged basal nuclei in keeping with epithelial growth. Patient 7 with the limbal lesion showed solar elastosis of the stromal collagen consistent with histological features of pterygium.

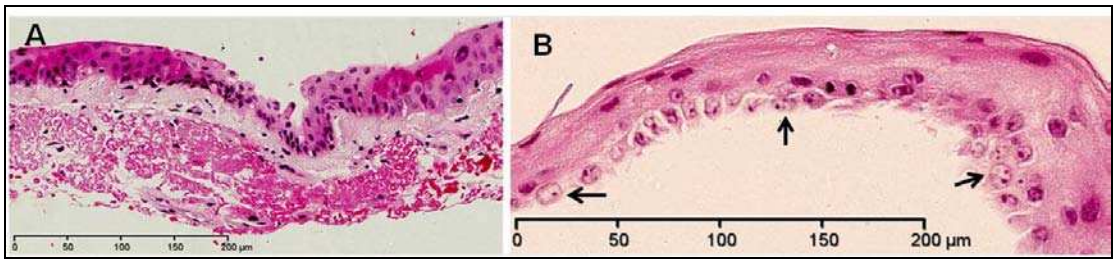

Figure 3-15: Light micrographs of tissue samples from control eyes (H&E stained). A: normal looking conjunctival epithelium overlying an area of elastotic degeneration of stromal collagen suggestive of pterygium in patient 7. B: A thin sheet of attenuated epithelium shows basal cell atypia with enlarged nuclei containing prominent nucleoli. Normal polarity towards surface layers is still maintained albeit with ill-defined cell borders (patient 6).

On IVCM the abnormal epithelium on cornea was hyper-reflective with distinct margins demarcating it from the normal corneal epithelium (Figure 3-16). It was multilayered and in the two patients with LSCD goblet cells could be seen in the superficial epithelium (within 20 to 30µm) (Figure 3-16 A). In all four patients dark cystic spaces were noted extending through the thickness of the epithelium. Pleomorphic and multinucleated cells were not observed in any layer. Cell borders were ill-defined. Hyper-reflective bright dots in the basal and suprabasal cells were seen only in the patient with regenerative atypia (Figure 3-16 B).

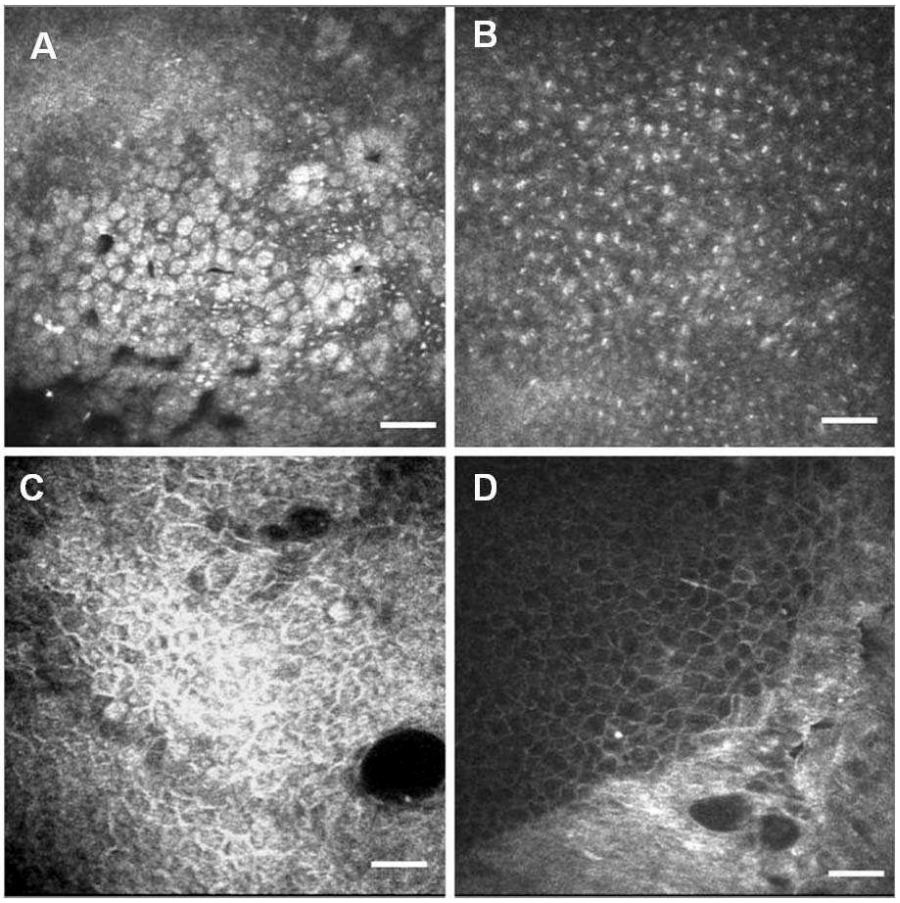

Figure 3-16: IVCM images of corneal surface for four of the control group. A: Abundant goblet cells, some organized in rosettes, are seen amongst hyper-reflective conjunctivalised epithelium. This is a hallmark of limbal stem cell deficiency (patient 5). B: The patient had goblet cells and cysts as seen in limbal stem cell deficiency but his basal layer showed prominent hyper-reflective dots that corresponded to basal cells with regenerative atypia (patient 6). C: Hyper-reflective epithelium with large cystic spaces are seen in the epithelium of the limbal 'pterygium –like' lesion (patient 7). D: Bright conjunctival epithelial cells with ill-defined cell margins are seen. The sheet is sharply demarcated from the darker corneal epithelium which shows well defined cells of normal mid-epithelial layer. Two dark cystic spaces are also seen (patient 8). Scale bar 50µm

3.2.4 Discussion:

The gold standard in diagnosis of CIN is histological examination of a biopsy of the conjunctival or limbal aspect of the lesion, when clinically apparent. Biopsy of the corneal epithelial layer too is possible, particularly

with the technique of alcohol delamination (Dua et al., 2006) whereby the removed epithelium is preserved as a sheet and fixed flat. With this technique however, no subepithelial tissue is removed and invasion of subepithelial tissue if any, by the lesion cannot be studied. However, it is not certain whether IVCM would be able to pick up cells invading the stroma. Studies on invasive squamous carcinoma would be needed to ascertain this. In this study all examined areas of Bowman's zone and stroma underlying the CIN were normal. IVCM offers a very useful diagnostic tool to examine the ocular surface at the cellular and sub-cellular level in a relatively non-invasive manner. Although morphological features of CIN as seen by IVCM have been described, the diagnostic criteria have not been defined. In this study we undertook a comprehensive examination of four patients with histologically diagnosed CIN, at presentation, during response to topical medication and after complete resolution. Based on our observations and morphological features reported in the literature (Guthof et al., 2006, Messmer, 2008) together with histological correlation of the lesions removed at biopsy, we are able to propose certain diagnostic IVCM features, which will allow the clinician to make a clinical diagnosis with reasonable certainty to initiate medical treatment. These features include

1. Hyper-reflective pleomorphic cells of varying shapes and sizes especially in the middle layers of the CIN. The middle cell layers also have bright dots, which correspond to prominent nuclei of the cells.

Within some cells two bright dots were visible. These correspond to two nuclei (mitotic cells) seen on histology in some cells of the middle layer.

2. At the edge of the lesions the hyper-reflective CIN cells contrast with the darker normal cells, which are also smaller in size with a regular uniform morphological appearance. The cell density of the adjoining normal epithelium was almost twice as much as the CIN cell density.
3. A 'starry night sky' pattern of the basal layer. The numerous bright dots are produced by the prominent nucleoli. The nuclei were very large and light-staining on histology but were not seen on IVCM. The cell borders of the basal layer too were indistinct or invisible on IVCM and also on histology. As the size of the bright dots corresponded to the size of the nucleoli it is reasonable to assume that the bright dots represent images of the nucleoli. These dots were smaller than the bright dots seen in the middle layers, which most probably represent the nuclei of this layer. There was a distinct difference in size of the nuclei between cells of the basal and middle layers with the basal nuclei being almost 2.5 times larger. Both the cell borders and nuclei were not imaged by IVCM giving the dark background to the bright images of the nucleoli. The actual size of nucleoli in normal or dysplastic corneal epithelium is not mentioned in the literature, however evidence of increased nucleolar size in neoplastic tissues has been well documented in other studies.(Zink et al., 2004)

4. The virtual absence of sub-basal corneal nerves was also noticed within areas involved by the CIN compared to adjacent non affected regions. This probably represents a limitation of the imaging technique wherein the high reflectivity of the CIN cells is close to the high reflectivity of the nerves, rendering them difficult to detect. As the lesions resolve and CIN cells are replaced by normal cells, the sub-basal nerves 're-appear' probably related to the increased contrast. At the advancing edge of the CIN, where the lesion extended as finger-like projections, sub-basal nerves could be seen in the intervening normal areas, again indicating that they had not degenerated but were merely not imaged.

Histologically nuclei in CIN were found to be larger than normal, being vesicular with more dispersed but coarsely clumped chromatin. Nucleoli in CIN were also found to be larger than normal, more eosinophilic and subjectively with well delineated borders from the surrounding nuclear chromatin. They were also typically more central in location within the nucleus. Nucleoli of normal cells were subjectively smaller, more basophilic with ill-defined margins that merged with the adjacent nuclear chromatin. These changes could explain the hyporeflective nature of such nuclei on IVCM imaging providing a contrast for the nucleoli enabling them to present as hyper-reflective dots.

Prominent large nuclei at various epithelial levels have been seen in conditions of regenerative atypia associated with rapid cellular turnover

and during wound healing. We have also noticed this in patients with trachoma and keratoconus with scarring and rigid contact lens wear (unpublished observations). It is unlikely that any single feature mentioned above, in isolation will be diagnostic of CIN but taken together will provide a reasonably certain diagnosis which could then be confirmed by biopsy if needed. The correlation of the IVCM features with the histopathology in our cases supports this conclusion. Table 3-3 summarises the ocular surface criteria on IVCM in CIN and non-neoplastic conjunctivalisation disorders.

Table 3-3: Summary of IVCM criteria in CIN compared to non-neoplastic conjunctivalisation.

IVCM in Corneal Intraepithlial Neoplasia	IVCM in Conjunctivalisation
1. Middle cells: Hyper-reflective, pleomorphic multinucleated & well defined borders 2. At borders: pleomorphic cells contrast with normal epithelial pattern 3. Basal cells: hyporeflective, ill-defined, with bright nucleoli 3-4µm (Starry night sky pattern) 4. Invisible sub-basal nerves in CIN areas	1. Bright ill-defined middle layer cells 2. Goblet cells & Cystic changes 3. No pleomorphism 4. Bright basal nuclei could be seen in regenerative atypia with visible sub-basal nerves

Increasingly, IVCM is being used to discern tissue micro-anatomy at a resolution previously only achieved by conventional histology. Many IVCM descriptors have been assigned to specific cell types, often without direct histological correlation. This study is therefore useful in that such a direct

correlation has been accomplished. It does however have at least three limitations: (a) IVCM provides en face images of cells compared to cross sectional images of tissue histology. The comparison therefore is not like-for-like but as IVCM imaging will always remain predominantly en face and histology will be cross sectional, the comparison is important. It is only by such comparison that some validity can be ascribed to cell morphology revealed with IVCM images. Moreover, in two cases we did perform impression cytology, which too provides en face images. Here the comparison is more valid but suffers from the limitation that impression cytology yields only the anterior 2 to 4 layers of cells, unlike histology where the entire thickness can be studied. (b) Fixation required for histology results in shrinkage of tissue. Morphometric comparison between living tissue and fixed tissue has to be viewed in this context. However, since formalin fixation causes negligible (skin) (Dauendorffer et al., 2009) to 7% (liver) (Riley and Ruggiero, 2008) shrinkage of tissue, a size comparison, taken in this context can still be appropriate. (c) It is difficult to obtain IVCM and histology images from exactly the same site of the tissue being examined. The HRTII-RCM confocal microscope used in this study is equipped with a side mounted digital camera that monitors the exact position of contact of the microscope objective lens with the cornea. Biopsy can be targeted to the site thus examined but it is impossible to say that the location was identical. However, as the appearances were similar over large areas scanned by IVCM and multiple

histological sections it is reasonable to assume that the correlation made is justified.

Chapter Four

4 In Vivo Confocal Microscopy in Corneal Oedema with Histopathological Correlation

4.1 INTRODUCTION

Corneal oedema is a clinical condition characterized by increased corneal thickness due to excessive accumulation of water into (hydrophilic) stromal layers usually secondary to decreased function or disease of the corneal endothelium. The important causes include late stages of Fuchs Endothelial Dystrophy (FED) and surgical trauma, commonly associated with cataract surgery (Pseudophakic bullous keratopathy). Bullous keratopathy represents an advanced stage of chronic corneal oedema where the corneal epithelium is affected and presents multiple cystic collections of water, termed bullae, of various sizes. This accumulation of water could be intra-epithelial or subepithelial causing separation of the basal epithelium from the underlying Bowman's zone (BZ).

For many years penetrating keratoplalsty (PK) has been the definitive treatment of corneal oedema with endothelial dysfunction. In PK the whole cornea including the oedematous stroma and bullous epithelium is replaced by donor tissue. With the advent of lamellar endothelial keratoplasty (EK) in the form of Descemets stripping endothelial

keratoplasty (DSEK) or Descemets membrane endothelial keratoplasty (DMEK) the oedematous stroma and epithelium are retained and only the diseased endothelium is replaced. Clinical experience has substantiated the many advantages of these techniques over PK (Melles, 2006, Tan and Mehta, 2007, Bahar et al., 2008). However, it has also been observed that excessively or chronically oedematous corneas do not clear in the same manner as early cases (personal observations). Certain changes, presumably permanent, appear to occur following longstanding corneal oedema raising the question whether EK successfully restores normality and perhaps whether the indications for EK need to be refined in the light of changes induced by chronic oedema.

It is important therefore to elucidate in detail the changes that occur in the cornea as a consequence of chronic oedema. In vivo confocal microscopy (IVCM) has proven to be a very useful non-invasive imaging tool to investigate cellular changes in various corneal disorders. In this study we examined by IVCM the changes occurring in all layers of oedematous corneas and in a proportion that subsequently underwent PK. We were able to correlate these to histological findings. Our aim was to identify and document specific changes that would form the basis of further studies to evaluate the persistence or reversal of these changes following EK.

4.2 PATIENTS & METHODS:

In this observational case series twenty patients with corneal oedema, attending the Queen's Medical Centre, Nottingham University Hospitals, England, UK (14 women and 6 men in the age range of 56-85y) were included. The diagnosis of corneal oedema was based on history, slit lamp examination and central corneal thickness (CCT) measured by ultrasonic pachymetry (Tomey SP-3000, Pachymeter, Tomey Corporation, Nagoya, Japan).

The patients fell into two groups, those with Fuchs endothelial dystrophy (FED) (11 patients, 9 females and 2 males) and non-Fuchs cases (9 patients, 4 males and 5 females) which included 5 with pseudophakic bullous keratopathy and 4 due to other causes (recurrent HSV endothelial/stromal keratitis n=2, glaucoma with filtration surgery n=1, unknown n=1). Among the FED patients 5 were also pseudophakic. Patients' demographics and presenting features are given in Table 4-1.

Table 4-1: Demographic and preoperative clinical features of patients with corneal oedema . The first 11 cases had Fuchs endothelial dystrophy (FED).

No.	Age/Sex/Eye	BCVA	Pachymetry(µm)	Epithelial Bullae	Lens status	Operation
Patients						
1	70y / F / R	6\36	760	Y	cataract	Triple
2	72y / M / R	6\36	598	Y	cataract	Triple
3	69y / F / R	6\36	642	Y	cataract	Triple
4	75y / M / R	6\30	588	N	pseudophakia	PK
5	56y / F / L	6\18	730	N	clear lens	PK
6	75y / F / R	1\60	NA	Y	pseudophakia	PK
7	75y / F / R	6\18	776	Y	pseudophakia	DSEK
8	75y / F / R	6\36	760	N	pseudophakia	PK
9	69y / F / L	6\36	672	N	clear lens	DSEK
10	81y / F / R	6\60	792	Y	pseudophakia	DSEK
11	73y / F / L	6\9 CL	597	N	clear lens	DSEK
12	81y / F / L	2\60	NA	N	cataract	Triple
13	57y / M/ R	6\36	663	Y	pseudophakia	PK
14	82y / F / R	2\60	NA	N	cataract	Triple
15	73y / F / L	CF	670	Y	pseudophakia	PK
16	68y / F / L	6\24	688	N	clear lens	PK
17	81y / M / L	6\18	624	Y	cataract	Triple
18	85y / M / L	6\18	633	N	pseudophakia	DSEK
19	70y / M/ R	6\36	NA	Y	pseudophakia	DSEK
20	78y / F / L	6\36	NA	Y	pseudophakia	DSEK
Controls						
21	59y / M / R	6/6	NA	N	Clear lens	N/A
22	22y / F / L	6/5	NA	N	Clear lens	N/A
23	72y / M / R	6/6	NA	N	Clear lens	N/A
24	24y / M / R	6/5	NA	N	Clear lens	N/A
25	30y / M / R	6/6	NA	N	Clear lens	N/A
26	21y / M / L	6/5	NA	N	Clear lens	N/A

CF= counting fingers, CL= with contact lens, DSEK= Descemet Stripping Endothelial Keratoplasty, N= No, NA= not available, N/A = not applicable, PK= Penetrating Keratoplasty, Triple = Triple procedure (cataract extraction + IOL implantation + Penetrating keratoplasty), Y= Yes.

All patients underwent routine assessment of visual acuity, pachymetry and slit lamp examination. In vivo confocal microscopy (IVCM) of the affected cornea was also done in all patients as described in (chapter two). Oblique IVCM images of areas examined were also obtained. Oblique images are the nearest the equipment can get to providing in-vivo cross sectional images resembling those obtained in histology sections.

A control group of six people with normal corneas (5 males and 1 female aged 21 – 72years) were examined with IVCM to compare their results with those of the study group.

IVCM examination was performed postoperatively in a subgroup of 4 cases operated with DSEK to compare the results with preoperative findings. Two were examined in the early postoperative period at months 7 and 8 (cases 11 and 7) and two in the late postoperative period at months 20 and 26 (cases 9 and 18). For the purpose of sub-basal nerve density measurement, nerve tracing and length was performed with 'Neuron J' software as described in chapter two.

13 corneal samples obtained by PK were processed for light microscopy (see chapter two). Three representative samples were further examined by electron microscopy (case 2, 16 & 17, Table 4-1). Morphometric calculation of nuclear length was carried out using the software of the Nanozoomer as illustrated in Figure 4-6. Nuclei of all the sub-epithelial cells in a given 40x field of the histology sections were measured. Twice as many nuclei of the corresponding corneal

stroma were also randomly selected and measured. When two nuclei were overlapping or lay very close to each other they were avoided. The average nuclear size was determined and compared for the two sets of cells. 3 patients, 3 fields each, were thus analysed. IVCM features were analysed and correlated with histopathological findings.

4.3 RESULTS

All patients presented with gradual deterioration of vision which was at its worst on waking in the morning. Three patients had painful bullous keratopathy. Best Corrected Visual Acuity (BCVA) preoperatively ranged between 6/9 (log MAR 0.17) and CF (log MAR 1.7) in the affected eye and the average central corneal thickness (CCT) was 679 ± 69µm (588 – 792µm). Slitlamp biomicroscopy revealed corneal scarring in two non FED cases only. Thirteen patients underwent penetrating keratoplasty (PK) of which 6 had a triple procedure (combined with lens extraction and implant). Seven patients underwent Descemets stripping endothelial keratoplasty (DSEK) of which five were pseudophakic. Table 4-2 shows the histological and IVCM findings in all subjects with corneal oedema.

Table 4-3 presents a brief descriptive data of IVCM patterns in corneal oedema.

Table 4-2: Summary of the main IVCM findings in corneas with oedema.

No.	Subepithelial Fibroblasts		Sub-basal Nerve Density mm/mm²	BZ / Stromal Granularity	Keratocyte Changes	Endothelial changes
	Histology	IVCM				
1	Y	Y	2.21	N	Y	Y
2	Y	Y	3.085	N	Y	Y
3	Y	Y	2.814	Y	Y	Y
4	N	N	Nil	N	N	Y
5	N	N	7.814	Y	Y	Y
6	N	N	1.131	Y	Y	Y
7	n/a	Y	5.65	Y	Y	Y
8	Y	Y	Nil	Y	Y	Y
9	n/a	Y	4.621	N	Y	Y
10	n/a	N	5.161	N	Y	Y
11	n/a	Y	6.586	N	N	Y
12	Y*	Y	6.415	Y	Y	Y
13	Y	Y	Nil	Y	Y	Y
14	N	N	2.392	N	Y	n/a
15	N	N	4.802	N	Y	n/a
16	N	N	Nil	N	Y	Y
17	Y*	Y	4.324	Y	Y	Y
18	n/a	Y	Nil	Y	Y	Y
19	n/a	N	6.766	N	Y	Y
20	n/a	N	Nil	Y	Y	n/a

BZ= Bowman's zone. n/a= sample not available (in DSEK). * Visible scar on Slitlamp examination

Table 4-3: A concise description of IVCM findings in corneal oedema with corresponding percentages and light microscopic histological features.

Corneal changes	Number (%)	IVCM patterns	Histology features
Sub-epithelial 'fibroblasts'	11 (55%)	Bright round to oval figures 10-20µm in size randomly distributed between basal epithelium and Bowman's zone	Cells with elongated slender nuclei 10.7 ± 4.1µm (Mean± SD)in length between basal epithelium and Bowman's zone
Sub-basal nerve density	14 (70%) 06(30%)	4.47 ± 2.05 mm/mm² (Mean ± SD) No sub-basal nerves were detected.	Not applicable
Bowman's zone / **Anterior stroma**	20(100%) 12 (60%)	Loss of normal reflective pattern (K- structures. (Kobayashi et al., 2006)) Fine or coarse granularity with variable reflectivity	No corresponding changes
Keratocyte changes	19 (95%)	Hyper-reflective expanded cell bodies and processes Dark small para-nuclear intracellular vacuoles (10-20µm) Large extracellular lacunae (40-100µm) in-between the keratocytes.	No corresponding changes
Descemets membrane (DM) & Endothelial changes	11(55%) 6(30%)	Fuchs endothelial dystrophy (FED): classical strawberry-like changes. Non-FED: polymegathism, thickened or ill-defined cell borders, prominent nuclei and reduced cell density to 512 ± 105cell/mm² (Mean ± SD).	FED: thickened multilaminated DM with inner excrescences on endothelial side. Attenuated endothelial cells with reduced cell density. Non-FED: attenuated endothelial cells with reduced cell density. DM thickened in 1 case.

4.3.1 Epithelial Bullae

On IVCM, epithelial bullae appeared as dark round areas with well defined margins. The majority of these were intraepithelial, within the mid-epithelial layers (Figure 4-1 A-C). These changes were seen in 11 cases of this group where the basal layer was intact without evidence of separation from BZ. The larger spaces, located superficially, were around 100µm. The size became smaller towards the basal layers. The appearance and change in size from superficial to deep layers is illustrated in Figure 4-1 E-I.

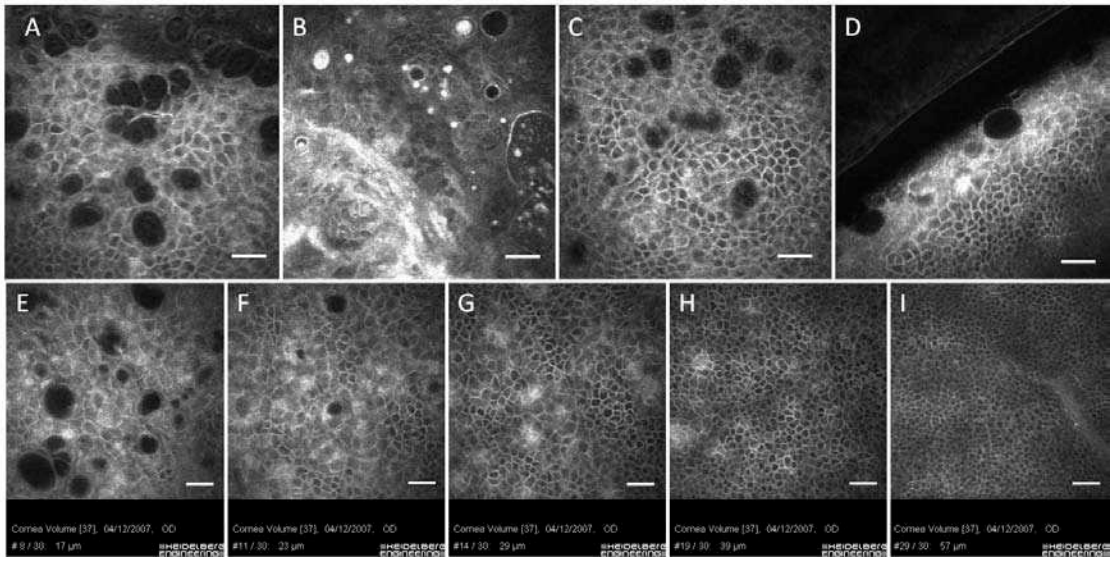

Figure 4-1: IVCM of epithelial bullae in corneal oedema. A-C en face images for cases 2, 3 & 7 respectively show epithelial bullae as empty dark round areas within corneal epithelial layers. D: oblique view of case 19 shows bullae within superficial layers. E – I [at focal depths of 17, 23, 29, 39, 57µm respectively]: Volumetric images show epithelial bullae becoming smaller from middle to basal epithelium where they disappear revealing an intact basal epithelial layer. Scale bar 50µm.

Of these 11 cases, histology was available for 10 cases. Histological sections showed superficial bullae in case 1 only (Figure 4-2 A). Cases 2 and 3, which had FED, showed sub-epithelial separation without

evidence of intraepithelial cystic spaces on light microscopy (Figure 4-2 B&C). No similar changes were visible in the other samples.

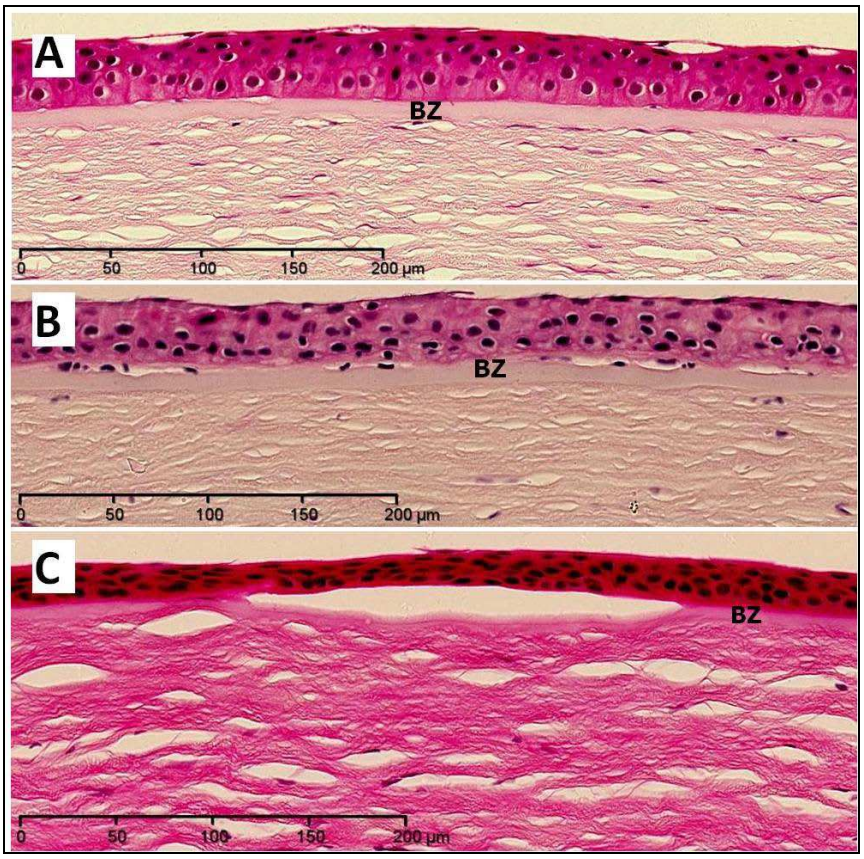

Figure 4-2: Light micrograph of corneal epithelial oedema : A (case1): superficial epithelial bullae are seen without separation of basal layer. B and C (cases 2 & 3): areas of basal epithelial separation from Bowman's zone (BZ). (haematoxylin and eosin stain).

4.3.2 Subepithelial fibroblasts and scarring

On histology cells with elongated thin nuclei, resembling keratocyte nuclei were seen lying beneath the basal epithelium and above Bowman's zone (Figure 4-3A). On IVCM these cells appeared as bright dots in the sub-basal plane (Figure 4-3B).

In some eyes, the basal epithelial cells were separated from the Bowman's zone by an accumulation of collagen 'scar tissue' with cells resembling keratocyte nuclei as described above. These cells were termed keratocyte derived cells (KDC). The collagen scar tissue was undulating and extended into the plane of the basal epithelial layer at places (Figure 4-3C). On IVCM the corresponding area presented as islands of (basal) epithelial cells surrounded by hyper-reflective (scar) tissue within which were bright dots which corresponded to the nuclei of the cells (Figure 4-3D). On oblique images the collagenous material presented as a continuous hyper-reflective, undulating, sub-basal sheet (Figure 4-3E).

In 2 eyes (case 3 &13), in addition to sub-basal scarring, there were one or more layers of scar tissue noted within the epithelium resembling reduplication of the basement membrane (figure 3F) and the epithelium itself was thickened (Figure 4-3F). On IVCM such layers were seen within the mid-epithelium as hyper-reflective patches or lines in en face or oblique sections respectively (Figure 4-3 G & H). At places there were breaches in the Bowman's zone with excessive deposition of 'scar tissue-collagen' and increased presence of cells (Figure 4-3I). On IVCM scar tissue always presented as hyper-reflective areas whether it was beneath (Figure 4-3E) or within the epithelium (Figure 4-3H). When the scar tissue was excessive, a meshwork of hyper-reflective strands was seen on IVCM (Figure 4-3J). Occasionally isolated islands of epithelium were seen totally embedded

within thick layer of fibrous tissue in histological sections (Figure 4-3K) and clearly illustrated on IVCM (Figure 4-3L).

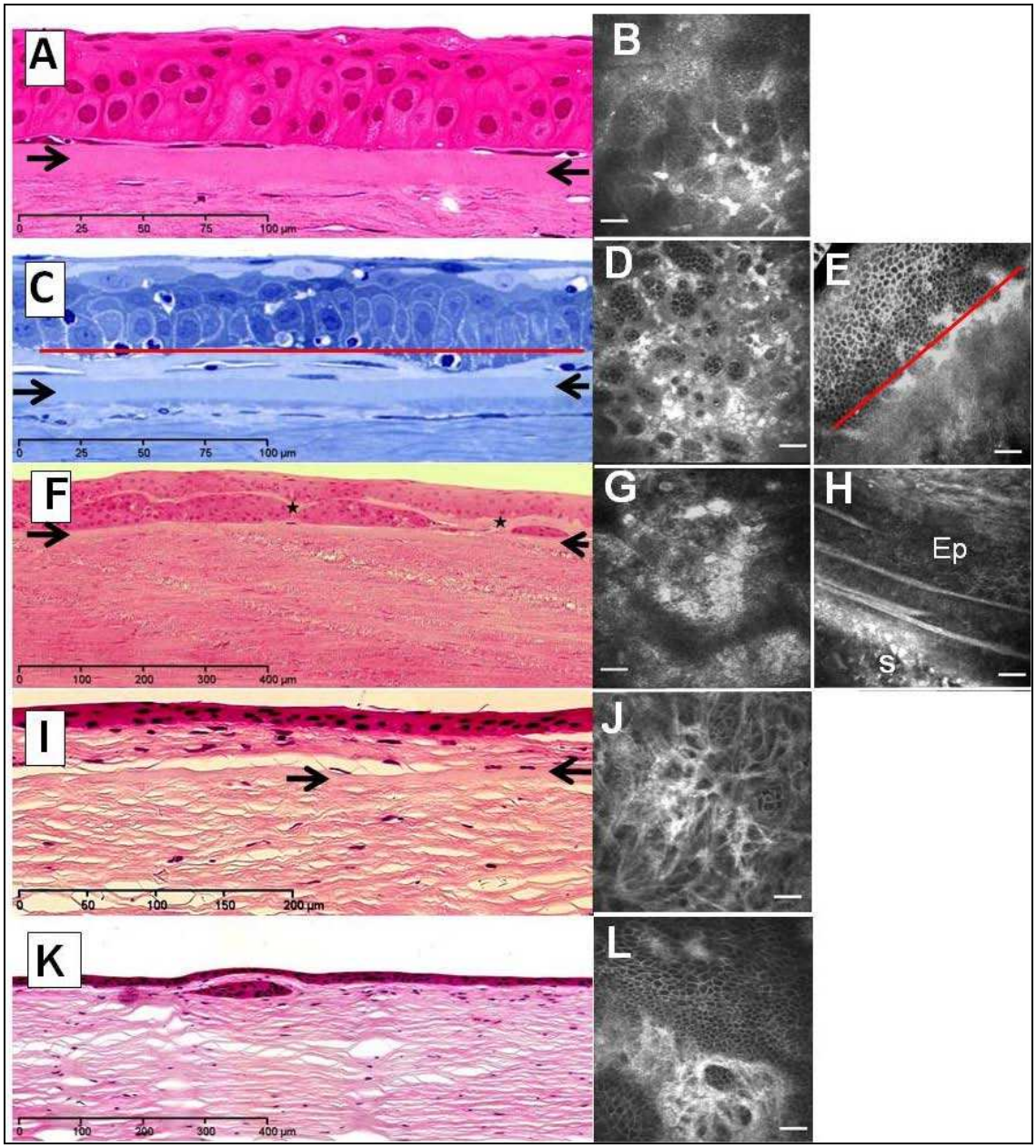

Figure 4-3: Light micrographs (left column) and IVCM images (right columns) of cases with corneal oedema. A, (case 1) shows flat elongated fibroblasts located between the epithelium and Bowman's zone (facing arrows = Bowman's zone) (H & E). B, A corresponding IVCM en face image of the same area taken pre-operatively, shows the subepithelial cells as bright oval figures. C, (case 2) Histology shows the deposition of collagen tissue with flat cells above Bowman's zone. The basal epithelium has an undulating profile corresponding to the variations in thickness of the collagen deposit (toluidine blue). D, Corresponding IVCM en face image shows small 'islands' of basal epithelial cells surrounded by bright collagen tissue containing brighter oval cells as described above. The red line (in C and E) represents one focal plane where both collagen tissue and basal cells would be imaged thus giving the appearance of 'islands

of cells' surrounded by collagen tissue. E, Oblique view of the same area clearly illustrating the subepithelial collagen layer of varying thickness with an undulating basal epithelium. F, (case 13) Histology section shows subepithelial collagen tissue with occasional flat cells. In addition, intraepithelial scar tissue is also seen, which is continuous with the sub-basal scar tissue at 2 places (star). The epithelium is multilayered and thicker than normal. G, en face IVCM image of the same area taken pre-operatively showing bright 'patches' with oval cells in the mid-epithelium corresponding to the intraepithelial scar tissue. H, Corresponding oblique IVCM image showing the intra-epithelial scar tissue as bright lines sandwiching layers of epithelium (Ep). The sub-epithelial scar tissue (s) with flat cells is also visible. I, (case 17) Histology shows attenuation and break in Bowman's zone. This corresponds with hypercellular and abundant subepithelial scar tissue. J, en face IVCM of the area shows a meshwork of hyper-reflective strands corresponding to the collage tissue. K, On histology the Bowman's zone is completely absent. There is excessive cellular scar tissue with islands of epithelium. L, en face IVCM showing the bright patches of scar tissue surrounding epithelial islands. (A, F, I & K are stained with H&E. C with toluidine blue. Scale bar in IVCM images = 50µm).

On volumetric IVCM the subepithelial KDC appeared as round or oval bright structures, 10 – 20µm in size in en face images, between levels of basal epithelium and BZ (Figure 4-4 A to E). The KDC were randomly distributed within a bright background and were more prominent in FED cases. Oblique views on IVCM were very useful in illustrating the exact location of these cells. They showed cells within BZ (Figure 4-4F) or in fibrous tissue septa extending within the epithelium (Figure 4-4G). Intraepithelial septa of scar tissue (Figure 4-4H) with epithelial islands were also seen in corneas of patients who did not undergo PK but had DSEK instead (Figure 4-4I).

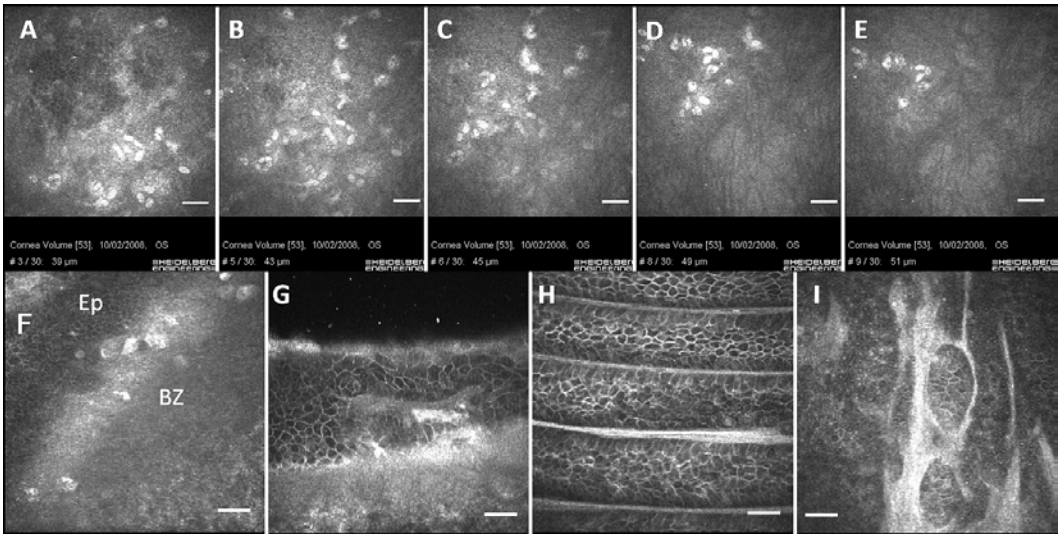

Figure 4-4: IVCM of subepithelial fibrosis and fibroblasts. A to E: Volumetric corneal images at successive depths in (case 18) show fibroblast nuclei at the level of basal epithelium (39µm) (A), becoming gradually fewer as we approach Bowman's zone (E) (51µm). F-G. Oblique views show bright fibroblast nuclei between epithelium (Ep) and Bowman's zone (BZ) (F, case 13) and within intra-epithelial fibrous septa (G case 18) that can take various patterns (H & I case 13 & 18 respectively). Scale bar 50µm.

With electron microscopy the Bowman's zone was noted to be thickened and irregular with a layer of scar tissue containing horizontally oriented elongated cell nuclei, on its anterior surface. At places the scar tissue extended anteriorly between basal cells. The posterior demarcation of Bowman's zone appeared quite normal. At places there were breaks in the Bowman's zone with increased scar tissue at these sites (Figure 4-5).

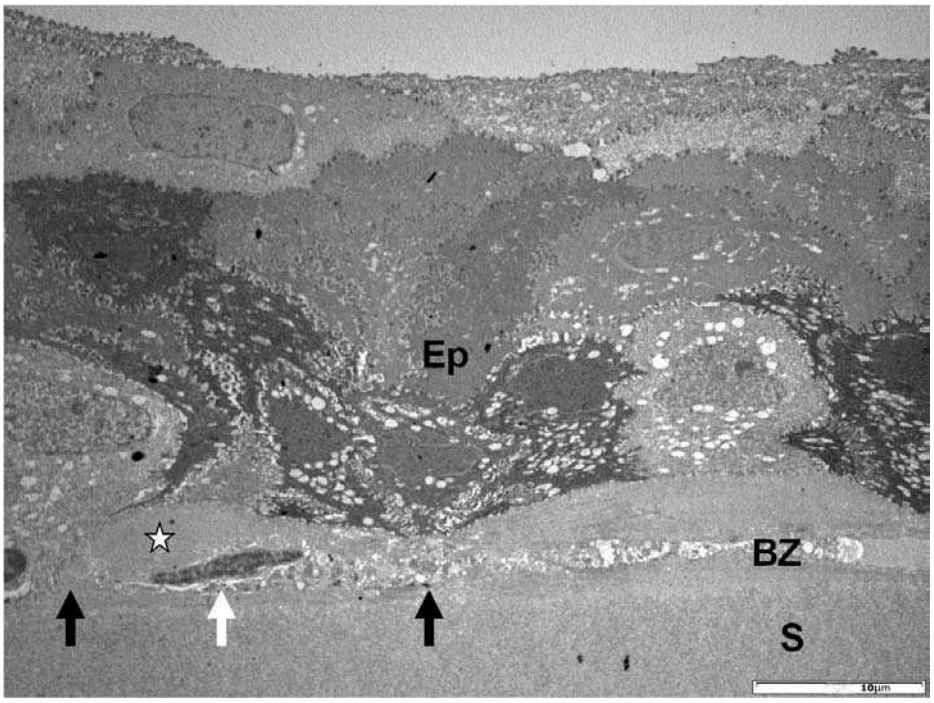

Figure 4-5: Transmission Electron micrograph of cornea with FED (case 2) showing epithelium (Ep), Bowman's zone (BZ) and anterior stroma (S). Breaks in BZ (black arrows) were seen close to a subepithelial spindle-like fibroblast (white arrow) with additional BZ-like material (star) located anterior to Bowman's zone and beneath epithelium. Scale bar 10µm.

4.3.2.1 Cell morphometry

In Histopathological sections the cells (KDC) located between epithelium and Bowman's zone had slender elongated nuclei comparable in shape and size to keratocyte nuclei seen in the anterior stroma (Figure 4-6). The length of subepithelial KDC nuclei was calculated in 3 cases. They ranged from 6 to 21.8µm with an average of 10.7±4.1µm (Mean±SD). In comparison, the keratocyte nuclei measured from 3.7 to 20.8µm with an average of 10.8±3.8µm (Figure 4-6). The difference in average nuclear length between the 2 groups was not statistically significant ($p=0.9$).

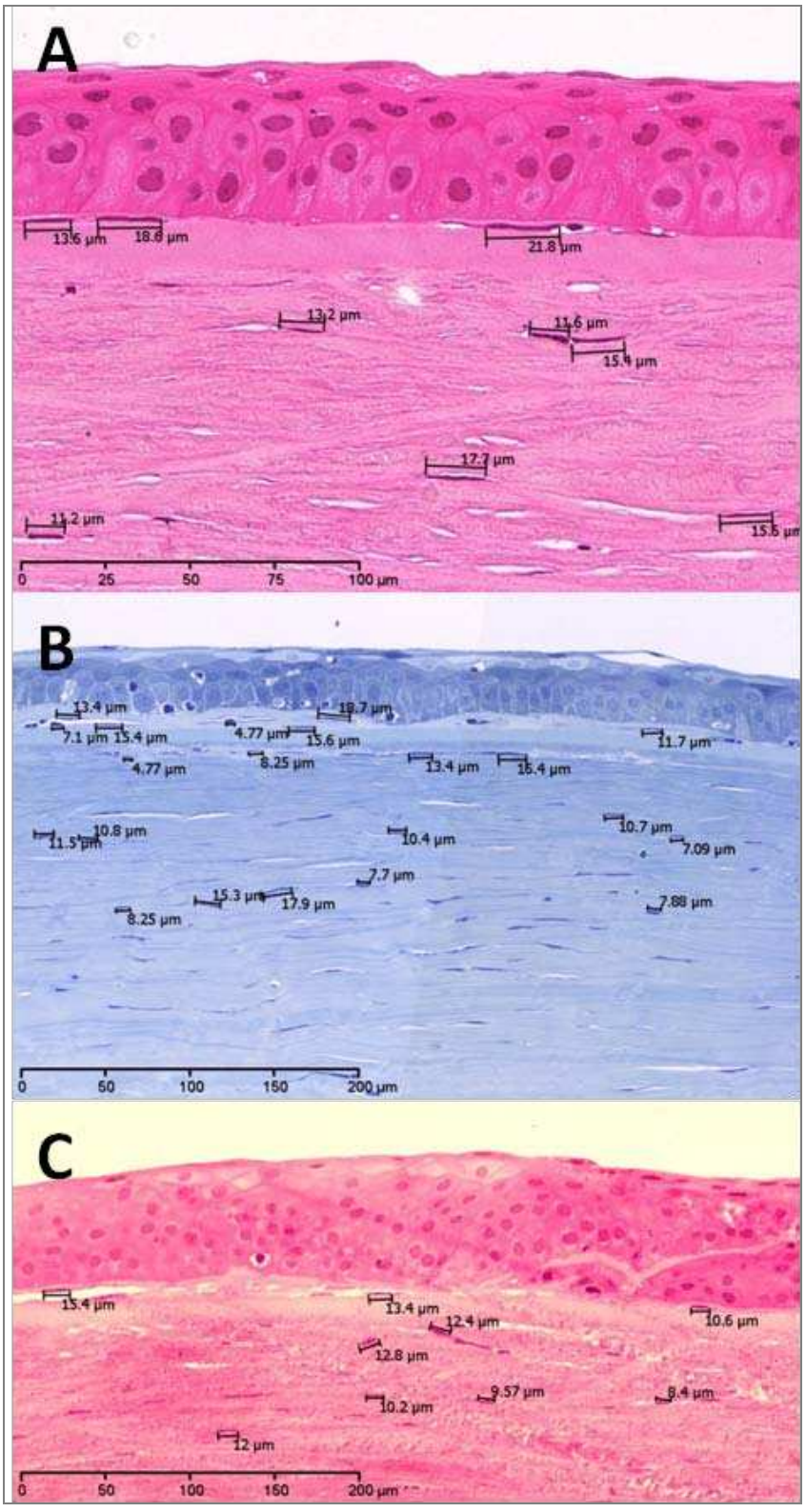

Figure 4-6: Light micrographs of corneas with subepithelial fibrosis in case 1(A), 2 (B) and 13 (C) to show nuclear morphometry. Subepithelial fibroblast nuclear size ranges from 6 to 21.8µm with an average of 10.7± 4.1µm (Mean ± SD) Keratocyte nuclear size ranges from 3.7 to 20.8µm with an average of 10.8 ± 3.8µm.(A & C = H&E stain, B = toluidine blue)

These cells were seen on histology and with IVCM in 7 of 13 (53.8%) full thickness corneal samples. The remaining 6 samples did not show these cells on histology nor by IVCM. IVCM alone illustrated these KDC in 4 of the 7 cases that had undergone DSEK and hence samples were not available for histological examination. Thus by IVCM subepithelial fibrous tissue was seen in 11 (55%) corneas of which 9 did not show any visible clinical scarring on slit lamp examination (table 2). Seven (63.6%) of the 11 FED cases showed evidence of such subepithelial scar tissue on IVCM.

4.3.3 Sub-basal corneal nerves

In 6 cases (30%) no sub-basal corneal nerves could be demonstrated in the oedematous central cornea by IVCM while in the remaining 14 patients (70%) the mean central sub-basal nerve density was significantly reduced to 4.47 ± 2.05 mm/mm² (Mean ± SD). When the oedema was sectorial, IVCM of the non-oedematous part showed the presence of sub-basal nerves that were not seen in the adjacent oedematous area (Figure 4-7).

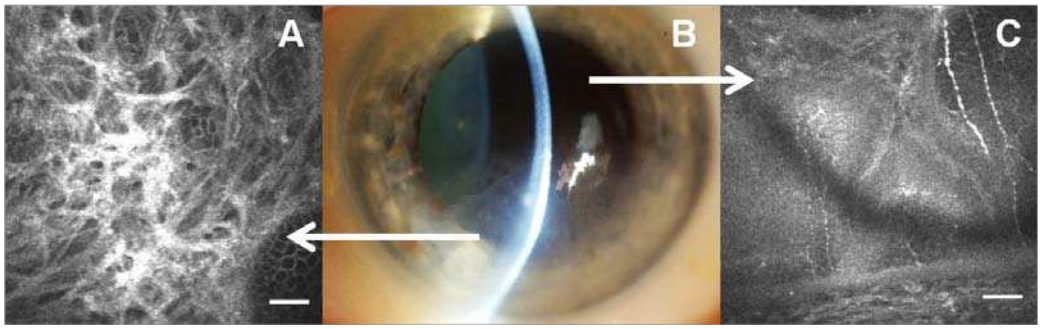

Figure 4-7: Slit-lamp corneal photograph (B) of case 17 shows marked oedema of the inferior half. IVCM image of oedematous parts (A) shows sub-epithelial fibrosis with no detectable sub-basal nerves that are visible on IVCM of superior non-oedematous area (C). IVCM focal depth 57 – 58µm. Scale bar 50µm.

4.3.4 Bowman's zone (BZ) and Anterior Stroma

IVCM features of the BZ showed a marked deviation from normal. Apart from the associated scar tissue described above, in all cases the fibrillary K-structures (Kobayashi et al., 2006) were absent while in 5 cases BZ presented a branching pattern of fine dark lines (Figure 4-8 A & B). Furthermore, fine or coarse granularity with a variable degree of reflectivity was noted in the anterior stroma in 12 of the 20 cases (Figure 4-8 C & D).

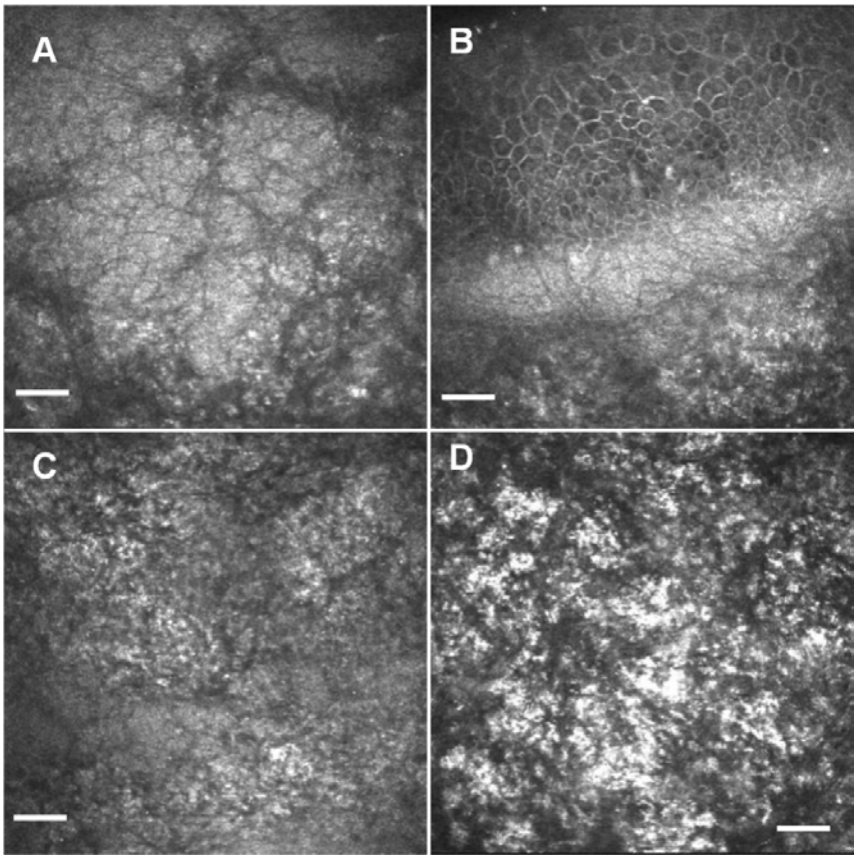

Figure 4-8: IVCM images of Bowman's zone and anterior stroma in corneal oedema. Fine arborizing dark lines could be seen in en face (A) and oblique (B) views replacing K-structures. Anterior stromal granularity was either fine (C) or coarse hyper-reflective (D) in appearance obscuring all keratocyte nuclei. Scale bar 50µm.

4.3.5 Stromal keratocyte changes

On IVCM stromal keratocytes showed hyper-reflective expanded cell bodies and processes with darker small intracellular “vacuoles” as well as extracellular “lacunae” seen as larger empty round to oval spaces in-between the keratocytes (Figure 4-9). The remarkable brightness of the cytoplasm in contrast to the surrounding extracellular matrix enabled sharp demarcation of the keratocyte borders with enhanced visualisation of interconnecting cell processes. The inter-cellular lacunae were about 40-100µm in diameter while the intra-cytoplasmic vacuoles were 10-20µm and located in the vicinity of the keratocyte nuclei. These changes were most obvious within midstromal layers at a focal depth of 200-400µm in 19 (95%) of the cases. In the FED group all corneas showed these morphological changes.

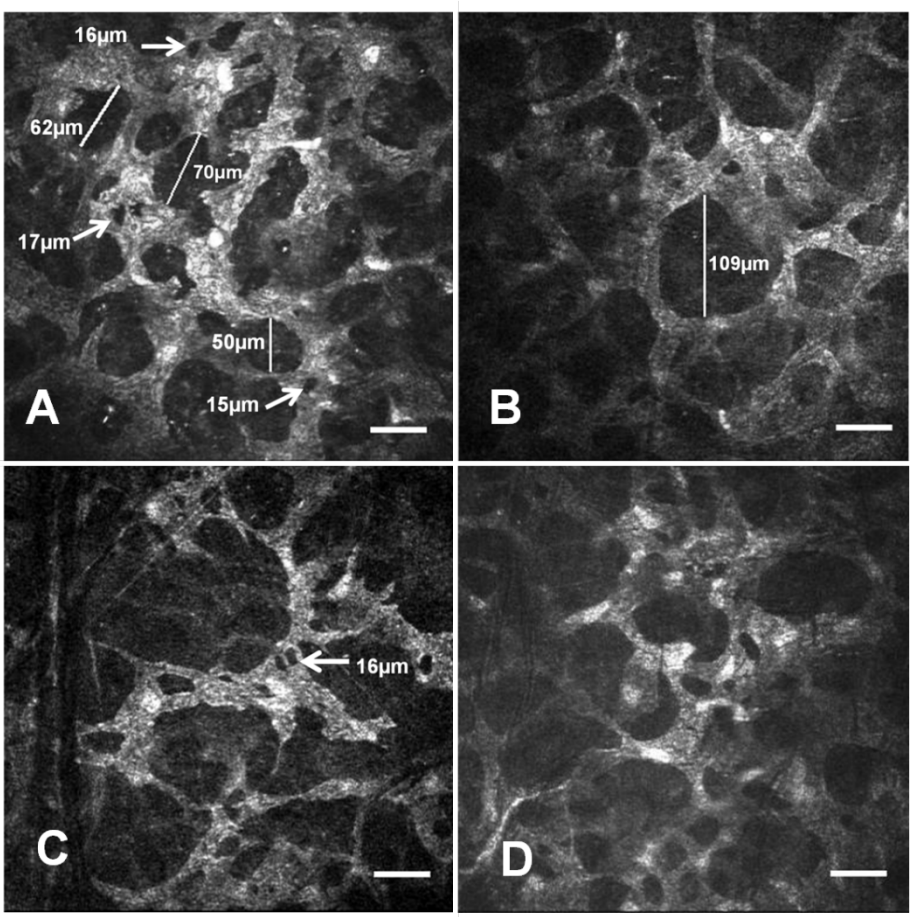

Figure 4-9: IVCM images of stromal keratocytes in corneal oedema illustrated in 4 cases (A case2) (B case1) (C case16) (D case5). Hyper-reflective expanded cell bodies and processes with reduced nuclear density. Dark small intracellular vacuoles (10 – 25µm) are visible close to the nuclei (arrows). Extracellular lacunae (between 40 and more than 100µm) were seen as larger empty round to oval spaces between the keratocyte processes. Scale bar 50µm.

Corresponding stromal changes could not be seen on histopathological sections examined by light microscopy. Transmission electron microscopy was performed in three samples (case 2, 16 & 17) where lipid material was seen within stromal keratocytes in one case (Figure 4-10) without evidence of cytoplasmic vacuoles or extracellular lacunae.

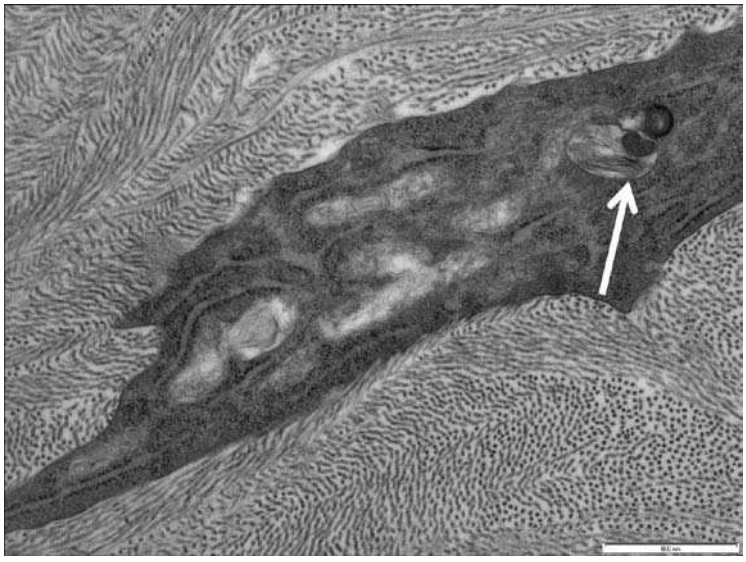

Figure 4-10: Transmission electron micrograph of oedematous cornea in case 16 illustrating a keratocyte within the stromal matrix. Intracytoplasmic deposits of lipid material (arrow) could be seen without evidence of vacuolation. Scale bar 600nm.

4.3.6 Stromal corneal nerves:

Tortuous curvilinear nerves were detected by IVCM in two cases within the midstromal (case 18) and deep layers (case 3) (Figure 4-11). The nerve width in these cases was 5 – 6µm. Neuronal structures could not be detected with histological preparation and staining methods used in this study.

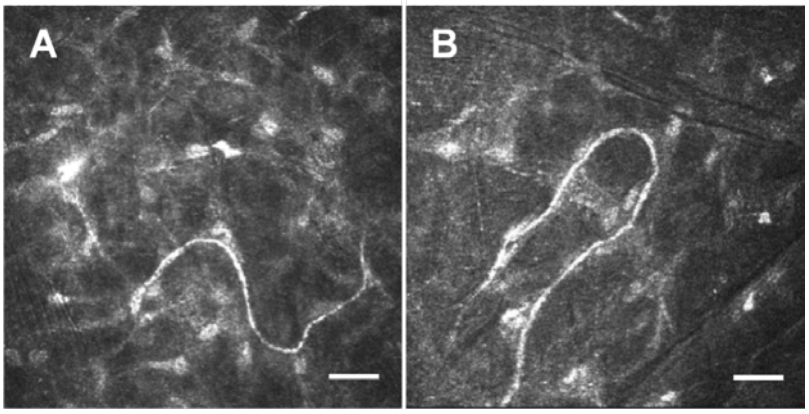

Figure 4-11: IVCM images showing tortuous stromal nerves in corneal oedema within 209µm (A, case 18) and 382µm (B, case 3) of stromal depth. Scale bar 50µm.

4.3.7 Descemet's membrane (DM) and Endothelium

On IVCM the classical strawberry-like pattern of DM and endothelium was seen in all cases of FED. This pattern comprised dark round 10 – 30 um areas with bright centres all within a bright background (Figure 4-12A). They corresponded to the excrescences of thickened DM seen on light microscopy. Another co-existing pattern of bright round 15 - 35µm shapes within dark circles was occasionally noticed (Figure 4-12B). Oblique IVCM views illustrated these projections arising from DM (Figure 4-12C). The normal endothelial pattern could not be identified on IVCM of FED patients.

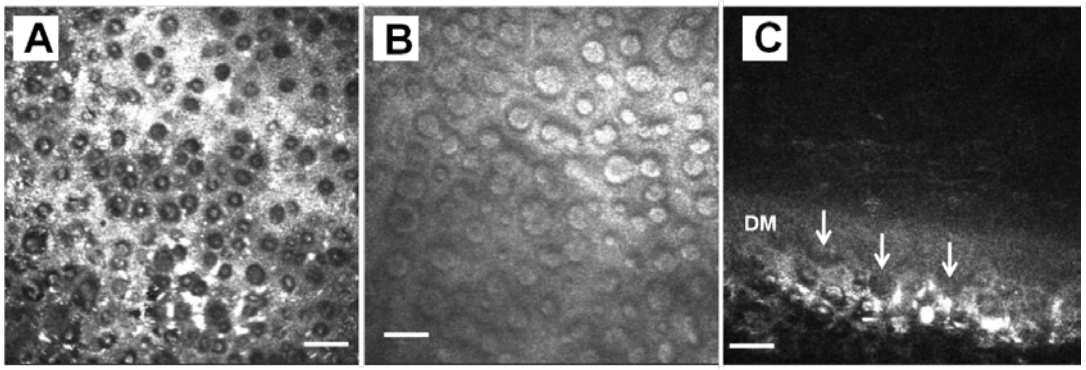

Figure 4-12: IVCM images of Descemet's membrane (DM) in FED-related corneal oedema in case 8 (A & C) and case 2 (B) . Dark round figures with bright centres representing wart-like projections form the classical strawberry-like pattern (A) seen in all FED cases. A novel coexistent pattern of bright round shapes within dark circles (B) was occasionally seen. Oblique view illustrated these excrescences as they extend from DM (C). Scale bar 50µm.

On histology of all 7 FED samples the DM was thickened and multilaminated with wart-like projections towards the endothelial side (Figure 4-13A). At certain areas these projections were seen buried

within an overlay of outer collagenous material identified by colour contrast between the two parts on H & E stain (Figure 4-13B). This collagenous overlay caused the endothelial side to be flat rather than corrugated. Endothelial cells were attenuated and reduced in number.

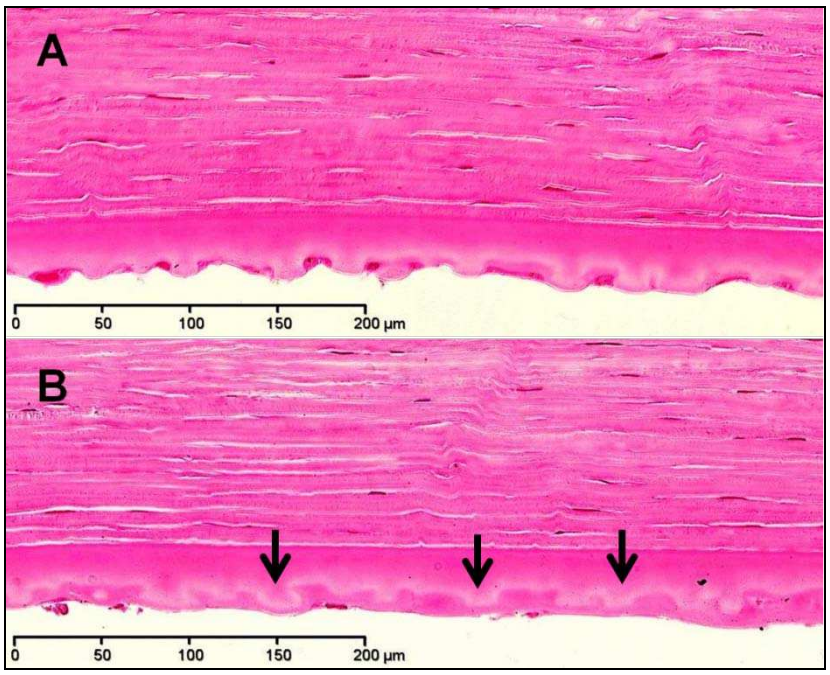

Figure 4-13: Light micrographs of Descemets membrane (DM) in Fuchs endothelial dystrophy (case 1) show thickening of the membrane with corrugated endothelial surface at one area caused by wart-like projections (A). In another area (B) DM excrescences are buried in excessive overlay of collagenous material resulting in flatter endothelial surface. The colour contrast between the two components gives a well demarcated outline to these projections (black arrows). (H& E stain)

In non-FED cases IVCM of endothelium showed loss of the normal honey-comb pattern with features of polymegathism, thickened or ill-defined cell borders, prominent nuclei and reduced cell density (Figure 4-14A). All these features were seen in 6 (including 3 pseudophakic eyes) of the 9 non-FED cases (12, 13, 16, 17, 18 and 19). Another pattern with occasional guttae shown as dark round spots could be

noticed in case 17 without evidence of hyper-reflective nuclei (Figure 4-14B). The average endothelial cell count (ECD) was remarkably low (512 ± 105 cells/mm² Mean ± SD).

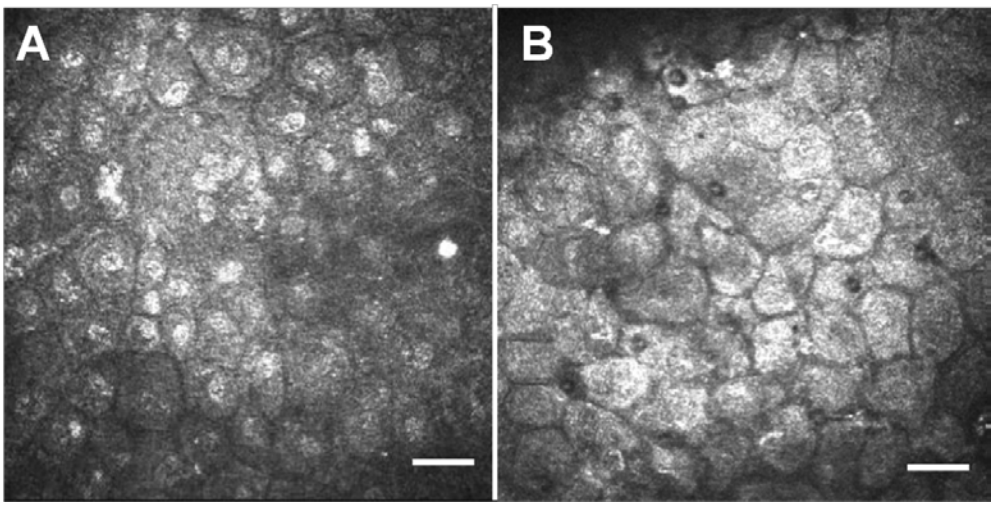

Figure 4-14: IVCM images of endothelium in non-FED related corneal oedema. Polymegathism, reduced cell density and prominent nuclei are seen in A. Occasional guttae represented by dark round spots can be seen in B (case 17) without visible nuclei. Scale bar 50µm.

On histopathology endothelial cells were reduced in number in all non-FED samples (Figure 4-15A). Descemet's membrane was thickened and multilaminated in one case (no. 17) mainly in the oedematous part of the cornea where occasional buried guttate excrescences were also noticed (Figure 4-15B) confirming those seen on IVCM (Figure 4-14B).

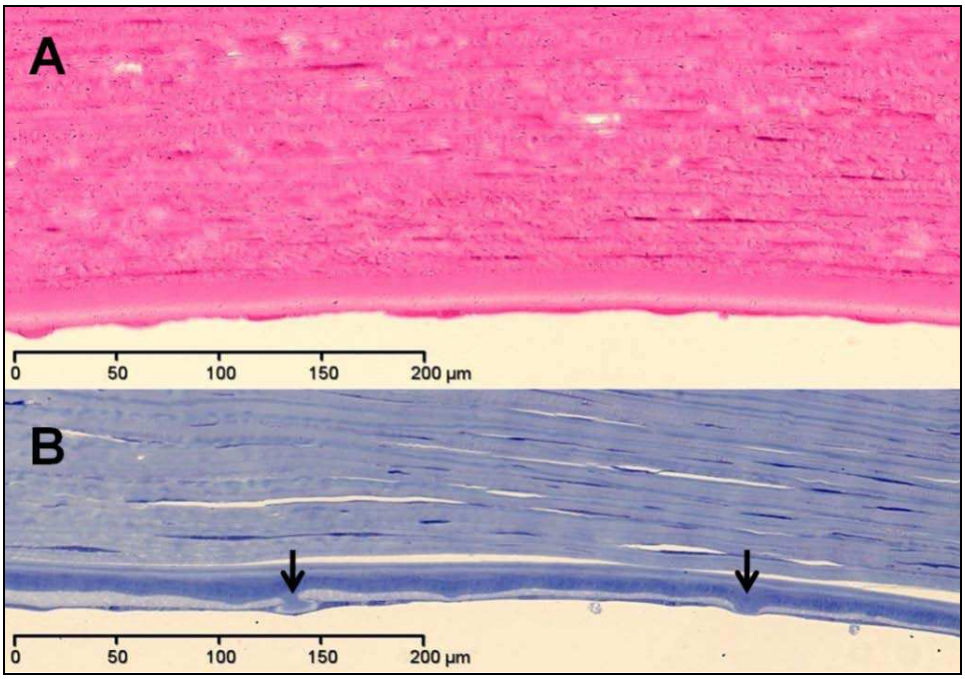

Figure 4-15: Light micrographs of Descemet's membrane (DM) and endothelium in non-FED related corneal oedema. DM thickening is seen in (A) as well as embedded excrescences (arrows) in B. (A stained with H&E. B with toluidine blue)

4.3.8 Control Group

IVCM findings in the control group showed normal patterns of basal epithelium, sub-basal nerves and Bowman's zone on en face and oblique views (Figure 4-16A-C). These findings were compared to histological features of anterior cornea studied in normal corneal tissue obtained from a donor cornea used for a DSEK procedure (case 18) (Figure 4-16D). Sub-basal nerve density of 19.3± 2.2 mm/mm² (Mean ± SD) was significantly higher than the average density in corneal oedema study group ($p = 0.001$).

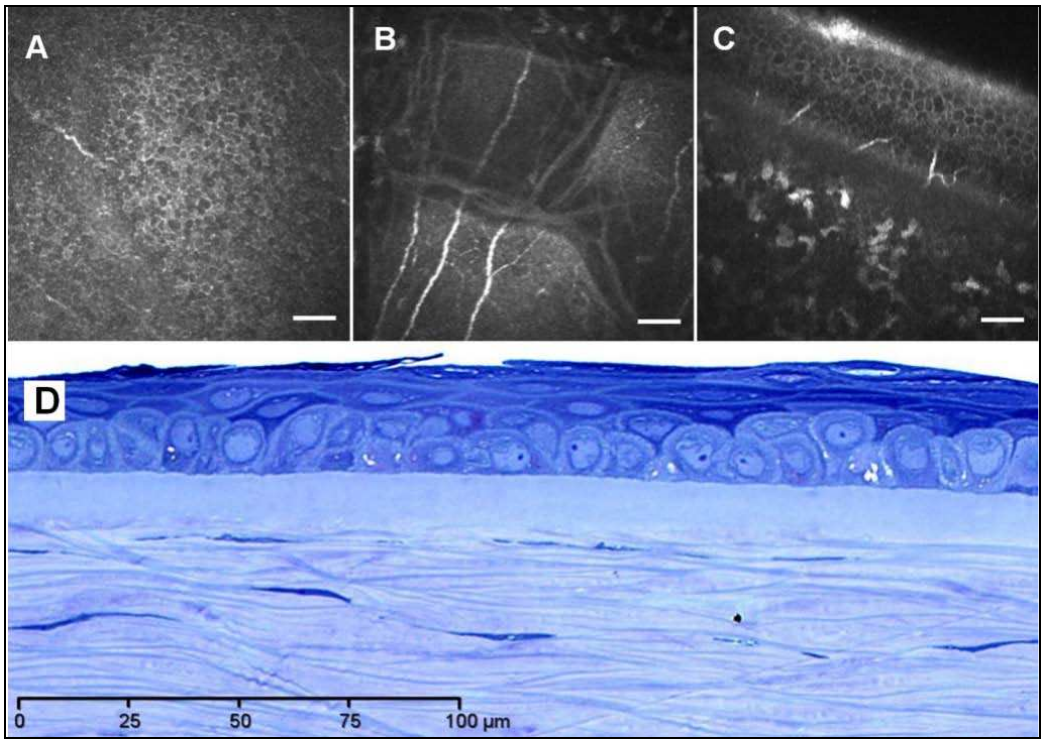

Figure 4-16: IVCM images and light micrograph of normal (control) cornea. Normal patterns of basal epithelium, sub-basal nerves and Bowman's zone with K-structures could be seen on en face views (A & B) in controls. Oblique view (C) confirmed intactness of anterior corneal layers. Histological cross-section in a normal cornea is shown in (D) stained with toluidine blue. Scale bar in IVCM 50µm.

No evidence of sub-basal fibrosis could be detected and stromal keratocyte nuclei were clearly demarcated with faint reflectivity of cell bodies and processes (Figure 4-17A). Due to the markedly reduced reflectivity, lacunae and vacuoles could not be readily identified throughout the stromal layers. Straight mid-stromal nerves (Figure 4-17B) with normal honey-comb pattern of the endothelium (Figure 4-17C) were clearly visible in the control group.

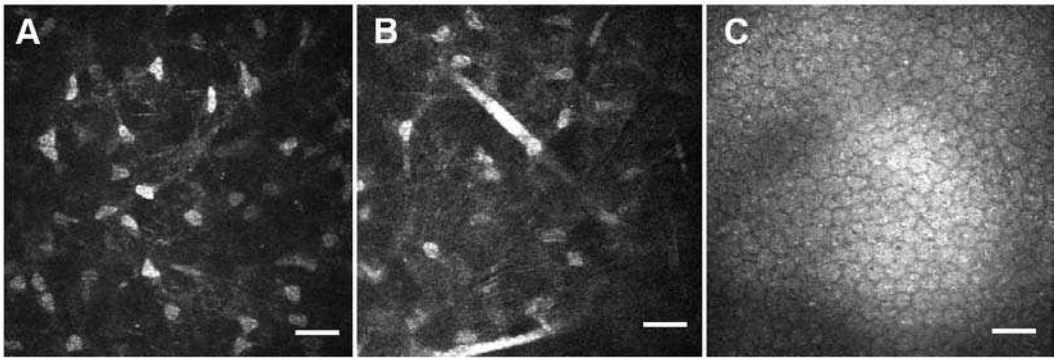

Figure 4-17: IVCM images of intact cornea in controls show normal reflectivity of stromal keratocytes (A), straight mid-stromal nerves (B) as well as normal honeycomb endothelial pattern (D). Scale bar 50µm.

4.3.9 Postoperative subgroup

Postoperative IVCM findings in 4 cases (no. 7, 9, 11 & 18 in Table 4-1) operated with DSEK are summarized in Table 4-4.

Table 4-4: Summary of postoperative IVCM findings in cases 7, 9, 11 & 18 following DSEK.

Case	Postoperative IVCM(months)	BCVA	Sub-epithelial 'fibroblasts' + cell density cell / mm² (Mean ± SD)	Sub-basal nerve density mm/mm² (Mean ± SD)	Bowman's zone/ Anterior stroma	Keratocyte changes
7	8	6/9	Visible (157 ±11) (Preoperative density= 155 ± 38)	No visible sub-basal nerves	No change from pre-operative state	Low reflectivity without visible lacunae. Well defined nuclei
9	20	6/9	Visible (243 ± 64) (Preoperative density= 239 ± 16)	9.8 ± 1.0 (Preoperative = 4.6 ± 1.8)	No change from Pre-operative state	Low reflectivity without visible lacunae. Well defined nuclei
11	7	6/9	Very few	7.5 ± 0.8 (Preoperative = 6.5 ± 1.1)	Intact	Low reflectivity without visible lacunae.
18	26	6/9	Visible with faint scar	3.2 ± 2 (Preoperative was nil)	No change from Pre-operative state	Low reflectivity, less obvious lacunae

4.3.9.1 Sub-epithelial fibrosis:

In 3 cases IVCM showed persistence of subepithelial fibroblasts that were associated with fibrous bands in one case (patient 18 in Table 4-1) despite improvement of BCVA to 6/9. The random distribution of these cells did not enable reliable cell density measurements. However, this value could be calculated in two cases (see Table 4-4) and did not show significant change postoperatively (Figure 4-18). The forth case (11) showed no evidence of subepithelial fibrosis 7months postoperatively, compared to just a few of these cells seen in the preoperative IVCM scan.

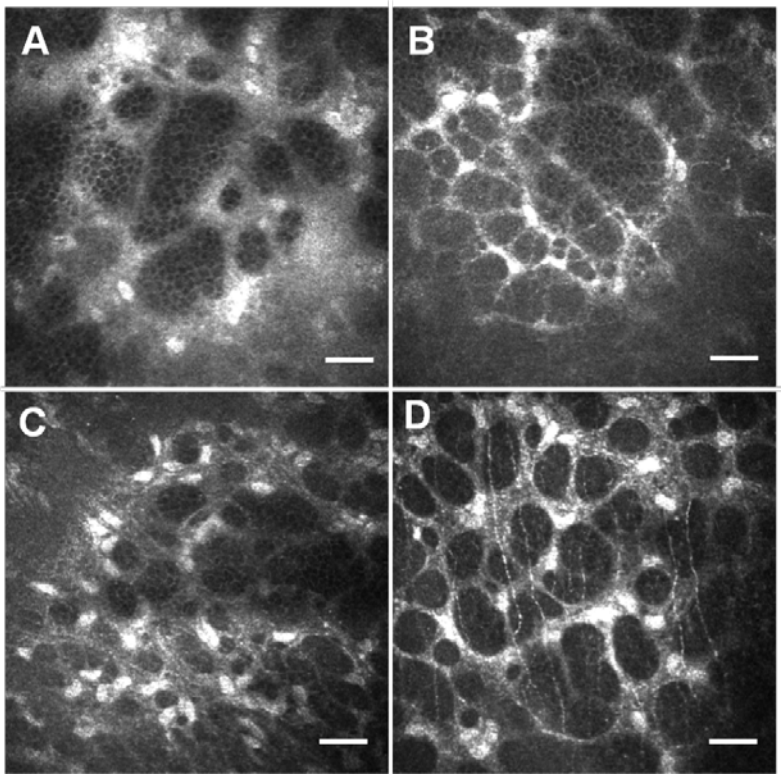

Figure 4-18: IVCM images of corneas in 2 cases who underwent DSEK to show sub-epithelial fibroblasts pre- (A & C) and post-operatively (B & D). Their densities are given in Table 4-4 and were not significantly different pre-and post-operatively. Scale bar 50µm.

4.3.9.2 Sub-basal nerves:

Post DSEK these nerves were detected in 3 cases and were not visible in one. The average central nerve density was 6.83 ± 3.35 mm/mm² (Mean ± SD) which was not significantly better than preoperative value of 4.47 ± 2.05 mm/mm². One case (18) who had no detectable sub-basal nerves preoperatively showed postoperative improvement to 3.2 ± 1.5mm/mm² whereas a third case (11) had an increase from 4.6 +/-1.8mm/mm² to 9.8 +/- 1mm/mm² (Mean+/- SD). Nevertheless, all these postoperative values were significantly below the average density of sub-basal corneal nerves in the control group.

4.3.9.3 Bowman's zone and anterior stroma:

Postoperative IVCM did not reveal any significant change in the features of Bowman's zone and anterior stroma from what was noticed preoperatively (Figure 4-8).

4.3.9.4 Stromal keratocyte changes:

Postoperatively all 4 cases showed a variable degree of reduction in reflectivity of stromal keratocytes compared to preoperative IVCM (Figure 4-19). This was more obvious in case 7 and 9 (Figure 4-19 E & F respectively) where lacunae and vacuoles were absent thus improving visibility of keratocyte nuclei that appeared well defined. This contrasted with cases 11 and 18 where the keratocytes were obscured by hyper-reflective cell bodies and processes (Figure 4-19G & H). Keratocyte nuclei

that were obscured preoperatively became more visible and well defined postoperatively.

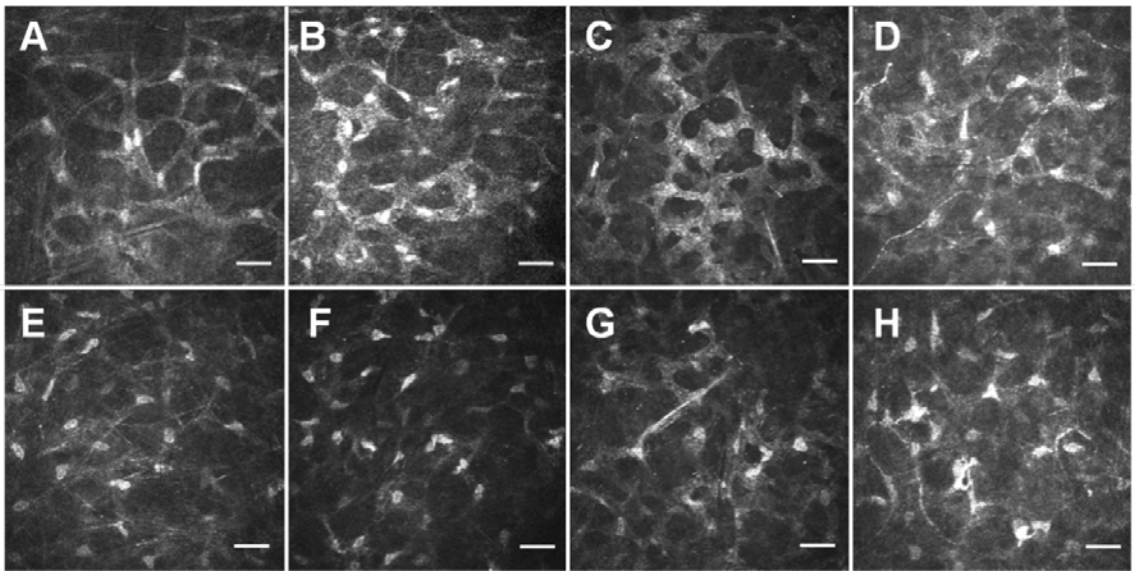

Figure 4-19: IVCM images of stroma before and after DSEK in 4 cases. A – D (case 7, 9, 11 & 18 respectively) show preoperative changes with hyper-reflective keratocyte processes and sharply demarcated lacunae. These were less obvious in corresponding postoperative frames (E – H) where the keratocyte nuclei were better visible due to low reflectivity of the keratocyte processes. Scale bar 50µm.

4.4 DISCUSSION:

IVCM has been widely used as a non-invasive imaging tool to study histological details of various corneal conditions. However IVCM studies of corneal oedema in FED and non-FED conditions have been limited in number and lack histopathological correlation (Mustonen et al., 1998a, Chiou et al., 1999b, Grupcheva et al., 2001b). In this study we attempted to illustrate definitive pathological changes in corneal oedema by IVCM and to correlate them with corresponding histopathological features.

4.4.1 Epithelial changes

At the epithelial level IVCM was able to illustrate cystic changes associated with epithelial oedema. IVCM through volume scans, showed these cysts to be located within the middle layers i.e. intraepithelial rather than subepithelial in 11 cases of this group with almost intact basal layer without evidence of separation from the basement membrane/Bowman's zone. Histological sections showed epithelial separation and bullae formation in 2 cases with no clear evidence of intraepithelial cystic spaces on light microscopy. Epithelial cells were otherwise histologically unremarkable at all layers. It is very likely that histological processing of tissue samples could result in tissue dehydration which might explain the finding of fewer epithelial cysts in histological sections compared to IVCM.

It is assumed in the literature that the accumulation of water and formation of cysts in the epithelium result in permanent changes (Iwamoto and De Voe, 1971, Eagle et al., 1989, Mustonen et al., 1998a). However, our study shows that water accumulation within epithelial layers does not represent or cause permanent disruption to these layers since surface epithelium clinically resumes its normal appearance following successful DSEK with subsequent improvement of corneal oedema. This was confirmed by showing unremarkable epithelium on IVCM post-DSEK in 4 of the cases.

4.4.2 Subepithelial 'fibroblasts'

This is the first study to document the presence of subepithelial fibroblasts in corneal oedema with IVCM. In this study sub-epithelial fibroblasts, alone and in association with fibrous tissue, were found to be comparable in location, shape, size and orientation in both IVCM and light microscopy of corresponding histological cross sections (Figure 4-3 & Figure 4-6). Their oval or rounded shapes on en face IVCM and their slender elongated appearance in histological cross-sections suggests that these nuclei have a flat discoid shape oriented parallel to the corneal surface (Figure 4-3A & B). Despite their random distribution IVCM showed similarity between these nuclei and keratocyte nuclei in terms of reflectivity, shape, size and orientation whereas cell morphometry on histological sections confirmed this similarity in size. It is worth considering that cross sections in histology do not always go through the maximum dimension of the nucleus, a feature that partly explains the variation in nuclear length measurements shown in histopathology slides (Figure 4-6) (Muller et al., 1995, Jester et al., 1994).

The undulating profile accorded to the basal epithelial layers by the accumulated sub-basal collagen tissue accounted for 'islands' of cells and scar tissue to be visualised at the same focal plane on IVCM. The en face images of this arrangement presented as a characteristic 'Swiss cheese' pattern (Figure 4-3D & Figure 4-18). Oblique views were even better in illustrating the exact plane of these cells within the anterior cornea

(Figure 4-3E & Figure 4-4F). On volumetric IVCM scan the bright structures representing en face images of cells/nuclei in the fibrous layer between Bowman's zone and basal epithelium extended for 12µm across the Z (volume) scans. This suggests that the cellular fibrous tissue was approximately 12µm thick and was distinguishable from the underlying Bowman zone and the overlying basal epithelial cells.

The narrow septa that were seen to extend into the epithelium were very similar to confocal images of 'fingerprint lines' of basement membrane dystrophy, reported previously (Labbe et al., 2006). In our cases of chronic corneal oedema, the patients did not have basement membrane dystrophy. The lines therefore relate to a rucking or folding of the basement membrane with associated sub-basal scar tissue and probably represent a similar pathology as seen in epithelial basement membrane dystrophy (Laibson, 1976, Labbe et al., 2006).

In previous IVCM work on FED similar patterns were noticed by other investigators but presented with speculative and inaccurate interpretation due to lack of histopathological correlation (Mustonen et al., 1998a, Guthoff et al., 2006).

Of the 11 FED patients these cells were visualized by IVCM in 7 cases (63.6%). None of these had clinically visible (slitlamp examination) corneal scarring preoperatively. IVCM and histopathology correlated well in all the 13 full thickness corneal samples with regard to presence or absence of fibroblastic changes.

In chronic corneal oedema sub-epithelial fibrosis is mentioned in the literature as a late feature resulting from epithelial separation in progressive corneal oedema (Iwamoto and De Voe, 1971, Eagle et al., 1989). In this study although all corneas with FED were devoid of clinically visible fibrotic changes, IVCM was able to detect the presence of subepithelial fibroblasts in 63.6% of them. This probably highlights the very early (subclinical) stage of subepithelial fibrosis in longstanding corneal oedema. These cells initially produce thin layer of collagenous material seen on light and electron microscopy sections, possibly causing the hyper reflective appearance surrounding the nuclear figures on IVCM (Swiss cheese pattern).

When corneal oedema persists this pattern disappears as the sheet of fibrous tissue between basal epithelium and Bowman's zone becomes more continuous. Some fibrous septa extend into the overlying epithelial layers resulting in epithelial irregularity with patterns resembling reduplication of basement membrane (Figure 4-3 G & I). At this stage the collagen fibres may present as a bright meshwork of interwoven fibres on IVCM (Figure 4-3K) while epithelial islands may be seen totally surrounded by fibrous tissue both histologically (Eagle et al., 1989) and on IVCM (Figure 4-3 G, L & M). In an early electron microscopic study of FED Iwamoto & De Voe mentioned similar findings of epithelial islands separated by continuations of subepithelial connective tissue (Iwamoto and De Voe, 1971).

The origin of these cells could be a fibroblastic transformation of stromal keratocytes that had migrated through breaks in Bowman's zone (Iwamoto and De Voe, 1971), or pre-existing mesenchymal stem cells at the subepithelial level. Such transformation could be stimulated by epithelial separation and bullae formation associated with progressively increasing corneal oedema (Eagle et al., 1989). In a recent study Said and co-workers illustrated the migration of stromal keratocytes through breaks in Bowman's zone to populate the amniotic membrane transplanted on corneas with bolluos keratopathy (Said et al., 2009).

In this study cell morphometry showed close similarity in nuclear size between these cells and anterior stromal keratocytes whereas the electron microscopic illustration of a break in Bowman's zone may also support the keratocyte origin of these cells. The exact role of these cells is unclear. They seem to be part of the wound healing response in bullous keratopathy. Interestingly, in a small subgroup we were able to confirm by IVCM the persistence of these cells following successful DSEK with clinical improvement of corneal oedema and BCVA.

Recently Morishige *et al* used Second Harmonic Generation microscopy with fluorescent probes to detect the presence of subepithelial fibrous tissues – not the cells – in corneal oedema and predict their time of accumulation relative to the duration of oedema (Morishige et al., 2009) Our study demonstrates the role of IVCM as a useful in vivo non-invasive real-time imaging method to detect the presence of subepithelial

fibroblasts even in the early stages of corneal oedema. The cells appear early in the pathogenesis of corneal oedema as they could be detected even before endothelial transplant was indicated especially in FED where the BCVA was 6/9 (data not presented).

4.4.3 Sub-basal corneal nerves

These nerves have been studied extensively with IVCM by other investigators (Patel and McGhee, 2005, Oliveira-Soto L and N., 2001). In this study sub-basal nerves were absent in 30% of the cases and reduced to 4.47 ± 2.05 mm/mm² (Mean ± SD) in 70%. This is significantly lower than the value of 19.3 ± 2.2 mm/mm² (Mean ± SD) in the control group which is comparable to the value of 21.6mm/mm² reported by other investigators in normal corneas using HRTII-RCM similar to the one used in this stud (Patel and McGhee, 2005). Depressed corneal sensitivity in FED was first mentioned by Professor Fuchs when he described the condition for the first time in 1910 (Fuchs, 1910). Yet IVCM studies on FED and non-FED related corneal oedema did not cover these changes in detail (Grupcheva et al., 2001b, Mustonen et al., 1998a, Chiou et al., 1999b). In the small postoperative subgroup it was clear that sub-basal nerves were better visualised on IVCM with significant increase in nerve density following successful DSEK (see Table 4-4). However the overall average nerve density was not significantly better than preoperative value.

4.4.4 Bowman's zone and anterior stromal Granularity:

Kobayashi et al described certain IVCM patterns of Bowman's zone in the normal cornea, which they termed K-structures using HRTII-RCM (Kobayashi et al., 2006). These fibrillar structures were best seen with this type of confocal microscope machine and considered to represent one of the features of the intact normal cornea. In our study Bowman's zone lost this reflective pattern in all cases of corneal oedema possibly due to the effect of excessive water content disrupting the normal arrangement of collagen fibrils. This effect is thought to involve the anterior stromal layers as well giving rise (in 60% of cases) to granularity of variable coarseness and reflectivity, which frequently obscured all anterior keratocyte nuclei. In 5 of the cases Bowman's zone showed fine dark lines of dendritic pattern previously described by Jester et al as basement membrane of basal epithelium (Jester et al., 1992). In this study the oblique view showed this pattern throughout the whole Bowman's zone thickness suggesting that it represents the Bowman's zone rather than the basement membrane which is much thinner than this layer. Postoperatively these changes remained irreversible despite remarkable improvement in BCVA possibly indicating the presence of permanent degenerative stromal changes with undetermined or no clinical significance.

4.4.5 The morphological changes of keratocytes

On IVCM keratocyte changes were seen practically in all cases of corneal oedema. Lacunae and smaller intracellular vacuoles were visualised on IVCM in close proximity to keratocyte nuclei along with hyper-reflective expanded keratocyte cell bodies and processes. All these changes were better visualised in mid-stromal rather than anterior stromal layers possibly due to the higher keratocyte density with straight interwoven collagen fibrils in the anterior layers (Muller et al., 2001).

Mustonen *et al* mentioned the presence of stromal lacunae as an IVCM finding in 24% of corneas with FED (Mustonen et al., 1998a) without giving further details of keratocyte morphology. They used a white light slit scanning confocal microscope (SSCM) with poor resolution images compared to the yield of HRTII-RCM used in this study. Postoperatively stromal keratocytes were better visible (Figure 4-19E & F) and tended to show less brightness approaching the normal pattern seen in the control group (Figure 4-17A). Thus it can be inferred that these keratocyte changes are reversible. Histologically these changes could not be linked to distinct features on light microscopy in our study. As these lacunae represent water accumulation within stromal lamellae it is possible that tissue dehydration through the use of fixatives could account for the lack of corresponding changes on light microscopy. Even when frozen section processing was conducted in part of the sample taken from case 2 to avoid the fixatives no evidence of stromal hydro-accumulation could be

noticed. Electron microscopy (EM) revealed intracytoplasmic deposition of lipid material (Figure 4-10). However, other EM studies on FED (Iwamoto and De Voe, 1971, Yuen et al., 2005) and bullous keratopathy (Akhtar et al., 2001) have recorded changes consistent with IVCM findings of our study. Iwamoto & De Voe (1971) described the keratocytes in one FED case to be fatter than normal whereas Akhtar *et al* (2001) and Yuen *et al* (2005) mentioned intracellular vacuoles within degenerate keratocytes as well as electron lucent lacunae throughout the stroma in bullous keratopathy.

The most likely cause of the increased reflectivity of the keratocytes observed in corneas with oedema is keratocyte activation. One other possibility is that high water content within stromal extracellular matrix has made the keratocytes with their interconnecting processes appear brighter/hyper-reflective compared to normal. Coexisting intracellular oedema might explain the remarkable expansion and hyper-reflectivity of stromal keratocytes in corneal oedema. Keratocyte activation is a term commonly used to describe hyper-reflective keratocytes in IVCM literature (Vesaluoma et al., 2000, Sonigo et al., 2006). The process of activation is well known in the literature to describe the response of stromal keratocytes to a variety of corneal injuries (physical, chemical or infectious) (Fini, 1999). This response involves transformation of keratocytes into repair fibroblasts that was studied by several investigators like Kitano and Goldman (Kitano and Goldman, 1966) and

Matsuda and Smelser (Matsuda and Smelser, 1973) using the rabbit model as well as Jester *et al* in a cat model (Jester et al., 1995).

The first noticeable sign of activation is the increase in keratocyte size in association with other changes in cytoplasmic organelles and the nucleus. This is also associated with synthesis of substances like integrins, fibronectin and matrix metalloproteinases required for wound healing. As progressive stromal oedema eventually involves the epithelium it is possible that the epithelial injury induces keratocyte activation. Previous studies in the context of refractive surgery have shown that keratocyte activation (and subsequent scarring) is more with PRK than after LASIK, where the epithelium is intact (Park and Kim, 1999, Mohan et al., 2003, Ambrosio and Wilson, 2003). In this study we have demonstrated that the elongated keratocyte derived cells, presumably fibroblasts, were located in the subepithelial region in 55% of the cases (63.6% of FED cases) (Table 4-3) and probably represent cells that have originated from activated stromal keratocytes. Recently another study by Morishige *et al* (2009) suggested possible fibroblastic transformation of stromal keratocytes in 10 of 31 cases of corneal oedema using immunofluorescent probes (Morishige et al., 2009) thus giving further evidence of the existence of transformed keratocytes in the oedematous corneal stroma. The response to successful DSEK with clinical improvement in corneal clarity and vision has been traced in a small subgroup in this study with a tendency to restore normal IVCM stromal patterns partially or completely

(Table 4-4 & Figure 4-19). However this needs further study in a larger group over a longer postoperative follow up period.

4.4.6 Descemets membrane and Endothelium

On light microscopy Descemets membrane appeared thickened and multilaminated with guttate excrescences as well as reduced endothelial cells in all FED corneal samples. This correlated well with IVCM, which illustrated the classical strawberry–like pattern in all FED cases with total obscuration of endothelial cells borders. This appearance is well described in the literature as hypo-reflective round images, 10 – 30µm large with bright centres all within a hyper-reflective background (Mustonen et al., 1998a, Chiou et al., 1999b, Vincent et al., 2005). In this study we noticed another co-existing pattern of Descemets membrane guttae by IVCM. They appeared as hyper-reflective round figures within dark circles about 15 – 35µm large. This variation in reflectivity patterns could be explained by variable shapes and sizes of these excrescences as well as their nature of being bare in some areas and buried in others.

In non-FED cases the above patterns were not noticed on IVCM. Endothelial cell changes including polymegathism and prominent hyper-reflective nuclei as well as reduced cell density, were observed. This clear IVCM imaging of endothelium could be explained by the almost normal thickness of Descemets membrane with absence of warty projections

seen in histological sections of this subgroup. Further work is needed to compare morphological changes in degenerate endothelium on IVCM with those seen with scanning electron microscopy of endothelial sheets obtained via DSEK in order to have better interpretation of IVCM findings.

Our study was not designed to correlate the severity of changes with the duration of edema, however in this study 3 FED cases presented with symptomatic corneal edema within less than 1year following successful cataract operation, a forth case in 2years and the fifth case after 5.5years. In non-FED cases all those with PBK were symptomatic in the first postoperative year. However Descemets membrane / endothelial changes comparable to those seen in FED were illustrated in case 17 only.

4.5 CONCLUSION

This is the first study where IVCM features of FED and non-FED corneal oedema are well compared to histopathological findings. It demonstrates the versatility and utility of IVCM to detect fine and early pathological changes associated with this condition in a non-invasive real-time manner. Histological changes related to subepithelial fibroblasts, reduced sub-basal corneal nerves and stromal keratocyte morphology have been well documented in this study. With increasing popularity of DSEK this work supports the role of IVCM in quantitative evaluation of histological features in corneal oedema both preoperatively and throughout post-

DSEK follow up period for better correlation with clinical outcomes. The persistence of histological changes with regard to sub-basal nerves, subepithelial fibroblasts and hyper-reflective keratocytes, in the host cornea after successful endothelial transplantation is important. It suggests that even though the oedema clears and corneal transparency improves, it does not return to a completely normal state. The implications of the persistent changes are unclear at this stage but longer term follow up of a larger number of patients will improve our understanding of these changes.

Chapter Five

5 In Vivo Confocal Microscopy of Keratoconus with Histopathological Correlation.

5.1 BACKGROUND:

Keratoconus is a well known and relatively common shape-deformity of the cornea. The histological changes in corneal structure are well documented (Teng, 1963, Scroggs and Proia, 1992, Fernandes et al., 2008). The mechanism by which the cornea becomes ectatic to produce a progressive conical deformity has not been fully established. Histopathological work has yielded some clues. Teng and co-workers believed that the process starts with damage of the basal corneal epithelium that results in degradation of the basal lamina and the Bowman's zone through the effect of released proteases (Teng, 1963). On the other hand Scroggs et al hypothesized that the pathological mechanism initially starts with stromal thinning that is consequently followed by abnormalities in Bowman's zone and epithelium (Scroggs and Proia, 1992).

The diagnosis of keratoconus is essentially clinical. Early cases are difficult to detect but corneal topographic devices have enabled us to

diagnose early keratoconus using curvature, elevation and corneal thickness related nomograms (Rabinowitz, 1996). Topography also allows close monitoring of progression throughout life (Ambrosio et al., 2006). In vivo confocal microscopy (IVCM) provides a non-invasive imaging method that shows changes in the cornea at a cellular level effectively giving histological features in a living cornea. Although comparison of IVCM finding with light microscopic histology has been performed in the past it was only done on two cases and carried out at a time when the resolution of the IVCM images was relatively poor (Hollingsworth et al., 2005a, Efron and Hollingsworth, 2008).

In this study we examined 11 cases of keratoconus where IVCM was carried out and subsequently had corneal transplantation providing tissue for histological examination. We report our findings picked up with confocal imaging and their correlation with histology.

5.2 DESIGN:

Observational case series with evaluation of diagnostic technology

5.3 METHODS:

Eleven eyes of 11 patients (2 females and 9 males; age range of 20 – 39years) diagnosed as keratoconus, attending the Queen's Medical Centre, Nottingham, UK, were included in the study. The diagnosis was based on clinical signs seen on slitlamp and/or topography. These patients were treated with either penetrating keratoplasty (PK) or deep

anterior lamellar keratoplasty (DALK) due to contact lens intolerance and poor best corrected visual acuity. Best corrected visual acuity (BCVA) was recorded for all patients. IVCM examination was carried out at 24 to 48 hours prior to surgery. Figure 5-1 illustrates slitlamp photographs of 6 representative corneas of the group.

Table 5-1 summarises the main demographic and pre-operative clinical features of the study group.

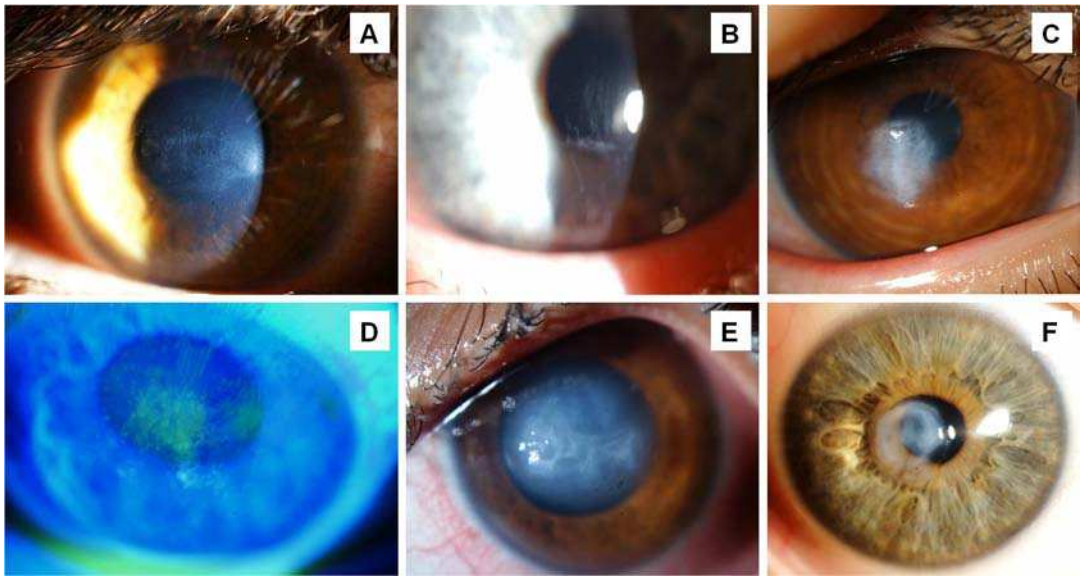

Figure 5-1: Slitlamp photographs of 6 corneas for patients with keratoconus. A – C show corneas with various patterns of apical scarring in cases 3, 5 and 6 respectively. D illustrates epithelial changes in case 7 highlighted with fluorescein staining. E & F show central corneal scarring following resolved hydrops in case 8 & 11 respectively.

Table 5-1: Demographic and preoperative clinical features of 11 cases with keratoconus recruited for "in vivo confocal microscopy" study.

No	Age/ Sex/ Eye	BCVA	Corneal Scar	Resolved Hydrops	Operation
1	32/ M/ R	6\36	N	N	DALK
2	39/ M/ L	6\36	N	N	DALK
3	25/ F/ R	6\60	Y	N	DALK
4	30/ M/ L	6\60	Y	N	DALK
5	24/ M/ L	6\24	Y	N	DALK
6	20/ M/ R	6\12	Y	N	DALK
7	30/ F/ R	6\18	Y	N	DALK
8	22/ M/ L	6\18	Y	Y	PK
9	35/ M/ R	6\9	Y	Y	PK
10	23/ M/ R	2\60	Y	Y	PK
11	30/ M/ R	6\36	Y	Y	PK

BCVA= Best Corrected Visual Acuity. DALK= Deep Anterior Lamellar Keratoplasty. PK= Penetrating Keratoplasty

5.3.1 In Vivo Confocal Microscopy:

IVCM was carried out on all cases as described in (chapter two) to scan the central 5-6mm zone of cornea. Paracentral scanning was performed in cases 2, 3, 10 and 11. Images were captured at each point through the thickness of the cornea, giving a total number of 200-300 frames per cornea. Volumetric mode of scan was performed to illustrate the level of structural changes within various corneal layers.

5.3.2 Histopathology:

Full or partial thickness corneal samples (from PK or DALK) were processed for light microscopy as described in chapter two. Slides were

viewed with the Nanozoomer Digital Pathology scanner (NDP C9600 series, Hamamatsu Photoincs K.K. Hamamatsu city, Japan) using the associated software for high magnification views and cell morphometry. Histopathological findings of specimen were compared to features of corresponding IVCM sections to establish a reliable correlation.

Cell morphometry: Where cellular abnormalities were detected, cell morphometry with the inbuilt software was performed to measure the basal epithelial nuclear size. This was done in 5 samples with features of regenerative atypia. It was also done in 2 samples with normal looking corneal epithelium that was found to be unremarkable clinically on slit lamp and IVCM, for the purpose of comparison. These measurements were compared to those already done in two samples of corneal intraepithelial neoplasia (CIN) (a condition known to have increased basal cell nuclear size) already reported in chapter three. Morphometry of the nuclei was carried out on basal cells that were enlarged or elongated with obvious cytoplasmic vacuoles and prominent nucleoli. In all groups the selection was focused on the biggest nuclei to compare the maximum size that can be found in each group (Figure 5-5). The values obtained from the three groups were analysed with one-way ANOVA test to check the significance of difference in nuclear size among these groups. P value ≤ 0.05 was considered to be statistically significant.

5.4 RESULTS

BCVA ranged between 6/12 – 2/60 where 9 cases had visible corneal central scar ranging from fine linear subepithelial fibrosis (Figure 5-1A&B) to fully established opaque stromal scar (Figure 5-1C, E & F). 4 cases had history of acute hydrops that resolved prior to keratoplasty (see Table 5-1). Associated epithelial keratopathy in the form of 'Hurricane keratopathy' (Dua and Gomes, 2000) was occasionally seen (Figure 5-1D). Two cases had no visible corneal scar or epithelial changes on slitlamp. Four cases underwent PK while 7 had DALK. Of the 11 corneal samples obtained, 4 were of full thickness and 7 of subtotal anterior stroma, all processed for histological examination by light microscopy.

Table 5-2 summarizes the IVCM and light microscopic (LM) findings in 11 cases of the study group. Table 5-3 presents a descriptive summary of the pathological changes in keratoconus seen with IVCM and light microscopy.

Table 5-2: Summary of IVCM and histological findings in 11 cases with keratoconus.

No		Epithelial changes			BZ		Stroma		DM breaks
		RA	Irregularity	Thinning	Breaks	Loss	Scar	Folds	
1	IVCM	N	N	N	Y	N	N	Y	N
	LM	N	N	N	N	N	N	N	N
2	IVCM	N	N	N	Y	N	N	Y	N
	LM	N	N	N	N	N	N	N	N
3	IVCM	Y	Y	N	Y	Y	Y	Y	N
	LM	Y	Y	N	Y	Y	Y	N	N
4	IVCM	Y	Y	N	Y	N	Y	Y	N
	LM	Y	Y	N	Y	N	Y	N	N
5	IVCM	Y	Y	N	Y	N	Y	Y	N
	LM	Y	Y	N	Y	N	Y	N	N
6	IVCM	N	Y	Y	Y	N	Y	Y	N
	LM	N	Y	Y	Y	N	Y	N	N
7	IVCM	Y	Y	N	Y	N	Y	Y	N
	LM	Y	Y	N	Y	N	Y	N	N
8	IVCM	Y	Y	Y	Y	Y	Y	Y	Y
	LM	Y	Y	Y	Y	Y	Y	N	Y
9	IVCM	N	Y	N	Y	N	Y	N	N
	LM	N	Y	N	Y	N	Y	N	N
10	IVCM	N	Y	N	Y	N	Y	Y	N
	LM	N	Y	N	Y	N	Y	N	N
11	IVCM	Y	Y	Y	Y	N	Y	Y	N
	LM	N	Y	Y	Y	N	Y	N	N

BZ= Bowman's zone. DM= Descemet's membrane. LM= light microscopy.
N= Nil. RA= Regenerative atypia. Y= Yes

Table 5-3: Descriptive summary of the pathological changes in keratoconus noticed on light and in vivo confocal microscopy.

Pathological changes (n / %)	Light microscopic features	IVCM patterns
Epithelial changes:		
Regenerative atypia (5 / 45%)	Enlarged / elongated basal epithelial cells with cytoplasmic vacuoles, vesicular nuclei and prominent nucleoli.	Basal epithelial cells with hyper-reflective prominent nuclei.
Irregularity (9 / 82%)	Undulating profile of basal epithelium. Basal epithelial down-growth filling Bowman's zone defects. Increased epithelial thickness	Islands / sheets of corneal epithelium interrupted by bright bands / areas of scarring. Hyper-reflective nuclear figures (of fibroblasts) can be seen occasionally next to scar areas.
Thinning (3 / 27%)	1-2 cell layer epithelium with thin, enlarged cells overlying stromal scars.	Large epithelial cells with bright nuclei, occasionally arranged in a whorled pattern, overlying hyper-reflective subepithelial scar.
Bowman's zone:		
Breaks (9 / 82% on light microscopy) (11 / 100% on IVCM)	Small (<20µm) to large (>100µm) gaps filled with epithelial downgrowth, acellular stromal matrix or migrating keratocytes.	Dark bands about 10-100µm wide within hyper-reflective Bowman's zone arranged in narrow crack-like pattern with occasional circular disposition or wider straight bands though which keratocyte nuclei can be visualised.
Extensive loss (2 / 18%)	Corneal epithelium growing directly on underlying stroma.	Basal epithelium, sub-basal nerves and anterior stromal keratocyte nuclei are all visualised at the same focal plane on en face images with no features of Bowman's zone.
Stroma		
Scarring		
Superficial lenticular (3 / 27%)	Fibrous tissue in-between basal epithelium and Bowman's zone. Frequent fragments of Bowman's zone are seen within stromal layers.	Finger-like bright extensions from the main scar tissue surrounding sheets of basal epithelium.
Deep stromal (1 case)	Areas of extreme stromal thinning throughout the corneal section.	Moderately hyper-reflective stromal background with randomly distributed brighter nuclei.
Folds (10 / 90%)	No evidence on light microscopy.	Alternate dark and bright parallel stromal bands in various directions virtually interrupting midstromal nerve courses.
Descemet's membrane breaks (1 / 0.1%)	Gaps with rolled edges	Dark well defined areas with sharp edges at the level of Descemet's membrane.

5.4.1 Epithelial changes:

Remarkable changes involving the epithelial layer thickness and cell morphology were noticed histologically and on IVCM in 9 (81%) cases.

5.4.1.1 Regenerative atypia

On histology in 5 cases (3, 4, 5, 7 & 8) (45%) morphological changes consistent with regenerative atypia were noticed mainly among the basal epithelial cells. These features included variable degree of pleomorphism, cell elongation and cytoplasmic vacuolation as well as relatively enlarged vesicular nuclei with dispersed chromatin and prominent nucleoli (Figure 5-2 A-C). These changes were obvious even when Bowman's zone was intact (Figure 5-2C). However features indicative of dysplasia, namely loss of polarity and mitotic figures were not observed in histological sections.

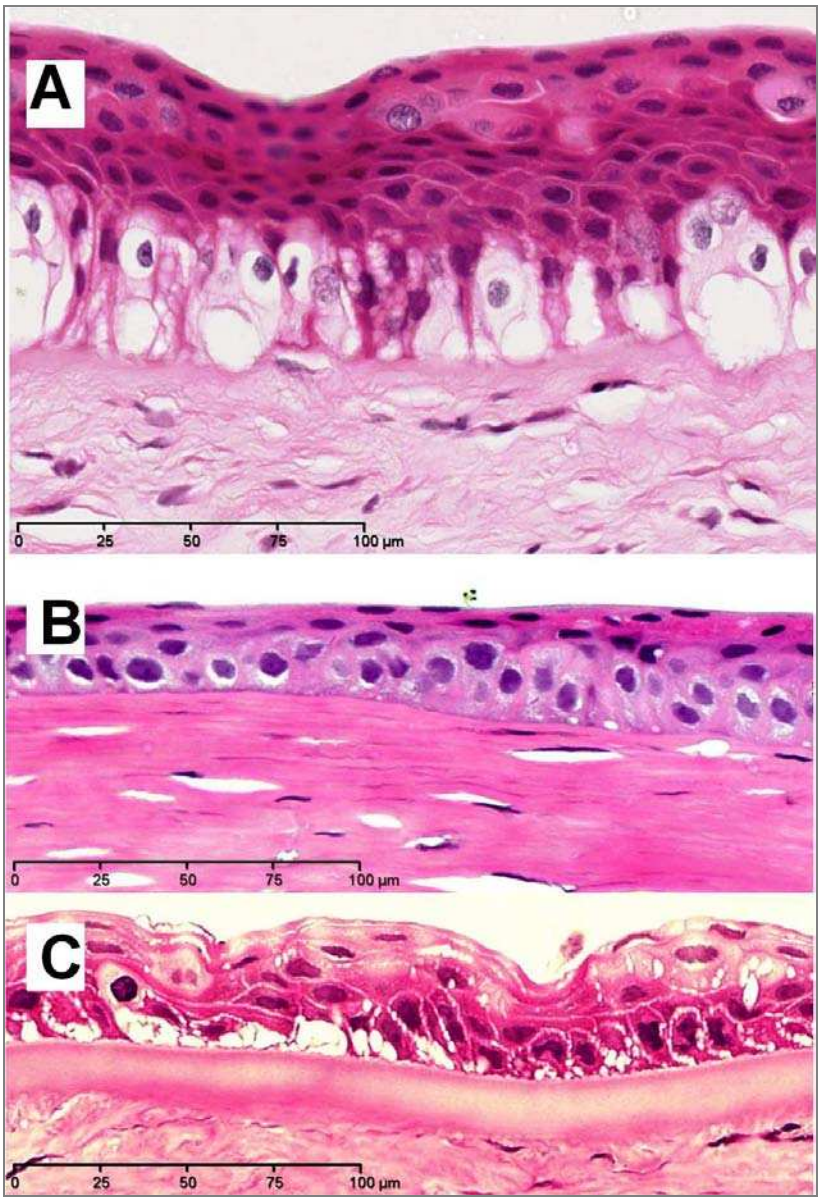

Figure 5-2:Light micrographs show epithelial changes in keratoconus consistent with regenerative atypia. Basal cell elongation and vacuolation with vesicular enlarged nuclei can be seen in A (case 3) & B (case 8) with subepithelial scar. Bowman's zone is missing in A & B but present in C. Similar epithelial changes were seen even with an intact Bowman's zone in C (case 5).

On IVCM for the same cases basal epithelial cells showed bright dots 4 – 9µm in size representing prominent nuclei with moderately ill-defined

cell borders (Figure 5-3). The sub-basal corneal nerves were clearly visualized in all cases (Figure 5-3B – D).

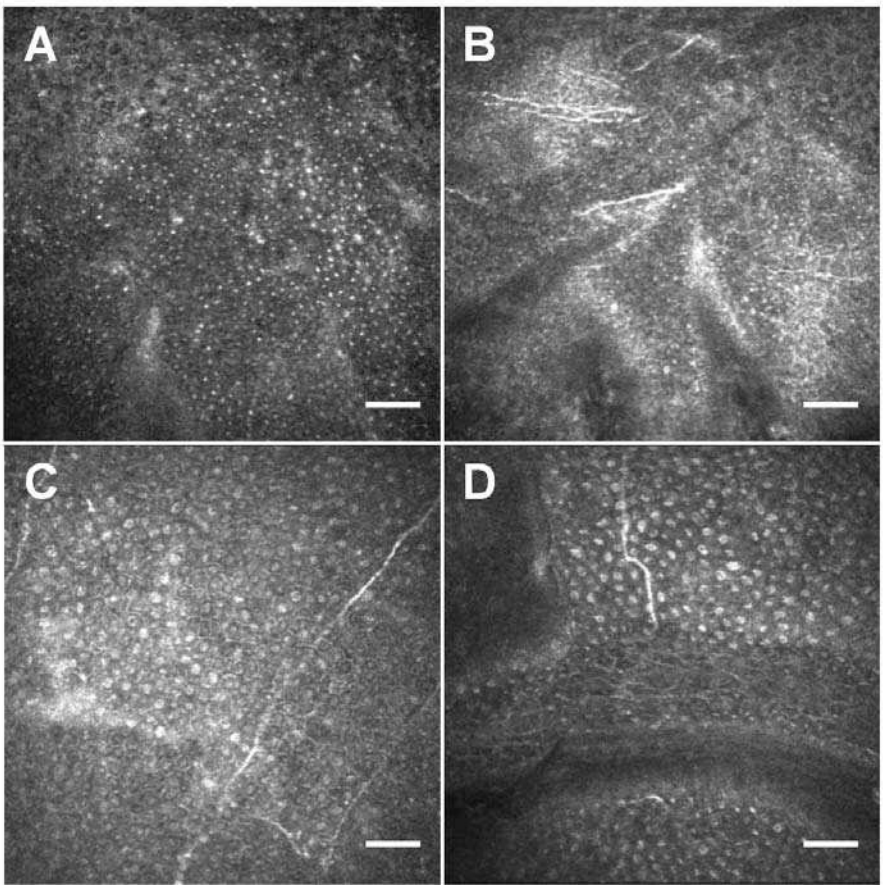

Figure 5-3: IVCM images showing basal epithelial changes in keratoconus. Bright nuclei 4 – 9µm in size can be seen within ill-defined cell borders. Sub-basal nerves are visible in all cases (A&B from case 3, C from case 8, D from case 5). Scale bar 50µm.

Epithelial changes changes were not detected on light and confocal microscopy in case 1 and 2 (Table 5-1) who did not show clinically visible corneal scarring (Figure 5-4).

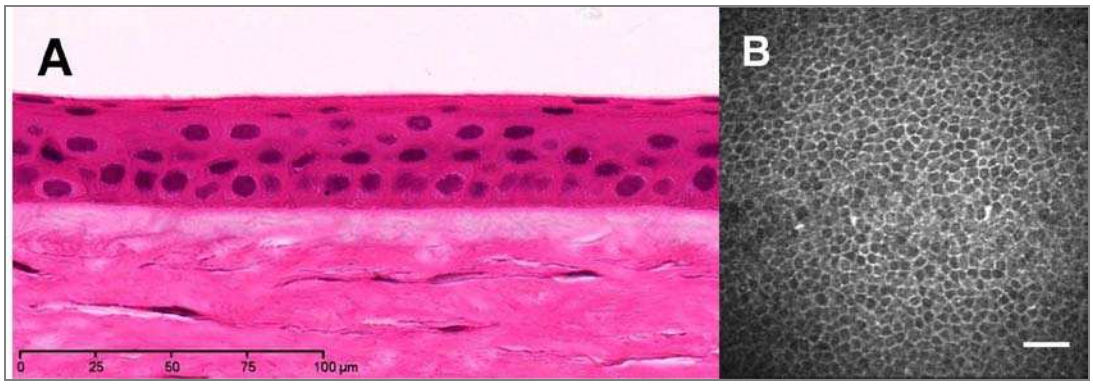

Figure 5-4: Light micrograph (A) and IVCM image (B) of the cornea in case 1 of keratoconus group showing normal appearance and pattern of basal epithelium. (H&E stain in A. Scale bar 50µm in B)

Cell morphometry revealed an average size of 8.13 ± 1.11µm (M± SD) (range 6.14 – 11.30µm) for the basal nuclei in regenerative atypia whereas in clinically and histologically normal epithelium the average basal nuclear size was 7.96 ± 0.917µm (M± SD) (range 6.79 – 9.96µm). The difference was not statistically significant between the 2 groups (P= 0.9). The average basal nuclear size in CIN group was 14.04 ± 4.81µm (M± SD) (range 7.98 – 28.50µm) (Figure 5-6). The difference was statistically significant (P= 0.000) between the nuclear size in CIN compared to each of regenerative atypia and normal epithelium groups (Table 5-4 & Figure 5-6). Figure 5-5 illustrates examples of morphometric measurements of nuclear sizes in basal epithelium seen in clinically and histologically normal epithelium (Figure 5-5A), regenerative atypia (Figure 5-5B) and CIN (Figure 5-5C).

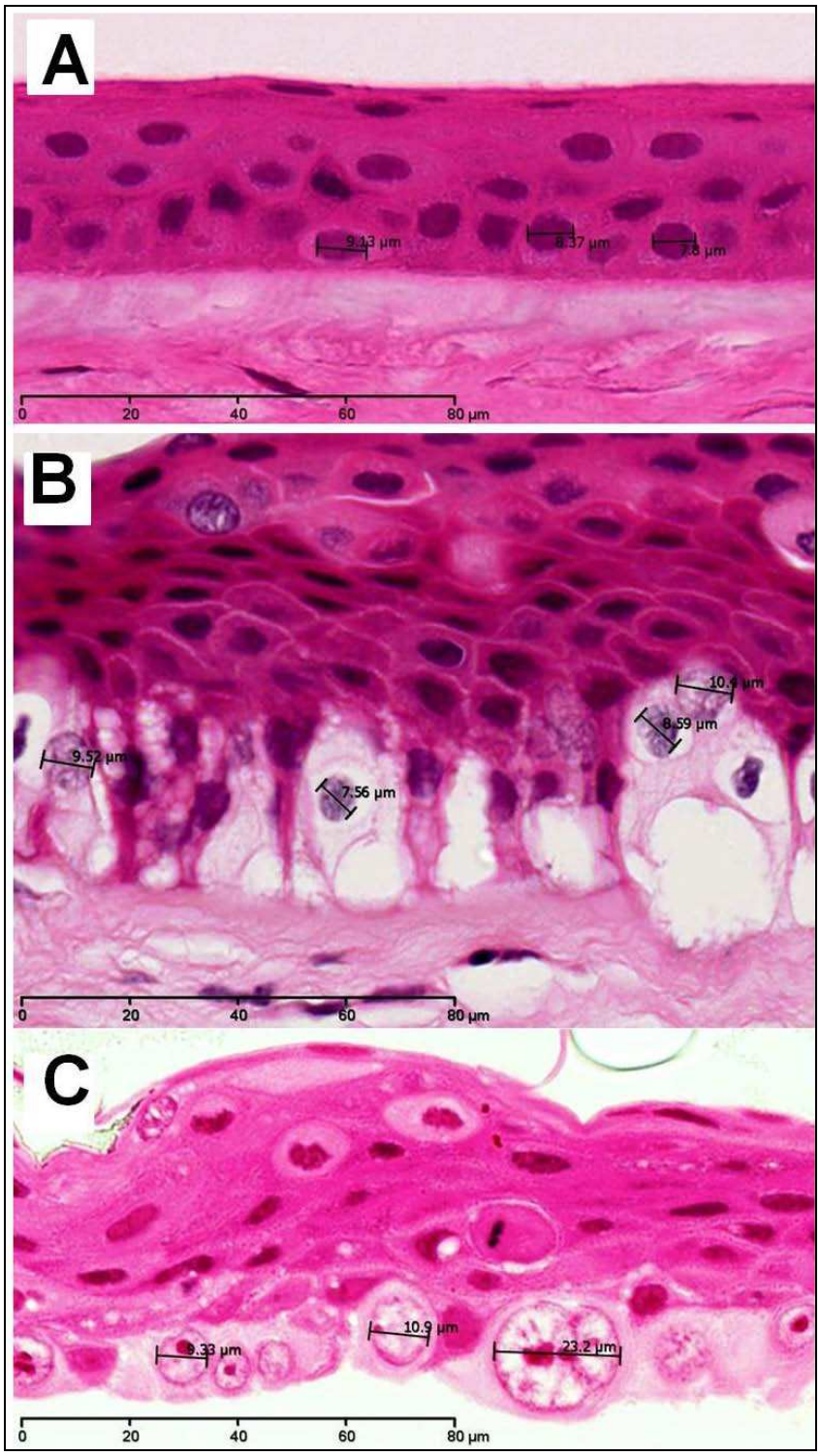

Figure 5-5: Light micrographs showing morphometric measurements of basal epithelial nuclei in normal looking epithelium (A), regenerative atypia (B) and corneal intraepithelial neoplasia (C). (H&E stain).

Table 5-4: Difference in nuclear size of corneal basal epithelium in three groups.

Corneal Basal Epithelium	NORMAL	RA	P value	CIN	P value
Nuclear size (Mean ± SD)	7.96 ± 0.91	8.13 ± 1.11	0.9	14.04 ± 4.81	0.000

CIN= Corneal intraepithelial neoplasia, RA= Regenerative Atypia

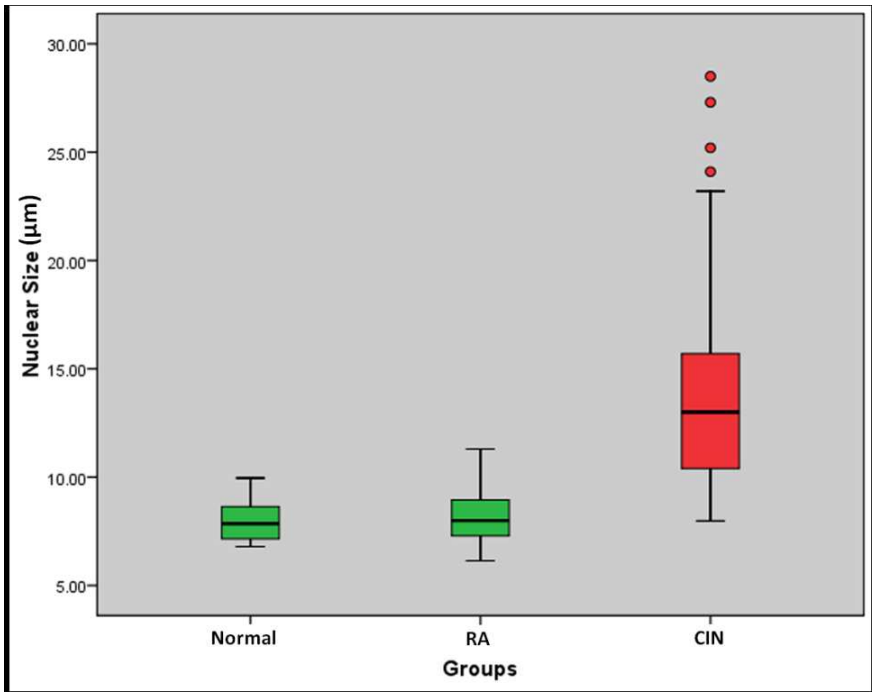

Figure 5-6: Boxplot diagram highlights the difference in mean and range of basal epithelium nuclear size values in cases with normal epithelium, regenerative atypia (RA) and Corneal intraepithelial Neoplasia (CIN). The latter group shows significant increase in basal nuclear sizes compared to the former two groups.

5.4.1.2 Epithelial irregularity:

All 9 cases (81%) who presented with corneal scarring showed features of epithelial irregularity both histologically and on IVCM. Figure 5-7 illustrates representative light micrographs of corneal sections from 5 cases of the study group. The development of a convoluted profile of the basal epithelium was noticed (Figure 5-7 A,B & C). In 2 of the 9 cases

small epithelial downgrowths were seen extending into areas of breaks or degradation of Bowman's zone (Figure 5-7 D) whereas in other areas larger downgrowths, resembling the rete pegs of epidermis in skin, were noted over sub-epithelial scarring (Figure 5-7 E). Areas with increased epithelial thickness to over 10 cell layers were noticed in 2 samples (Figure 5-7 A&D).

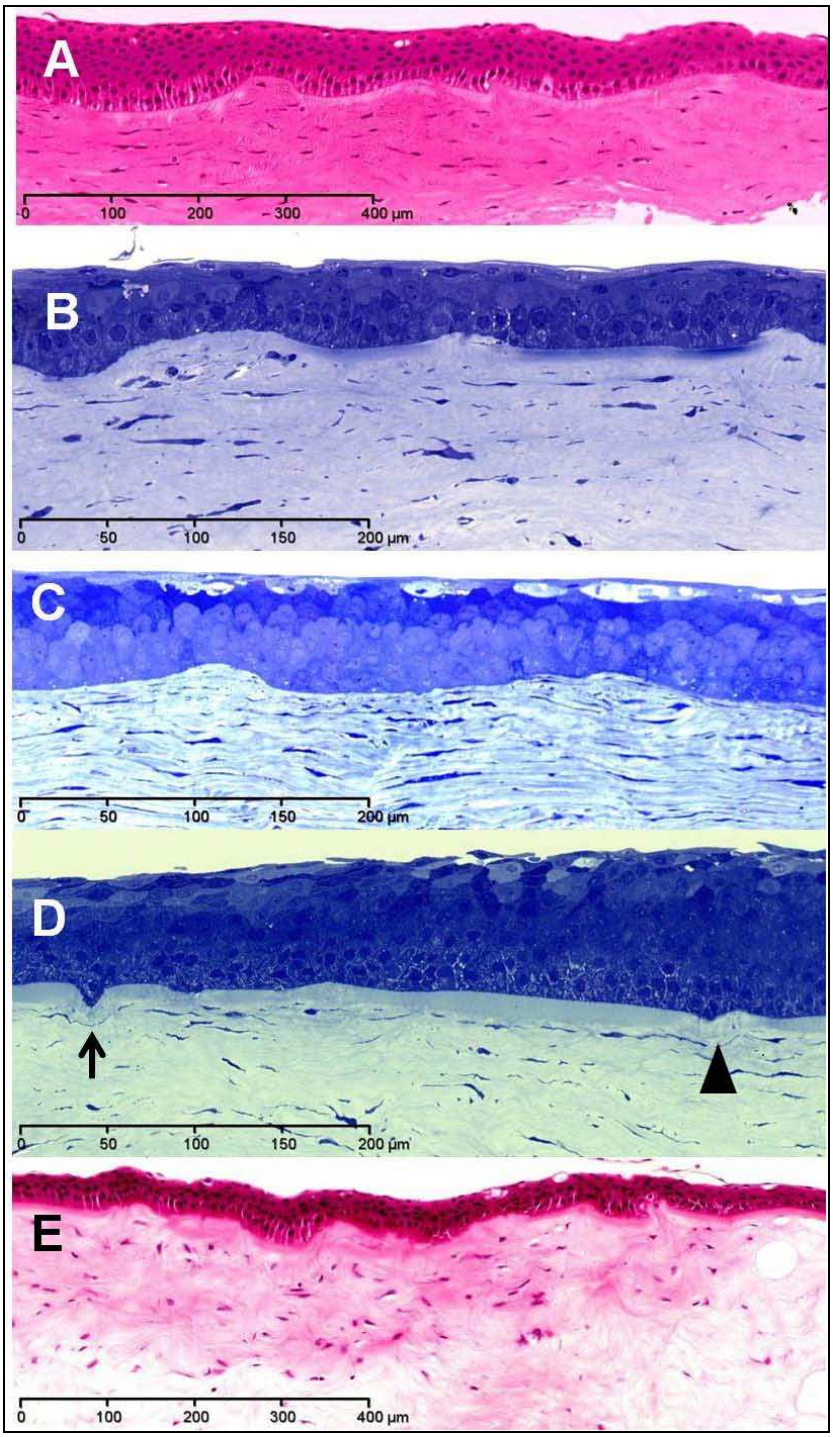

Figure 5-7 Light micrographs of cross sections in keratoconus illustrating irregular undulating profiles of basal epithelium in A (case 7), B (case 6) and C (case 8). Epithelial downgrowths into Bowman's zone breaks (arrow) or area of Bowman's zone degradation (arrowhead) are seen in D (case 4) occasionally resembling rete pegs of epidermis in E (case 5). (A and E stained with Heamatoxylin and Eosin, B, C & D stained with toludine blue).

On IVCM en face images basal epithelial layers were seen interrupted by bright bands (Figure 5-8 A,B&C) or sheets (Figure 5-8 D&E) of subepithelial scar tissue or undulating Bowman' zone creating bays and islands of epithelium surrounded by hyper-reflective collagenous tissue. In some cases IVCM was able to show bright figures of keratocyte / fibroblast nuclei within the sub-epithelial fibrous tissue (Figure 5-8 E).

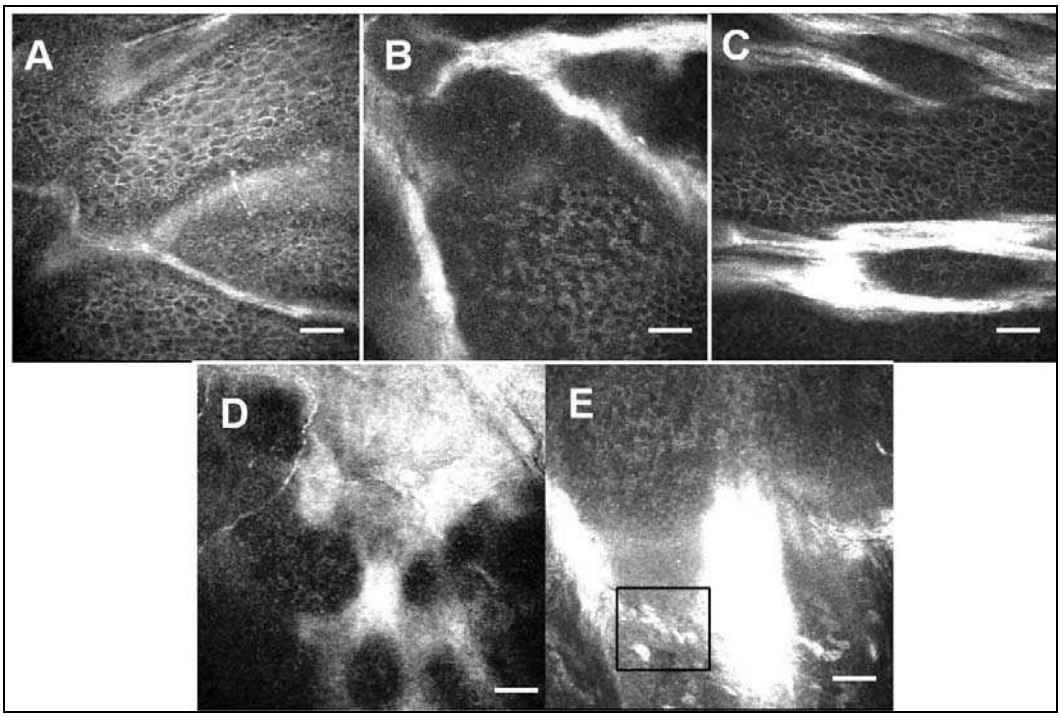

Figure 5-8: IVCM images in keratoconus illustrating basal epithelium interrupted by hyper-reflective ridges (A in case 5) or bands of collagenous tissue (B in case 7) occasionally surrounding islands of basal epithelium (C & D in case 6 & 8 respectively). Bright nuclear figures of fibroblasts / keratocytes can be seen in relation to scar tissue (square in E in case 4). Scale bar 50µm.

5.4.1.3 Epithelial thinning:

This feature was noticed histologically in three cases (no. 6, 8 & 11 in Table 5-1) (27%). In two cases (no. 6 & 11 Figure 5-1C & F) remarkable thinning of corneal epithelium was noticed over zones of prominent superficial lenticular scar associated with a break and loss of Bowman's zone. In case 6 abrupt changes in epithelial thickness were noticed at the edges of the scar (Figure 5-9 A). The corresponding IVCM images showed bays of basal epithelium bounded by bright finger–like extensions of fibrous bands from the main mass of the scar (Figure 5-9B). In case 11 changes in epithelial thickness were gradual along the sides of the lenticular scar (Figure 5-9C). The corresponding en face IVCM image showed bright elongated epithelial nuclei arranged in a whorled pattern within a hyper-reflective background of the scar tissue (Figure 5-9D). Oblique view showed elongated epithelial cells on top of the prominent scar tissue (Figure 5-9E). In case 8 extreme epithelial thinning was associated with remarkable stromal thinning and scarring illustrated later in figure 17A.

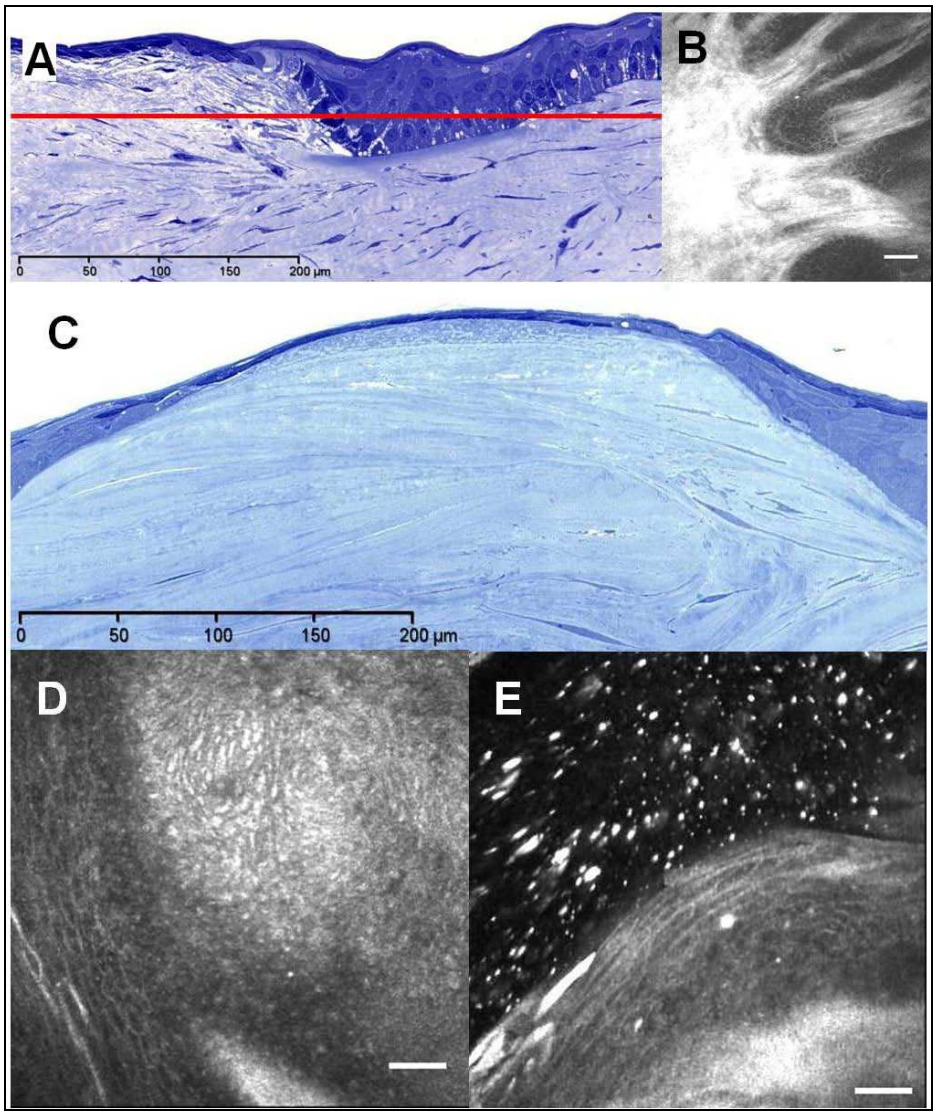

Figure 5-9: Light and in vivo confocal micrographs showing epithelial thinning over a superficial lenticular scar in keratoconus. A (case 6), rapid increase in epithelial thickness from apex to the periphery of scar is seen. The red line indicates the level of focal plane in IVCM (toluidine blue). B, corresponding IVCM image shows hyper-reflective finger like extensions from the scar surrounding sheets of epithelium. C (case 11), gradual increase in epithelial thickness is noticed on the periphery of the scar (toluidine blue). Corresponding IVCM en face image shows bright elongated epithelial nuclei in a whorled pattern within a hyper-reflective background (D). These cell appeared elongated on oblique view (E). Scale bar 50µm.

Epithelial changes were not seen in the remaining 2 cases (1 & 2 Table 5-1) who showed unremarkable epithelium both histologically and on IVCM (Figure 5-10).

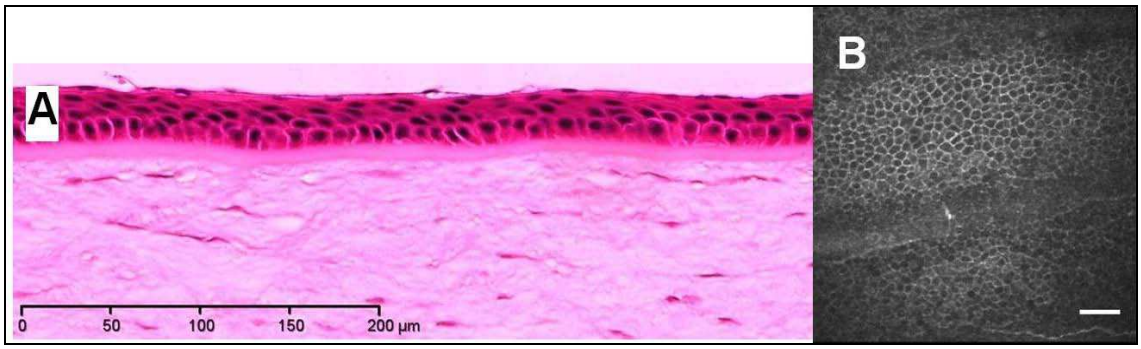

Figure 5-10: Light micrograph (A) and IVCM image (B) of keratoconus case 2 (Table 5-1) with unremarkable corneal epithelium. Scale bar 50µm.

5.4.2 Bowman's zone changes:

5.4.2.1 Breaks:

Histological sections showed breaks in Bowman's zone of variable lengths that could range from less than 20µm (Figure 5-11A) up to 100µm or more (Figure 5-11B). These gaps were either empty (Figure 5-11B) or densely occupied by spindle cells resembling keratocytes propagating from subjacent anterior stromal layers (Figure 5-11C). In certain areas these breaks were filled with basal epithelial cells (Figure 5-11D). These changes were obvious in 9 histological samples (82%) while the remaining 2 (from case 1 & 2 Table 5-1) did not show evidence of Bowman's zone breaks (Figure 5-4A & Figure 5-10A). Oblique IVCM views were comparable to histological cross sections in illustrating Bowman's

zone breaks occupied with stromal cells presumably keratocytes (Figure 5-11E&F in case 7).

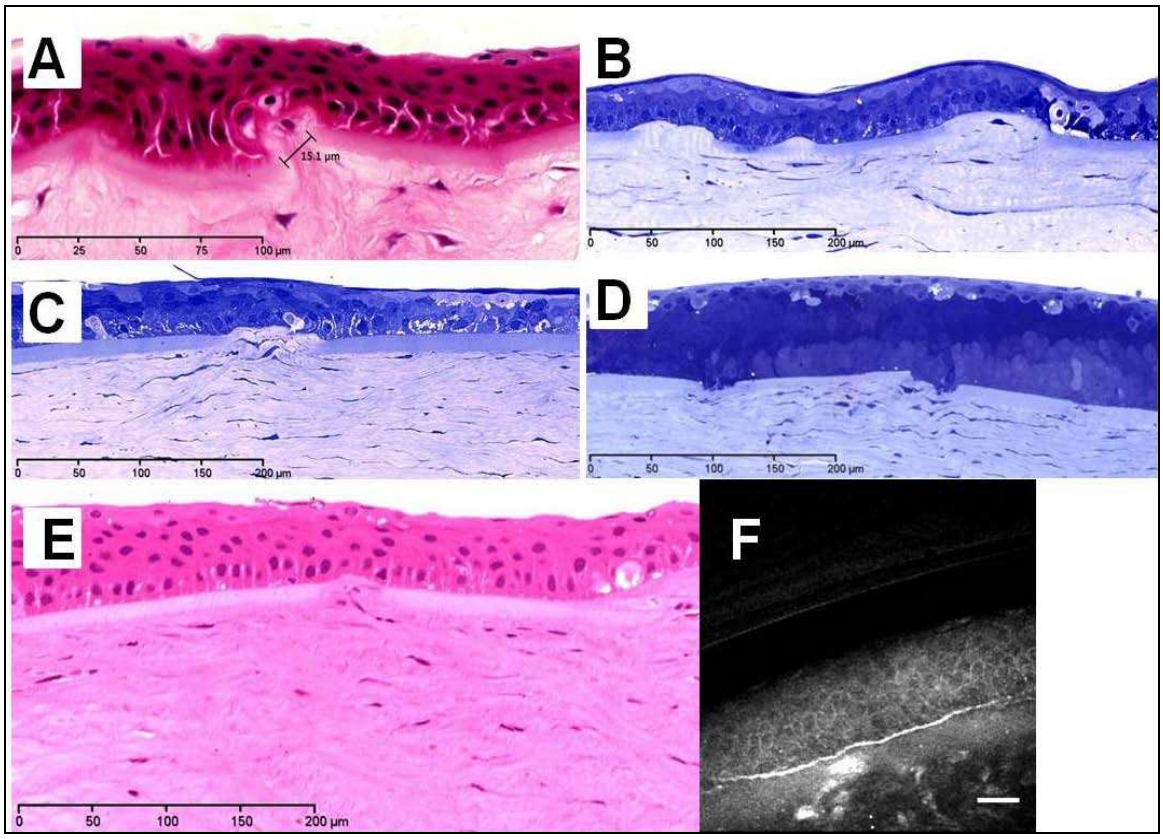

Figure 5-11: Microscopic views of Bowman's zone breaks in keratoconus. A – E, Light micrographs in cases 5, 6, 4, 8 & 7 respectively. Breaks in Bowman's zone are noticed to be small (A), large (B), empty (B), filled with presumed keratocytes (C) or basal epithelial cells (D). In case 7 these breaks were comparable in light (E) and IVCM (F). (H&E in A & E. Toluidine blue in B, C & D. Scale bar 50µm in F).

IVCM at the level of basal epithelium and Bowman's zone illustrated dark bands of variable width and direction occasionally connected to each other (Figure 5-12). These bands appeared as 'cracks' or gaps, which were 10 – 100µm in width. The narrow ones gave the Bowman's a crack-like pattern running as dark lines within the relative brightness of Bowman's zone (Figure 5-12A) occasionally forming circular figures (Figure 5-12B).

The wider dark bands were rather straight and presented like “gaps” in Bowman’s zone within which bright keratocyte nuclei could be seen (Figure 5-12C & D) with frequent interconnections (Figure 5-12E & F). When sub-basal nerves passed in the same area their courses were interrupted by these gaps (Figure 5-12E & Figure 5-13). Thus the overall result was visualization of basal epithelium, sub-basal corneal nerves and anterior keratocyte nuclei all at the same focal plane in en face images of IVCM.

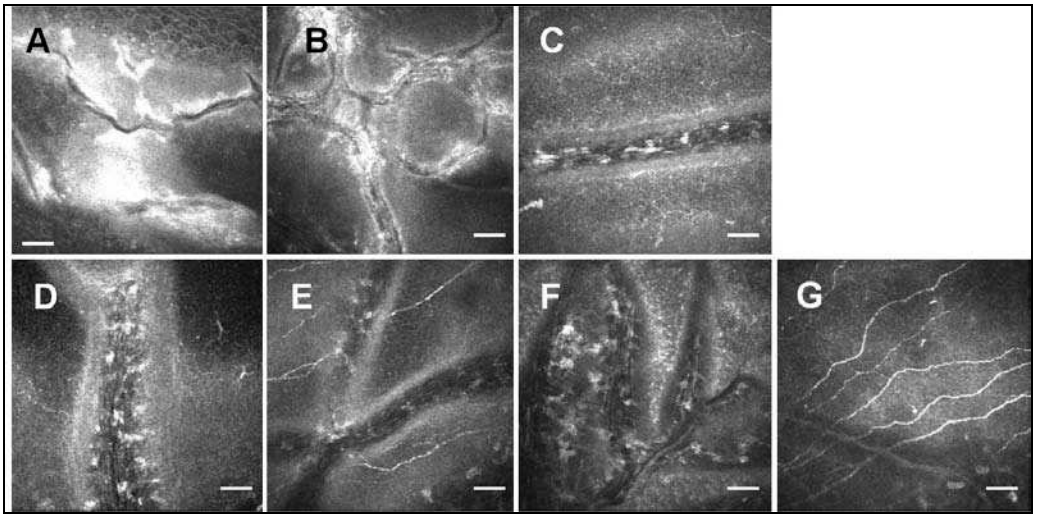

Figure 5-12: IVCM images showing patterns of Bowman’s zone breaks in keratoconus. The Bowman’s zone gives a bright background within which narrow dark lines are seen running in curvilinear (A) and circular (B) courses. A second pattern presents as wider dark straight bands running horizontally (C) and vertically (D) through which keratocytes can be seen. Occasional interconnections of these wide gaps at certain places can be seen in E & F with interruption of the sub-basal nerves. Images C & E show these breaks in cases 1 & 2 respectively that had no visible corneal scarring (table 1). G, Bowman’s zone with normal pattern of K-structures could be seen in a clear paracentral cornea in case 10. Scale bar 50µm. (A & D from case11, B & F from cases 7 & 3 respectively).

Volumetric IVCM scanning illustrated these 2 patterns of Bowman’s zone breaks in a consistent manner as shown in Figure 5-13. As the focal plane was advanced from basal epithelium these gaps were visualised clearly

through Bowman's zone, virtually interrupting sub-basal nerves, to disappear at the level of anterior stroma.

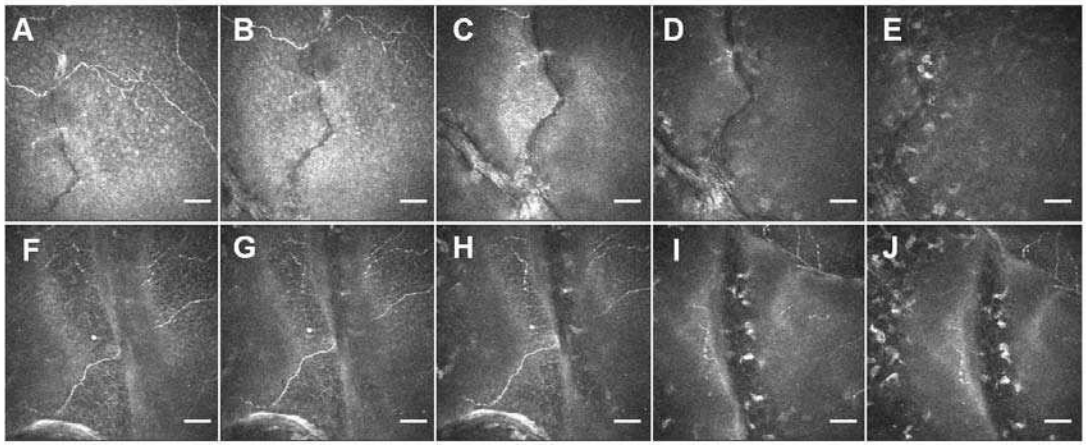

Figure 5-13: Volumetric IVCM images showing that the level of dark lines representing breaks are within the Bowman's zone. The focal plane passes from basal epithelium through Bowman's zone to the anterior stroma where the dark lines disappear. A – E show crack-like pattern, F – J show wider 'gap' pattern. Scale bar 50µm.

These changes were seen by IVCM in all cases including case 1 (Figure 5-12C) & 2 (Figure 5-12E) who showed no histological evidence of Bowman's zone breaks (Figure 5-4A & Figure 5-10A respectively) with no clinically visible corneal scarring preoperatively (Table 5-1). A third pattern possibly related to breaks in Bowman's zone was noticed on IVCM as interconnected bright bands forming irregular round and oval shapes similar to the pattern of distribution of Bowman's zone breaks (Figure 5-14). This was noticed in 5 cases (4, 5, 6, 7 & 9 in Table 5-1) all had clear histological evidence of Bowman's zone breaks occupied by keratocytes.

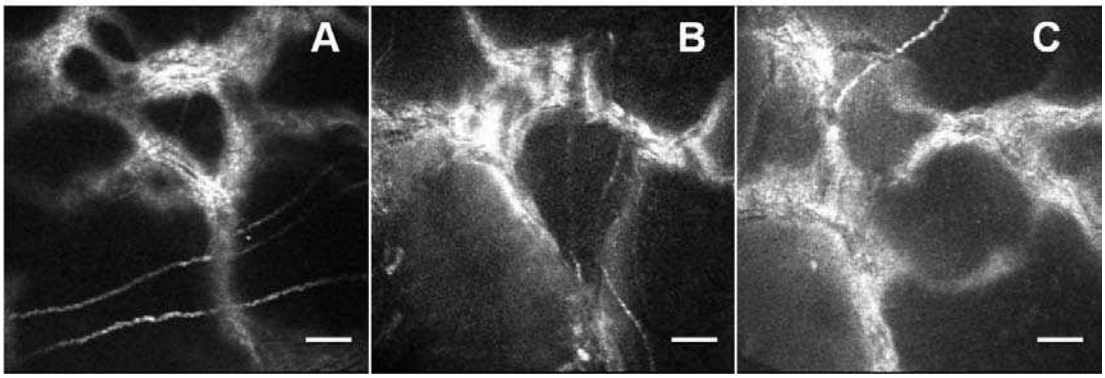

Figure 5-14: IVCM images in 3 keratoconus cases (A, B and C in case 4, 5 and 7 respectively) showing hyper-reflective curvilinear bands at the level of sub-basal nerves and Bowman's zone forming irregular circular patterns. Scale bar 50µm.

5.4.2.2 Loss of Bowman's zone

In areas where Bowman's zone was missing over wide areas as seen in histology sections the basal epithelium appeared to settle directly on the underlying stroma. These features were seen in cases 3 and 8. A representative section from case 8 is shown in Figure 5-15A. IVCM of the same cornea showed areas where basal epithelial cells, sub-basal nerves and bright nuclear figures of keratocytes were all visualised at the same focal plane. The bright reflective pattern of Bowman's zone and patterns of breaks were conspicuously absent (Figure 5-15B-D).

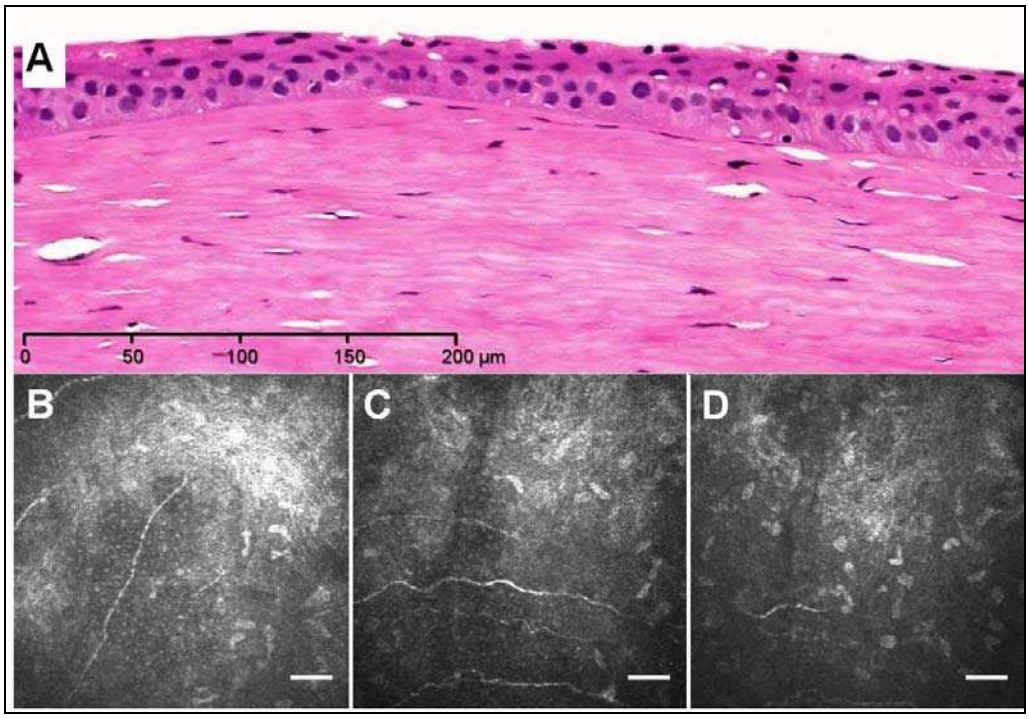

Figure 5-15: A: Light micrograph of corneal cross section in case 8 showing area of total loss of Bowman's zone with the corneal epithelium sitting directly on the stroma. IVCM en face images of the same cornea show basal epithelium and sub-basal nerves visualised at the same focal plane (B & C). The reflective pattern of an intact Bowman's zone or the dark lines representing breaks are missing. At deeper levels keratocyte nuclei became more obvious (D). scale bar 50µm.

5.4.3 Stromal changes

5.4.3.1 Superficial Lenticular Scar:

In 3 samples (27%) superficial lenticular stromal scar associated with a break and loss of Bowman's zone was noticed on light microscopy (Figure 5-9 C & Figure 5-16 A&B). This scar was seen at the apex of the corneal deformity and associated with thinning of overlying epithelium. The corresponding IVCM pattern for this type of scar has been already described in Figure 5-9B (case 6) with a similar pattern seen in case 7

where bright nuclear figures within the scar were also visible (Figure 5-16C).

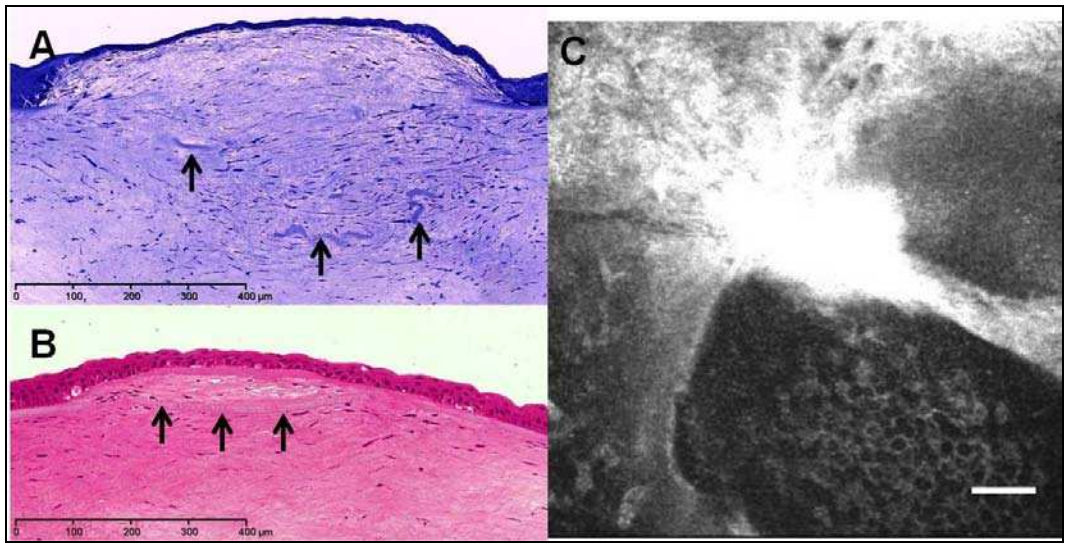

Figure 5-16: Microscopic views of superficial stromal lenticular scar in keratoconus. A & B are light micrographs of sections in keratoconus case 6 & 7 respectively, showing superficial lenticular scar with fragments of Bowman's zone (arrows). The IVCM image in case 7 (C) shows sheets of normal looking basal epithelium interrupted by hyper-reflective scar within which bright fibroblast nuclei are seen. This pattern is similar to the one shown in figure 9B for case 6. (toluidine blue in A, H&E in B, scale bar 50µm in C).

5.4.3.2 Deep stromal scar:

Deep stromal scarring associated with remarkable thinning was seen in certain areas of the corneal sample from case 8 (Figure 5-17A). The scar was indicated by loss of regularity of the stromal lamellae that were populated with random nuclear figures consistent with fibroblasts. The Bowman's zone showed multiple breaks whereas the overlying epithelium was progressively thinned (tissues are highlighted in a pseudocolour image Figure 5-17B). IVCM views taken at mid-stromal levels showed

bright nuclear figures randomly distributed within a hyper-reflective background consistent with stromal scarring (Figure 5-17C-E).

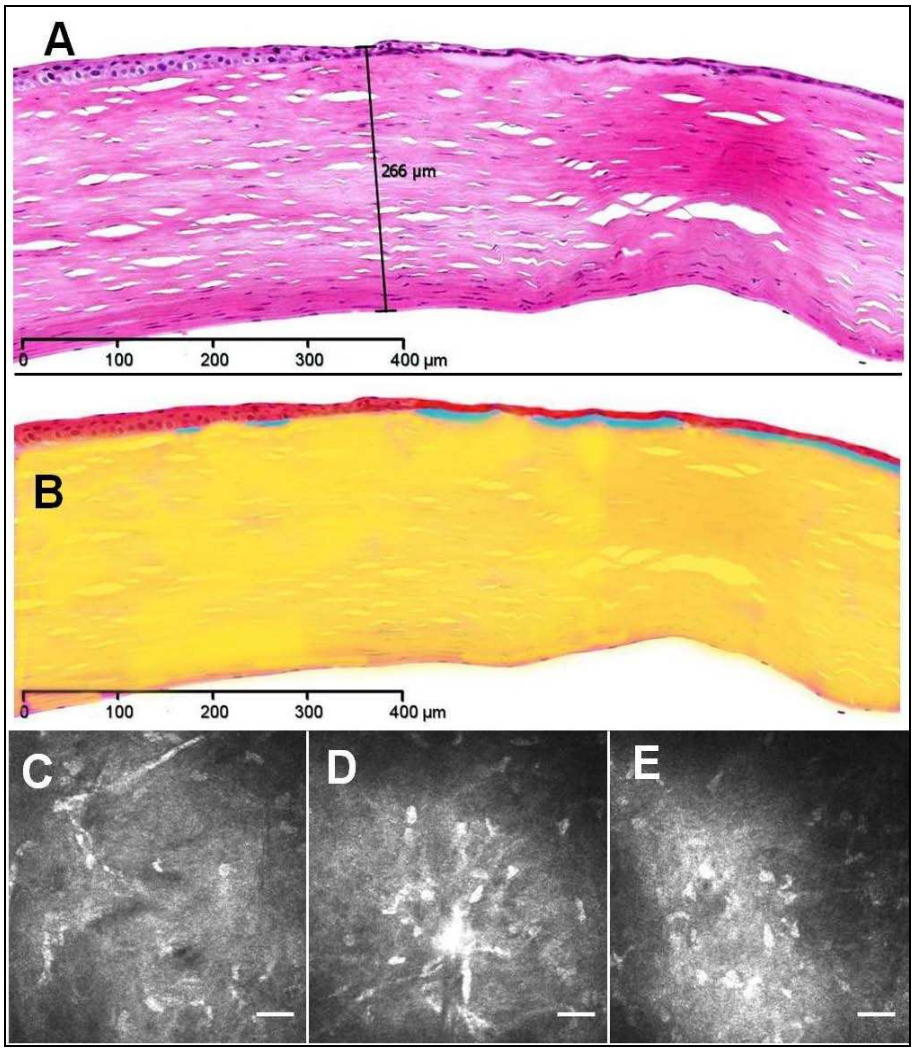

Figure 5-17: A, light micrograph of corneal cross section in keratoconus case 8 (H&E stain) showing area of remarkable stromal thinning associated with deep scarring indicated by irregular stromal lamellae populated with nuclear figures consistent with fibroblasts. Note the progressive thinning of the epithelium overlying this area. The darker eosinophilic hue on the right side of the section is induced by tissue compression during sample sectioning. B, a pseudocolour image highlights the changes in Epithelium (red) Bowman's zone (blue) and stroma (yellow). C-D, IVCM images of mid-stroma at 103, 128 & 155µm of focal depth respectively for the same case showing randomly distributed nuclear figures within a hyper-reflective background of scar tissue. Scale bar 50µm.

5.4.3.3 Stromal folds

IVCM revealed confluent dark lines about 10µm wide within the stroma in 10 cases of the study group (90%) (Figure 5-18). These lines were noticed to have almost parallel courses running in various directions and frequently alternating with brighter ones. Occasionally the courses of stromal nerves were interrupted by these stromal 'folds' (Figure 5-18B). On light microscopy no specific corresponding stromal histological changes were noted.

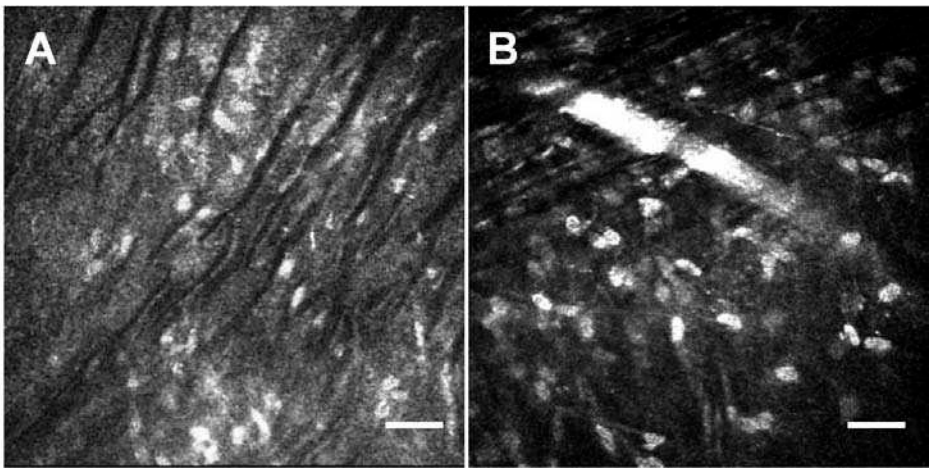

Figure 5-18: IVCM images showing stromal folds in keratoconus cornea represented as multiple parallel dark and bright lines running in various directions with occasional 'interruption' of stromal nerves. Scale bar 50µm.

5.4.4 Descemet's membrane:

5.4.4.1 Breaks:

Breaks in Descemet's membrane were noticed in the corneal sample of case 8 (Table 5-1, Figure 5-1E) with a history of acute hydrops followed

by dens central scarring. The histological sections showed central rupture of Descemet's membrane with rolled edges (Figure 5-19 A-C). IVCM showed dark well defined areas with sharp edges interrupting the continuity of endothelium (Figure 5-19 D&E).

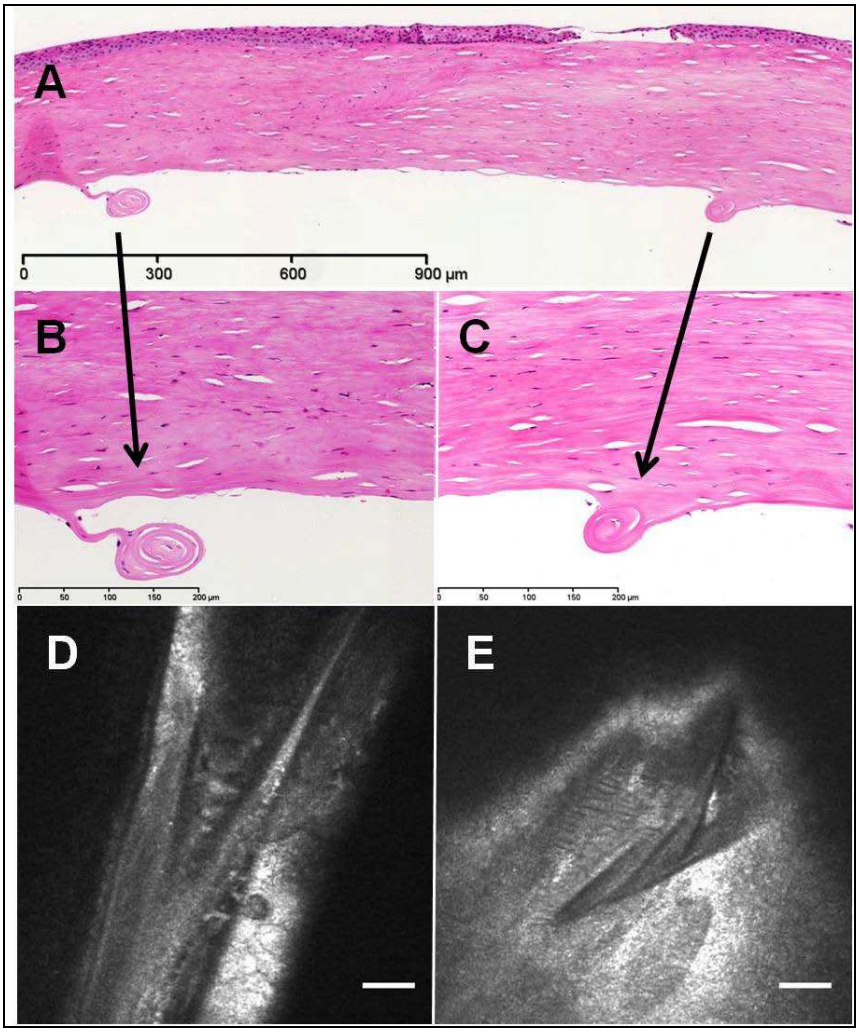

Figure 5-19: Microscopic views of Descemet's membrane (DM) breaks. A-C: light micrographs of keratoconus case 8 illustrate a break in DM with rolled edges shown in a full view (A) and magnified views (B&C). IVCM images (D&E) show dark well defined areas with sharp edges at the level of endothelium interrupting continuity of DM. (H&E in A-C, scale bar 50µm in D&E).

5.4.4.2 Scar:

In case 10 the histological sample revealed a small well demarcated area of scar in Descemet's membrane (Figure 5-20) that was not visualised on corresponding IVCM.

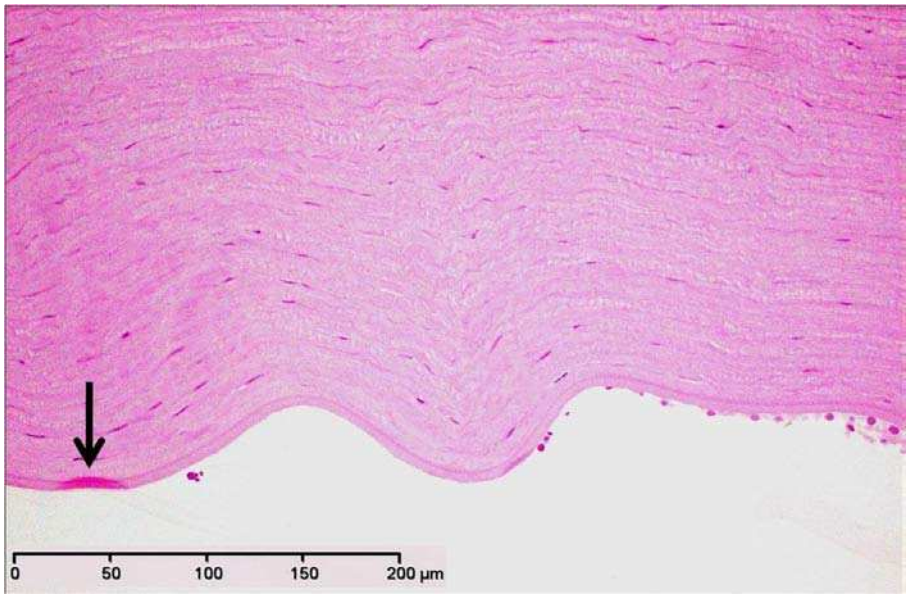

Figure 5-20: Light micrograph of cross section in keratoconus cornea in case 10 shows sharply demarcated area of Descemet's membrane scar (arrow). (H&E stain).

5.5 DISCUSSION

5.5.1 Epithelial Changes in Keratoconus

Epithelial thinning is well documented in the literature as one of the common histopathological features of keratoconus seen by light microscopy (Teng, 1963, Scroggs and Proia, 1992, Fernandes et al., 2008). However on IVCM studies of keratoconus two pathological features were mentioned within epithelial layers namely elongated superficial cells

and hyper-reflective nuclei of the middle and basal cells (Hollingsworth et al., 2005a, Somodi et al., 1996, Ucakhan et al., 2006). In our study epithelial thinning was noticed in 3 histological sections over areas of superficial and deep stromal scars indicating that epithelial thinning is associated with underlying stromal scarring. The corresponding IVCM images showed epithelial cell morphology similar to that described above but we were able to demonstrate a whorled arrangement of bright nuclei on en face and oblique views. It is possible that the higher resolution afforded by our instrument enabled us to pick up this pattern. A whorled or vortex pattern of epithelium highlighted by fluorescein staining in keratoconus, has been previously reported by slitlamp examination. (Dua et al., 1993, Dua and Gomes, 2000).

Importantly in this study, features consistent with regenerative atypia of the basal epithelium were noticed on histological sections in 5 cases of keratoconus all of which were associated with subepithelial scarring visible on slitlamp examination. Such metaplastic changes induced by this process have not been reported before in keratoconus histopathology. These changes appeared almost similar to regenerative atypia changes mentioned in epithelial lining of other organs in response to rapid turnover induced by inflammatory conditions (Terano et al., 2002, Vaidyanathan et al., 2002, Genta and Rugge, 2006). Interestingly the whorl pattern seen in the epithelium of keratoconus patients is also postulated to be related to the increased turnover of epithelium in these

corneas especially in patients wearing rigid contact lenses where constant apical rubbing causes increased cell shedding. It is worth mentioning that some of the inter- and intra-cellular spaces noticed in the basal epithelium on light microscopy were possibly created during histological processing most probably due to weak cytoplasmic skeleton and cellular adhesions associated with regenerative atypia. On IVCM such changes of prominent hyper-reflective nuclei of the basal epithelium have been previously reported and were believed to represent corneal epithelial metaplasia (Guthoff et al., 2006) or related to general thinning of the corneal epithelium ((Hollingsworth et al., 2005a).

Our study suggests that these morphological changes are related to regenerative atypia. We have previous reported such changes by light and in vivo confocal microscopy in corneal Intraepithelial Neoplasia (CIN) where they represent neoplastic atypia (Alomar et al., 2011). This morphological similarity between neoplastic dysplasia and RA applies to epithelial cells in other organs and frequently presents a challenge for proper histological diagnosis (Genta and Rugge, 2006, Vaidyanathan et al., 2002). However the two conditions can be differentiated by smaller nuclear size, less dispersed chromatin, less number of prominent nucleoli and fewer – if any – mitotic figures in regenerative atypia where polarity is also preserved throughout the epithelial layers (Genta and Rugge, 2006).

Our morphometric analysis (figure 6) revealed no significant difference between basal nuclear sizes in corneas with regenerative atypia and normal epithelium in the same study group. However the difference was highly significant when these values were compared to nuclear sizes in dysplastic basal epithelium of Corneal Intraepithelial Neoplasia (CIN) diagnosed clinically and confirmed histologically in 2 cases in a previous study (Alomar et al., 2011). With the selection of the largest nuclei in each group an ascertainment bias was considered to increase confidence in the ability to discriminate between dysplasia in CIN and metaplasia induced by regenerative atypia on the basis of nuclear size.

On IVCM the two conditions can be differentiated by the presence of pleomorphic and multinucleated cells in the middle layers together with masking of the sub-basal nerves in CIN (Alomar et al., 2011) in contrast to regenerative atypia seen in advanced cases of keratoconus where there was an absence of multinucleated cells and the nerves were clearly visible as reported herein.

We further believe that regenerative atypia could describe the corneal epithelial changes seen in keratoconus given the fact that this process is a desirable homeostatic response to epithelial injury that resolves once the inciting / provoking factors are removed or treated, a condition that clinically applies to the majority of keratoconus patients who show surface epithelial changes, occasionally in the form of hurricane keratopathy which resolves with topical lubricants and reduction in the duration of

hard contact lens wear (Dua and Gomes, 2000). These findings are in keeping with the theory that describes basal epithelial degeneration as the provocative factor for accelerated keratocyte apoptosis in the pathogenesis of keratoconus (Teng, 1963, Wilson et al., 1996). However this does not contradict the existence of an ongoing process of regeneration to compensate for any epithelial cell loss (Teng, 1963). When this balance is disrupted, as it is frequently and commonly encountered in keratoconus patients, epithelial changes are likely to be exacerbated.

Epithelial irregularity in keratoconus is related to the sub-epithelial changes of scarring and Bowman's zone breaks with occasional incursions of basal epithelium in these gaps (Teng, 1963, Sherwin et al., 2002). The undulating profile of basal epithelium seen on light microscopic explains the patterns of reflectivity seen on IVCM. Another form of epithelial irregularity seen was the variability / increase in thickness similar to that reported in previous studies of keratoconus (Scroggs and Proia, 1992, Kaas-Hansen, 1993). All IVCM patterns related to epithelial changes in keratoconus were not seen in corneas devoid of scarring on slitlamp examination, therefore it can be reasonably concluded that epithelial changes are secondary to or associated with stromal pathology.

5.5.2 Bowman's zone:

The three IVCM patterns of Bowman's zone changes, namely crack-like pattern, wide dark band pattern and hyper-reflective curvilinear pattern, could all be correlated with histological changes observed on light microscopy. In relation to the wide dark band pattern two patients did not show corresponding histological changes. In a histological study, Scroggs and Proia (Scroggs and Proia, 1992) reported absence of Bowman's zone breaks in multiple sections of about 20% of their patients. They considered these patients to represent 'atypical' keratoconus. However, despite lack of histological detection of breaks, we were able to demonstrate changes on IVCM. This could be due to the fact that IVCM enables enface visualization of a much larger surface area compared to histology where the breaks could be missed in the sections viewed.

Previous histological studies on keratoconus have described the corneal tissue response to breaks in Bowman's zone (Teng, 1963, Scroggs and Proia, 1992, Fernandes et al., 2008, Kaas-Hansen, 1993). The spindle – like nuclear figures seen within Bowman's breaks have been reported in other studies and confirmed to be keratocytes from the anterior stroma (Sridhar et al., 2001, Said et al., 2009) with the capability for fibroblast and myofibroblast transformation in response to wound repair (Fini, 1999, Said et al., 2009). Based on this we can hypothesize that initially the Bowman's zone breaks are acellular and appear as the 'crack-like lines' on IVCM. These later widen to from the wide band like pattern seen on IVCM

and finally, are populated with keratocyte derived cells and scar tissue representing the hyper-reflective curvilinear lines as seen on IVCM. Interestingly some of the changes seen by IVCM were not visible on slit lamp examination suggesting the difference in resolution of the two modalities of examination. We also noted that the Bowman's zone breaks were filled with basal epithelium in 2 samples of the study group only. In a detailed histopathological study of keratoconus Teng has commented on this and concluded that Bowman's zone breaks are less likely to be replaced by tissue from damaged epithelium (Teng, 1963).

On IVCM, where the above described patterns were seen, there was a complete lack of K-structures of normal Bowman's zone (Kobayashi et al., 2006). Although we consistently observed the three different patterns, others who have studied keratoconus have not commented on this (Somodi et al., 1996, Hollingsworth et al., 2005b, Efron and Hollingsworth, 2008, Ucakhan et al., 2006, Niederer et al., 2008). Hollingsworth et al in their study mentioned abnormal IVCM findings at the level of Bowman's zone in 57% of keratoconus cases without any description or illustration. Thus we claim that the Bowman's zone changes described herein constitute a novel aspect of this study. We believe that these patterns described are fairly specific to keratoconus and can be considered with other clinical and topographic features to confirm the diagnosis especially in early or equivocal cases. Moreover it can help to follow the progression of keratoconus.

Damage to Bowman's zone was noticed to be extensive in histological sections of severe cases of keratoconus with resultant growth of surface epithelium directly on the underlying stroma. These changes correlated well with corresponding IVCM images that were able to show basal epithelium along with sub-basal nerves and keratocyte nuclei without evidence of patterns of normal or abnormal Bowman's zone. This finding re-enforces the use of IVCM in detecting microstructural changes in keratoconic cornea.

5.5.3 Stromal & Descemet's membrane changes in keratoconus:

In keratoconus, scarring occurs in all layers of the cornea from Bowman's zone, through superficial and deep stroma, to the Descemet's membrane. The progression of scarring tends to relate to the severity of the condition, progressing from superficial to deep. Bowman's zone scarring occurs early followed by superficial stromal lenticular scar and deep scarring. The latter is a less common feature and has been commented by others as well (Fernandes et al., 2008, Scroggs and Proia, 1992).

Alternating dark and bright bands within stromal layers have been well documented in other IVCM studies of keratoconus (Ucakhan et al., 2006, Efron and Hollingsworth, 2008) and considered to represent Vogt's striae classically observed on slitlamp biomicroscopy. Efron & Hollingsworth

noticed these bands in 45% of their cases while Ukakhan et al reported similar findings in 50% of their cases. We noticed these IVCM bands in 10 (90%) of the 11 study cases including 2 cases with no evidence of Vogt's striae on preoperative examination. Descemet's membrane breaks were noticed on IVCM in one case of the study group who had a history of resolved acute hydrops. The IVCM pattern of Descemet's membrane break illustrated in this study correlated well with the rolled edges of the Descemet's membrane break seen on histological section with light microscopy. Although this feature is well documented in the histopathology of keratoconus (Scroggs and Proia, 1992, Fernandes et al., 2008) our study is the first to report this pattern in the literature of IVCM. It adds to the IVCM observations on keratoconus giving the clinician a comprehensive guide on the IVCM reflectivity patterns in keratoconus.

The concept of corneal shape remodelling in keratoconus can be considered as a possible result of a cycle of events starting from the disruption of Bowman's zone with the formation of multiple breaks. This is followed by keratocyte occupation of these gaps with subsequent fibroblastic transformation that lays variable amounts of fibrous tissue. With further loss of Bowman's zone material as well as keratocyte apoptosis these fibrotic changes can later expand transversely and vertically to end up with corneal shape deformation. The role of other mechanical forces like the intraocular pressure and forceful frequent rubbing of a cornea with already weakened anterior lamellae would

possibly have an additive effect in the process of corneal shape remodelling. The rate of progression of this cycle may be determined by the provocative factors.

Chapter Six

6 In vivo Confocal Microscopy in Corneal Dystrophy with Histopathological Correlation.

6.1 INTRODUCTION

Corneal dystrophies involve a group of genetically inherited disorders that can affect various corneal layers resulting in certain microstructural as well as gross morphological changes. The clinical consequences of such changes could be limited to recurrent corneal irritation and erosion with stable vision in epithelial dystrophies (Waring et al., 1978a) or the vision could be significantly impaired in stromal and endothelial dystrophies later in life to an extent that corneal graft will finally be justified (Waring et al., 1978a, Waring et al., 1978b). Recurrence of corneal dystrophic material years following a successful graft is well documented in stromal dystrophies (Auw-Haedrich et al., 1996, Marcon et al., 2003).

The histological features of the majority of corneal dystrophies are well described and are a standard feature in ocular pathology texts especially the stromal and endothelial types. In vivo confocal microscopy (IVCM) has been used to identify the reflectivity patterns

of these disorders at various corneal layers in order to get a more comprehensive understanding of the microstructural details via this non-invasive real time imaging tool that promises to improve clinical evaluation of involved corneas (Werner et al., 1999b, Ciancaglini et al., 2001a, Labbe et al., 2006, Chiou et al., 1999a, Kobayashi et al., 2007). Not all studies included histopathological correlation with IVCM in corneal dystrophy and the aim of this study is to compare IVCM patterns with corresponding histological findings in a variety of corneal dystrophies in order to achieve a reliable corroborated interpretation of IVCM features that might help establish clinically useful diagnostic criteria besides those seen with slitlamp biomicroscopy.

6.2 PATIENTS AND METHODS:

Eight patients, 1 male and 7 females with an age range of 25 – 74 years, all seen in the eye clinic at Nottingham University hospitals, Queens Medical Centre, Nottingham, UK, were included. All cases were diagnosed with one of the known corneal dystrophies based on their clinical features. Figure 6-1 illustrates slitlamp photographs of 4 cases of the study group while Table 6-1 summarises the demographic and clinical features of all the cases that could be classified according to their clinical diagnosis into the following conditions and groups:

1. **Bowmans zone corneal dystrophy (n=1): Case 1** was a 49 year old female suffered from gradual drop of vision in her left eye over the preceding year not corrected with contact lenses. Her best

corrected visual acuity (BCVA) was 6/9 and 6/24 in the right and left eyes respectively. Slitlamp examination revealed reticular fishnet–like central subepithelial opacities in both corneas, being worse in the left eye (Figure 6-1A). Central corneal thickness was 548µm and 560µm in right and left eyes respectively. A clinical diagnosis of Reis-Bucklers' corneal dystrophy was considered and she underwent left deep anterior lamellar keratoplasty (DALK).

2. **Macular dystrophy (n=2): Case 2** (Table 6-1) was a female aged 25 years who presented with slowly progressive drop of vision associated with photophobia over the past 2 years. Her BCVA was 6/12 in each eye and the slitlamp examination revealed bilateral greyish white central corneal opacities of ill-defined edges involving epithelium and stroma, being worse in the left eye (Figure 6-1 B). Case 3 was a 74 years old female who presented with visual deterioration in her left eye over 2 years. On clinical examination she had BCVA of 6/9 and 6/24 in the right and left eyes respectively along with central corneal diffuse punctuate opacities surrounded by peripheral larger roundish opacities (Figure 6-1C). The right eye was already operated with penetrating keratoplasty (PK). Both patients underwent left PK.
3. **Granular dystrophy (n=4):** 2 cases in this subgroup (no. 4 & 5 Table 6-1) presented with primary granular corneal deposits seen as crumb-like opacities with clear intervening stroma on slitlamp examination. Case 4 (Table 6-1), a 52 years old female, presented with history of severely painful episodes of recurrent corneal

erosion in both eyes for two years. Her BCVA was 6/9 in each eye and the slitlamp examination revealed multiple corneal granular deposits protruding through the epithelium being worse in the right eye. Case 5 (Table 6-1), a 46 years old female, had BCVA of 6/12 in the right eye which showed corneal deposits with intact epithelium (Figure 6-1D). She had a clear left corneal graft done 1 year before. Both cases underwent right deep anterior lamellar keratoplasty (DALK). Case 6 (Table 6-1), a 50 years old female presented with moderate drop of vision (BCVA 6/12) associated with recurrent fine granular superficial deposits in the right eye 1 year following PK. She underwent alcohol delamination (Dua et al., 2006) of the central 8mm zone of the right corneal epithelium. Case 7 (Table 6-1), a 69 years old female, presented with deeper and more extensive recurrent fine granular deposits in the right eye with BCVA of 6/18 following PK done 2 years before. She underwent right repeat PK.

4. **Lattice dystrophy (n=1).** A 62-year-old male (case 8 Table 6-1) presented with gradual drop of vision with photophobia in the right eye that had undergone a corneal graft 15 years before. BCVA was 6/18 and 6/6 in the right and left eye respectively and slitlamp examination revealed lattice-like stromal opacities in the right corneal graft. He was diagnosed with recurrent lattice dystrophy and treated with repeat PK to his right eye.

All cases were examined preoperatively with IVCM as described in chapter two. 8 tissue samples including 1 sheet of corneal epithelium, 3 anterior lamellar and 4 full thickness corneal buttons were obtained for histological processing. Heamatoxylin & Eosin (H&E), toluidine blue and Alcian blue dyes were used to prepare sections for light and electron microscopy (see chapter two). IVCM images were then compared with histopathological sections to correlate the findings observed with the two diagnostic modalities.

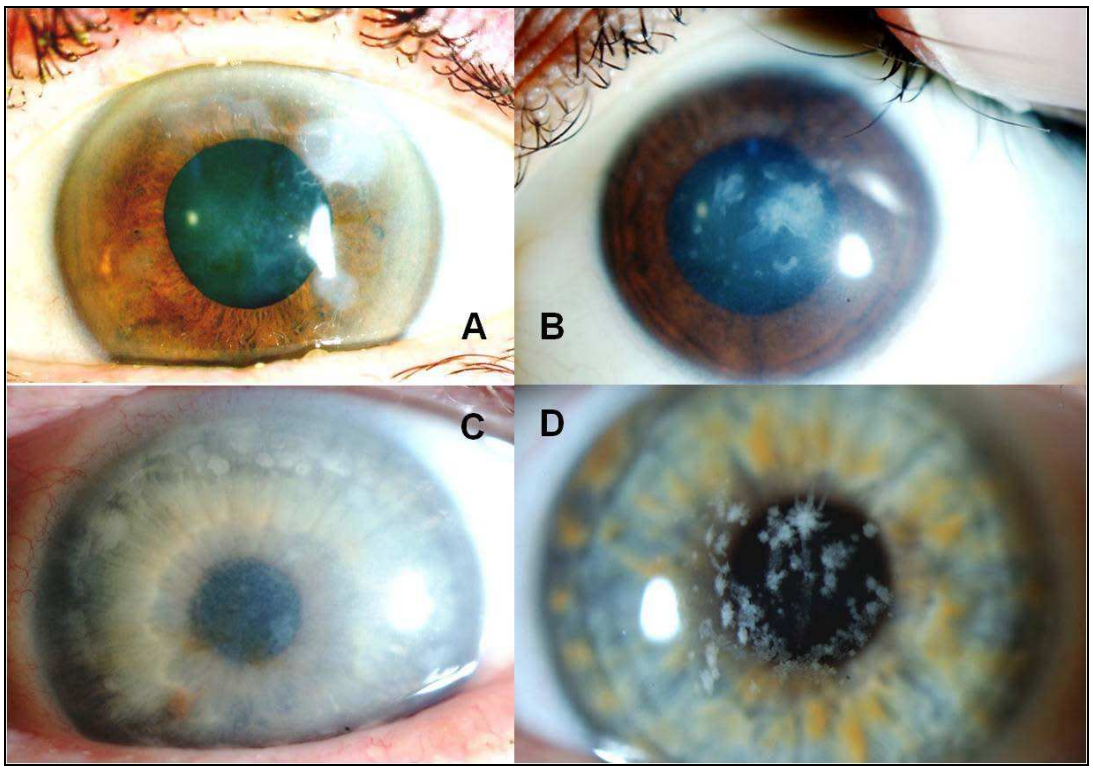

Figure 6-1: Diffuse slitlamp corneal photographs of 4 cases with corneal dystrophies. A (case1) shows central honeycomb opacities affecting Bowman's zone. B (case2) shows multiple opacities with hazy intervening stroma in macular dystrophy. C (case3) shows hazy central cornea with multiple peripheral roundish opacities in macular dystrophy. D (case5) shows multiple breadcrumb like opacities with clear intervening stroma in granular dystrophy.

Table 6-1: Summary of demographic and clinical features of 8 cases with various corneal dystrophies included in this study.

No.	Age/ Sex/ Eye	BCVA	Clinical features	Diagnosis	Operation
1	49 /F / L	6\24	Drop of vision, fishnet central corneal subepithelial opacities	Bowman's zone dystrophy	DALK
2	25 /F / L	6\12	Drop of vision, photophobia, central corneal opacities with ill-defined edges	Macular dystrophy	PK
3	74 /F / L	6\24	Drop of vision, intact epithelium, central stromal opacification	Macular dystrophy	PK
4	52 /F /R	6\9	RCE, photophobia, irregular epithelial surface, multiple coarse breadcrumb like corneal opacities with clear intervening stroma	Granular dystrophy	DALK
5	46 /F /R	6\12	Drop of vision, multiple coarse breadcrumb like central corneal opacities with clear intervening stroma	Granular dystrophy	DALK
6	50 /F /R	6\12	Drop of vision, fine epithelial opacities in otherwise clear corneal graft	Recurrent granular dystrophy	Alcohol Delamination
7	69 /F /R	6\18	Drop of vision, fine breadcrumb-like opacities in corneal graft epithelium & superficial stromal	Recurrent granular dystrophy	PK
8	62 /M /R	6\18	Drop of vision, photophobia, lattice like stromal opacities in right corneal graft	Recurrent lattice dystrophy	PK

BCVA= Best Corrected Visual Acuity. DALK= Deep Anterior Lamellar Keratoplasty, PK= Penetrating Keratoplasty.

RCE= Recurrent Corneal Erosion.

6.3 RESULTS:

6.3.1 Bowman's zone corneal dystrophy:

Histopathological corneal sections from case1 revealed extensive loss of Bowman's zone that was replaced by superficial stromal scar. The overlying epithelium showed irregularity in thickness with undulating profile of the basal epithelium. The cellular polarity was well preserved (Figure 6-2A). The corresponding IVCM images showed areas of basal epithelium surrounded by hyper-reflective bands of scar tissue (Figure 6-2B). Bright oval figures of fibroblast / keratocyte nuclei were clearly seen within the scar corresponding to sub-epithelial spindle–like presumed fibroblast nuclei seen in histological sections (Figure 6-2C). On volumetric scan neither the normal reflectivity pattern of Bowman's zone nor sub-basal nerves could be visualised (Figure 6-3). No evidence of deposit material could be seen on light or confocal microscopy.

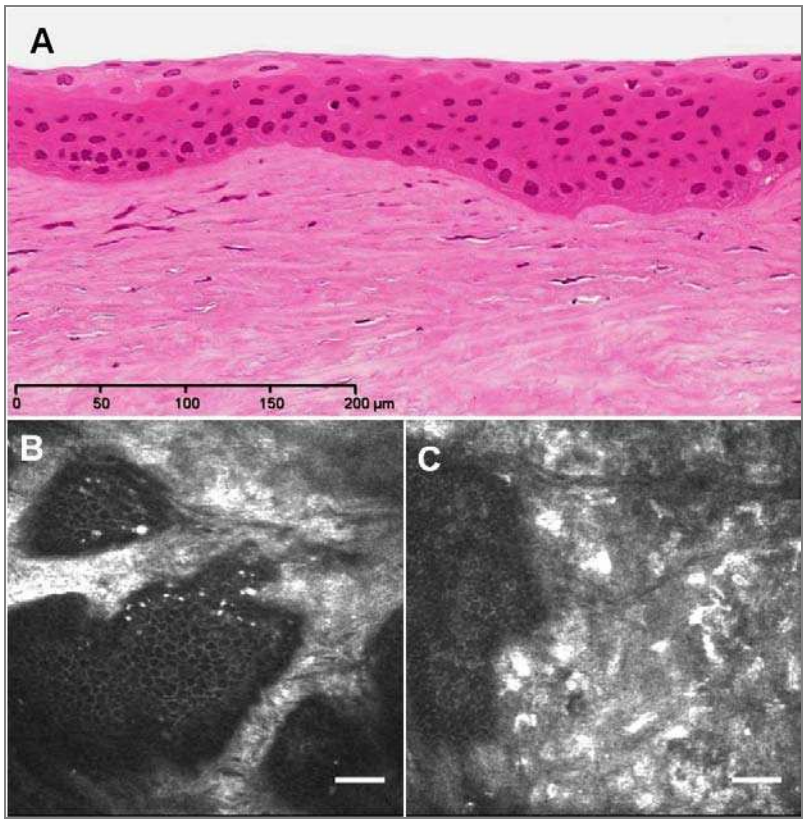

Figure 6-2: Histological changes in Bowman's zone corneal dystrophy. A, light micrograph of corneal cross section from case 1 sample showing total replacement of Bowman's zone by superficial stromal cellular scar with undulating profile of the overlying epithelium without clear evidence of material deposition. Corresponding en face IVCM images showed basal epithelia sheets interrupted by hyper-reflective bands of subepithelial scar with isolated epithelial islands (B) and bright nuclear figures of fibroblasts (C). Scale bar 50µm. (A stained with H&E)

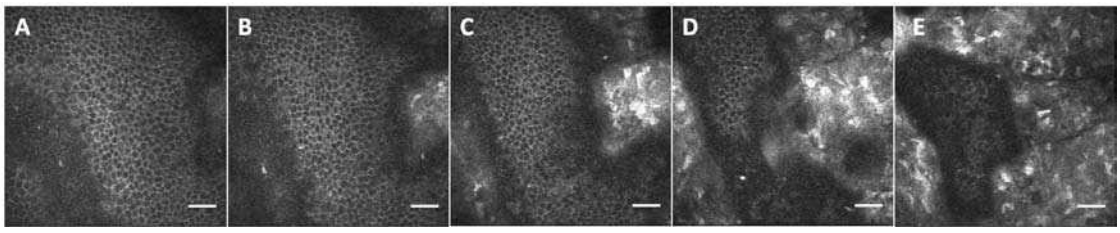

Figure 6-3: Volumetric IVCM images from case 1 with Bowman's zone dystrophy taken at successive focal plane depth of 66, 70, 76, 89 and 102µm from A to E respectively showing patterns of basal epithelium overlying subepithelial scar without evidence of normal patterns of Bowman's zone or sub-basal nerves. Scale bar 50µm.

6.3.2 Macular Corneal Dystrophy:

Histological sections of corneal samples revealed widespread deposits stained positively with alcian blue indicating its acid mucopolysaccharide nature (Figure 6-4). Within stromal layers these deposits appeared to accumulate within the spindle-like vacuolated keratocytes of variable sizes within which red-stained nuclei could be seen (Figure 6-4A from case 3). Extracellular stromal deposits could be seen as well (Figure 6-4B from case 4). Subepithelial deposits within scar tissues associated with breaks or even total loss of Bowman's zone were clearly seen in both cases (Figure 6-4 A&B). Endothelial cells were also involved and in case 3 Descemet's membrane excrescences could be seen as well (Figure 6-4C).

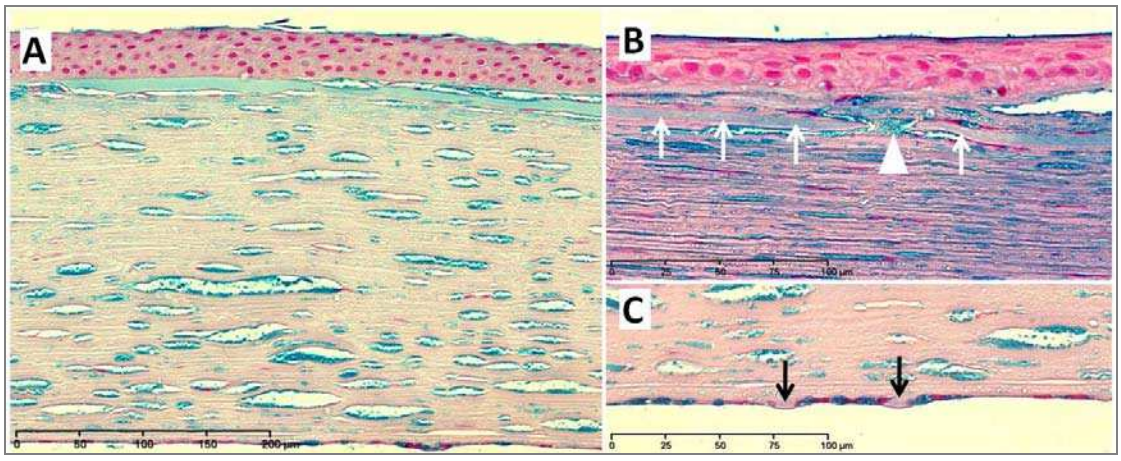

Figure 6-4: Light micrographs of sections from 2 cases with macular corneal dystrophy. A (case 3) shows well demarcated accumulations of mucopolysaccharides within vacuolated keratocytes. B (case2) illustrates extracellular stromal and subepithelial deposits filling a break (arrow head) in Bowman's zone (white arrows). C (case 3) shows involvement of endothelium with Descemet's membrane excrescences (black arrows). (Stained with alcian blue).

IVCM images revealed frequent areas of subepithelial hyper-reflective scar-like tissue seen adjacent to basal epithelium and sub-basal corneal nerves (Figure 6-5 A). The normal reflectivity pattern of Bowman's zone was largely undetectable in both cases even in oblique views (Figure 6-5 B).

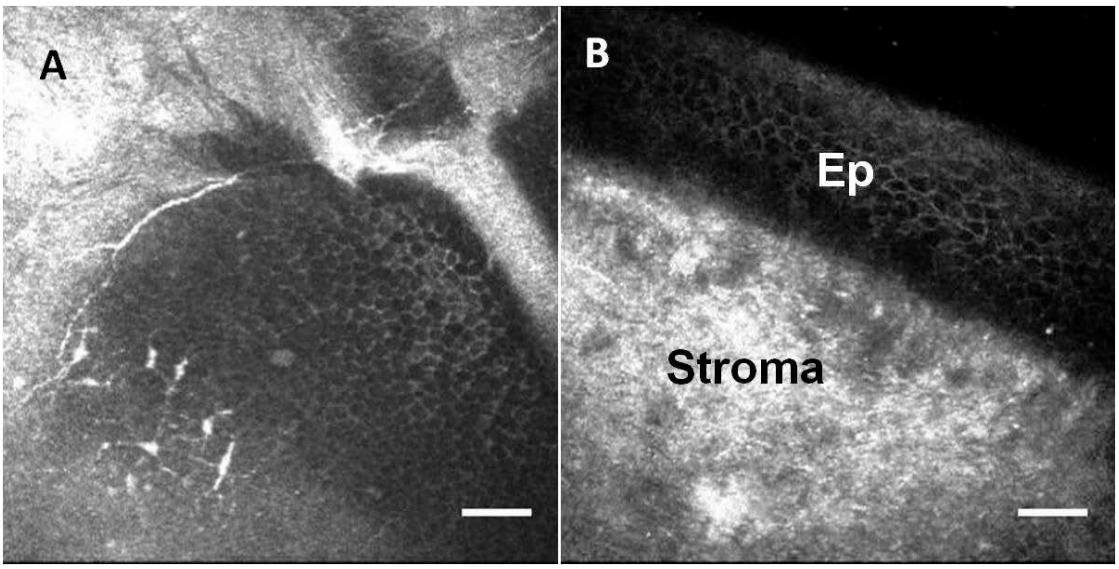

Figure 6-5: IVCM images of cornea in case 3 with macular dystrophy showing hyper-reflective scar-like pattern at subepithelial levels interrupting continuity of the basal epithelium on enface view (A). No evidence of Bowman zone could be seen in oblique view (B). Ep= epithelium. scale bar 50µm.

Interestingly in case 3 the stromal layers showed multiple hyper-reflective amoeboid figures within a bright background replacing keratocyte nuclei mostly at middle and deep stromal layers (Figure 6-6C). This pattern was not seen in case 2 where keratocyte nuclei were completely overshadowed by homogenously increased reflectivity of stromal layers.

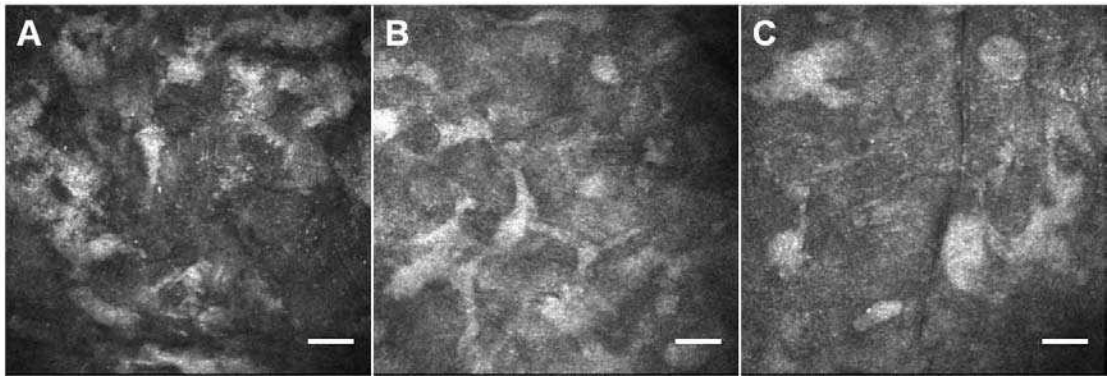

Figure 6-6: IVCM images of cornea in case 3 with macular dystrophy showing amoeboid hyper-reflective figures seen at middle and deep stromal levels replacing normal keratocyte nuclei. Focal plane depths are 159, 318 and 369µm in images A to C respectively. Scale bar 50µm.

Endothelial cells in case 2 showed normal pattern with scattered hyper-reflective deposits (Figure 6-7 A) while in case 3 the endothelium was ill-defined with frequent dark spots with bright centres representing guttae of Descemet's membrane (Figure 6-7B).

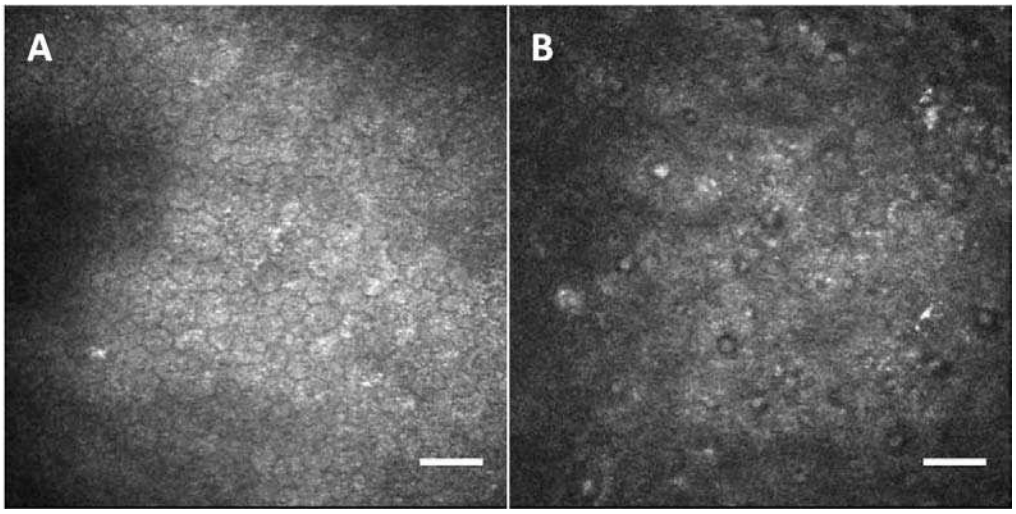

Figure 6-7: IVCM images of corneal endothelium in macular dystrophy showing scattered hyper-reflective spots with reasonably normal pattern in case 2 (A). In case 3 (B) the endothelium is ill-defined with multiple guttae of Descemet's membrane. Scale bar 50µm.

6.3.3 Granular corneal dystrophy

Histopathological sections revealed multiple clumps of eosinophilic hyaline material stained homogenously with H&E within stromal layers (Figure 6-8). In case 4 Bowman's zone was extensively lost with irregular overlying epithelium related to anteriorly located deposits (Figure 6-8A). In case 5 these deposits showed limited breaches in Bowman's zone with relatively intact regular epithelium (Figure 6-8B).

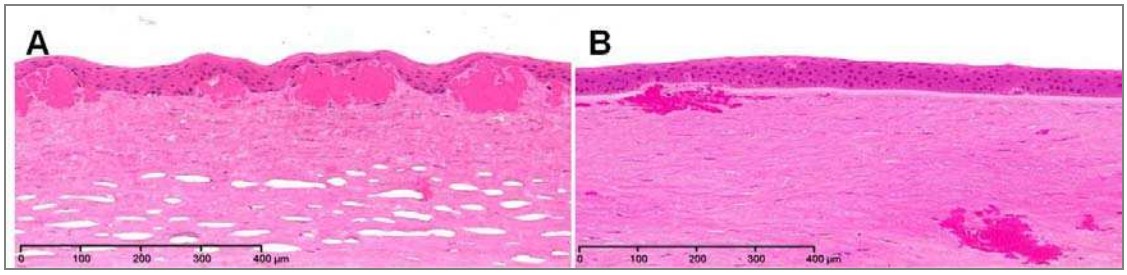

Figure 6-8: Light micrographs of sections from case 4 & 5 with granular corneal dystrophy. A (case 4) shows multiple superficial stromal hyaline deposits disrupting Bowman's zone with irregular overlying epithelium. B (case 5) limited breach in Bowman's zone is seen with relatively regular surface epithelium. (H&E stain).

IVCM images revealed multiple hyper-reflective geographical areas with ragged edges representing granular deposits (Figure 6-9). In case 4 the deposits showed non-homogenous reflectivity with bright round spots within paler areas surrounding sheets of corneal epithelium without evidence of sub-basal nerves or normal Bowman's zone pattern (Figure 6-9 A). In case 5 the deposits were homogenously brighter with clear adjacent sub-basal nerves (Figure 6-9 B&C).

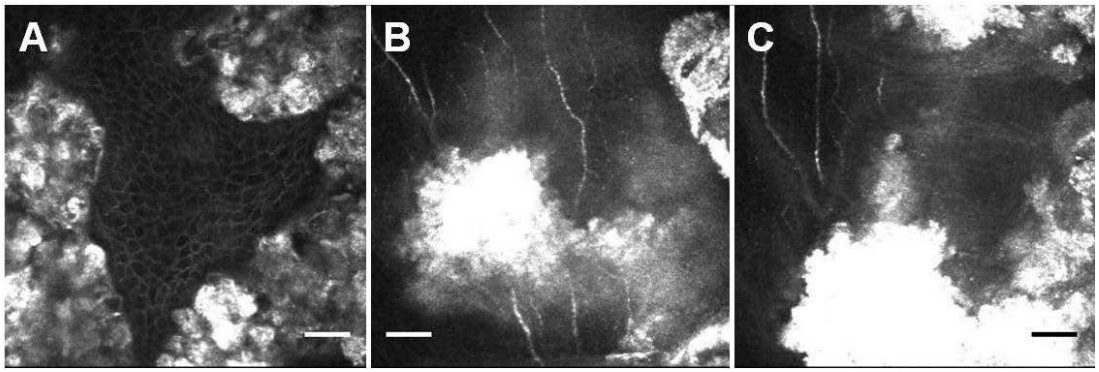

Figure 6-9: IVCM images of cornea in case 4 & 5 with granular dystrophy. Non-homogenous hyper-reflective deposits with multiple round bright figures can be seen in A (case 4) surrounding a sheet of epithelium. Brighter deposits at the level of Bowman zone can be seen in B & C (case 5) with visible sub-basal nerves. Focal plane depths are 37, 54 and 60µm in images A-C respectively. Scale bar 50µm.

In case 6 with recurrent granular dystrophy electron microscopy of the epithelial sheet revealed multiple dark electron-dense areas representing extracellular granular deposits (Figure 6-10 A). In case 7 the deposits were seen in anterior stromal layers with extensive loss of Bowman's zone associated with irregular epithelium (Figure 6-10 B).

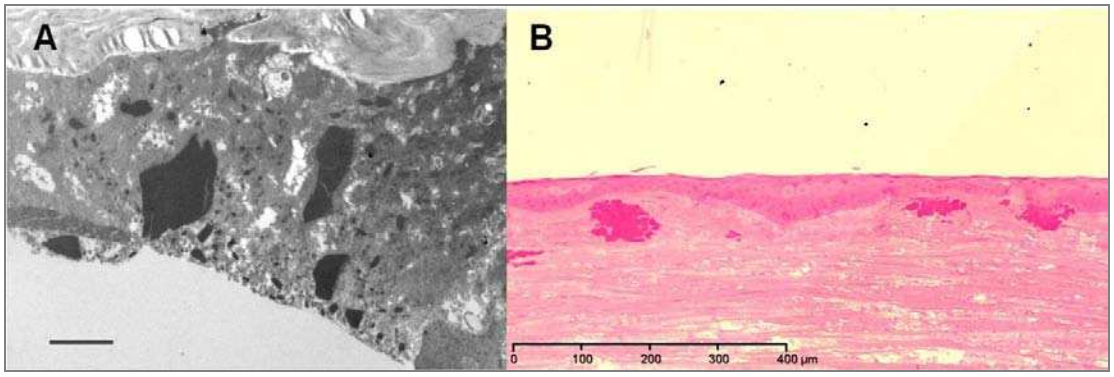

Figure 6-10: Microscopic views in recurrent granular corneal dystrophy. A, Transmission electron micrograph of corneal epithelium from case 6 showing multiple electron-dense (dark) deposits in recurrent granular dystrophy. B, light micrograph of section from case 7 shows stromal eosinophilic hyaline deposits in recurrent granular dystrophy. (Scale bar =2µm in A. H&E stain in B).

Corresponding IVCM images in case 6 showed multiple bright snowflake like structures at the level of basal epithelium close to Bowman's zone representing early granular deposits (Figure 6-11 A&B). Compared to primary deposits they were smaller and not exceeding 50µm in size. In case 7 these deposits were larger and located deeper within stromal layers (Figure 6-11C).

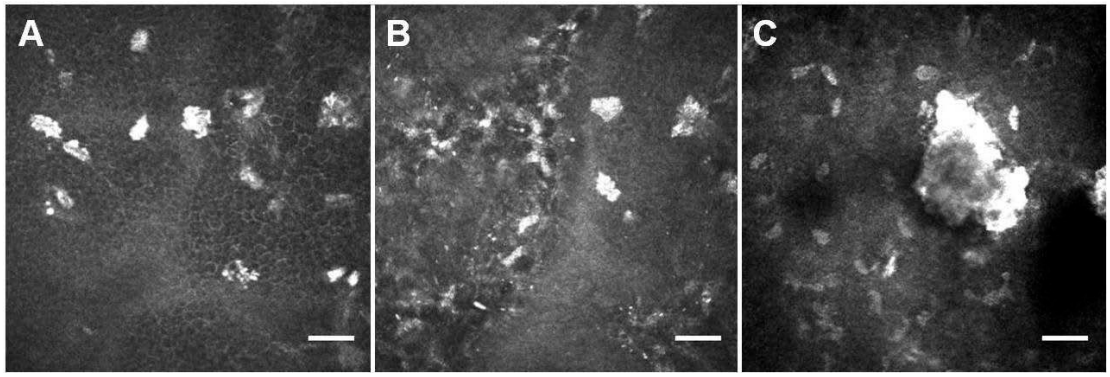

Figure 6-11: IVCM images of cornea with recurrent granular dystrophy. Snowflakes – like figures are seen at basal epithelial level (A) and close to Bowman's zone (B) (case 6). Deeper stromal deposits can be seen in C (case 7). Scale bar 50µm.

6.3.4 Lattice corneal dystrophy.

Histopathology of corneal sections revealed deposition of amyloid material that was deeply stained with toluidine blue and consistent with lattice dystrophy (Figure 6-12). A break in Bowman's zone was noticed with deposition of dystrophic material at subepithelial and anterior stromal levels (Figure 6-12A). Deep stromal material was noticed as well (Figure 6-12B).

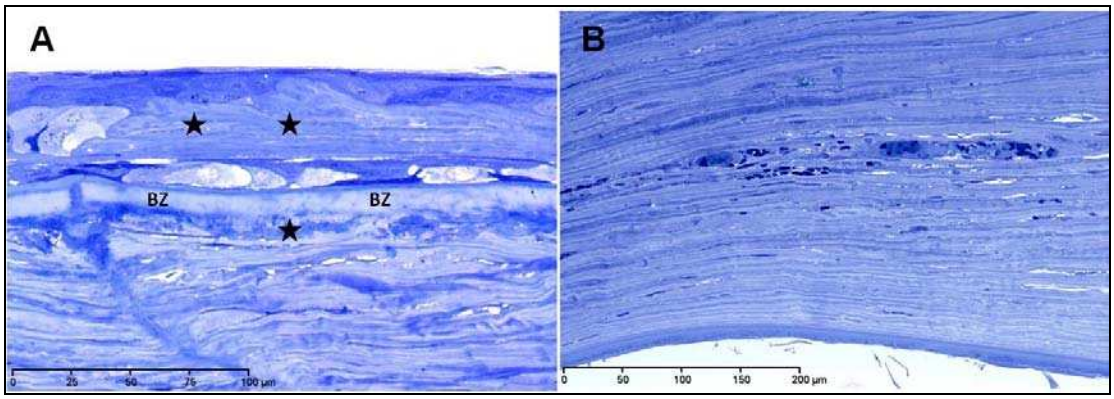

Figure 6-12: Light micrographs of corneal sections from case 8 with Lattice dystrophy. Amorphous material (consistent with amyloid) stained with toluidine blue (stars) can be seen above and below Bowman's zone (BZ) in A as well as within deep stromal layers in B.

On IVCM hyper-reflective broad areas were noticed at the level of basal epithelium similar to reflectivity patterns of scar tissues (Figure 6-13A). Dark cyst-like areas and bright round to oval figures were frequently seen within these bright scar-like areas. No evidence of sub-basal nerves or Bowman's zone patterns could be visualised. In deep stromal levels branching hyper-reflective bands ranging between 12 and 40µm in width similar to stromal nerves were noticed as well (Figure 6-13 B&C). The keratocyte nuclei were clearly visible throughout the stromal thickness.

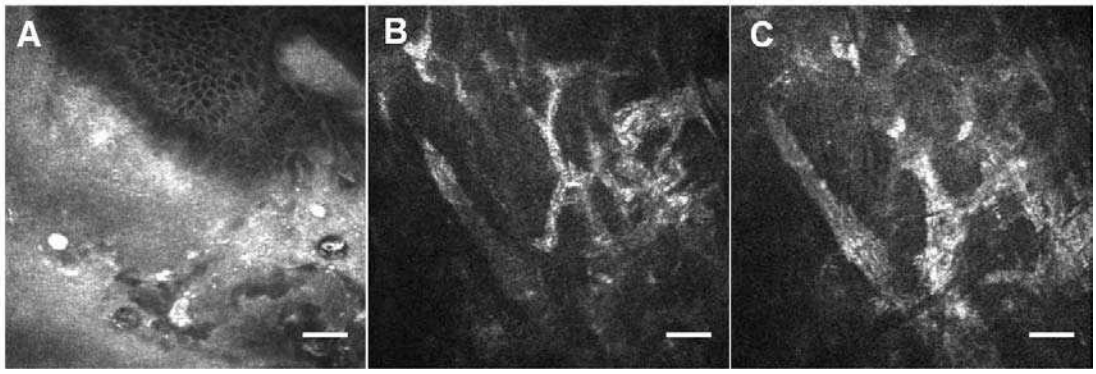

Figure 6-13: IVCM images of cornea in case 8 with lattice dystrophy. Broad hyper-reflective areas are noticed at the basal epithelial level in A with scattered bright round and dark cyst-like figures. In deep stromal layers hyper-reflective branching bands 12 – 40µm wide are visible (B) next to well demarcated keratocyte nuclei (C). Scale bar 50µm.

6.4 DISCUSSION:

IVCM has been applied widely to describe various corneal dystrophies (Werner et al., 1999b, Chiou et al., 1999a, Grupcheva et al., 2001a, Kobayashi et al., 2007, Kobayashi and Sugiyama, 2007, Labbe et al., 2006). However histopathological correlation with samples obtained from the same patients has been limited to 2 papers only (Chiou et al., 1999a, Kobayashi et al., 2007).

This study recruited 8 cases with various corneal dystrophies for correlation between IVCM criteria and histopathological features.

In **corneal dystrophy of Bowman's zone (CDB)** 2 types have been identified histologically: Reis-Bucklers' (CDBI) and Thiel-Behnke's (CDBII) dystrophy (Kuchle et al., 1995, Ridgway et al., 2000). The first type is associated with earlier onset of visual impairment, usually in the second decade of life, along with epithelial irregularity and geographical opacities

/ deposits at the level of Bowman's zone seen on slitlamp examination (Kuchle et al., 1995, Ridgway et al., 2000). The second type presents with later onset of visual impairment with a honeycomb-shaped opacities at the level of Bowman's zone (Kuchle et al., 1995, Ridgway et al., 2000). Histologically both conditions are characterised by loss of Bowman's zone but differ in the presence of band –shaped granular deposits in Bowman's zone in Reis-Bucklers' dystrophy, while in Thiel-Behnke's an undulant fibrocellular tissue replaces Bowman's zone (Kuchle et al., 1995, Ridgway et al., 2000). In case 1 neither slitlamp nor light microscopic examination revealed any clear sign of corneal deposits so the diagnostic features were more consistent with those reported in Thiel-Behnke's dystrophy. The IVCM and histological findings can be correlated as follows:

1. Corneal epithelial irregularity: The undulating profile of basal epithelium seen on histological cross sections explains the pattern of basal epithelial sheets interrupted by bright bands of subepithelial scar seen on en face IVCM images. This pattern is attributed to the loss of Bowman's zone with subsequent formation of anterior stromal scar, quite similar to the changes seen in keratoconus cases with significant disruption of Bowman's zone (see chapter 5 for more details). The long history of recurrent corneal erosion associated with Bowman's zone dystrophy is clearly related to corneal epithelial irregularity.
2. The sub-epithelial scar was frequently seen with presumed fibroblast nuclei in a pattern similar to what was seen in corneal oedema and

keratoconus (see chapter 4 & 5). The random and irregular arrangement of these nuclei within scar tissue seen on light microscopy and IVCM is thought to be useful to differentiate these cells from normal keratocytes.

The extensive loss of Bowman's zone was reflected on IVCM by loss of the normal reflectivity pattern of K-structures seen in intact Bowman's zone (Kobayashi et al., 2006) as well as invisibility of sub-basal corneal nerves. Kobayashi and Sugiyama (2007) described IVCM features in Thiel-Behnke's dystrophy with presence of focal deposits within corneal epithelial and Bowman's zone levels (Kobayashi and Sugiyama, 2007). However the published images were more consistent with reflectivity pattern of scar tissue without clear evidence of presence of deposits that were obviously visible in IVCM images of Reis-Bucklers' dystrophy published in the same paper (Figure 1-19). Moreover they did not describe the patterns of epithelial irregularity associated with subepithelial fibrosis reported in this study. We couldn't identify any kind of granular deposits on either mode of examination, light microscopy or IVCM.

Macular corneal dystrophy is an autosomal recessive disorder that results in diffuse stromal haze due to widespread deposition of glycosaminoglycan (GAG). In histology the deposits are well reported to accumulate within vacuolated keratocytes as well as in extracellular matrix (Garner, 1969, Rodrigues and Krachmer, 1988). In this study keratocyte nuclei were not visible on IVCM in both cases. The hyper-

reflective amoeboid patterns seen in case 3 were comparable to the pattern of distribution of the dystrophic material seen on histopathological sections. In these sections the spindle-like vacuolated keratocytes laden with alcianophilic deposits were better demarcated in case 3 compared to case 2. It would be possible that these amoeboid figures seen on IVCM might represent GAG-filled keratocytes. Moreover the endothelial involvement was more obvious in case 3 with frequent Descemet's membrane guttae formation seen on IVCM, a finding that confirmed the need for PK rather than DALK in that lady. Kobayashi et al [2007] reported homogenous stromal hyper-reflectivity with no keratocyte nuclei on IVCM of macular dystrophy similar to our findings in case 2 (Kobayashi et al., 2007). However the amoeboid stromal pattern as well as the endothelial changes seen in case 3 were not mentioned in previous studies with IVCM.

Granular corneal dystrophy is an autosomal dominant disorder characterised by the accumulation of circumscribed discrete breadcrumb like opacities within the central corneal anterior stroma sparing the periphery (Rodrigues and Krachmer, 1988)**.** In granular dystrophy the reflectivity pattern seen on IVCM in this study is consistent with what was mentioned in previous studies (Werner et al., 1999b, Kobayashi et al., 2007). In case 4 the superficial stromal deposits were paler on IVCM than those seen in case 5 that is in addition to the clear visibility of basal epithelial sheets in between these deposits in the former case indicating

corneal epithelial irregularity. This was clearly related to the history of recurrent corneal erosion mentioned in case 4. Recurrence of corneal dystrophies has been reported to occur 2-25 years following a successful corneal graft (Rodrigues and Krachmer, 1988, Lyons CJ et al., 1994, Marcon et al., 2003). The superficial recurrent granular deposits seen in case 6 were mainly epithelial and appeared smaller than those found in primary cases 4 & 5. The epithelial origin of these recurrent deposits has been strongly suggested by other investigators who described vortex patterns on presentation (Lyons CJ et al., 1994, Auw-Haedrich et al., 1996, Traversi et al., 2006). The snowflakes pattern of these deposits seen on IVCM is close to the findings described by Werner et al (1999).

In our study IVCM was able to confirm the exact level of these deposits in a way that supported the decision for proper treatment with alcohol delamination in case 6 and PK in case 7 who proved to have deeper involvement.

In **lattice corneal dystrophy** deposits of amyloid material are localised within subepithelial and stromal layers presenting clinically as filamentous branching opacities (Rodrigues and Krachmer, 1988). In this study the subepithelial deposits were viewed on IVCM as hyper-reflective areas at the level of basal epithelium. This scar–like reflectivity on IVCM was described by other investigators who also mentioned the branching bright bands within stromal layers that were found in our study (Chiou et al., 1999a, Rosenberg et al., 2001, Kobayashi et al., 2007). Only one study

used HRTII-RCM machine similar to the one used in our study to yield IVCM images of reasonable quality (Kobayashi et al., 2007).

6.5 CONCLUSION

This study has produced a reliable set of IVCM criteria supported by histological evidence in a group of corneal dystrophies so that it complements what has already been published. Careful scanning has resulted in a new IVCM pattern in macular dystrophy. In this study the ability of IVCM to confirm endothelial involvement in macular dystrophy did support the priority of PK over DALK as a definitive treatment in case 3 with macular dystrophy. Early cases of recurrent granular dystrophy can be further evaluated with IVCM to confirm the need for alcohol delamination in case the deposits are found to be limited to the epithelial layers.

Chapter Seven

7 In vivo Confocal Microscopy in the diagnosis and management of Acanthamoeba Keratitis

7.1 INTRODUCTION:

Acanthamoeba keratitis (AK) is a painful potentially blinding corneal infection that has been increasingly reported in association with soft contact lens wear (Pfister et al., 1996). The causative organism, Acanthamoeba, is a ubiquitous free-living amoeba found in water and soil. We present two cases in whom the decision to treat for acanthamoeba keratitis was based on IVCM findings, with favourable outcomes. Novel IVCM presentations of cysts as 'signet rings' and 'bright spots' in addition to the classical 'double wall' images, were noted. In both cases acanthamoeba were confirmed on culture as well. IVCM can provide early evidence of acanthamoeba infection. Treatment, when initiated whilst the organism is largely confined to the epithelium as was done in these two patients, can result in healing with minimal scarring.

7.2 PATIENTS AND MANAGEMENT:

7.2.1 Case 1:

A 24 year female contact lens wearer presented with a 1 mm diameter paracentral stromal infiltrate (Figure 7-1A) with no overlying ulcer, in her left eye. Her vision was 6/6. Routine IVCM examination with Rostock Cornea Module attached to HRT II (Heidelberg Engineering, Germany) and scrapes for culture were taken. IVCM showed classical intraepithelial cysts with dendritic cell infiltration (Figure 7-1B and C). Anti-acanthamoeba treatment (Polyhexamethylene biguanide 0.02% and Propamidine 0.1%) antibiotics Polyfax eye ointment (Polymixin B 10,000 IU and Bacitracin zinc 500 IU) and ciprofloxacin 0.3%, were initiated. Repeat IVCM showed decrease in number of cysts and dendritic cells on day 7 (Figure 7-1D) which had disappeared by week 9 (Figure 7-1E) when the lesion had completely healed with a nebular stromal scar (Figure 7-1F). Cultures were positive for acanthamoeba but no bacteria or fungi were grown. Her vision remained 6/6.

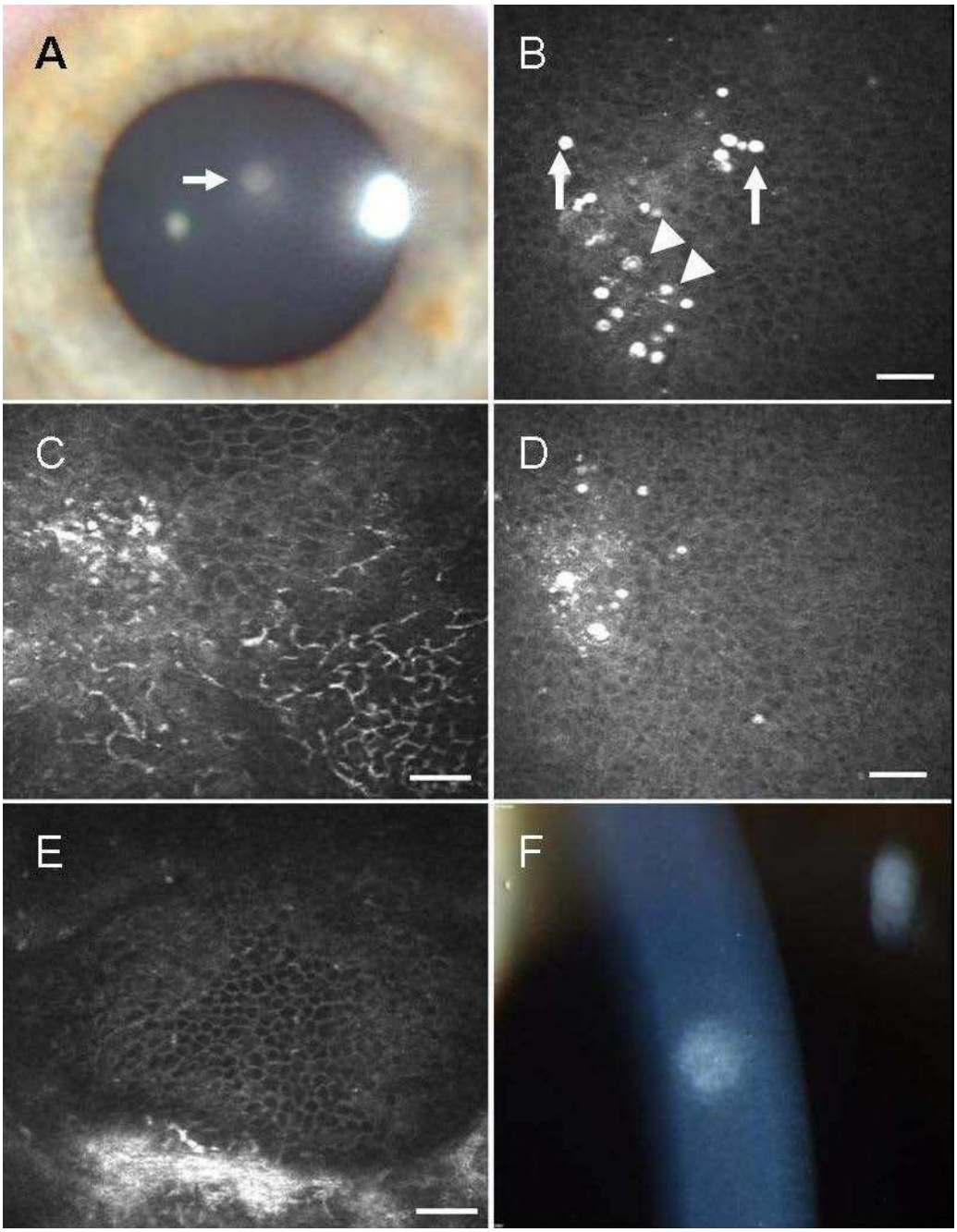

Figure 7-1: (A) Clinical slit lamp photomicrograph (diffuse illumination) of case 1 showing corneal stromal infiltrate (arrow). (B) IVCM (pre-treatment) showing double walled cysts (arrow heads) and 'bright spot' cysts (arrows). (C) IVCM (pre-treatment) showing dendritic cells. (D) IVCM (day 7) showing reduced number of cysts. (E) IVCM (week 9) showing absence of cysts. (F) Slit lamp broad beam illumination (week 9) showing residual subepithelial nebular scar.

7.2.2 Case 2:

The second patient was a 28 year female contact lens wearer who presented 4 weeks after onset of bilateral symptoms of photophobia, irritation and slightly reduced vision (6/9 in each eye). The corneal findings included pseudentritic keratitis bilaterally (Figure 7-2 A and B) and subepithelial infiltrates in the left eye. IVCM showed intraepithelial acanthamoeba cysts (Figure 7-2 C (double walled) and D (signet rings and bright spots) with dendritic cells. No cysts were observed in the stroma. The patient was treated as described above with anti-acanthamoeba and antibiotic medication. IVCM examination 11 weeks later showed decrease in number of cysts (Figure 7-3 A-C). 2 months after clinical diagnosis and initiation of treatment culture of corneal epithelium samples revealed acanthamoeba only with no fungi or bacteria. Her vision improved to 6/6 with no stromal scarring.

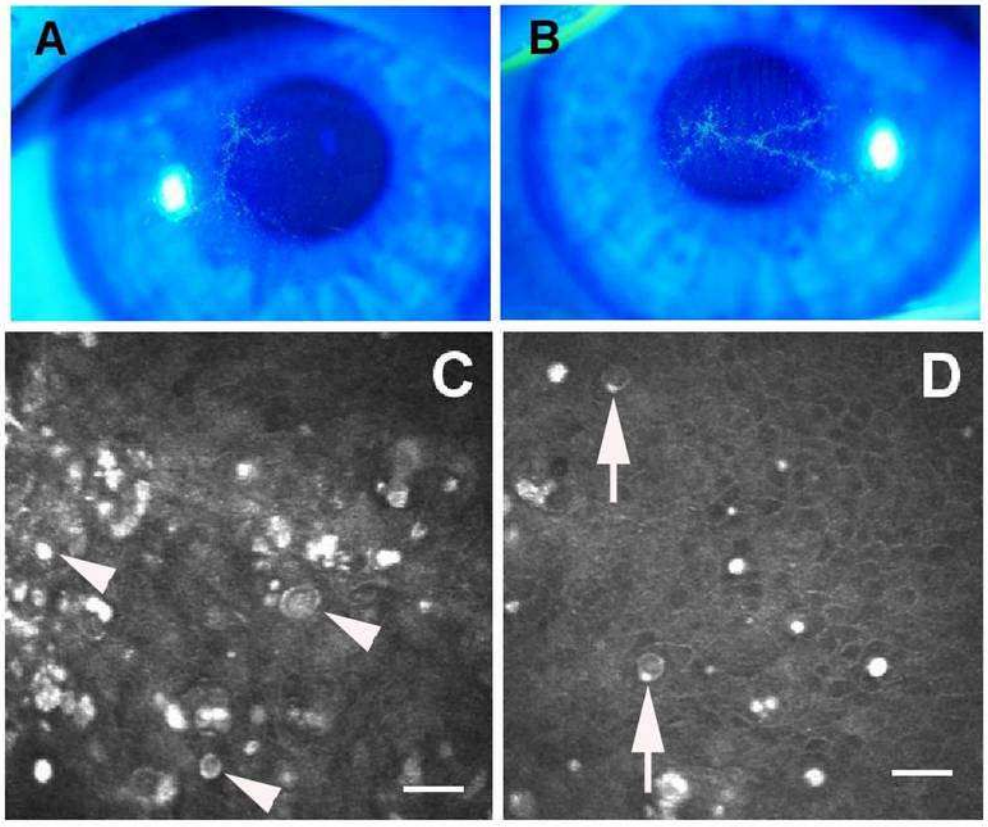

Figure 7-2: (A) and (B) Clinical photograph of right and left eyes respectively in case 2 showing pseudodendritiform lesions (fluorescein dye stained photomicrograph, diffuse illumination). (C) IVCM (pre-treatment) showing intraepithelial double walled (arrowheads) and 'bright spot' cysts. (D) IVCM (pre-treatment) showing 'signet ring' cysts (arrows) and 'bright spot' cysts.

7.2.3 IVCM images with new cystic forms:

IVCM features of acanthamoeba cysts included the classical double walls (Figure 7-1 B and Figure 7-2 C), bright hyper reflective spots (Figure 7-1 B and Figure 7-2 C and D) and bright 'signet ring' images (Figure 7-2 D). The latter represent a novel IVCM manifestation of acanthamoeba cysts. The transition from the 'bright spot image' to the 'signet ring' image is clearly illustrated in Figure 7-3 A-C. In Figure 7-3A two 'bright spots' are

noted at 25µm depth. In the next frame (Figure 7-3 B) at 27µm depth, the upper spot remains as a bright spot but the lower one shows a double wall configuration. At a depth of 31µm (Figure 7-3C) the upper cyst shows a double wall configuration and the lower one assumes a 'signet ring' configuration. This clearly illustrates that these different manifestation represent the level at which the cysts are scanned and 'bright spots' though not always specific for acanthamoeba, should not be ignored when suspecting AK.

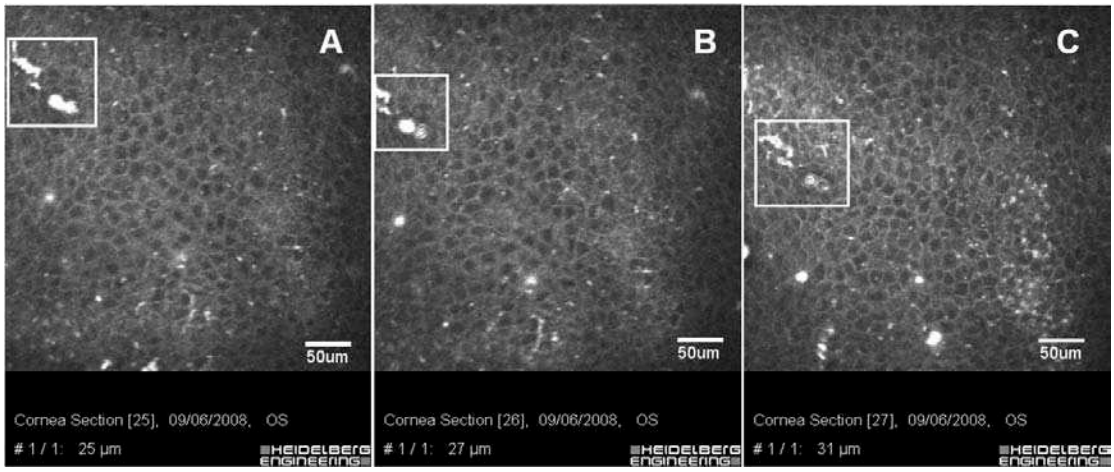

Figure 7-3: (A) IVCM (week 11) at 25µm depth. A pair of 'bright spot' cysts are seen (outlined in square). (B) IVCM of same area as in 'A' at 27µm depth. The top 'bright spot' cyst remains as such but the lower one now has a double wall appearance. (C) IVCM of same area as in 'A' at 31µm depth. The top 'bright spot' cyst now has a double wall appearance and the lower one now presents a 'signet ring' appearance.

7.3 DISCUSSION

Pseudodendritiform lesions, radial perineuritis and ring or double ring abscesses are associated with AK (Lindquist et al., 1988) but the manifestation can often be varied and atypical (Parmar et al., 2006, Mathers et al., 1996). As in our second patient, bilateral involvement in AK is uncommon but has been reported (Lim et al., 2008). Our first case was atypical whilst the second one had the recognised pseudo dendrites. In one large study Mathers et al (1996) confirmed that AK could clinically resemble bacterial keratitis, with stromal infiltrates as well as herpetic keratitis with punctate epithelial Keratopathy, dendritiform lesions, anterior stromal haze and scarring, decreased corneal sensation, disciform keratitis, iritis, and recurrent or persistent epithelial defects (Mathers et al., 1996). The variable virulence as well as the ability to exist in resistant cystic forms under hostile environmental conditions have been suggested to alter the clinical presentation of AK (Mathers et al., 1996). There may be a case for IVCM in all patients with atypical keratitis. The advantage of IVCM has been emphasized in previous studies with some authors proposing that the true incidence of AK would be higher with the use of confocal microscopy than just relying on culture methods (Parmar et al., 2006, Mathers et al., 1996). More recently in a larger retrospective study Parmer et al (Parmar et al., 2006) performed IVCM in 63 cases of suspected AK. In 54 cases (85.7%) cysts were detected and

all of them showed a favourable response to treatment. However, the yield of positive cultures in this group was relatively low (9/29 [31%]), whereas the yield of corneal biopsy was only 50% (2/4). As illustrated by these two cases, IVCM can also be used to monitor response to treatment by estimating the density of cysts over time, which may also help in determining the frequency of instillation of topical medication. These cases suggest that encystment in early infection with acanthamoeba can be confined to the epithelium and routine treatment can successfully eradicate this with a good prognosis.

Chapter Eight

8 In Vivo Confocal Microscopy in Miscellaneous cases

In this chapter 3 miscellaneous cases will be discussed on individual basis as each case presented with unique features that could not be included in a group of cases sharing common diagnostic and pathological criteria. However an effort has been made to compare and relate some of IVCM findings in these individual cases to those already discussed in previous groups and chapters with an emphasis on the diagnostic value of IVCM examination.

The conditions included in this chapter are:

1. Interstitial keratitis – related corneal scarring
2. Paraproteinic Crystalline Keratopathy in localized conjunctival B-cell lymphoma
3. Amiodarone Keratopathy in keratoconus

8.1 CASE 1: INTERSTITIAL KERATITIS-RELATED CORNEAL SCARRING

A 27 year old male presented with poor vision in his right eye for about 12years (since 1994). The drop of vision went painlessly and rapidly in that eye without clear records about the actual diagnosis as he lived in Rwanda when the problem started first. No history of traumatic or other ocular problems could be recalled. He had a left corneal graft done at age 14 without clear information about its indication. On clinical presentation his BCVA was 6/24 and 6/9 in the right and left eye respectively. Slit lamp exam revealed moderate right corneal haze with widespread stromal thinning and scarring. Fine double-contour lines at the level of Descemet's membrane could be seen within the central 4mm zone of the right cornea consistent with breaks in Descemet's membrane. Deep corneal neovascularisation was seen as ghost vessels extending from 6 to 9 o'clock limbal positions to the area of Descemets membrane breaks. The left eye showed clear corneal graft and the rest of his ocular examination was unremarkable. A clinical diagnosis of interstitial keratitis- induced right corneal scarring was considered and the patient underwent right penetrating keratoplasty. IVCM was performed preoperatively and the corneal button was processed in histopathology lab to produce 5µm sections stained with Periodic Acid Schiff (PAS) as well as Heamatoxylin & Eosin (H&E).

8.1.1 Results:

8.1.1.1 Epithelial irregularity with Rolled up Bowman's zone

On histological sections undulate profile of epithelial layers was noticed in areas where Bowman's zone was found to be rolled up (Figure 8-1).

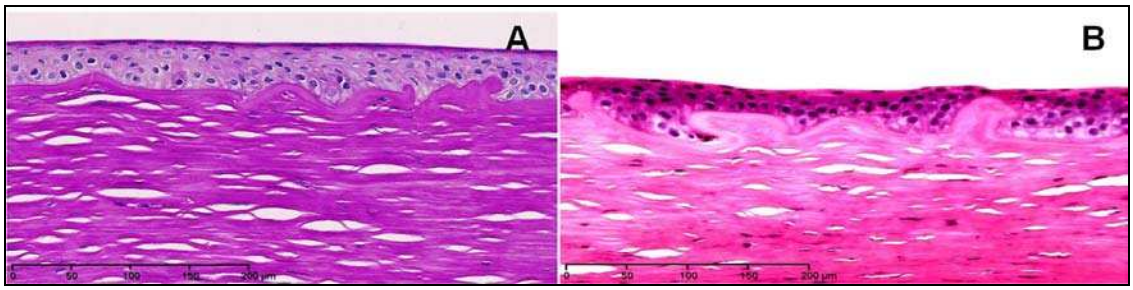

Figure 8-1: Light micrographs of corneal sections from case1 showing areas of rolled up Bowman's zone with associated irregularity of overlying epithelium. (A stained with PAS, B stained with H&E).

Corresponding IVCM images revealed epithelial sheets interrupted by sharply demarcated hyper-reflective curvilinear bands showing wavy or sinusoidal edges (Figure 8-2 A&B). They were 40–100µm in width and intersecting sub-basal nerves could be seen in certain frames running across these bands (Figure 8-2C).

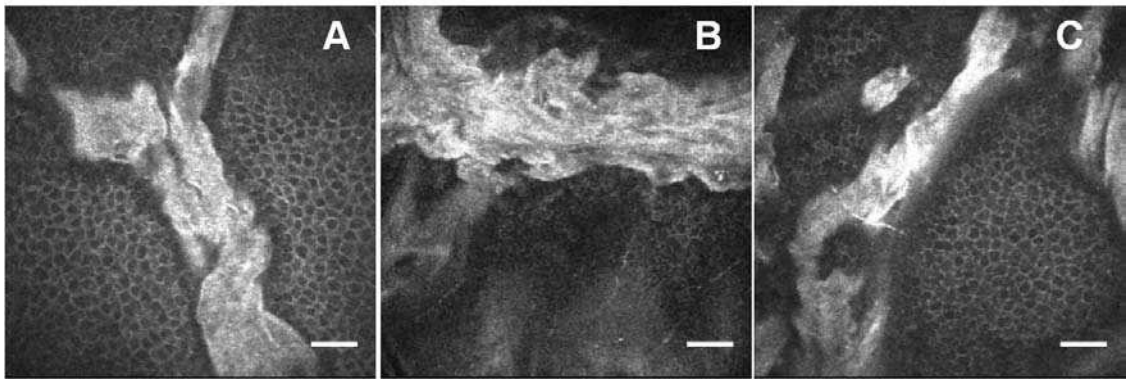

Figure 8-2: IVCM en face images of the cornea in case1 showing sharply demarcated hyper-reflective bands with wavy or sinusoidal edges running in vertical (A) and horizontal (B) directions interrupting the basal epithelial layers. Sub-basal nerves can be seen crossing over these bands in (C). These bands correspond in pattern and location to rolled up Bowman's zone in figure1. Scale bar 50µm.

8.1.1.2 Breaks in Bowman's zone

These breaks were noticed in certain parts of the histological sections (Figure 8-3A). On IVCM dark bands of variable width and direction were seen at the level of Bowman's zone and sub-basal nerves (Figure 8-3B). Bright keratocyte nuclei could be seen within these bands as well so that in some frames these nuclei were seen at the same focal plane with basal epithelium and sub-basal nerves (Figure 8-3C & D).

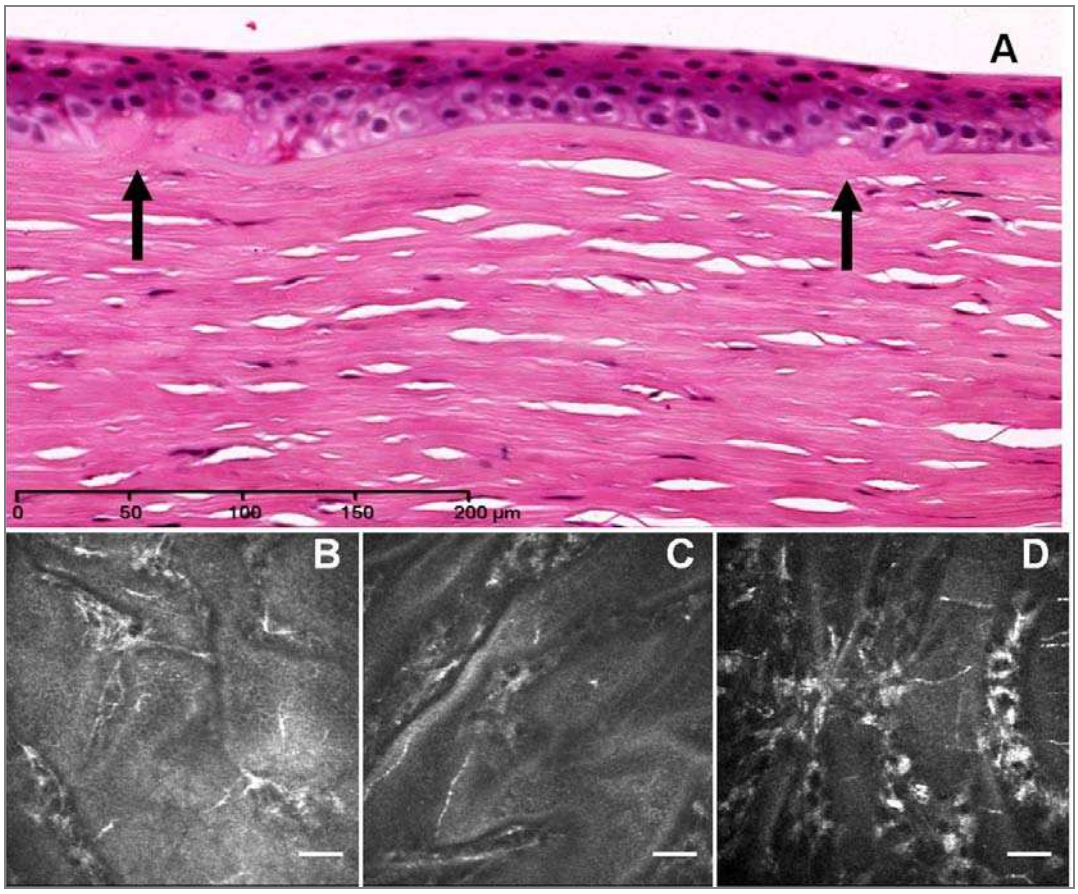

Figure 8-3: Microscopic views of Bowmans zone breaks in case 1. A, light micrograph of a corneal section (H&E stained) showing 2 breaks in Bowman's zone (arrows). Corresponding IVCM images (B – D) show dark wide bands at Bowman's zone level running in various directions and occupied by keratocyte nuclei. These bands are consistent with breaks in Bowman's zone where basal epithelium and sub-basal nerves are seen at the same level as well. Scale bar 50µm.

8.1.1.3 Anterior stromal scarring with loss of Bowman's zone

In other areas of the histological sections the epithelial irregularity was associated with hyaline / acellular anterior stromal scarring growing at subepithelial levels along with extensive loss of Bowman's zone (Figure 8-4A). Corresponding IVCM images revealed wide areas of hyper-

reflective scar tissue interrupting the basal epithelium along with visible sub-basal nerves all visualised at the same focal plane (Figure 8-4B&C). These scar areas presented a different pattern to that seen in Figure 8-2 of rolled up Bowman's zone.

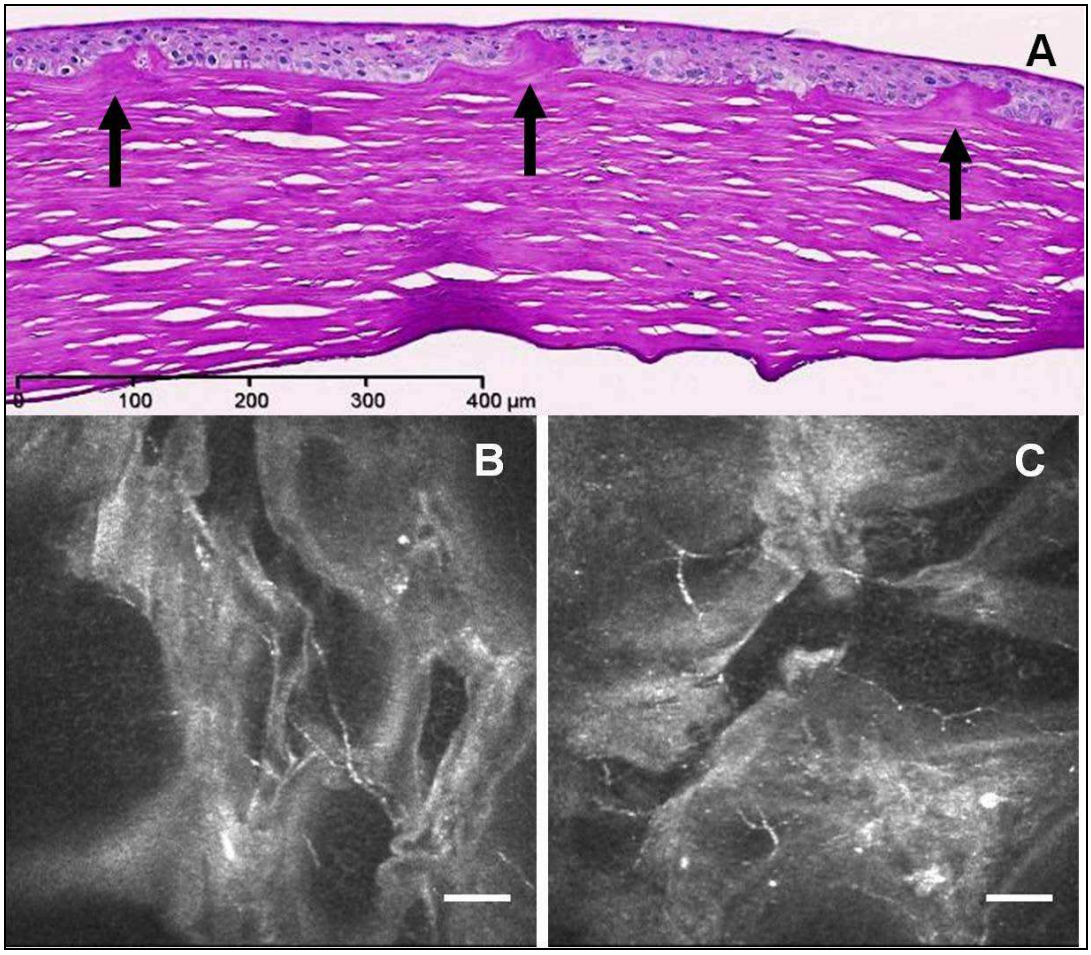

Figure 8-4: A, light micrograph of corneal section in case1 (PAS stain) showing areas of anterior stromal acellular fibrosis with irregular overlying epithelium and loss of Bowman's zone. Corresponding IVCM enface images (B & C) show wide hyper-reflective areas of subepithelial scarring seen at the same level of sub-basal nerves. Note irregular shapes and lack of sharp demarcation in certain areas of scar tissue compared to the patterns in figure1. Scale bar 50µm.

8.1.1.4 *Deep stromal scarring*

The stroma in histological sections revealed areas of extensive deep stromal scarring associated with remarkable thinning (Figure 8-5A). IVCM images taken at various stromal levels revealed increased reflectivity within middle and deep stromal layers with randomly scattered bright nuclei (Figure 8-5B&C).

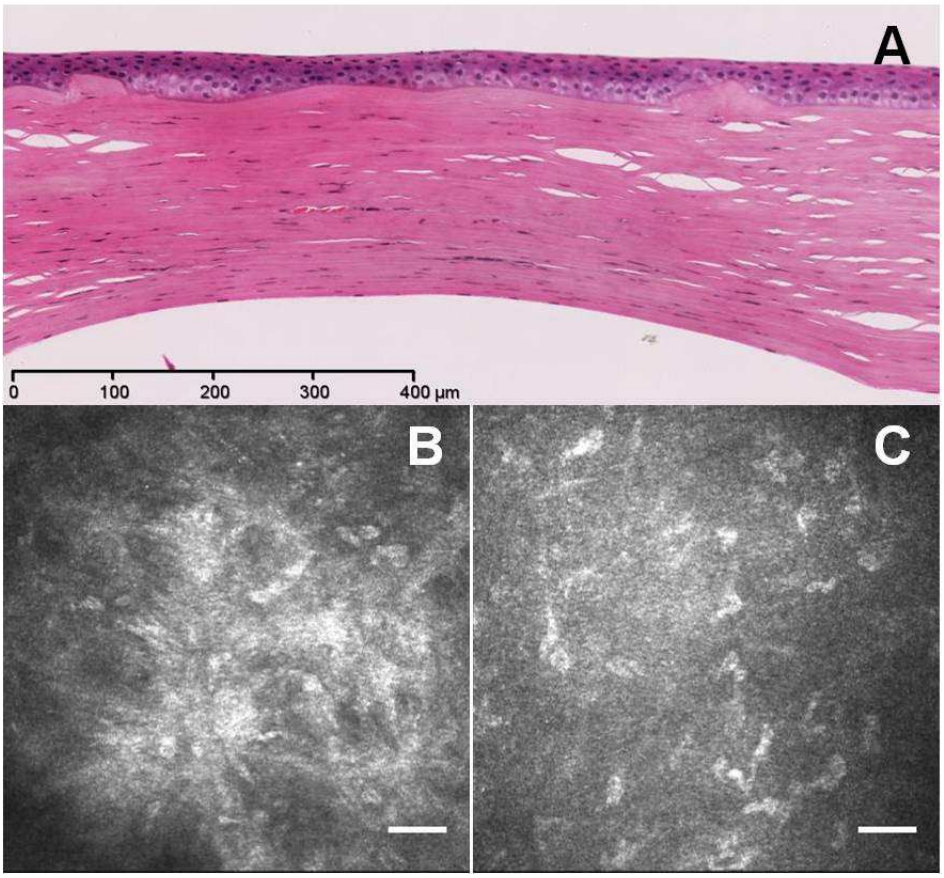

Figure 8-5: A, Light micrograph of corneal section in case1 showing extensive fibrosis involving the whole stromal thickness. Corresponding IVCM images reveal hyper-reflective scar tissue within middle (B) and deep (C) stromal layers at 130µm and 419µm of focal plane depth respectively. Randomly distributed nuclear figures can be seen within the scar areas.H&E stain in A. Scale bar 50µm in B & C.

8.1.1.5 Descemet's membrane changes

Descemet's membrane showed multiple areas of folds on histological sections (Figure 8-6A) as well as an area of break with rolled edges (Figure 8-6 B-D).

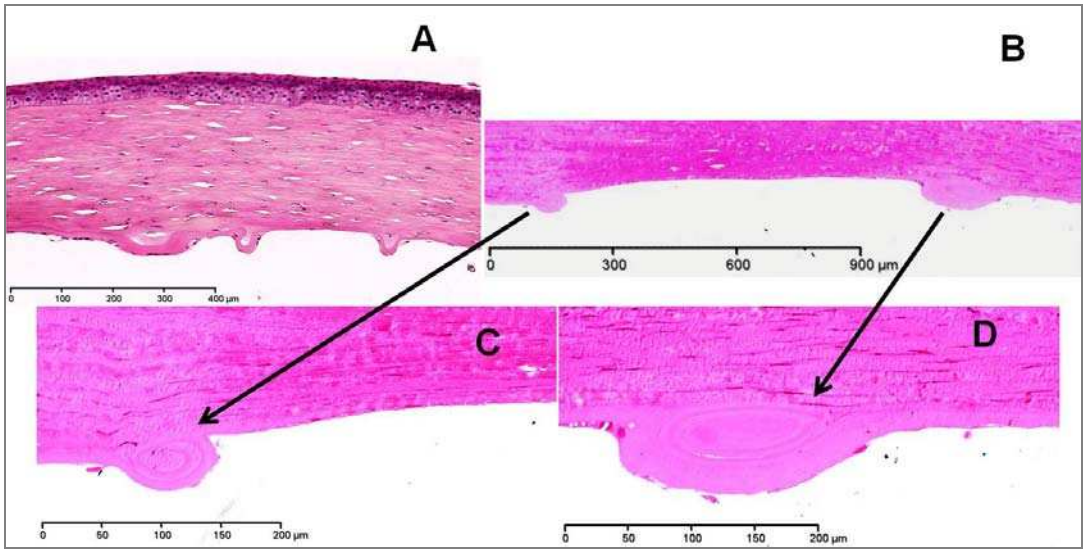

Figure 8-6: Light micrographs of corneal sections in case1 showing folds in Descemet's membrane (A) as well as an area of break with rolled up edges (B) seen at higher magnification in C and D. (H&E stain).

On IVCM the images revealed alternate bright and dark bands at the level of Descemets membrane running in curvilinear courses with occasional trapezoid pattern (Figure 8-7A&B). The endothelium appeared attenuated on histological sections while IVCM revealed enlarged cells with visible nuclei and reduced density (Figure 8-7 C).

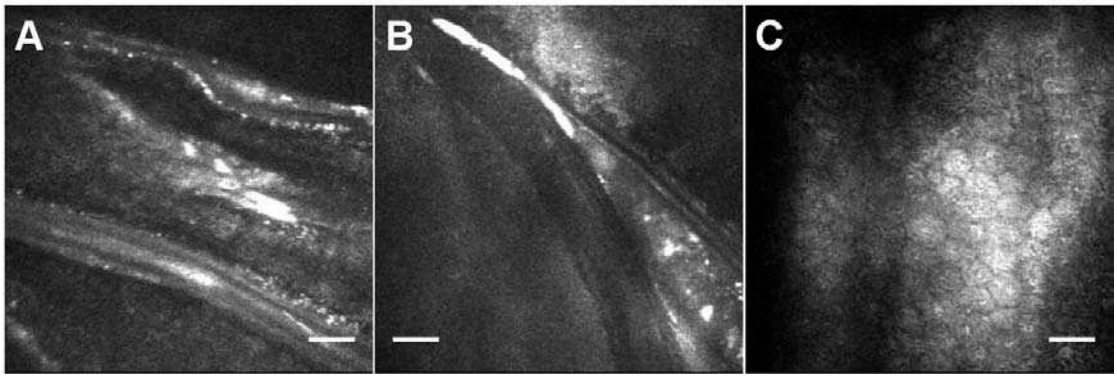

Figure 8-7: IVCM images of the cornea in case 1 show alternating dark and bright lines at the level of Descemet's membrane (A) consistent with the folds seen in Figure 8-6. A trapezoid pattern is seen in (B) which is consistent with a break in Descemet's membrane. In other areas the endothelial cells appear to be enlarged with visible nuclei (C). Scale bar 50µm.

8.1.2 Discussion:

This cornea showed features of widespread stromal scarring on histology that was associated with wrinkling of Bowman's zone as well as the Descemet's membrane. Unlike scar tissue Bowman's zone is characterised on histology by a distinct regular thickness and clear edges especially towards the epithelial side. When this layer was rolled up in this case these edges remained clear and thus the IVCM pattern of sharply demarcated bright bands with wavy and sinusoidal edges correlated better with areas of rolled Bowman's zone seen on histology. IVCM criteria of Bowman's zone have been well reported by other investigators in normal (Kobayashi et al., 2006) and diseased cornea (Kobayashi and Sugiyama, 2007). However this pattern of rolled Bowman's zone is not mentioned before and may provide clinicians with additional value of the role of IVCM in detailed corneal examination.

This pattern was distinct from the reflectivity of subepithelial scar seen in other parts of the cornea as well as in conditions previously investigated (see chapter 5 for scarring in keratoconus).

Frequent breaks in Bowman's zone were also noticed histologically, a finding that correlated with the IVCM pattern of wide dark bands occupied by keratocytes seen at the level of Bowman's zone with sub-basal nerves. This is similar to what was found in keratoconus as regard to IVCM patterns of Bowman's zone breaks (see chapter 5). Stromal scarring was another type of fibrosis in this case presenting histological and IVCM features similar to those found in keratoconus (see chapter 5 for details).

The folds in Descemets membrane seen on histological sections were reflected on IVCM as alternate bright and dark bands with sharp edges while the triangular figures on IVCM were more consistent with Descemet's membrane breaks that were comparable to those seen in keratoconus (see chapter 5 case 8). These IVCM criteria of Descemet's membrane changes have not been reported yet in the literature.

It has been postulated from the features seen in histopathology that the extensive shrinkage of the stromal scarring has led to multiple wrinkles and folds in both Bowman's zone and Descemets membrane suggesting the presence of myofibroblasts in the scar tissue. Although this cornea showed some histological and IVCM features that were comparable to those already seen in keratoconus cases the possibility of resolved

interstitial keratitis could not be ruled out especially with the existence of deep ghost blood vessels within corneal stroma on slitlamp examination.

8.1.3 Conclusion

These findings support the reliability of IVCM criteria of certain pathological changes that can arise from different aetiological factors.

8.2 CASE 2: LOCALISED CONJUNCTIVAL B CELL LYMPHOMA WITH PARAPROTEINIC CRYSTALLINE KERATOPATHY

8.2.1 Patient and Management

A 44y old lady was referred to the cornea clinic in Queen's Medical centre by her optician who noticed suspicious lattice-like corneal deposits in her right eye on routine examination. Her BCVA was 6/6 in each eye and slitlamp examination revealed a fleshy diffusely elevated conjunctival lesion about 10x20mm in the right upper bulbar conjunctiva (Figure 8-8A) along with similar but smaller lesions in the left upper and lower fornicial conjunctiva (Figure 8-8B). The right cornea showed discreet crystalline linear deposits in criss-cross pattern within the deep stromal layers in a similar appearance to lattice corneal dystrophy (Figure 8-8C&D). The left

cornea was clear and the rest of her ocular examination was unremarkable.

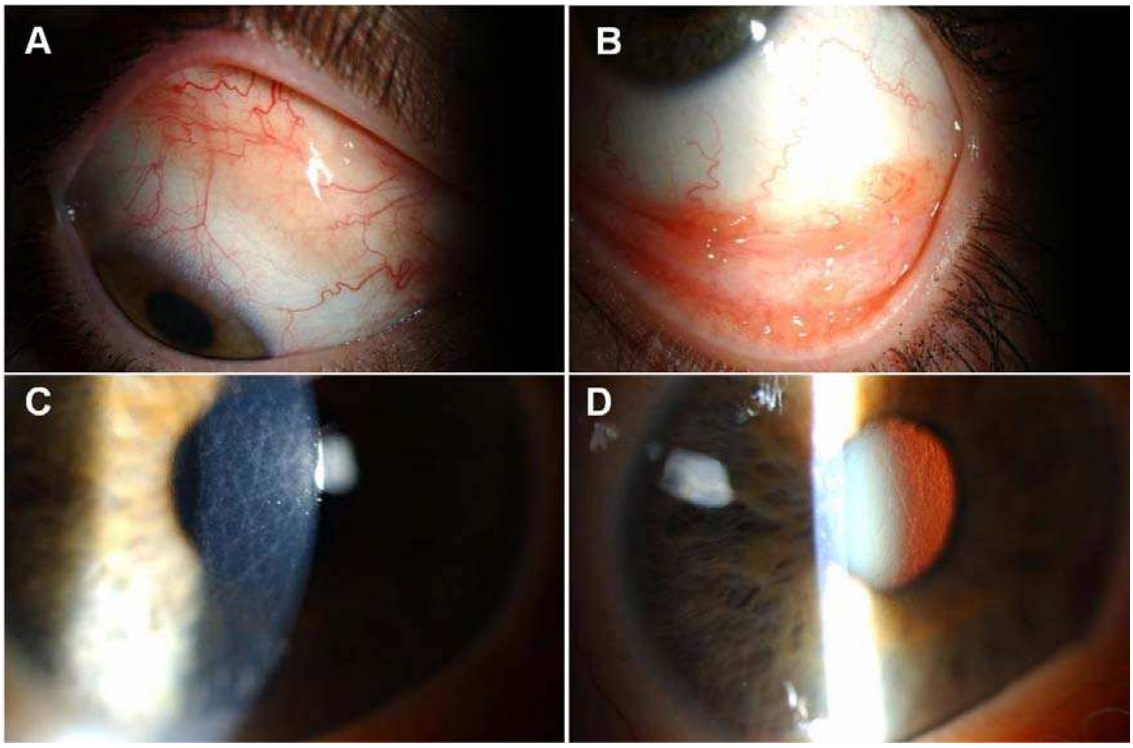

Figure 8-8: Slitlamp micrographs of eyes in case 2. A, Right eye shows diffusely elevated lesion in the upper bulbar conjunctiva. B, left eye has multiple small lesions in the lower conjunctival fornix. C, right cornea shows interlacing fine linear deposits in deep stromal layers. D, the right corneal deposits are highlighted by transillumination.

IVCM done for both eyes revealed the presence of hyper-reflective stromal deposits that appeared as irregular snowflake-like figures within the middle stromal layers (Figure 8-9A). At deeper pre-Descemet's levels these deposits presented as confluent intersecting bright lines (Figure 8-9B) along with normal endothelial pattern (Figure 8-9C).

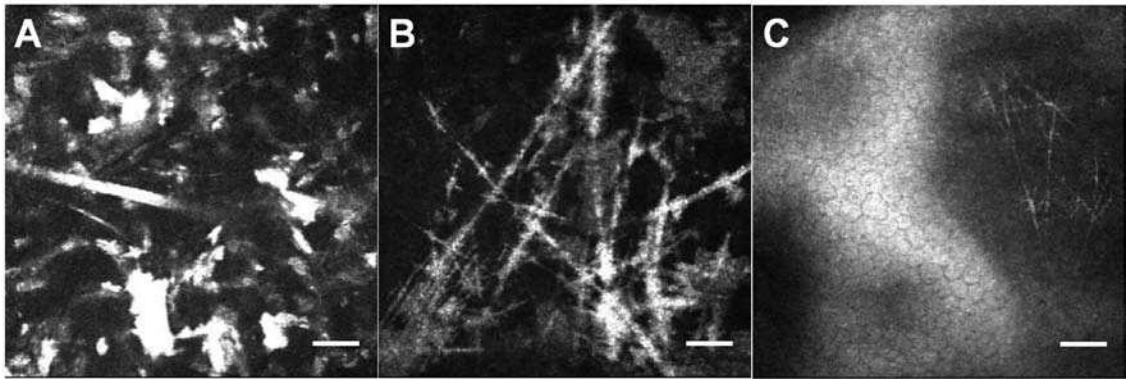

Figure 8-9: IVCM en face images of the right cornea in case2 showing hyper-reflective snowflake-like deposits within the middle stroma in (A) as well as interlacing straight lines in the pre-Descemet's layers in (B). the endothelium shows normal pattern in (C). Focal plane depth is 263µm and 476µm in A and B respectively. Scale bar 50µm.

A clinical diagnosis of B-cell lymphoma of the conjunctiva was considered for which a conjunctival biopsy was taken from the left eye for histopathological examination. The initial result showed nodular lymphoid infiltrates within the subepithelial stroma mostly showing lymphoplasmacytoid features (Figure 8-10A). With immunohistochemistry the vast majority of cells were CD20 & CD79a positive B- lymphocytes with a very low proliferative index well under 10%. This appearance was consistent with non-Hodgkin's marginal zone B-cell Lymphoma. However the possibility of lymphoplasmacytic lymphoma was excluded through further investigations that revealed no evidence of paraproteins in blood or urine. Based on this exclusion of systemic involvement she was treated with orbital radio-therapy alone that resulted in complete resolution of her conjunctival lesions. On further follow up visits tiny glistening refractile deposits were noted in the bulbar conjunctiva in both eyes. These persisted even 2 years following the treatment (Figure

8-10B). Corresponding IVCM revealed highly reflective dots ≤10µm in size widely spread within superficial epithelial layers with occasional aggregates in cystic spaces (Figure 8-10C).

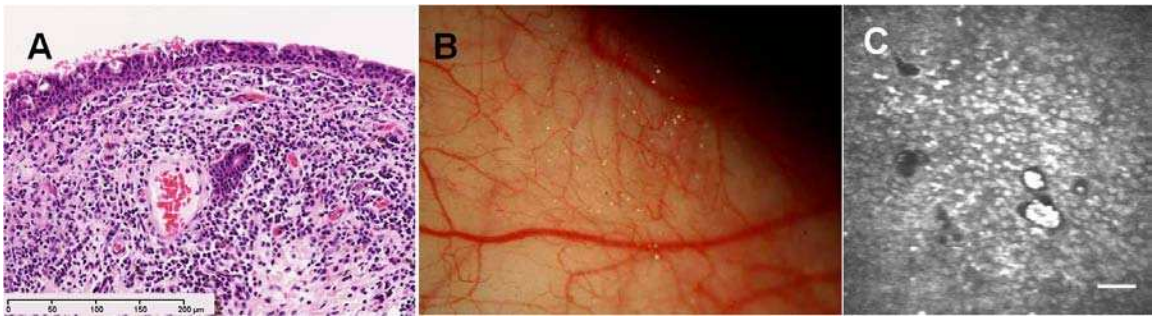

Figure 8-10: A, light micrograph of conjunctival tissue shows intense nodular lymphocytic infiltration representing a low grade B cell non-Hodgkin's lymphoma in keeping with "marginal zone lymphoma". B, Diffuse slitlamp photograph of the right eye showing tiny glistening particles on bulbar conjunctiva. C, IVCM image of bulbar conjunctiva showing highly reflective dots≤10µm in size within superficial epithelium with occasional aggregates in cystic spaces (A stained with H&E).(IVCM focal depth 19µm, scale bar 50µm).

8.2.2 Discussion:

Paraprotein crystalline keratopathy is a term used to describe corneal involvement with deposits in lymphoproliferative disorders associated with hyper-gammaglobulineamia including plasma cell myeloma (multiple myeloma), B cell non-Hodgkin's lymphomas, essential cryoglobulineamia and monoclonal gammopathy (Aronson and Shaw, 1959, Henderson et al., 1993, Froussart et al., 2001, Garibaldi et al., 2005). Despite their rare incidence corneal deposits in paraproteinemic disorders have been reported to be bilateral and frequently associated with significant visual impairment as the first presenting clinical feature (Froussart et al., 2001) such that corneal graft was justified in many instances (Garibaldi et al.,

2005). In other cases corneal changes were asymptomatic and noticed during routine ocular examination but they were still considered to be the first sign of the systemic disorder. On slitlamp examination the corneal deposits could be found at any level from the epithelium to the deep stromal layers taking the form of tiny dots (Buerk and Tu, 2002, Froussart et al., 2001) or as lattice- like pattern (Stirling et al., 1997). The deposits could be of mid-peripheral location sparing the centre (Henderson et al., 1993). They are mostly composed of IgG kappa light chain (Garibaldi et al., 2005) although cases with gamma chain–positive deposits have been reported (Stirling et al., 1997).

IVCM imaging of such deposits has been published in a case report of a patient diagnosed with plasma cell myeloma who showed bilateral corneal diffuse haze with tiny globular crystalls in anterior stroma that were seen as confluent bright dots on IVCM (Buerk and Tu, 2002).

The origin of these crystalloid deposits was suggested to be heamatogenous through molecular diffusion from the limbal vascular loops (Henderson et al., 1993). In their major review Garibaldi et al (2005) reported that all previuos cases of paraprotein crystalline keratopathy were seen in systemic disorders associated with hypergammaglobulinemea, hence resulting in bilateral involvement. They listed all reports of single or two cases published between 1947 and 2000. A recent case report of a similar condition has been published in 2011 (Lisch and Saikia, 2011).

Our case represents the first instance where these corneal deposits are seen with a localised conjunctival B cell lymphoma suggesting direct corneal infiltration with paraprotiens produced by a nearby lesion. In fact the right upper bulbar conjunctival lesion was found to be larger on initial examination compared to the smaller lesions in the left eye that occupied mainly the lower conjunctival fornix. This may explain the early involvement of the right cornea while the left remained clear.

In their analysis of 117 cases of conjunctival lymphoid tumors Schields et al (2001) reported the development of systemic lymphoma in 17% of the cases at a mean of 21 months following their initial ocular diagnosis (Shields et al., 2001). Systemic lymphoma was found more often in those with midbulbar, forniceal or multiple conjunctival tumors. They recommended long-term systemic follow-up of all cases with conjunctival lymphoid tumors as systemic lymphoma can manifest many years later.

8.2.3 Conclusion

This case report confirms the importance of full conjunctival examination in all conditions of corneal crystalline deposits in order to exclude the presence of an associated localised conjunctival lymphoma that requires appropriate treatment and lifetime follow-up.

8.3 CASE 3: AMIODARONE KERATOPATHY IN KERATOCONUS

8.3.1 Patient and Management

A 65 years old man was referred to the corneal clinic in Queens Medical Centre, Nottingham, UK, for his bilateral corneal changes. He was on amiodarone for one year and stopped it three months prior to referral. Patient noticed slight reduction in the right visual acuity. He was slightly concerned as his son was recently diagnosed to have keratoconus. He had worn hard contact lenses since 1975 and changed to rigid gas permeable lens recently. On clinical examination his best contact lens corrected visual acuity (BCLVA) was 6/9 and 6/6 in the right and left eye respectively. Slit-lamp examination revealed bilateral conical cornea with paracentral thinning and Vogt striae being more remarkable in the right eye. Superficial golden brown ‘‘pigment’’ deposits arranged in a semicircular fashion were noticed in the inferior region of the base of the cone in both eyes (Figure 8-11A). Detailed examination revealed multiple fine lines radiating from the ends of the pigmented semicircle in a pattern close to that seen in cornea verticillata (Figure 8-11B).

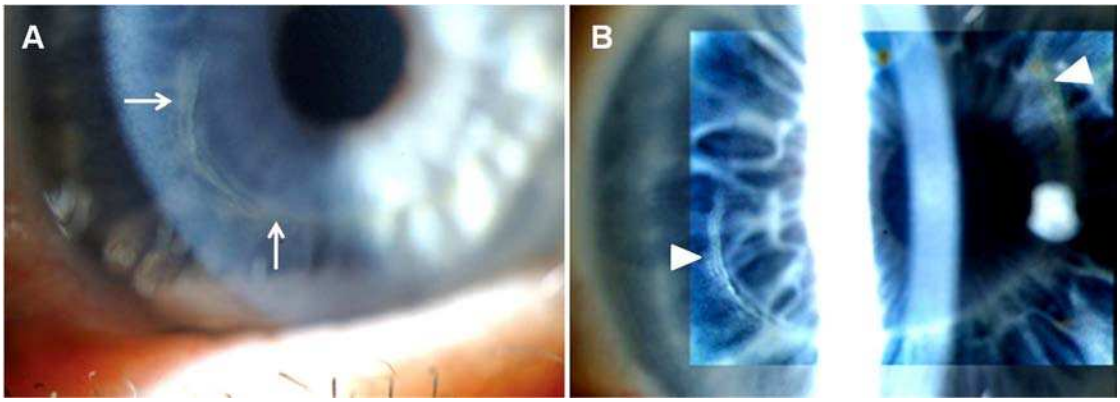

Figure 8-11: Slitlamp photographs of the left cornea in case3 showing the semicircular golden brown epithelial deposits around the base of the cone. Multi-branching pattern can be seen between the arrows in (A) while the full extent of the semicircular deposit line is seen between the arrowheads within the enhanced corneal photograph in (B).

Using Cobalt blue filter during slitlamp examination did not highlight this semicircle as it usually does in Fleischer ring of keratoconus. Corneal topography confirmed the diagnosis of bilateral keratoconus while the rest of his ocular examination was unremarkable. Based on these clinical findings the brownish semicircular corneal deposits were diagnosed to be amiodarone – induced keratopathy (or cornea verticillata) rather than Fleischer ring of keratoconus.

IVCM was performed and showed confluent bright dots 3 – 5 µm in size within the epithelial and superficial stromal layers (Figure 8-12A). When Bowman's zone was approached these dots were fading as more sub-basal nerves were seen (Figure 8-12B). In oblique view it was clear that Bowman's zone was not involved with these dots (Figure 8-12C). IVCM of Fleischer ring seen in keratoconus revealed bright 3 – 10µm spots that

were less confluent within the epithelium compared to those seen in amiodarone keratopathy (Figure 8-12D).

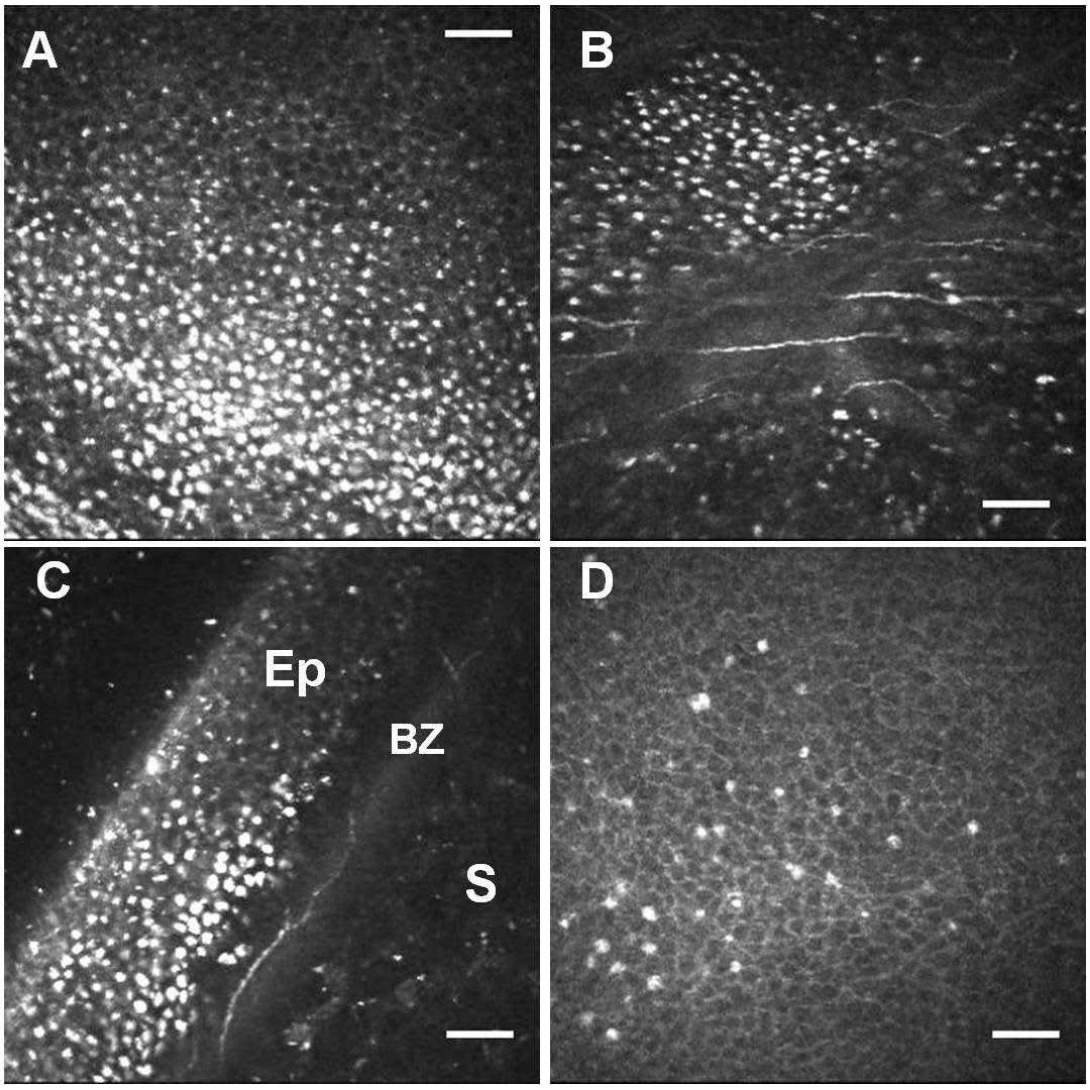

Figure 8-12: A – C, IVCM images of cornea in case3 showing confluent bright dots 3 – 5 µm in size within the corneal epithelium (A) fading gradually at the level of Bowman's zone highlighted by the presence of sub-basal nerves (B). Oblique view in (C) shows these dots densely accumulated in the epithelium (Ep), non-visualised in Bowman's zone (BZ) and scattered within the anterior stroma (S). Enface IVCM image (D) of Fleischer ring in keratoconus shows the scarcely distributed bright ferritin deposits within corneal epithelium. Scale bar 50µm.

8.3.2 Discussion

Cornea verticillata is the most common ocular side effect seen in patients taking amiodarone while other less common side effects include lens opacities and ischaemic optic neuropathy (Mantyjarvi et al., 1998).

Cornea verticillata presents on slitlamp examination as fine superficial lines that swirl from a point below the centre of the cornea and radiate to the peripheral cornea in a vortex-like pattern. The condition is generally asymptomatic and unlikely to affect the vision (Reasor and Kacew, 2001). However coloured halos, blurred vision, glare, dry eyes with irritation have been reported (Mantyjarvi et al., 1998).

The pathogenesis of amiodarone keratopathy is thought to result from the accumulation of the amphiphilic drug and its active metabolite secreted into the tear film in the corneal epithelium (Pollak and Tan, 1999) although a threshold serum concentration must be reached to produce a significant drug excretion through the lacrimal gland (Orlando et al., 1984). Corneal deposits are strongly related to the daily dose and duration of treatment (Kaplan and Cappaert, 1982, Ghosh and McCulloch, 1984). In an electron microscopic study the deposits were described as lysosome-like intracytoplasmic membranous lamellar bodies in corneal epithelial cells, stromal keratocytes and endothelial cells (Ghosh and McCulloch, 1984). Four grades of amiodarone keratopathy have been described: Grade 1 indicates tiny brownish epithelial opacities arranged in a horizontal line in the inferior third of the cornea. Grade 2 is seen when

the line show branches and Grade 3 when these branches increase in number and form a whorl – like pattern. Grade 4 was added later to indicate irregular brown pigment clumps seen with the whorl pattern (Orlando et al., 1984).

On the other hand keratoconus-related Fleischer ring presents as a brownish circular pigmentation of the epithelium around the base of the cone well highlighted on illumination through the cobalt blue filter during slitlamp examination of the cornea. It is usually seen in 50 – 70% of patients with keratoconus (Bron, 1988). This ring is formed by inter- and intracellular deposition of ferritin in the basal epithelium although the pathogenesis of iron deposition remains unclear (Iwamoto and De Voe, 1976, Rose and Lavin, 1987). In our observation ferritin and perhaps other deposits tend to occur along points of abrupt change in corneal surface steepness. This feature has also been mentioned by other investigators (Vongthongsri et al., 1999).

The IVCM pattern of amiodarone keratopathy was described in previous studies that reported similar findings of bright dots 1 - 9µm in size seen within the basal epithelium, Bowman's zone, stromal keratocytes and endothelial cells in cornea involved with stage 2 & 3 of keratopathy (Ciancaglini et al., 2001b, Ucakhan et al., 2005). However in our case IVCM could not show any evidence of deposits in Bowman's zone that was well highlighted in the oblique view as a clear layer between the dot-containing basal epithelium and anterior stroma.

In case of Fleischer ring of keratoconus in our experience IVCM revealed scanty hyper-reflective dots within the basal epithelium compared to the confluent dots seen in amiodarone keratopathy. They are difficult to be visualised and in a recent study Fleischer ring could not be seen on IVCM in 30% of keratoconus cases [Ukakhan 2006].

8.3.3 Conclusion

Our case emphasizes the importance of history taking besides slitlamp biomicroscopy in the clinical evaluation of keratoconus cases. The role of IVCM in confirming the diagnosis of amiodarone keratopathy with the ability to differentiate it from Fleischer of keratoconus have been well illustrated in this case report.

Chapter Nine

9 Summary & Conclusion

9.1 SUMMARY:

In this study a total of 65 cases were recruited among whom 53 underwent surgical procedures that offered tissue samples for histopathological examination to correlate with corresponding IVCM. The correlative analysis of histological sections with corresponding IVCM images has resulted in the following outcomes:

In ocular surface disease (**chapter one**) a set of IVCM criteria has been established in corneal/conjunctival intra-epithelial neoplasia (CIN) to be considered collectively to diagnose and differentiate this dysplastic condition from non-neoplastic conjunctival overgrowth onto the corneal surface. The morphological / metaplastic changes induced by regenerative atypia of corneal epithelium have been well studied histologically and correlated with the changes in reflectivity patterns seen on IVCM in cases of limbal stem cell deficiency (LSCD) (chapter one). Similar changes have been found in keratoconus on light and in vivo confocal microscopy (**chapter five**) where careful analysis of basal epithelial cells has confirmed a significant difference in the average size of the enlarged

vesicular nuclei in CIN compared to the average nuclear size of basal epithelium in regenerative atypia and normal looking basal epithelium.

In metaplasia prominent nuclei were hyper-reflective on IVCM at the level of middle and basal epithelium while in CIN only prominent nucleoli were seen as hyper-reflective dots at the level of basal epithelium. IVCM has illustrated the distribution of isolated islands of conjunctival epithelium within normal looking corneal epithelium in cases of partial LSCD where the slitlamp examination revealed intact corneal surface even with fluorescein staining.

In corneal oedema **(chapter four)** we detected through IVCM for the first time the presence of subepithelial fibroblasts in 11 (55%) corneas even in cases with minimal deposition of collagen material. This has been correlated well with corresponding histological sections examined under light microscopy especially in cases of Fuch's endothelial dystrophy FED) that presented no evidence of corneal scarring on pre-operative slitlamp examination. As a first scientific advantage this finding has corrected a longstanding wrong interpretation of similar figures reported in the IVCM of FED in a previous study. The second clinical advantage came from the fact that these subepithelial cells were detected with similar density following successful Descemets Stripping Endothelial Keratoplasty (DSEK) with clinical and visual improvement. Another interesting finding was the universal reduction of sub-basal corneal nerves that were totally

undetectable in 70% of these decompensated corneas. Keratocyte changes with increased hype-reflectivity of cytoplasmic cell bodies and processes have been clearly detected with IVCM in 95% of the cases without comparable changes on light and electron microscopy. Extracellular large lacunae and intracellular smaller vacuoles were highlighted in IVCM images with superior resolution compared to previously published ones thanks to the high resolution of HRTII-RCM machine used in our study. Therefore IVCM has proven its ability for quantitative evaluation of corneas with FED through detecting these microstructural changes long before keratoplasty is justified as well as following successful DSEK procedures, an issue that needs more elaborate research work.

In keratoconus **(chapter five)** the universal finding of IVCM patterns for Bowman's zone breaks is not reported in the literature before. 3 patterns, namely the crack-like pattern, the wide dark bands and the scar-filled bright curvilinear pattern have been identified.

More interesting was the visualizing of the second pattern on IVCM of two corneas that did not show clear evidence of Bowman's zone breaks on histological sections. Therefore IVCM can be considered with other clinical and topographic features to confirm the diagnosis of keratoconus especially in early or suspected recurrences postkeratoplasty.

The IVCM reflective patterns of corneal scarring have been well illustrated in this study including those seen in corneal oedema (**chapter four**) and keratoconus (**chapter five**), thus offering a comprehensive understanding of the IVCM illustration in many varieties of corneal fibrosis. Table 9-1 summarises the types and stages of corneal fibrosis included in this study with corresponding histological and IVCM features.

Table 9-1: Various types of corneal fibrosis illustrated on light and confocal microscopy.

Types of corneal fibrosis	Light microscopy	IVCM en face	IVCM oblique
Subepithelial fibroblasts with minimal collagen in FED	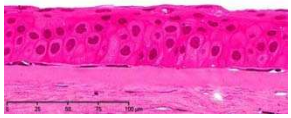	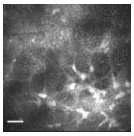	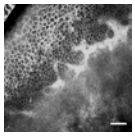
Subepithelial fibroblasts with intra-epithelial fibrous bands in chronic corneal oedema	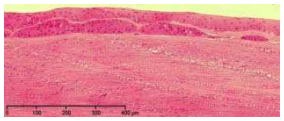	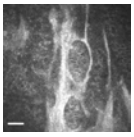	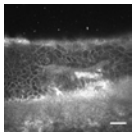
Loose subepithelial fibrocellular scarring in chronic corneal oedema	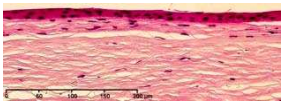	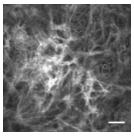	
Scar-filled Bowman's zone breaks in keratoconus	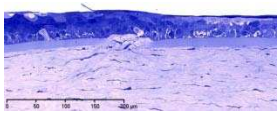		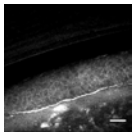
Superficial lenticular stromal scar in advanced keratoconus	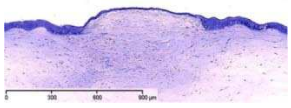	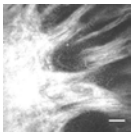	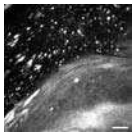
Deep stromal scarring in advanced keratoconus	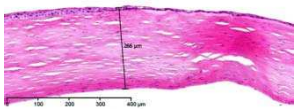	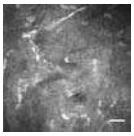	

Breaks of Descemet's membrane were illustrated with IVCM in one case of keratoconus group as dark well-defined areas with sharp edges at the level of endothelium interrupting continuity of Descemet's membrane. This is the first time to illustrate such pathology in IVCM literature.

In corneal dystrophy (**chapter six**) the IVCM pattern in a case of Bowman's zone corneal dystrophy (CDB) correlated well with the light microscopic findings that were more consistent with Thiel-Behnke's rather than Reis-Buckler's dystrophy. Similar correlation has been has been done in another case with macular corneal dystrophy with a novel ' ameoboid' pattern on IVCM described for the first time. We assume that these IVCM patterns could be useful diagnostic criteria besides other clinical features of corneal dystrophy to confirm the diagnosis.

Clinically the choice for penetrating keratoplasty (PK) in macular dystrophy was confirmed by IVCM findings of endothelial involvement. Similarly in recurrent granular dystrophy IVCM confirmed the level of corneal layer involvement with recurrent deposits thus supporting the choice of alcohol delamination in one case and PK for the other one.

In Acanthamoeba keratitis (**chapter seven**) a new form of Acanthamoeba cysts described as 'signet ring' was illustrated clearly on serial IVCM sections taken at different focal depths to show the change in reflectivity patterns of these cysts within the epithelial layers. Clinicians

should be aware of this form in IVCM findings of cases with suspected acanthamoeba keratitis.

In **chapter eight** IVCM and LM detected pathological findings similar to those seen in keratoconus but in a case clinically diagnosed with interstitial keratitis. This confirms the reliability of IVCM criteria of certain pathological changes that can arise from different aetiological factors.

In another case it showed the difference between deposits in Amiodarone keratopathy and ferritin deposits in Fleischer ring seen in keratoconus.

Finally in this study novel IVCM patterns in various pathological conditions have been described and illustrated for the first time in the literature. These are listed in Table 9-2.

Table 9-2: Summary of novel IVCM patterns described in this study with corresponding disorders.

IVCM patterns	Illustrations
Starry night sky in CIN	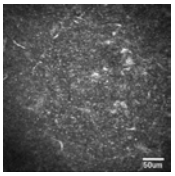
Swiss Cheese holes pattern in subepithelial fibroblasts in FED	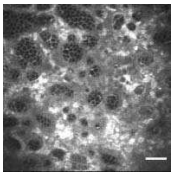
Bowman's zone breaks in keratoconus: 1. Crack-like pattern 2. Dark wide bands	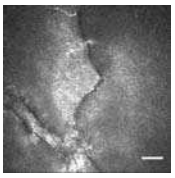 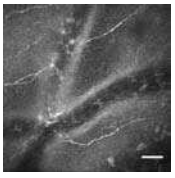
Amoeboid pattern in macular dystrophy	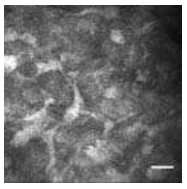
Signet ring form of Acanthamoeba cysts.	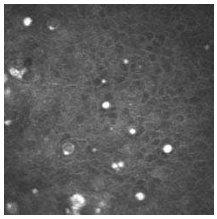

9.2 CONCLUSION:

This study has provided a quality scientific evidence for proper interpretation of IVCM features for both clinicians and histopathologists.

This study has established IVCM criteria for certain corneal and ocular surface disorders that can be applied for diagnostic purposes in addition to other clinical features. Based on these outcomes further work is required to verify IVCM role for clinical evaluation of conditions like corneal oedema, FED and keratoconus in larger series and for longer follow up periods.

Bibliography

AKHTAR, S., BRON, A. J., HAWKSWORTH, N. R., BONSHEK, R. E. & MEEK, K. M. (2001) Ultrastructural morphology and expression of proteoglycans, betaig-h3, tenascin-C, fibrillin-1, and fibronectin in bullous keratopathy. *Br J Ophthalmol,* 85**,** 720-31.

AL-AQABA, M. A., FARES, U., SULEMAN, H., LOWE, J. & DUA, H. S. (2010) Architecture and distribution of human corneal nerves. *British Journal of Ophthalmology,* 94**,** 784-789.

ALOMAR, T., S. , NUBILE, M., LOWE, J. & DUA, H., S. (2011) Corneal Intraepithelial Neoplasia: In Vivo Confocal Microscopic Study With Histopathologic Correlation. *American Journal of Ophthalmology,* 151**,** 238-247.

AMBROSIO, R., JR., ALONSO, R. S., LUZ, A. & COCA VELARDE, L. G. (2006) Corneal-thickness spatial profile and corneal-volume distribution: tomographic indices to detect keratoconus. *J Cataract Refract Surg,* 32**,** 1851-9.

AMBROSIO, R. & WILSON, S. E. (2003) LASIK vs LASEK vs PRK: Advantages and indications. *Seminars in Ophthalmology,* 18**,** 2-10.

ARONSON, S. B., 2ND & SHAW, R. (1959) Corneal crystals in multiple myeloma. *AMA Arch Ophthalmol,* 61**,** 541-6.

AUW-HAEDRICH, C., LOEFFLER, K. U., SUNDMACHER, R. & WITSCHEL, H. (1996) Characteristic distribution of deposits in recurrent granular corneal dystrophy. *Ger J Ophthalmol,* 5**,** 132-6.

BAHAR, I., KAISERMAN, I., MCALLUM, P., SLOMOVIC, A. & ROOTMAN, D. (2008) Comparison of Posterior Lamellar Keratoplasty Techniques to Penetrating Keratoplasty. *Ophthalmology,* 115**,** 1525-1533.

BENITEZ DEL CASTILLO, J. M., WASFY, M. A., FERNANDEZ, C. & GARCIA-SANCHEZ, J. (2004) An in vivo confocal masked study on corneal epithelium and subbasal nerves in patients with dry eye. *Invest Ophthalmol Vis Sci,* 45**,** 3030-5.

BERGMANSON, J. P., SHELDON, T. M. & GOOSEY, J. D. (1999) Fuchs' endothelial dystrophy: a fresh look at an aging disease. *Ophthalmic Physiol Opt,* 19**,** 210-22.

BERLAU, J., BECKER, H.-H., STAVE, J., ORIWOL, C. & GUTHOFF, R. F. (2002) Depth and age-dependent distribution of keratocytes in healthy human corneas. *J Cataract Refract Surg* 611 - 616.

BOHNKE, M. & MASTERS, B. R. (1999) Confocal Microscopy of The Cornea. *Progress in Retina and Eye Research* 18**,** 553 - 628.

BOURNE, W. M. (2001) Cellular Changes in Transplanted Human Cornea. *Cornea,* 20**,** 560 - 569.

BRAGHEETH, M. A. & DUA, H. S. (2005) Corneal sensation after myopic and hyperopic LASIK: clinical and confocal microscopic study. *Br J Ophthalmol* 89**,** 580-585.

BRAGHEETH, M. A. E.-N. M. (2004) Lamellar corneal refractive surgery. *PhD Thesis, University of Nottingham*.

BRASNU, E., BOURCIER, T., DUPAS, B., DEGORGE, S., RODALLEC, T., LAROCHE, L., BORDERIE, V. & BAUDOUIN, C. (2007) In vivo confocal microscopy in fungal keratitis. *Br J Ophthalmol,* 91**,** 588-591.

BRON, A. J. (1988) Keratoconus. *Cornea,* 7**,** 163-9.

BROWN HH, GLASGOW BJ, HOLLAND GN & RY., F. (1989) Keratinizing corneal intraepithelial neoplasia. *Cornea,* 8**,** 220-4.

BRUGIN, E., GHIRLANDO, A., GAMBATO, C. & MIDENA, E. (2007) Central corneal thickness: z-ring corneal confocal microscopy versus ultrasound pachymetry. *Cornea,* 26**,** 303-7.

BUERK, B. M. & TU, E. (2002) Confocal microscopy in multiple myeloma crystalline keratopathy. *Cornea,* 21**,** 619-20.

BUHREN, J., BAUMEISTER, M. & KOHNEN, T. (2001) Diffuse lamellar keratitis after laser in situ keratomileusis imaged by confocal microscopy. *Ophthalmology,* 108**,** 1075-81.

BUHREN, J. & KOHNEN, T. (2003) Stromal haze after laser in situ keratomileusis Clinical and confocal microscopy findings. *J Cataract Refract Surg***,** 1718–1726.

CALVILLO, M. P., MCLAREN, J. W., HODGE, D. O. & BOURNE, W. M. (2004) Corneal Reinnervation after LASIK: Prospective 3-Year Longitudinal Study. *Invest. Ophthalmol. Vis. Sci.,* 45**,** 3991-3996.

CAVANAGH, H. D., EL-AGHA, S., PETROLL, W. M. & JESTER, J. V. (2000) Specular Microscopy, Confocal Microscopy, and Ultrasound Biomicroscopy: Diagnostic Tools of the Past Quarter Century. *Cornea,* 19**,** 712 - 722.

CAVANAGH, H. D., JESTER, J. V., ESSEPIAN, J., SHIELDS, W. & LEMP, M. A. (1990) Confocal Microscopy of the Living Eye. *CLAO* 16**,** 65-73.

CAVANAGH, H. D., PETROLL, W. M., ALIZADEH, H., HE, Y.-G., MCCULLEY, J. P. & JESTER, J. V. (1993) Clinical and Diagnostic Use of In Vivo Confocal Microscopy in Patients with Corneal Diseases. *Ophtlamology,* 100**,** 1444-1454.

CHIOU, A. G., BEUERMAN, R. W., KAUFMAN, S. C. & KAUFMAN, H. E. (1999a) Confocal microscopy in lattice corneal dystrophy. *Graefes Arch Clin Exp Ophthalmol,* 237**,** 697-701.

CHIOU, A. G. Y., KAUFMAN, S. C., BEUERMAN, R. W., OHTA, T., SOLIMAN, H. & KAUFMAN, H. E. (1999b) Confocal microscopy in cornea guttata and Fuchs' endothelial dystrophy. *Br J Ophthalmol,* 83**,** 185-189.

CHIOU, A. G. Y., KAUFMAN, S. C., BEUERMAN, R. W., OHTA, T., YAYLALI, V. & KAUFMAN, H. E. (1999c) Confocal microscopy in the iridocorneal endothelial syndrome. *Br J Ophthalmol,* 83**,** 697-702.

CIANCAGLINI, M., CARPINETO, P., DORONZO, E., NUBILE, M., ZUPPARDI, E. & MASTROPASQUA, L. (2001a) Morphological evaluation of Schnyder's central crystalline dystrophy by confocal microscopy before and after phototherapeutic keratectomy. *J Cataract Refract Surg,* 27**,** 1892-5.

CIANCAGLINI, M., CARPINETO, P., ZUPPARDI, E., NUBILE, M., DORONZO, E. & MASTROPASQUA, L. (2001b) In vivo confocal microscopy of patients with amiodarone-induced keratopathy. *Cornea,* 20**,** 368-73.

CRUESS, A. F., WASAN, S. M. & WILLIS, W. E. (1981) Corneal epithelial dysplasia and carcinoma in situ. *Can J Ophthalmol,* 16**,** 171-5.

DABBS, T. & GLASS, M. (1992) Fiber-optic confocal microscope: FOCON. *Applied Optics,* 31**,** 3030 - 3035.

DAUENDORFFER, J. N., BASTUJI-GARIN, S., GUERO, S., BROUSSE, N. & FRAITAG, S. (2009) Shrinkage of skin excision specimens: formalin fixation is not the culprit. *Br J Dermatol,* 160**,** 810-4.

DAWSON, D. G., HOLLEY, G. P., GEROSKI, D. H., III, G. O. W., GROSSNIKLAUS, H. E. & EDELHAUSER, H. F. (2005) Ex Vivo Confocal Microscopy of Human LASIK Corneas with Histologic and Ultrastructural Correlation. *Ophthalmology***,** 634 - 644.

DE NICOLA, R., LABBE, A., AMAR, N., DUPAS, B. & BAUDOUIN, C. (2005) In vivo confocal microscopy and ocular surface diseases: anatomical-clinical correlations. *J Fr Ophtalmol,* 28**,** 691-8.

DHALIWAL, J. S., KAUFMAN, S. C. & CHIOU, A. G. (2007) Current applications of clinical confocal microscopy. *Curr Opin Ophthalmol,* 18**,** 300-7.

DUA, H. S., GOMES, J. A. & SINGH, A. (1994) Corneal epithelial wound healing. *Br J Ophthalmol,* 78**,** 401-8.

DUA, H. S. & GOMES, J. A. P. (2000) Clinical course of hurricane keratopathy. *Br. J. Ophthalmol. 2000;;,* 84**,** 285-288.

DUA, H. S., LAGNADO, R., RAJ, D., SINGH, R., MANTRY, S., GRAY, T. & LOWE, J. (2006) Alcohol Delamination of the Corneal Epithelium: An Alternative in the Management of Recurrent Corneal Erosions. *Ophthalmology,* 113**,** 404-411.

DUA, H. S., SHANMUGANATHAN, V. A., POWELL-RICHARDS, A. O., TIGHE, P. J. & JOSEPH, A. (2005) Limbal epithelial crypts: a novel anatomical structure and a putative limbal stem cell niche. *Br J Ophthalmol,* 89**,** 529-32.

DUA, H. S., WATSON, N. J., MATHUR, R. M. & FORRESTER, J. V. (1993) Corneal epithelial cell migration in humans: 'hurricane and blizzard keratopathy'. *Eye (Lond),* 7 (Pt 1)**,** 53-8.

EAGLE, R. C., JR., LAIBSON, P. R. & ARENTSEN, J. J. (1989) Epithelial abnormalities in chronic corneal edema: a histopathological study. *Trans Am Ophthalmol Soc,* 87**,** 107-19; discussion 119-24.

ECKARD, A., STAVE, J. & GUTHOFF, R. F. (2006) In Vivo Investigations of the Corneal Epithelium With the Confocal Rostock Laser Scanning Microscope (RLSM). *Cornea,* 25**,** 127-131.

EFRON, N., AL-DOSSARI, M. & PRITCHARD, N. (2009) In vivo confocal microscopy of the bulbar conjunctiva. *Clin Experiment Ophthalmol,* 37**,** 335-44.

EFRON, N. & HOLLINGSWORTH, J. G. (2008) New perspectives on keratoconus as revealed by corneal confocal microscopy. *Clin Exp Optom,* 91**,** 34-55.

ERIE, J. C. (2003) CORNEAL WOUND HEALING AFTER PHOTOREFRACTIVE A 3-YEAR CONFOCAL MICROSCOPY STUDY. *Trans Am Ophthalmol Soc* 101**,** 287-328.

ERIE, J. C., CAMPBELL, R. J. & LIESEGANG, T. J. (1986) Conjunctival and corneal intraepithelial and invasive neoplasia. *Ophthalmology,* 93**,** 176-83.

ERIE, J. C., MCLAREN, J. W., HODGE, D. O. & BOURNE, W. M. (2005) Recovery of Corneal Subbasal Nerve Density After PRK and LASIK. *American Journal of Ophthalmology,* 140**,** 1059-1059.

ERIE, J. C., PATEL, S. V., MCLAREN, J. W., HODGE, D. O. & BOURNE, W. M. (2003) Keratocyte Density in the Human Cornea After Photorefractive Keratectomy. *Arch Ophthalmol,* 121**,** 770-776.

ERIE, J. C., PATEL, S. V., MCLAREN, J. W., NAU, C. B., HODGE, D. O. & BOURNE, W. M. (2002a) Keratocyte density in keratoconus. A confocal microscopy study. *American Journal of Ophthalmology,* 134**,** 689-695.

ERIE, J. C., PATEL, S. V., MCLAREN, J. W., RAMIREZ, M., HODGE, D. O., MAGUIRE, L. J. & BOURNE, W. M. (2002b) Effect of Myopic Laser In Situ Keratomileusis on Epithelial and Stromal Thickness: A Confocal Microscopy Study. *Ophthalmology,* 109**,** 1447-1452.

FERNANDES, B. F., LOGAN, P., ZAJDENWEBER, M. E., SANTOS, L. N., CHEEMA, D. P., JR. & BURNIER, M. N. (2008) Histopathological study of 49 cases of keratoconus. *Pathology,* 40**,** 623-626

FINI, M. E. (1999) Keratocyte and fibroblast phenotypes in the repairing cornea. *Prog Retin Eye Res,* 18**,** 529-51.

FROUSSART, F., CLAY, C., LEBLOND, V., CHAOUAT, D., D'HERMIES, F. & RENARD, G. (2001) Corneal crystalline deposits in monoclonal gammapathy: a report of two cases. *J Fr Ophtalmol,* 24**,** 738-43.

FUCHS, E. (1910) Dystrophia epithelialis corneae. *Graefe's Archive for Clinical and Experimental Ophthalmology,* Volume 76, / August, 1910**,** 478-508.

GARIBALDI, D. C., GOTTSCH, J., DE LA CRUZ, Z., HAAS, M. & GREEN, W. R. (2005) Immunotactoid keratopathy: a clinicopathologic case report and a review of reports of corneal involvement in systemic paraproteinemias. *Surv Ophthalmol,* 50**,** 61-80.

GARNER, A. (1969) Histochemistry of corneal macular dystrophy. *Invest Ophthalmol,* 8**,** 475-83.

GEGGEL, H. S., FRIEND, J. & BORUCHOFF, S. A. (1985) Corneal epithelial dysplasia. *Ann Ophthalmol,* 17**,** 27-31.

GENTA, R. M. & RUGGE, M. (2006) Assessing risks for gastric cancer: new tools for pathologists. *World J Gastroenterol,* 12**,** 5622-7.

GENTILE, C. M., BURCHAKCHI, A. I. & OSCAR, C. J. (2009) In Vivo Confocal Microscopy Study of Ocular Surface Neoplasia Manifesting After Radial Keratotomy and Laser In Situ Keratomileusis. *Cornea,* 28**,** 357-359.

GHECK, L., DUPAS, B., DENION, E., AMAR, N. & BAUDOUIN, C. (2007) Advantages of in vivo confocal microscopy for investigation of the pterygium. *J Fr Ophtalmol,* 30**,** 703-10.

GHOSH, M. & MCCULLOCH, C. (1984) Amiodarone-induced ultrastructural changes in human eyes. *Can J Ophthalmol,* 19**,** 178-86.

GRUPCHEVA, C. N., CHEW, G. S. M., EDWARDS, M., CRAIG, J. P. & MCGHEE, C. N. J. (2001a) Imaging posterior polymorphous corneal dystrophy by in vivo confocal microscopy. *Clinical and Experimental Ophthalmology***,** 256 - 259.

GRUPCHEVA, C. N., CRAIG, J. P., SHERWIN, T. & MCGHEE, C. N. J. (2001b) Differential Diagnosis of corneal oedema assisted by in vivo confocal microscopy. *Clinical and Experimental Ophthalmology***,** 133 - 137.

GRUPCHEVA, C. N., MALIK, T., CRAIG, J. P. & MCGHEE, C. N. J. (2001c) In vivo confocal microscopy of corneal epithelial ingrowth through a laser in situ keratomileusis flap buttonhole. *J Cataract Refract Surg* 1318–1322.

GRUPCHEVA, C. N., MCGHEE, C. N. J., DEAN, S. & CRAIG, J. P. (2004) In vivo confocal microscopic characteristics of iridocorneal endothelial syndrome. *Clinical and Experimental Ophthalmology,* 32**,** 275 - 283.

GRUPCHEVA, C. N., WONG, T., RILEY, A. F. & MCGHEE, C. N. J. (2002) Assessing the sub-basal nerve plexus of the living healthy human cornea by in vivo confocal microscopy. 30**,** 187-190.

GUTHOF, R. F., BAUDOUIN, C. & STAVE, J. (2006) *Atlas of Confocal Laser Scanning In-vivo Microscopy in Ophthalmology—Principles and Applications in Diagnostic and Therapeutic Ophthalmology,* Berlin, Springer.

GUTHOFF, R., BAUDOUIN, C. & STAVE, J. (2006) *Atlas of confocal laser scanning in-vivo microscopy in ophthalmology - principles and applications in diagnostic and therapeutic ophthalmology,* Berlin, Springer.

GUTHOFF, R. F., WIENSS, H., HAHNEL, C. & WREE, A. (2005) Epithelial innervation of human cornea: a three-dimensional study using confocal laser scanning fluorescence microscopy. *Cornea,* 24**,** 608-13.

HANSSENS M, KESTELYN P, VAN LIEFFERINGE T & PRAET M (1993) Primary corneal epithelial dysplasia (corneal intraepithelial neoplasia). *Bull Soc Belge Ophtalmol***,** 125-30.

HENDERSON, D. W., STIRLING, J. W., LIPSETT, J., ROZENBILDS, M. A., ROBERTS-THOMSON, P. J. & COSTER, D. J. (1993) Paraproteinemic crystalloidal keratopathy: an ultrastructural study of two cases, including immunoelectron microscopy. *Ultrastruct Pathol,* 17**,** 643-68.

HERNANDEZ-QUINTELA, E., MAYER, F., DIGHIERO, P., BRIAT, B., SAVOLDELLI, M., LEGEAIS, J.-M. & RENARD, G. (1998) Confocal Microscopy of Cystic Disorders of the Corneal Epithelium. *Ophthalmology,* 105**,** 63l - 636.

HOLLINGSWORTH, J. G., BONSHEK, R. E. & EFRON, N. (2005a) Correlation of the appearance of the keratoconic cornea in vivo by confocal microscopy and in vitro by light microscopy. *Cornea,* 24**,** 397-405.

HOLLINGSWORTH, J. G., EFRON, N. & TULLO, A. B. (2005b) In vivo corneal confocal microscopy in keratoconus. *Ophthalmic and Physiological Optics,* 25**,** 254-260.

HOLLINGSWORTH, J. G., EFRON, N. & TULLO, A. B. (2006) A longitudinal case series investigating cellular changes to the transplanted cornea using confocal microscopy. *Contact Lens and Anterior Eye,* 29**,** 135-141.

HOLLINGSWORTH, J. O., PEREZ-GOMEZ, I., MUTALIBT, H. A. & EFRON, N. (2001) A Population Study of the Normal Cornea using an in Vivo, Slit-Scanning Confocal Microscope. *Optometry and Vision Science,* 78**,** 706 - 711.

HORATANARUANG, O., CHANSANTI, O., MITARNUN, W. & TUNGSINMUNKONG, K. (2005) Isolated Corneal Intraepithelial Neoplasia. *J Med Assoc Thai* 88**,** S134-7.

HOSAL, B. M., ORNEK, N., ZILELIOGLU, G. & ELHAN, A. H. (2005) Morphology of corneal nerves and corneal sensation in dry eye: a preliminary study. *Eye (Lond),* 19**,** 1276-9.

IVARSEN, A., STULTIENS, B. A. T. & MØLLER-PEDERSEN, T. (2002) Validation of Confocal Microscopy Through Focusing for Corneal Sublayer Pachymetry. *Cornea,* 21**,** 700 - 704.

IWAMOTO, T. & DE VOE, A. G. (1971) Electron Microscopic Studies on Fuchs' Combined Dystrophy: II. Anterior Portion of the Cornea. *Invest. Ophthalmol. Vis. Sci.,* 10**,** 29-40.

IWAMOTO, T. & DE VOE, A. G. (1976) Electron Microscopical Study of the Fleischer Ring. *Arch Ophthalmol,* 94**,** 1579-1584.

JALBERT, I., STAPLETON, F., PAPAS, E., SWEENEY, D. F. & CORONEO, M. (2003) In vivo confocal microscopy of the human cornea. *Br. J. Ophthalmol***,** 225 - 236.

JESTER, J. V., BARRY, P. A., LIND, G. J., PETROLL, W. M., GARANA, R. & CAVANAGH, H. D. (1994) Corneal keratocytes: in situ and in vitro organization of cytoskeletal contractile proteins. *Invest Ophthalmol Vis Sci,* 35**,** 730-43.

JESTER, J. V., PETROLL, W. M., BARRY, P. A. & CAVANAGH, H. D. (1995) Expression of alpha-smooth muscle (alpha-SM) actin during corneal stromal wound healing. *Invest Ophthalmol Vis Sci,* 36**,** 809-19.

JESTER, J. V., PETROLL, W. M., FENG, W., ESSEPIAN, J. & CAVANAGH, H. D. (1992) Radial keratotomy. 1. The wound healing process and measurement of incisional gape in two animal models using in vivo confocal microscopy. *Investigative Ophthalmology & Visual Science,* 33**,** 3255-3270.

KAAS-HANSEN, M. (1993) The histopathological changes of keratoconus. *Acta Ophthalmol (Copenh),* 71**,** 411-4.

KALLINIKOS, P., BERHANU, M., O'DONNELL, C., BOULTON, A. J. M., EFRON, N. & MALIK, R. A. (2004) Corneal Nerve Tortuosity in Diabetic Patients with Neuropathy. *Invest. Ophthalmol. Vis. Sci.,* 45**,** 418-422.

KAPLAN, L. J. & CAPPAERT, W. E. (1982) Amiodarone keratopathy. Correlation to dosage and duration. *Arch Ophthalmol,* 100**,** 601-2.

KAUFMAN, S. C., MUSCH, D. C., BELIN, M. W., COHEN, E. J., MEISLER, D. M., REINHART, W. J., UDELL, I. J. & VAN METER, W. S. (2004) Confocal microscopy: A report by the American Academy of Ophthalmology. *Ophthalmology,* 111**,** 396-406.

KITANO, S. & GOLDMAN, J. N. (1966) Cytologic and histochemical changes in corneal wound repair. *Arch Ophthalmol,* 76**,** 345-54.

KOBAYASHI, A., FUJIKI, K., FUJIMAKI, T., MURAKAMI, A. & SUGIYAMA, K. (2007) In Vivo Laser Confocal Microscopic Findings of Corneal Stromal Dystrophies. *Arch Ophthalmol,* 125**,** 1168-1173.

KOBAYASHI, A. & SUGIYAMA, K. (2007) In Vivo Laser Confocal Microscopy Findings for Bowman's Layer Dystrophies (Thiel-Behnke and Reis-Bücklers Corneal Dystrophies). *Ophthalmology,* 114**,** 69-75.

KOBAYASHI, A., YOKOGAWA, H. & SUGIYAMA, K. (2006) In Vivo Laser Confocal Microscopy of Bowman's Layer of the Cornea. *Ophthalmology,* 113**,** 2203-2208.

KOBAYASHI, A., YOSHITA, T. & SUGIYAMA, K. (2005) In vivo findings of the bulbar/palpebral conjunctiva and presumed meibomian glands by laser scanning confocal microscopy. *Cornea,* 24**,** 985-8.

KUCHLE, M., GREEN, W. R., VOLCKER, H. E. & BARRAQUER, J. (1995) Reevaluation of corneal dystrophies of Bowman's layer and the anterior stroma (Reis-Bucklers and Thiel-Behnke types): a light and electron microscopic study of eight corneas and a review of the literature. *Cornea,* 14**,** 333-54.

LABBE, A., NICOLA, R. D., DUPAS, B., AUCLIN, F. & BAUDOUIN, C. (2006) Epithelial basement membrane dystrophy: evaluation with the HRT II Rostock Cornea Module. *Ophthalmology,* 113**,** 1301-8.

LABBÉ, A., NICOLA, R. D., DUPAS, B., AUCLIN, F. & BAUDOUIN, C. (2006) Epithelial Basement Membrane Dystrophy: Evaluation with the HRT II Rostock Cornea Module. *Ophthalmology,* 113**,** 1301-1308.

LAIBSON, P. R. (1976) Microcystic corneal dystrophy. *Trans Am Ophthalmol Soc,* 74**,** 488-531.

LEE, B. H., MCLAREN, J. W., HODGE, D. O. & BOURNE, W. M. (2002) Reinnervation in the Cornea after LASIK. *Invest Ophthalmol Vis Sci***,** 3660 - 3664.

LEE, G. A. & HIRST, L. W. (1995) Ocular surface squamous neoplasia. *Surv Ophthalmol,* 39**,** 429-50.

LIM, N., GOH, D., BUNCE, C., XING, W., FRAENKEL, G., POOLE, T. R. G. & FICKER, L. (2008) Comparison of Polyhexamethylene Biguanide and

Chlorhexidine as Monotherapy Agents in the Treatment of Acanthamoeba Keratitis. *American Journal of Ophthalmology,* 145**,** 130-135.

LINDQUIST, T. D., SHER, N. A. & DOUGHMAN, D. J. (1988) Clinical signs and medical therapy of early Acanthamoeba keratitis. *Arch Ophthalmol,* 106**,** 73-77.

LINNA, T. U., VESALUOMA, M. H., PEREZ-SANTONJA, J. J., PETROLL, W. M., ALIO, J. L. & TERVO, T. M. T. (2000) Effect of Myopic LASIK on Corneal Sensitivity and Morphology of Subbasal Nerves. *Invest. Ophthalmol. Vis. Sci.,* 41**,** 393-397.

LISCH, W. & SAIKIA, P. (2011) Immunotactoid Microtubular Corneal Deposits in Bilateral Paraprotein Crystalline Keratopathy and Atypical Corneal Immunoglobulin Deposition in a Patient with Dysproteinemia. *Cornea,* 30**,** 247

LYONS CJ, MCCARTNEY AC, KIRKNESS CM, FICKER LA, STEELE AD & NS., R. (1994) Granular corneal dystrophy. Visual results and pattern of recurrence after lamellar or penetrating keratoplasty. *Ophthalmology,* 101**,** 1812-7.

MALANDRINI, A., MARTONE, G., TRAVERSI, C. & CAPOROSSI, A. (2008) In vivo confocal microscopy in a patient with recurrent conjunctival intraepithelial neoplasia. *Acta Ophthalmologica,* 86**,** 690-691.

MALIK, R. A., KALLINIKOS, P., ABBOTT, C. A., VAN SCHIE, C. H., MORGAN, P., EFRON, N. & BOULTON, A. J. (2003) Corneal confocal microscopy: a non-invasive surrogate of nerve fibre damage and repair in diabetic patients. *Diabetologia,* 46**,** 683-8.

MANTYJARVI, M., TUPPURAINEN, K. & IKAHEIMO, K. (1998) Ocular side effects of amiodarone. *Surv Ophthalmol,* 42**,** 360-6.

MARCON, A. S., COHEN, E. J., RAPUANO, C. J. & LAIBSON, P. R. (2003) Recurrence of Corneal Stromal Dystrophies After Penetrating Keratoplasty. *Cornea,* 22**,** 19-21.

MASTERS, B. R. & BOHNKE, M. (2001a) Confocal Microscopy of the Human Cornea in vivo. *International Ophthalmology,* 23**,** 199-206.

MASTERS, B. R. & BOHNKE, M. (2001b) Three-Dimensional Confocal Microscopy of the Human Cornea in vivo. *Ophtlamic Research,* 33**,** 125 - 135.

MASTERS, B. R. & THAER, A. A. (1994) In vivo human corneal confocal microscopy of identical fields of subepithelial nerve plexus, basal epithelial, and wing cells at different times. *Microscopy Research and Technique,* 29**,** 350-356.

MASTROPASQUA, L. & NUBILE, M. (2002) *Confocal Microscopy of the Cornea,* Thorofare, NJ, Slack Inc.

MASTROPASQUA, L., NUBILE, M., LANZINI, M., CARPINETO, P., CIANCAGLINI, M., PANNELLINI, T., DI NICOLA, M. & DUA, H. S. (2006) Epithelial Dendritic Cell Distribution in Normal and Inflamed Human Cornea: In Vivo Confocal Microscopy Study. *American Journal of Ophthalmology,* 142**,** 736-744.e2.

MATHERS, W. D., J E SUTPHIN , R FOLBERG , P A MEIER, R P WENZEL & ., R. G. E. (1996) Outbreak of keratitis presumed to be caused by Acanthamoeba. *Am J Ophthalmol.,* 121**,** 129-42.

MATHERS, W. D., PETROLL, W. M., JESTER, J. V. & CAVANAGH, H. D. (1995) Basic science and applications of in vivo microscopy. . *Current Opinion in Ophthalmology , :,* 6**,** 86 -94

MATSUDA, H. & SMELSER, G. K. (1973) Electron microscopy of corneal wound healing. *Experimental Eye Research,* 16**,** 427-442.

MCLAREN, J. W., NAU, C. B., ERIE, J. C. & BOURNE, W. M. (2004) Corneal Thickness Measurement by Confocal Microscopy, Ultrasound, and Scanning Slit Methods. *AMERICAN JOURNAL OF OPHTHALMOLOGY* 137**,** 1011-1020.

MCLAREN, J. W., NAU, C. B., PATEL, S. V. & BOURNE, W. M. (2007) Measuring Corneal Thickness With the ConfoScan 4 and Z-Ring Adapter. *Eye & Contact Lens,* 33**,** 185-190 10.1097/ICL.0b013e31802b3114.

MEIJERING, E., JACOB, M., SARRIA, J. C., STEINER, P., HIRLING, H. & UNSER, M. (2004) Design and validation of a tool for neurite tracing and analysis in fluorescence microscopy images. *Cytometry A,* 58**,** 167-76.

MELLES, G. R. J. (2006) Posterior Lamellar Keratoplasty: DLEK to DSEK to DMEK. *Cornea,* 25**,** 879-881

MESSMER, E. (2008) In vivo confocal microscopy in healthy conjunctiva, conjunctivitis, and conjunctival tumors. IN REINHARD, T. (Ed.) *Essentials in Ophthalmology.* Heidelberg, Germany Springer Verlag.

MESSMER, E., MACKERT, M., ZAPP, D. & KAMPIK, A. (2006a) In vivo confocal microscopy of pigmented conjunctival tumors. *Graefe's Archive for Clinical and Experimental Ophthalmology,* 244**,** 1437-1445.

MESSMER, E. M., MACKERT, M. J., ZAPP, D. M. & KAMPIK, A. (2006b) In vivo confocal microscopy of normal conjunctiva and conjunctivitis. *Cornea,* 25**,** 781-8.

MINSKY, M. (1988) Memoir on inventing the confocal scanning microscope. *Scanning,* 10**,** 128-38.

MITOOKA, K., RAMIREZ, M., MAGUIRE, L. J., ERIE, J. C., PATEL, S. V., MCLAREN, J. W., HODGE, D. O. & BOURNE, W. M. (2002) Keratocyte density of central human cornea after laser in situ keratomileusis. *American Journal of Ophthalmology,* 133**,** 307-314.

MOHAN, R. R., HUTCHEON, A. E. K., CHOI, R., HONG, J., LEE, J., MOHAN, R. R., AMBRÓSIO, R., ZIESKE, J. D. & WILSON, S. E. (2003) Apoptosis, necrosis, proliferation, and myofibroblast generation in the stroma following LASIK and PRK. *Experimental Eye Research,* 76**,** 71-87.

MOHAY, J., WOOD, T. O. & MCLAUGHLIN, B. J. (1997) Long-term evaluation of corneal endothelial cell transplantation. *Trans Am Ophthalmol Soc,* 95**,** 131-151.

MOILANEN, J. A. O., VESALUOMA, M. H., MULLER, L. J. & TERVO, T. M. T. (2003) Long-Term Corneal Morphology after PRK by In Vivo Confocal Microscopy. *Invest. Ophthalmol. Vis. Sci.,* 44**,** 1064-1069.

MOLLER-PEDERSEN, T., CAVANAGH, H. D., PETROLL, W. M. & JESTER, J. V. (2000) Stromal wound healing explains refractive instability and haze development after photorefractive keratectomy : A 1-year confocal microscopic study. *Ophthalmology,* 107**,** 1235-1245.

MOLLER-PEDERSEN, T., LI, H. F., PETROLL, W. M., CAVANAGH H DWIGHT & V., J. J. (1998) Confocal Microscopic Characterization of Wound Repair after Photorefractive Keratectomy. *Invest Ophthalmol Vis Sci.,* 39**,** 487-501.

MORISHIGE, N., YAMADA, N., TERANISHI, S., CHIKAMA, T., NISHIDA, T. & TAKAHARA, A. (2009) Detection of subepithelial fibrosis associated with corneal stromal edema by second harmonic generation imaging microscopy. *Invest Ophthalmol Vis Sci,* 50**,** 3145-50.

MULLER, L. J., MARFURT, C. F., KRUSE, F. & TERVO, T. M. T. (2003) Corneal nerves: structure, contents and function. *Experimental Eye Research,* 76**,** 521-542.

MULLER, L. J., PELS, E. & VRENSEN, G. F. J. M. (2001) The specific architecture of the anterior stroma accounts for maintenance of corneal curvature. *Br J Ophthalmol,* 85**,** 437-443.

MULLER, L. J., PELS, L. & VRENSEN, G. F. (1995) Novel aspects of the ultrastructural organization of human corneal keratocytes. *Invest. Ophthalmol. Vis. Sci.,* 36**,** 2557-2567.

MULLER, L. J., VRENSEN, G. F., PELS, L., CARDOZO, B. N. & WILLEKENS, B. (1997) Architecture of human corneal nerves. *Invest. Ophthalmol. Vis. Sci.,* 38**,** 985-994.

MUSTONEN, R. K., MCDONALD, M. B., SRIVANNABOON, S., TAN, A. L. & DOUBRAVA, M. W. (1998a) In Vivo Confocal Microscopy of Fuchs' Endothelial Dystrophy. *Cornea,* 17**,** 493-503.

MUSTONEN, R. K., MCDONALD, M. B., SRIVANNABOON, S., TAN, A. L., DOUBRAVA, M. W. & KIM, C. K. (1998b) Normal Human Corneal Cell Populations Evaluated by In Vivo Scanning Slit Confocal Microscopy.

. *Cornea.,* 17**,** 485.

NATHAN EFRON, INMA PEREZ-GOMEZ, MUTALIBT, H. A. & HOLLINGSWORTH, J. (2001) Confocal Microscopy of The Normal HumanCornea. *Contact Lens and Anterior Eye* 16 - 23.

NIEDERER, R. L. & MCGHEE, C. N. (2010) Clinical in vivo confocal microscopy of the human cornea in health and disease. *Prog Retin Eye Res,* 29**,** 30-58.

NIEDERER, R. L., PERUMAL, D., SHERWIN, T. & MCGHEE, C. N. (2007a) Corneal innervation and cellular changes after corneal transplantation: an in vivo confocal microscopy study. *Invest Ophthalmol Vis Sci,* 48**,** 621-6.

NIEDERER, R. L., PERUMAL, D., SHERWIN, T. & MCGHEE, C. N. (2008) Laser scanning in vivo confocal microscopy reveals reduced innervation and

reduction in cell density in all layers of the keratoconic cornea. *Invest Ophthalmol Vis Sci,* 49**,** 2964-70.

NIEDERER, R. L., PERUMAL, D., SHERWIN, T. & MCGHEE, C. N. J. (2007b) Age-related differences in the normal human cornea: a laser scanning in vivo confocal microscopy study. *Br J Ophthalmol,* 91**,** 1165-1169.

OLIVEIRA-SOTO L & N., E. (2001) Morphology of corneal nerves using confocal microscopy. *Cornea,* 20**,** 374-384.

OLIVEIRA-SOTO, L. & EFRON, N. (2001) Morphology of Corneal Nerves Using Confocal Microscopy. *Cornea,* 20**,** 374-384.

ORLANDO, R. G., DANGEL, M. E. & SCHAAL, S. F. (1984) Clinical experience and grading of amiodarone keratopathy. *Ophthalmology,* 91**,** 1184-7.

PARK, C. K. & KIM, J. H. (1999) Comparison of wound healing after photorefractive keratectomy and laser in situ keratomileusis in rabbits1 1 Neither of the authors has a proprietary or financial interest in any material or method mentioned. *Journal of Cataract and Refractive Surgery,* 25**,** 842-850.

PARMAR, D. N., AWWAD, S. T., PETROLL, W. M., BOWMAN, R. W., MCCULLEY, J. P. & CAVANAGH, H. D. (2006) Tandem Scanning Confocal Corneal Microscopy in the Diagnosis of Suspected Acanthamoeba Keratitis. *Ophthalmology,* 113**,** 538-547.

PATEL, D. V., GRUPCHEVA, C. N. & MCGHEE, C. N. (2005a) Imaging the microstructural abnormalities of meesmann corneal dystrophy by in vivo confocal microscopy. *Cornea,* 24**,** 669-73.

PATEL, D. V., GRUPCHEVA, C. N. & MCGHEE, C. N. (2005b) In vivo confocal microscopy of posterior polymorphous dystrophy. *Cornea,* 24**,** 550-4.

PATEL, D. V. & MCGHEE, C. N. (2008) In vivo laser scanning confocal microscopy confirms that the human corneal sub-basal nerve plexus is a highly dynamic structure. *Invest Ophthalmol Vis Sci,* 49**,** 3409-12.

PATEL, D. V. & MCGHEE, C. N. J. (2005) Mapping of the Normal Human Corneal Sub-Basal Nerve Plexus by In Vivo Laser Scanning Confocal Microscopy. *Invest. Ophthalmol. Vis. Sci.,* 46**,** 4485-4488.

PATEL, D. V. & MCGHEE, C. N. J. (2006) Mapping the Corneal Sub-basal Nerve Plexus in Keratoconus by In Vivo Laser Scanning Confocal Microscopy. *Invest. Ophthalmol. Vis. Sci.,* 47**,** 1348-1351.

PATEL, D. V. & MCGHEE, C. N. J. (2009) In vivo confocal microscopy of human corneal nerves in health, in ocular and systemic disease, and following corneal surgery: a review. *British Journal of Ophthalmology,* 93**,** 853-860.

PATEL, D. V., PHUA, Y. S. & MCGHEE, C. N. J. (2006a) Clinical and microstructural analysis of patients with hyper-reflective corneal endothelial nuclei imaged by in vivo confocal microscopy. *Experimental Eye Research* 682–687

PATEL, D. V., SHERWIN, T. & MCGHEE, C. N. J. (2006b) Laser Scanning In Vivo Confocal Microscopy of the Normal Human Corneoscleral Limbus. *Invest. Ophthalmol. Vis. Sci.,* 47**,** 2823-2827.

PATEL, S. V., ERIE, J. C., MCLAREN, J. W. & BOURNE, W. M. (2007) Keratocyte density and recovery of subbasal nerves after penetrating keratoplasty and in late endothelial failure. *Arch Ophthalmol,* 125**,** 1693-8.

PATEL, S. V., MCLAREN, J. W., HODGE, D. O. & BOURNE, W. M. (2001) Normal Human Keratocyte Density and Corneal Thickness Measurement by Using Confocal Microscopy In Vivo. . *Invest Ophthalmol Vis Sci***,** 333–339.

PATEL, S. V., MCLAREN, J. W., HODGE, D. O. & BOURNE, W. M. (2002) Confocal Microscopy In Vivo in Corneas of Long-Term Contact Lens Wearers. *Invest. Ophthalmol. Vis. Sci.,* 43**,** 995-1003.

PEREZ-GOMEZ, I. & EFRON, N. (2003) Confocal microscopic evaluation of particles at the corneal flap interface after myopic laser in situ keratomileusis. *J Cataract Refract Surg***,** 1373 - 1377.

PFISTER, D. R., CAMERON, J. D., KRACHMER, J. H. & HOLLAND, E. J. (1996) Confocal microscopy findings of Acanthamoeba keratitis. *Am J Ophthalmol.,* 121**,** 119-28.

PISELLA, P.-J., AUZERIE, O., BOKOBZA, Y., DEBBASCH, C. & BAUDOUIN, C. (2001) Evaluation of Corneal Stromal Changes In Vivo after Laser In Situ Keratomileusis with Confocal *Ophthalomology***,** 1744–1750

POLLAK, P. T. & TAN, M. H. (1999) Elevation of high-density lipoprotein cholesterol in humans during long-term therapy with amiodarone. *Am J Cardiol,* 83**,** 296-300, A7.

POPPER, M., MORGADO, A. M., QUADRADO, M. J. & VAN BEST, J. A. (2004) Corneal cell density measurement in vivo by scanning slit confocal microscopy: method and validation. . *Ophthalmic Research,* 36**,** 270-6.

RABINOWITZ, Y. S. (1996) Tangential vs sagittal videokeratographs in the "early" detection of keratoconus. *Am J Ophthalmol,* 122**,** 887-9.

REASOR, M. J. & KACEW, S. (2001) Drug-induced phospholipidosis: are there functional consequences? *Exp Biol Med (Maywood),* 226**,** 825-30.

RIDGWAY, A. E., AKHTAR, S., MUNIER, F. L., SCHORDERET, D. F., STEWART, H., PERVEEN, R., BONSHEK, R. E., ODENTHAL, M. T., DIXON, M., BARRAQUER, R., ESCOTO, R. & BLACK, G. C. (2000) Ultrastructural and molecular analysis of Bowman's layer corneal dystrophies: an epithelial origin? *Invest Ophthalmol Vis Sci,* 41**,** 3286-92.

RILEY, T. R., 3RD & RUGGIERO, F. M. (2008) The effect of processing on liver biopsy core size. *Dig Dis Sci,* 53**,** 2775-2777.

ROBERSON, M. (1984) Corneal epithelial dysplasia. *Ann Ophthalmol.,* 16**,** 1147-50.

RODRIGUES, M. M. & KRACHMER, J. H. (1988) Recent advances in corneal stromal dystrophies. *Cornea,* 7**,** 19-29.

ROSE, G. E. & LAVIN, M. J. (1987) The Hudson-Stahli line. III: Observations on morphology, a critical review of aetiology and a unified theory for the formation of iron lines of the corneal epithelium. *Eye (Lond),* 1 (Pt 4)**,** 475-9.

ROSENBERG, M. E., TERVO, T. M. T., GALLAR, J., ACOSTA, M. C., MULLER, L. J., MOILANEN, J. A. O., TARKKANEN, A. H. A. & VESALUOMA, M. H. (2001) Corneal Morphology and Sensitivity in Lattice Dystrophy Type II (Familial Amyloidosis, Finnish Type). *Invest. Ophthalmol. Vis. Sci.,* 42**,** 634-641.

ROSENBERG, M. E., TERVO, T. M. T., IMMONEN, I. J., MULLER, L. J., GRONHAGEN-RISKA, C. & VESALUOMA, M. H. (2000a) Corneal Structure and Sensitivity in Type 1 Diabetes Mellitus. *Invest. Ophthalmol. Vis. Sci.,* 41**,** 2915-2921.

ROSENBERG, M. E., TERVO, T. M. T., PETROLL, W. M. & VESALUOMA, M. H. (2000b) In vivo confocal microscopy of patients with corneal recurrent erosion syndrome or epithelial basement membrane dystrophy. *Ophthalmology,* 107**,** 565-573.

SAID, D. G., MATHEW, M., SHAIKH, M. Y., MAHARAJAN, V. S., LOWE, J. & DUA, H. S. (2008) Diffuse keratoconjunctival proliferation: a novel clinical manifestation. *Arch Ophthalmol,* 126**,** 1226-1232.

SAID, D. G., NUBILE, M., ALOMAR, T., HOPKINSON, A., GRAY, T., LOWE, J. & DUA, H. S. (2009) Histologic features of transplanted amniotic membrane: implications for corneal wound healing. *Ophthalmology,* 116**,** 1287-95.

SCROGGS, M. W. & PROIA, A. D. (1992) Histopathological variation in keratoconus. *Cornea,* 11**,** 553-9.

SHERWIN, T., BROOKES, N. H., LOH, I. P., POOLE, C. A. & CLOVER, G. M. (2002) Cellular incursion into Bowman's membrane in the peripheral cone of the keratoconic cornea. *Exp Eye Res,* 74**,** 473-82.

SHIELDS, C. L., SHIELDS, J. A., CARVALHO, C., RUNDLE, P. & SMITH, A. F. (2001) Conjunctival lymphoid tumors : Clinical analysis of 117 cases and relationship to systemic lymphoma. *Ophthalmology,* 108**,** 979-984.

SIMO MANNION, L., TROMANS, C. & O'DONNELL, C. (2005) An evaluation of corneal nerve morphology and function in moderate keratoconus. *Cont Lens Anterior Eye,* 28**,** 185-92.

SOMODI, S., HAHNEL, C., SLOWIK, C., RICHTER, A., WEISS, D. G. & GUTHOFF, R. (1996) Confocal in vivo microscopy and confocal laser-scanning fluorescence microscopy in keratoconus. *Ger J Ophthalmol,* 5**,** 518-25.

SONIGO, B., IORDANIDOU, V., CHONG-SIT, D., AUCLIN, F., ANCEL, J. M., LABBE, A. & BAUDOUIN, C. (2006) In vivo corneal confocal microscopy comparison of intralase femtosecond laser and mechanical microkeratome for laser in situ keratomileusis. *Invest Ophthalmol Vis Sci,* 47**,** 2803-11.

SRIDHAR, M. S., VEMUGANTI, G. K., BANSAL, A. K. & RAO, G. N. (2001) Anterior stromal puncture in bullous keratopathy: a clinicopathologic study. *Cornea,* 20**,** 573-9.

STACHS, O., ZHIVOV, A., KRAAK, R., STAVE, J. & GUTHOFF, R. (2007) In vivo three-dimensional confocal laser scanning microscopy of the epithelial nerve structure in the human cornea. *Graefes Arch Clin Exp Ophthalmol,* 245**,** 569-75.

STIRLING, J. W., HENDERSON, D. W., ROZENBILDS, M. A., SKINNER, J. M. & FILIPIC, M. (1997) Crystalloidal paraprotein deposits in the cornea: an

ultrastructural study of two new cases with tubular crystalloids that contain IgG kappa light chains and IgG gamma heavy chains. *Ultrastruct Pathol,* 21**,** 337-44.

TAN, D. T. H. & MEHTA, J. S. (2007) Future Directions in Lamellar Corneal Transplantation. *Cornea,* 26**,** S21-S28

TENG, C. C. (1963) Electron microscope study of the pathology of keratoconus: I. *Am J Ophthalmol,* 55**,** 18-47.

TERANO, A., MORITA, K., NAKAMURA, T., OHKURA, Y., ONO, Y. & FUJIMORI, T. (2002) Barrett's esophagus. *J Gastroenterol,* 37**,** 685-90.

TIMO TERVO & MOILANEN, J. (2003) In vivo confocal microscopy for evaluation of wound healing following corneal refractive surgery. . *Progress in Retinal and Eye Research***,** 339–358.

TRAVERSI, C., MARTONE, G., MALANDRINI, A., TOSI, G. M. & CAPOROSSI, A. (2006) In vivo confocal microscopy in recurrent granular dystrophy in corneal graft after penetrating keratoplasty. *Clinical & Experimental Ophthalmology,* 34**,** 808-810.

TRIPATHI, R. C. & GARNER, A. (1972) The Ultrastructure of Preinvasive Cancer of the Corneal Epithelium. *Cancer Res,* 32**,** 90-97.

UCAKHAN, O. O., KANPOLAT, A., YLMAZ, N. & OZKAN, M. (2005) Amiodarone keratopathy: an in vivo confocal microscopy study. *Eye Contact Lens,* 31**,** 148-57.

UCAKHAN, O. O., KANPOLAT, A., YLMAZ, N. & OZKAN, M. (2006) In Vivo Confocal Microscopy Findings in Keratoconus. *Eye & Contact Lens: Science & Clinical Practice,* 32**,** 183-191.

VAIDYANATHAN, S., MCDICKEN, I. W., IKIN, A. J., MANSOUR, P., SONI, B. M., SINGH, G. & SETT, P. (2002) A study of cytokeratin 20 immunostaining in the urothelium of neuropathic bladder of patients with spinal cord injury. *BMC Urol,* 2**,** 7.

VANATHI M, TANDON R, SHARMA N, TITIYAL JS, PANDEY RM & RB., V. (2003) In-Vivo Slit Scanning Confocal Microscopy of Normal Corneas in Indian Eyes. *Indian J Ophthalmol,* 51**,** 225-230.

VESALUOMA, M., PEREZ-SANTONJA, J., PETROLL, W. M., LINNA, T., ALIO, J. & TERVO, T. (2000) Corneal Stromal Changes Induced by Myopic LASIK. *Invest. Ophthalmol. Vis. Sci.,* 41**,** 369-376.

VESALUOMA, M. H., LINNA, T. U., SANKILA, E.-M., WEISS, J. S. & TERVO, T. M. T. (1999) In vivo confocal microscopy of a family with schnyder crystalline corneal dystrophy. *Ophthalmology,* 106**,** 944-951.

VINCENT, A. L., PATEL, D. V. & MCGHEE, C. N. J. (2005) Inherited corneal disease: the evolving molecular, genetic and imaging revolution. *Clinical and Experimental Ophthalmology***,** 303 - 316.

VISSER, N., MCGHEE, C. N. J. & PATEL, D. V. (2009) Laser-scanning in vivo confocal microscopy reveals two morphologically distinct populations of stromal nerves in normal human corneas. *British Journal of Ophthalmology,* 93**,** 506-509.

VONGTHONGSRI, A., CHUCK, R. S. & PEPOSE, J. S. (1999) Corneal iron deposits after laser in situ keratomileusis. *Am J Ophthalmol,* 127**,** 85-6.

WAKUTA, M., CHIKAMA, T.-I., TAKAHASHI, N. & NISHIDA, T. (2008) A Case of Bilateral Corneal Epithelial Dysplasia Characterized by Laser Confocal Biomicroscopy and Cytokeratin Immunofluorescence. *Cornea,* 27**,** 107-110.

WARING, G. O., 3RD, RODRIGUES, M. M. & LAIBSON, P. R. (1978a) Corneal dystrophies. I. Dystrophies of the epithelium, Bowman's layer and stroma. *Surv Ophthalmol,* 23**,** 71-122.

WARING, G. O., 3RD, RODRIGUES, M. M. & LAIBSON, P. R. (1978b) Corneal dystrophies. II. Endothelial dystrophies. *Surv Ophthalmol,* 23**,** 147-68.

WARING, G. O., 3RD, ROTH, A. M. & EKINS, M. B. (1984) Clinical and pathologic description of 17 cases of corneal intraepithelial neoplasia. *Am J Ophthalmol,* 97**,** 547-59.

WEED, K. H., MACEWEN, C. J., COX, A. & MCGHEE, C. N. J. (2006) Quantitative analysis of corneal microstructure in keratoconus utilising in vivo confocal microscopy. *Eye,* 21**,** 614-623.

WERNER, L. P., WERNER, L., DIGHIERO, P., LEGEAIS, J.-M. & RENARD, G. (1999a) Confocal Microscopy in Bowman and Stromal Corneal Dystrophies. *Ophthalmology***,** 1697-1704.

WERNER, L. P., WERNER, L., DIGHIERO, P., LEGEAIS, J. M. & RENARD, G. (1999b) Confocal microscopy in Bowman and stromal corneal dystrophies. *Ophthalmology,* 106**,** 1697-704.

WILSON, S. E., HE, Y. G., WENG, J., LI, Q., MCDOWALL, A. W., VITAL, M. & CHWANG, E. L. (1996) Epithelial injury induces keratocyte apoptosis: hypothesized role for the interleukin-1 system in the modulation of corneal tissue organization and wound healing. *Exp Eye Res,* 62**,** 325-7.

WINCHESTER, K., MATHERS, W. D. & SUTPHIN, J. E. (1997) Diagnosis of Aspergillus keratitis in vivo with confocal microscopy. *Cornea,* 16**,** 27-31.

WINCHESTER, K., MATHERS, W. D., SUTPHIN, J. E. & DALEY, T. E. (1995) Diagnosis of Acanthamoeba keratitis in vivo with confocal microscopy. *Cornea,* 14**,** 10-7.

YUEN, H. K. L., RASSIER, C. E., JARDELEZA, M. S. R., GREEN, W. R., DE LA CRUZ, Z., STARK, W. J. & GOTTSCH, J. D. (2005) A Morphologic Study of Fuchs Dystrophy and Bullous Keratopathy. *Cornea,* 24**,** 319-327.

ZHANG, M., CHEN, J., LUO, L., XIAO, Q., SUN, M. & LIU, Z. (2005) Altered Corneal Nerves in Aqueous Tear Deficiency Viewed by In Vivo Confocal Microscopy. *Cornea,* 24**,** 818-824.

ZINK, D., FISCHER, A. H. & NICKERSON, J. A. (2004) Nuclear structure in cancer cells. *Nat Rev Cancer,* 4**,** 677-687.

APPENDICES

10 Appendix I

10.1 LIST OF PUBLICATIONS ARISING FROM WORK PRESENTED IN THIS THESIS

1. In vivo confocal microscopy in the diagnosis and management of acanthamoeba keratitis showing new cystic forms.

   Alomar T, Matthew M, Donald F, Maharajan S, Dua HS.

   Clin Experiment Ophthalmol. 2009 Sep;37(7):737-9. PMID: 19788672

2. Rings around cones.

   Said DG, Ho S, Mathew M, Alomar T, Dua HS.

   Br J Ophthalmol. 2009 Apr;93(4):423, 545. Epub 2008 Aug 21. PMID: 18718970

3. The role of limbal stem cells in corneal epithelial maintenance: testing the dogma.

   Dua HS, Miri A, Alomar T, Yeung AM, Said DG.

   Ophthalmology. 2009 May;116(5):856-63. PMID:19410942

4. Corneal intraepithelial neoplasia: in vivo confocal microscopic study with histopathologic correlation.

   Alomar TS, Nubile M, Lowe J, Dua HS.

   Am J Ophthalmol. 2011 Feb;151(2):238-47. Epub 2010 Dec 18.

PMID: 21168809

5. Corneal nerve aberrations in bullous keratopathy.

   Al-Aqaba M, Alomar T, Lowe J, Dua HS. Am J Ophthalmol. 2011 May;151(5):840-849.e1. Epub 2011 Feb 18. PMID: 21310389

6. Histological and Confocal Microscopy Changes in Chronic Corneal Edema: Implications for Endothelial Transplantation.
   Thaer S Alomar, Mouhamed Al-Aqaba, Trevor Gray, James Lowe and Harminder S Dua. Invest Ophthalmol Vis Sci. 2011 Oct;52(11):8193-8207.

10.2 PAPERS SUBMITTED AND UNDER REVISION FOR PUBLICATION

1. Localized Conjunctival B cell Lymphoma with Paraproteinic Crystalline Keratopathy.

   T S Alomar, Khalid Mahmood, Simon O' Connor, Keith Robson and H S Dua. Submitted to "International Ophthalmology" on 13 Dec 2011.

2. Histological and Confocal Microscopy Changes in Chronic Corneal Edema: Implications for Endothelial Transplantation.

   Thaer S Alomar, Mouhamed Al-Aqaba, Trevor Gray, James Lowe and Harminder S Dua. Accepted for oral and poster presentation at 2012 Oxford Ophthalmology Congress, 1-4 July 2012 Oxford, UK.

3. In Vivo Confocal Microscopy of Keratoconus with Histpathological Correlation.
   T S Alomar, Mouhamed Al-Aqaba, James Lowe and Harminder S Dua. Accepted for poster presentation at 2012 Oxford Ophthalmology Congress, 1-4 July 2012, Oxford, UK.

11 Appendix II:

11.1 LIST OF PRESENTATIONS FROM WORK PRESENTED IN THIS THESIS

1. In Vivo Confocal Microscopy of the Cornea. Dua HS and Alomar T. The 23rd Malaysia – Singapore Ophthalmic Congress, Malaysia, June 2007. Oral presentation
2. In Vivo Confocal Microscopy of Abnormal Cornea: Clinical & Pathological Correlation. Alomar T, Lowe J and Dua HS. European Association for Vision & Eye Research Conference (EVER 2008) Portoroz, Slovenia, Oct 2008. Oral presentation.
3. Diffuse keratoconjunctival diseases: an in vivo confocal microscopic study. Dua HS and Alomar T. European Association for Vision & Eye Research (EVER 2009), Portoroz, Slovenia, Sep30-Oct3 2009. Oral presentation.
4. In Vivo Confocal Microscopy in Corneal Oedema with Histopathological Correlation. Alomar T, Gray T, Lowe J and Dua HS. The14th Nottingham Eye Symposium, Nottingham, UK, Jan 2010. Poster presentation.
5. Corneal Intra-epithelial Neoplasia: In Vivo Confocal Microscopic Study with Histopathological Correlation. Alomar T, Lowe J and Dua HS. 15th Nottingham Eye Symposium, Nottingham, UK, Jan 2011. Oral presentation.
6. Histological and Confocal Microscopy Changes in Chronic Corneal Edema: Implications for Endothelial Transplantation.

Thaer S Alomar, Mouhamed Al-Aqaba, Trevor Gray, James Lowe and Harminder S Dua. Accepted abstract, The 2nd EuCornea Congress, Vienne, Austria Sep 2011.

7. In Vivo Confocal Microscopy in Keratoconus with Hitopathological correlation. Thaer S Alomar, Mouhamed Al-Aqaba, James Lowe and Harminder S Dua. Accepted Poster, The 2nd EuCornea Congress, Vienne, Austria Sep 2011.